Biodegradation and microbial upcycling of plastics

Inaugural Dissertation

for the attainment of the title of doctor
in the Faculty of Mathematics and Natural Sciences
at the Heinrich Heine University Düsseldorf
presented by

Jan Alexander de Witt
born in
Münster, Germany

Jülich
06.02.2024

This thesis has been conducted at the Institute of Bio- and Geosciences, IBG-1: Biotechnology, Forschungszentrum Jülich GmbH, from June 2020 until January 2024 under the supervision of Prof. Dr. Nick Wierckx.

Publications

The results presented in this dissertation have been published in the following original publications, are currently under revision or are in the process of being prepared as manuscript for submission:

de Witt, J., Luthe, T., Jensen, K., Polen, T., Wirtz, A., Frunzke, J., Wynands, B., Wierckx, N., (2024). Microbial upcycling of polyamides using engineered *Pseudomonas putida* – Invitation to revise and resubmit to *Nat. Microbiol.*

de Witt, J., Ostheller, M-E., Jensen, K., van Slagmaat C.A.M.R., Polen, T., Wynands, B., Wierckx, N., (2024). Increasing the diversity of Nylonases for polyamide degradation. – Manuscript in preparation.

Ackermann Y. S.[†], **de Witt J.**[†]**,** Mezzina M. P., Schroth C., Polen T., Nickel, P. I., Wynands B., and Wierckx N.[*] (2024). Bio-upcycling of even and uneven medium-chain-length diols and dicarboxylates using engineered *Pseudomonas putida*. *Microb. Cell Factories – In press*. doi:10.1186/s12934-024-02310-7

[†] YSA and JdW contributed equally to this study.

de Witt, J., Ernst, P., Gätgens, J., Noack, S., Hiller, D., Wynands, B., Wierckx, N., (2023). Characterization and engineering of branched short-chain dicarboxylate metabolism in *Pseudomonas* reveals resistance to fungal 2-hydroxyparaconate. *Metab. Eng.* 75, 205-216. doi:10.1016/j.ymben.2022.12.008

de Witt, J., Molitor, R., Gätgens, J., Ortmann de Percin Northumberland, C., Kruse, L., Polen, T., Wynands, B., van Goethem, K., Thies, S., Jaeger, K-E., Wierckx, N., (2023). Biodegradation of poly(ester-urethane) coatings by *Halopseudomonas formosensis*. *Microb. Biotechnol.* 17, e14362. doi:10.1111/1751-7915.1436

Thesis-associated publications

Tiso, T., Winter, B., Wei, R., Hee, J., **de Witt, J.,** Wierckx, N., Quicker, P., Bornscheuer, U., Bardow, A., Nogales, J., Blank, LM., (2022). The metabolic potential of plastics as biotechnological carbon sources – Review and targets for the future. *Metab. Eng.* 71, 77-98. doi:10.1016/j.ymben.2021.12.006

Other publications not covered in this thesis:

Kruse, L., Loeschcke, A., **de Witt, J.,** Wierckx, N., Jaeger, K-E., Thies, S., (2023). *Halopseudomonas* species: cultivation and molecular genetic tools. *Microb. Biotechnol.* 17, e14369. doi:10.1111/1751-7915.14369

Other publications in the form of posters or oral presentations:

Poster presentations

de Witt, J., Ortmann de Percin Northumberland, C., Gätgens, J., Noack, S., Wierckx, N., (2021). Isolation of bacteria degrading polyester-polyurethane coatings. *EFB2021 – virtual conference,* online.

de Witt, J., Polen, T., Wynands B., Wierckx, N., (2022). Engineering metabolism of polyamide oligomers in *Pseudomonas putida*. *PhD Workshop Topic 7: Towards a Sustainable Bioeconomy – Resources, Utilization, Engineering and AgroEcosystems*, Leipzig, Germany, November 2022.

de Witt, J., Polen, T., Wynands B., Wierckx, N., (2022). Engineering metabolism of polyamide oligomers in *Pseudomonas putida*. *Biocatalysis for the biological transformation of polymer science*, Cologne, Germany, June 2022.

de Witt, J., Jensen, K., Luthe, T., Polen, T., van Slagmaat, C.A.M.R., De Wildeman, S.M.A., Wynands B., Wierckx, N., (2023). Bio-upcycling of polyamides using engineered *Pseudomonas putida*. 2023 *Plastics Recycling and Upcycling GRC*, Manchester/NH, United States, July 2023.

Oral presentations

de Witt, J., Ortmann de Percin Northumberland, C., Gätgens, J., Noack, S., Wierckx, N., (2021). Isolation of bacteria degrading polyester-polyurethane coatings. *EFB2021 – virtual conference,* online. Flash poster, May 2021.

de Witt, J., Polen, T., Wynands B., Wierckx, N., (2022). Engineering metabolism of polyamide oligomers in *Pseudomonas putida*. *Biocatalysis for the biological transformation of polymer science*, Cologne, Germany, Flash poster, June 2022.

Additionally, the results were presented orally at intervals of six months at Glaukos project meetings in Ghent (December, 2021), Rome (July, 2022), Maastricht (December, 2022), Vigo (June, 2023), or online.

List of abbreviations

2.4-DHB	2,4-dihydroxybutyrate
2-HP	2-hydroxyparaconate
4-NPH	4-nitrophenyl hexanoate
6-AH	6-aminohexanal
AA	Adipic acid
Aco2	Cyclic Ahx-oligomers with $n \geq 2$
Ahx	6-aminohexanoate
Ahx_n	6-aminohexanoate oligomers with n units
AIC	Analytical ion current
ALDFG	Abandoned, lost, or discarded fishing gear
ALE	Adaptive laboratory evolution
ASA	Adipate semialdehyde
BDO	1,4-butanediol
BHET	Bis(2-hydroxylethyl) terephthalic acid
BSCD	Branched short-chain dicarboxylates
CAD	*cis*-aconitate decarboxylase
CDW	Cell dry weight
CO_2	Carbon dioxide
CoA	Coenzyme A
CRediT	Contributor Roles Taxonomy
DAD	Diode array detector
DALI	Distance matrix alignment
DCA	Dicarboxylic acid
DEG	Differentially expressed gene
DMSO	Dimethyl sulfoxide
DSC	Differential scanning calorimetry
DSF	Differential scanning fluorimetry
EG	Ethylene glycol

EU	European Union
FID	Flame ionization detector
FLD	Fluorescence detector
FRT	Flippase recognition site
GC	Gas chromatography
GEO	Gene expression omnibus
GRAS	Generally recognized as safe
HA	Hydroxy acid
*Haes*_PE-H	Polyester hydrolase from *Halopseudomonas aestusnigri*
HDO	1,6-hexanediol
HDPE	High-density polyethylene
*Hfor*_PE-H	Polyester hydrolase from *Halopseudomonas formosensis* FZJ
HMDA	1,6-hexamethylenediamine
HPLC	High-performance-Liquid-Chromatography
IDS	Iminodisuccinate
*Is*PETase	PETase from *Ideonella sakaiensis*
ITT	Itatartarate
LB	Lysogeny broth
LCC	Leaf-branch compost cutinase
lcl	Long-chain-length
mcl	Medium-chain-length
MeOH	Methanol
MHET	Mono(2-hydroxylethyl) terephthalic acid
Mn	Number average molecular weight
MSM	Mineral salt medium
Mt	Metric tons
Mw	Weight average molecular weight
N-tn	N-terminal nucleophile
NylA	Nylonase A - 6-aminohexanoate-cyclic-dimer hydrolase
NylB	Nylonase B - 6-aminohexanoate-oligomer exohydrolase
NylC	Nylonase C - 6-aminohexanoate-oligomer endohydrolase

NylC$_{TS}$	Thermostable NylC variant
NylD	Nylonase D - transaminase
NylE	Nylonase E - oxidoreductase
OD$_{600}$	Optical density at λ=600 nm
ODO	1,8-octanediol
OPA	*o*-phthaldialdehyde
PA	Polyamide
PA6	Polycaprolactam
PA6.6	Poly(hexamethylene adipamide)
PAS	*Per-Arnt-Sim*
PCR	Polymerase chain reaction
PDB	Protein data bank
PDI	Polydispersity index
PE	Polyethylene
PEA	Poly(ester-amide)
PE-H	Polyester hydrolase
PET	Poly(ethylene terephthalate)
PETase	PET hydrolase
PEU	Poly(ester-urethane)
PHA	Polyhydroxyalkanoates
PHB	Polyhydroxybutyrate
PLA	Polylactic acid
PP	Polypropylene
PS	Polystyrene
PU	Polyurethane
PVC	Poly(vinyl chloride)
RID	Refractive index detector
RNA-seq	RNA-sequencing
scl	Short-chain-length
SNP	Single nucleotide polymorphism
SNV	Single nucleotide variant

TA	Terephthalic acid
T_c	Crystallization temperature
TCA cycle	Tricarboxylic acid cycle (citrate cycle)
TEM	Transmission electron microscopy
TfH	*Thermobifida fusca* hydrolase
T_g	Glass transition temperature
TIC	Total ion current
T_m	Melting temperature
TPM	Transcripts per million
T_{rc}	Re-cooling temperature
ucl	Uneven-chain-length
WGS	Whole-genome sequencing
γ-Glu	γ-glutamylated

List of figures

List of tables

Contents

Summary

Plastics have undoubtedly revolutionized our daily lives, becoming irreplaceable in several sectors, including packaging, healthcare, and automotive industries. However, current end-of-life strategies cannot cope with the increasing global production, which exceeded 400 million tons in 2022, leading to a global plastic pollution crisis. Biological catalysis has the potential to overcome the drawbacks of conventional recycling, using enzymes and microbes for the depolymerization of plastics and their subsequent conversion to value-added compounds. To facilitate the transition towards a circular plastics economy, the overall goal of this thesis is to provide new biological end-of-life solutions for plastics. Therefore, the substrate range of the biotechnological workhorse *Pseudomonas putida* KT2440 was expanded with prevalent plastic hydrolysates providing them as feedstock for microbial upcycling. Deep metabolic engineering enabled the utilization of polyamide (PA) hydrolysates as a carbon source, while RNA-sequencing revealed the synthetic metabolic routes and how they mesh with the native metabolism. In parallel, new nylonase enzymes were discovered and characterized that showed activities towards PA and poly(ester-amides). In addition to PA-derived compounds, metabolic routes for dicarboxylic acids and diols were established and their combination yielded a powerful platform strain that fully metabolized a complex polyester mock hydrolysate. Moreover, rational metabolic design enabled the degradation of branched short-chain dicarboxylates, including itaconic acid, thereby further expanding the metabolic palette of *Pseudomonas* with plastic monomers. To close the life cycle of plastic waste, hydrolysates should not only be metabolized but also upcycled. This was achieved by converting the newly accessible plastic-derived feedstocks into polyhydroxyalkanoates, demonstrating, among others, the conversion of nylon to polyhydroxybutyrate through hydrolysis and microbial conversion. The resulting products are environmentally benign due to their biodegradability and resources are maintained in the material cycle, reducing the production of virgin fossil-based plastics. With regard to a circular plastics economy, it is essential to consider plastic coatings as an additional source of complexity in plastic waste. For this, the novel *Halopseudomonas formosensis* FZJ was isolated from a compost heap due to its ability to metabolize poly(ester-urethane) coatings. The detailed characterization of its metabolic pathways and enzymes provides the scientific basis for future bio-recycling processes of coated plastics and thus increasingly complex materials.

Zusammenfassung

Kunststoffe haben ohne Zweifel unser tägliches Leben revolutioniert und sind in verschiedenen Bereichen wie der Verpackungs-, Gesundheits- und Automobilindustrie unverzichtbar geworden. Die derzeitigen Strategien zur Entsorgung von Kunststoffen sind jedoch nicht in der Lage, die steigende Weltproduktion von über 400 Millionen Tonnen im Jahr 2022 zu bewältigen, was die globale Plastikkrise weiter verschärft. Die Biokatalyse besitzt das große Potenzial, die Nachteile des traditionellen Recyclings zu überwinden, indem sie Enzyme und Mikroorganismen für die Depolymerisierung von Kunststoffen und deren anschließende Umwandlung in höherwertige Produkte einsetzt. Um den Übergang zu einer Kreislaufwirtschaft für Kunststoffe zu erleichtern, besteht das übergeordnete Ziel dieser Arbeit darin, neue biologische Verwertungsmöglichkeiten für Kunststoffabfälle zu entwickeln. Daher wurde das Substratspektrum von *Pseudomonas putida* KT2440 um weit verbreitete Kunststoffhydrolysate erweitert werden, die damit als Ausgangsstoffe für mikrobielles Upcycling zur Verfügung stehen. Umfangreiches Optimieren des Stoffwechsels ermöglichte die Nutzung von Polyamid (PA) -Hydrolysaten und die exakten synthetischen Stoffwechselwege wurden durch RNA-Sequenzierung aufgedeckt. Parallel dazu wurden neue Nylonase-Enzyme entdeckt und charakterisiert, die gegenüber PA und Poly(ester-amiden) aktiv waren. Zusätzlich wurden Stoffwechselwege für Dicarbonsäuren und Diole etabliert, deren Kombination einen leistungsstarken Plattformstamm hervorbrachte, der ein komplexes Polyesterhydrolysat vollständig verstoffwechselte. Darüber hinaus ermöglichte die rationale Expression eines Stoffwechselweges und dessen Aufklärung den Abbau von verzweigten kurzkettigen Dicarbonsäuren, darunter Itaconsäure, wodurch das metabolische Repertoire um weitere Plastikmonomere erweitert wurde.

Um den Lebenszyklus von Plastikabfällen zu schließen, sollten Hydrolysate nicht nur verstoffwechselt, sondern auch wiederverwertet werden. Dies wurde durch die Umwandlung der neu zugänglichen Substrate in Polyhydroxyalkanoate erreicht, wobei unter anderem die Umwandlung von Nylon in Polyhydroxybutyrat durch Hydrolase und mikrobielle Umwandlung demonstriert wurde. Die dabei entstehenden Produkte sind aufgrund ihrer biologischen Abbaubarkeit umweltfreundlich und die Ressourcen bleiben im Wertstoffkreislauf erhalten. Im Hinblick auf eine kreislauforientierte Kunststoffwirtschaft ist es unerlässlich, Kunststoffbeschichtungen als zusätzliche Quelle der Komplexität zu betrachten. Zu diesem Zweck wurde das neue Bakterium *Halopseudomonas formosensis* FZJ aus einem Komposthaufen isoliert, welches in der Lage ist, Poly(ester-urethan)-Beschichtungen zu verstoffwechseln. Die detaillierte Charakterisierung seiner Stoffwechselwege und Enzyme bildet die wissenschaftliche Grundlage für zukünftige Bio-Recyclingprozesse von beschichteten Kunststoffen und damit komplexeren Materialien.

1 Introduction

1.1 From natural polymers to synthetic plastics

Polymers are macromolecules consisting of many repeating subunits and are essential for all life on earth. According to research on the origin of life, the formation of natural polymers such as RNA and proteins was essential for abiogenesis – the emergence of life from non-living matter (Damer and Deamer, 2020). Today, natural polymers are ubiquitous in nature and include DNA, silk, cellulose, and many more. Technological progress of humankind led to the creation of synthetic, human-made polymers designated as plastics. In contrast to the long history of natural polymers, plastics have a comparatively brief timeline but revolutionized human life at all levels over the past decades.

In the early 20th century, the increasing demand for electric cable insulation resulted in shortages of shellac, a natural polymer synthesized by the female lac bug *Kerria lacca*. The extraction of shellac was a labor-intensive process, requiring the manual scraping of tree bark inhabited by lac bugs. Both, the arduous extraction process and the unsaturated demand for shellac required the exploration of new alternatives that could be produced in large quantities. In 1907, Leo Baekeland achieved such a breakthrough by inventing a process in which polycondensation of phenol and formaldehyde resulted in the formation of Bakelite, the world's first synthetic polymer (American Chemical Society National Historic Chemical Landmarks; Thompson et al., 2009). Bakelite became a great commercial success due to its non-conductivity and resistance to heat and thus replaced shellac as insulator. The invention of Bakelite was revolutionary for humanity, as it paved the way for further replacements of natural polymers by plastics, overcoming material shortages, enabling technological advancements, and boosting innovations in many fields of application. During the 1930s, many plastics that are still relevant today were synthesized for the first time (Mueller, 1962). These include polyethylene (PE) (1933) and poly(hexamethylene adipamide) (1935), also known as nylon or polyamide 6.6 (PA6.6). In 1938, polycaprolactam (PA6) was invented to mimic the properties of PA6.6 without infringing the respective patent. Due to the beginning of World War II in 1939, the demand of plastics increased due to their applications in the

military sector. Poly(ethylene terephthalate) (PET), which is probably the most well-known plastic to the general public today, was invented in 1941 and the number of new-to-world plastics further increased over time (British Plastics Federation, 2014; Whinfield and Dickson, 1941).

The term *plastic* originates from the Greek word πλαστικός (plastikos), which can be translated into "having the ability to be shaped and molded". Such plasticity contributes to the success of plastics as it enables processing of raw materials such as extrusion, molding, or compression into various shapes including fibers, foils, bottles and many more. Once the raw materials are hardened, the obtained plastics can be divided into three main groups based on the mechanical-thermal behavior, namely thermoplastics, thermosetting plastics, and elastomers (Massy, 2017) (Figure 1.1-1). Thermoplastics consist of linear or branched polymer chains that are not cross-linked. When heat is applied, thermoplastics such as PA or PET become moldable again, theoretically allowing reversible re-processing as often as desired. A unique characteristic of thermoplastics is their crystallinity, which refers to the degree of structural order of the polymer chains. When cooled or stretched through processes like molding or extrusion, polymer chains undergo partial ordering known as crystallization (Mileva et al., 2018). This ordering and arrangement leads to chain folding into local lamellae, in which polymer chains interact *via* van der Waals forces. Depending on the polymer's molecular structure and the processing conditions, amorphous regions with no structural order can form. However, most thermoplastics, such as PE, PP, or PA, contain crystalline and amorphous regions and thus are designated as semi-crystalline plastics (Figure 1.1-1). Semi-crystalline plastics feature two important transition temperatures namely the melting temperature (T_m) and the glass transition temperature (T_g) that both define critical properties such as heat resistance (Cantor and Watts, 2011). The T_m defines the temperature at which crystalline states melt and transit to viscous, amorphous states. In contrast, at T_g, the glass transition occurs that describes the reversible transition of amorphous regions from brittle into a viscous state. Hence, the amorphous regions become softer and more flexible at temperatures above T_g (Okui, 1990). In semi-crystalline plastics such as PET, T_m (260 °C) is always higher than T_g (67-81 °C) resulting in its excellent mechanical properties at high temperatures (Thomsen et al., 2022).

A) Classification of plastics

| Thermoplastics | | | Thermosetting plastics | Elastomers |
| crystalline | semi-crystalline | amorphous | tightly cross-linked | loosely cross-linked |
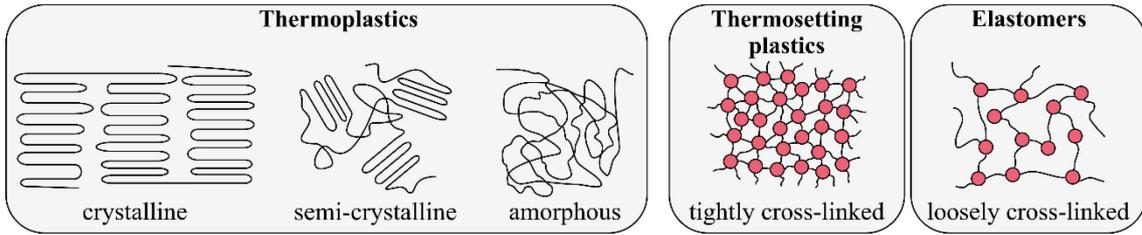
B) Selected structures of thermoplastics

polyolefins   **polyesters**

Polypropylene   Polyethylene   Poly(ethylene terephthalate)
(PP)   (PE)   (PET)

polyamides

Poly(hexamethylene adipamide)   Polycaprolactam
(PA6.6)   (PA6)

polyurethanes*   **poly(ester-urethanes)***
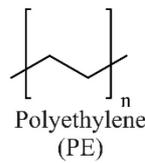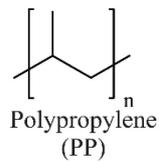
Polyurethane   Poly(ester-urethane)
(PU)   (PEU)
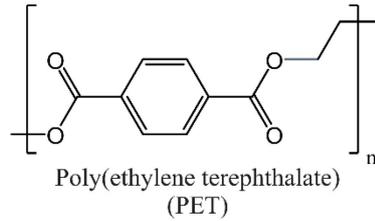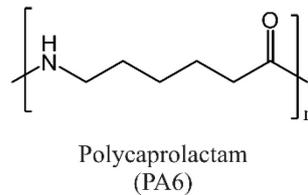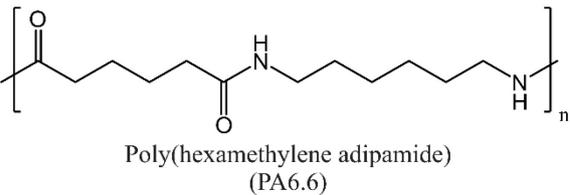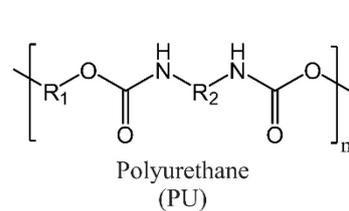
R_1 = Rest of diol R_1 = Rest of diol
R_2 = Rest of diisocyanate R_2 = Rest of diisocyanate
                                R_3 = Rest of dicarboxylate

Figure 1.1-1. Classification and molecular structures of plastics. (A) Classification of plastics with regard to their thermo-mechanical behavior. Thermoplastics can be divided into crystalline, semi-crystalline, and amorphous plastics. Thermosetting plastics and elastomers are tightly and loosely cross-linked *via* covalent bonds (red circles), respectively. **(B)** Chemical structures of thermoplastics categorized by their functional groups. Based on the degree of cross-linking and/or the type of monomers, polyurethanes and poly(ester-urethanes) can be thermoplastics, thermosetting plastics, or elastomers (*).

In contrast to thermoplastics, thermosetting plastics and elastomers cannot crystallize due to their cross-linked polymer chains. Moreover, they feature a different thermo-mechanical behavior depending on the degree of cross-linking. Contrary to the reversible moldability of

3

thermoplastics, thermosetting plastics, including polyurethanes or epoxy resins, remain solid but undergo decomposition when heat is applied. This characteristic is based on the network of tightly cross-linked polymer chains resulting in increased temperature resistance and mechanical strength compared to thermoplastics (Alauddin et al., 1995). Hence, thermosetting plastics are often used in the automotive or aerospace sector where high temperatures and forces are present. Conversely, elastomers are loosely cross-linked allowing sliding of the polymer chains. Thus, when exposed to heat or pressure, elastomers can temporarily change their shape but quickly return to their original form after the release of such factors (Zhai et al., 2022). Due to these characteristics, elastomers, such as natural or synthetic rubber, find extensive application in tire manufacturing. This utilization often involves a process known as vulcanization in which polymer chains are cross-linked *via* sulfur-bridges leading to greatly increased mechanical properties such as rigidity and durability (Akiba and Hashim, 1997) (Figure 1.1-1).

Depending on many parameters such as molecular structure and composition, plastics can feature a diverse range of advantageous properties, including durability, lightweight nature, non-conductivity, and inexpensive production, all of which paved the way for their current supremacy in human life. The majority of produced plastics are thermoplastic that are used in the packaging industry (44.8 %), followed by the building and construction sector (18.8 %), and other applications (13.2 %) including the textile industry (Geyer et al., 2017). Within the textile industry, PA are widely used due to their strength and durability. Moreover, fishing gear such as fishing nets consist of PA (Textile Exchange, 2022).

In addition to the core polymer, coatings are an important component of the final plastic product. Coatings are thin layers of polymers that are applied to material surfaces to enhance their appearance or physical properties. Utilized across various sectors such as fishery, automotive, aerospace and medical, coatings find applications in a broad spectrum of industries. Many coatings consist of poly(ester-urethane)s (PEUs), recognized for their exceptional mechanical attributes, including high strength, fatigue resistance, and resilience to abrasion (Hojabri et al., 2012; Quienne et al., 2020; Ye et al., 2020). Consequently, PEUs are used in a variety of coating applications, enhancing the longevity of materials and improving their resistance to chemical and biological factors. Depending on their chemical

composition, coatings can even be employed to tune the biodegradability of a material (Kim et al., 2023). However, it is important to note that coatings simultaneously add complexity to a material by increasing the variety of polymers it contains, and consequently, the number of molecular building blocks. Hence, coatings display a burden for traditional end-of-life solutions as described in chapter 1.3.

1.2 The global plastic crisis

Today, a life without plastics is inconceivable, given their extensive usage across a wide range of industries. The demand of plastics is steadily increasing every year and resulted in a new all-time high for global plastic production, which reached 400.3 million metric tons (Mt) in 2022 (PlasticsEurope, 2023). The immense quantity of durable and persistent plastics, coupled with insufficient disposal management, resulted in their spread and accumulation in all types of ecosystems. Today, plastics are so ubiquitous in nature, that they have been proposed as a geological indicator of the Anthropocene era, highlighting the plastic crisis we face today (Zalasiewicz et al., 2016).

About 60 % of all plastic ever produced, totaling approximately 4900 Mt, are accumulating in landfills or in the environment (Geyer et al., 2017). Plastics can have several direct impacts on terrestrial ecosystems such as habitat degradation, leaching of toxic compounds, or entanglement of wildlife (Hurley et al., 2020). Once plastics are released in terrestrial environments, they often spread into further ecosystems. In 2016, about 19-23 Mt of plastics entered aquatic ecosystems from land and this amount is predicted to surge to 90 Mt by 2030, following current trajectories (Borrelle et al., 2020). Natural transport of plastics caused by ocean currents, wind, or atmospheric transport resulted in the pollution of areas with no evident human activity such as the Arctic or deep seafloors (Bergmann et al., 2022). Moreover, plastics enter oceanic gyres leading to the formation of huge contaminated areas. The largest oceanic accumulation of plastics is the Great Pacific garbage patch that is predicted to contain 79 thousand tons of plastics within a floating area of 1.6 million km^2 (Lebreton et al., 2018). Additionally, the widespread use of plastics in local marine environments results in further pollution of aquatic ecosystems. Especially abandoned, lost,

or discarded fishing gear (ALDFG) gained increased attention over the past years. This is because ALDFG cause several environmental threats and damages such as ghost fishing, release of microplastics and toxins, dispersal of invasive alien species, and habitat degradation (Angiolillo and Fortibuoni, 2020; Barnes, 2002; Gilman et al., 2021). In addition to terrestrial and aquatic ecosystems, plastics are also present in the atmosphere in form of micro- and nanoplastics especially in proximity to industrial and urban locations (Allen et al., 2021; Chen et al., 2020). Moreover, their low density facilitates long-range and even global transport by atmospheric winds, which can rain down as so-called plastic rain (Brahney et al., 2020).

The uncontrolled release of plastics into the environment goes hand in hand with the release of microplastics, which are particles with a size of 1-5,000 μm. Microplastics are formed upon deterioration and fragmentation of larger plastics during usage, such as wear particles from tires or textiles, or after disposal (Hale et al., 2020). Despite or precisely because of their small particle size, microplastics pose a threat to all levels of ecosystems. This include release of toxic compounds, ingestion and harm of diverse organisms, and accumulation in the food chain that ironically could also affect human health (Hale et al., 2020; Nelms et al., 2019). Microplastics can even fragment into smaller particles called nanoplastics (<1 μm particles) (Hartmann et al., 2019; Lambert and Wagner, 2016; Van Cauwenberghe and Janssen, 2014). It was estimated that this fragmentation could generate more than 10^{14} times greater numbers of nanoparticles greatly facilitating their spread in terrestrial, aquatic, and atmospheric ecosystems with yet unknown consequences (Besseling et al., 2019; Hale et al., 2020; Van Cauwenberghe and Janssen, 2014).

Overall, the pollution of the entire globe with (micro-/nano-) plastics underlines humanity's inability to manage the overwhelming and increasing amounts of plastic waste. Plastic pollution is most evident in developing countries, where waste collection and recycling systems are often inefficient or non-existent. Nevertheless, humanity faces a global problem as natural transport of plastics occurs through ecosystems. Simultaneously, plastic waste is actively exported by developed to developing countries, creating a psychological distance from plastic pollution (Barnes, 2019). To solve the plastic crisis, we need global solutions as well as efficient and sustainable end-of-life strategies.

1.3 Conventional end-of-life solutions for plastic waste

The increasing environmental pollution by plastics is a threat to all life on earth. In order to tackle this hazard, adequate end-of-life strategies for post-consumer plastic waste need to be implemented. Today, current end-of-life solutions for plastic waste can be divided into three main categories, namely landfilling, incineration, and recycling (Geyer et al., 2017) (Figure 1.3-1). Landfilling is seen as the least environmentally preferred option, as valuable resources remain unused and fail to reenter the material cycle, while mismanagement simultaneously contributes to environmental pollution (Kosior and Mitchell, 2020). Incineration also results in the loss of valuable resources, but it can at least be used for energy recovery. However, incineration of plastics waste releases greenhouse gases and carries the risk to emit hazardous compounds into the atmosphere, which facilitates the climate change (Wu et al., 2021a). Both end-of-life solutions are part of a linear plastic economy, in which virgin plastics are produced from fossil resources and disposed without material recovery after their usage. In 2020, 35 % of post-consumer plastics waste was recycled in the EU, while 42 % underwent energy recovery *via* incineration, and 23 % were disposed in landfills (PlasticsEurope, 2022). Overall, the recycling rates in the EU have more than doubled from 2006 to 2020. In contrast to this, only 16 % of plastic waste is collected for recycling worldwide, while 25 % is incinerated and 59 % is disposed in (unmanaged) landfills (Hundertmark et al., 2018). For some plastics, such as PA, recycling rates are below 5 %, highlighting the long road ahead for establishing a fully circular plastic economy (Textile Exchange, 2022).

In contrast to linear end-of-life strategies, recycling aims to conserve resources by keeping them in the material cycle, thereby reducing the need for the production of virgin materials (Figure 1.3-1). Due to the versatility of plastics waste, several recycling methods have been established including mechanical and chemical recycling. Mechanical recycling is widely used for thermoplastics due to their ability to be repeatedly melted and formed into new products by extrusion. Prior to its reprocessing, various steps including sorting, grinding, washing, and drying of post-consumer plastics waste are required (Schyns and Shaver, 2021). Ideally, plastics waste can be endlessly recycled back in a closed-loop without

reducing the quality of the recycled plastic, which is called primary recycling (Figure 1.3-1). In contrast to the linear plastics economy, primary recycling contributes to a circular economy for plastics avoiding the production of virgin materials. Today, primary recycling of PET bottles, designated as bottle-to-bottle recycling, is the only industrial relevant large-scale process of primary recycling (Benyathiar et al., 2022). This is due to so-called super-clean recycling technologies that were developed for PET, decontaminating post-consumer PET to the purity of virgin PET (Welle, 2011). However, in the absence of such super-clean technologies, mechanical recycling typically yields reduced-quality products caused by impurities such as plasticizers or the material's heterogeneity (Pietroluongo et al., 2020). As a result, the materials are downcycled, which culminates in their disposal after several cycles of downcycling as shown for PP or PE (Eriksen et al., 2019). Downcycling can be explained by the immiscibility of certain polymers with each other when melted, resulting in phase separation that hinders further reprocessing (Schyns and Shaver, 2021). Moreover, tiny amounts of poly(vinyl chloride) (PVC) (>100 ppm) can already induce degradation of polyesters, such as PET, during processing, preventing its mechanical recycling (Paci and La Mantia, 1999). A prominent example of downcycling, also designated as secondary recycling, is the conversion of waste tires into crumb rubber, which can be used for the production of rubberized asphalt (Thiounn and Smith, 2020). Depending on the material, secondary recycling may eventually lead to the production of non-recyclable materials. Overall, mechanical recycling is a sensitive recycling strategy and thus highlights the importance of plastic sorting but also of product design to facilitate primary recycling.
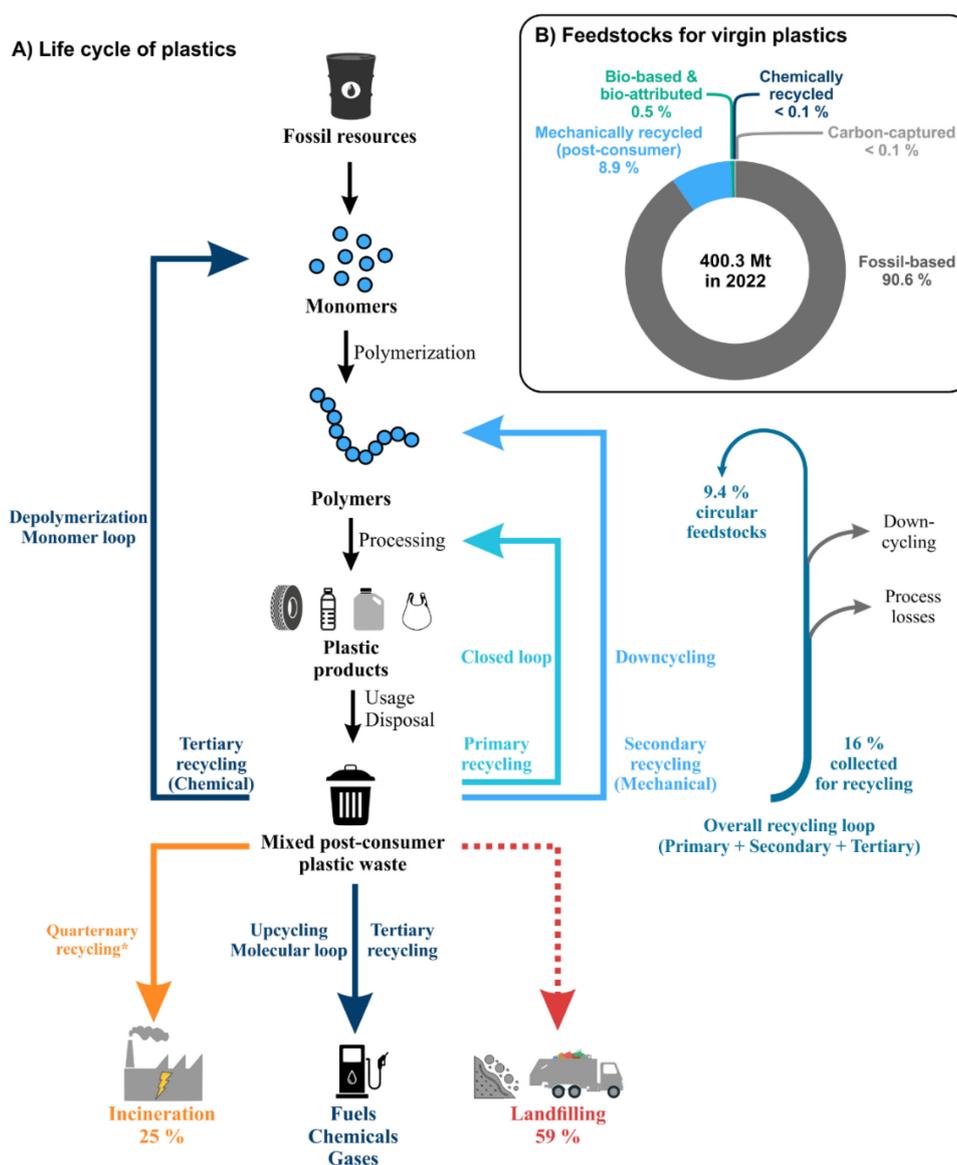
Figure 1.3-1. Life cycle of plastics and traditional end-of-life solutions. (A) Mixed post-consumer plastic waste can be treated by landfilling, incineration, or recycling. Worldwide, 59 % of post-consumer plastic waste is landfilled, 25 % is incinerated for energy recovery and 16 % are collected for recycling. Recycling can be divided into primary, secondary, tertiary, and quaternary technologies. Primary recycling results in a closed-loop for materials. Secondary recycling maintains polymer chains, but products typically show reduced quality (downcycling). In contrast, tertiary recycling depolymerizes plastics and building blocks can be either re-polymerized (monomer loop) or upcycled (molecular loop) to value-added compounds. Quaternary recycling for energy recovery is not classified as 'recycling' by the EU (*). Due to process losses and downcycling, only 9.4 % of plastics are within a circular economy. **(B)** Consequently, 90.6 % of virgin plastics are produced from fossil-based resources. Modified from Tournier et al. (2023) and PlasticsEurope (2023).

An alternative to primary and secondary recycling is tertiary recycling, also known as feedstock or chemical recycling. In contrast to these two recycling strategies, tertiary recycling depolymerizes plastics into their monomers, which can either be purified for re-polymerization (monomer loop) or used as feedstock for the production of various compounds such as fuels (molecular loop) (Figure 1.3-1) (Achilias et al., 2007; Ellis et al., 2021). Among tertiary recycling technologies, pyrolysis, that is the thermal depolymerization of plastics in inert atmospheres, is the most powerful strategy as it can deconstruct a broad range of mixed plastics (Yadav et al., 2023). This includes the polymer backbones of PE, PP, PET, PVC, or polystyrene (PS) (Li et al., 2022). In addition to pyrolysis, chemical depolymerization can also be utilized for the deconstruction of plastics. For this, homogenous or heterogeneous catalysts are used in the presence of oxygen, high pressures and at elevated temperatures, to depolymerize a variety of plastics (Hackler et al., 2022; Kolganov et al., 2023). Moreover, several other chemical processes such as solvolysis and hydrogenolysis can be applied to chemically depolymerize plastics (Beghetto et al., 2021). However, tertiary recycling typically requires a high energy input, non-recyclable catalysts, and hazardous chemicals, while being sensitive to feedstock contaminations (Ellis et al., 2021).

In contrast to the described recycling technologies, quaternary recycling, also known as energy recycling, is often considered a recycling method of last resort. That is because plastics waste is burned to recover energy from the process that goes along with the loss of valuable resources (Lee et al., 2017). Moreover, this waste to energy process results in the release of greenhouse gases and toxic compounds (Wu et al., 2021a) and is not classified as 'recycling' by the EU:

> *" 'recycling' means any recovery operation by which waste materials are reprocessed into products, materials or substances whether for the original or other purposes. It includes the reprocessing of organic material but does not include energy recovery and the reprocessing into materials that are to be used as fuels or for backfilling operations"*

> Directive 2008/98/EC of the European Parliament and of the Council of 19 November 2008 on waste and repealing certain directives – Chapter 1, Article 3, Definition 17.

Nevertheless, energy recycling is still preferable to landfilling as it reduces the environmental plastic pollution and can be used to substitute fossil energy sources such as coal.

In 2022, the majority of plastics was part of a linear economy as 90.6 % of virgin plastics were produced from fossil resources, while 9.4 % originated from circular feedstocks such as mechanical (8.9 %) or chemical (<0.1 %) recycling (Figure 1.3-1). Moreover, landfilling and incineration displayed the dominant end-of-life solutions, while 16 % of plastics waste was collected for recycling at the end of the product's lifetime. Process losses and downcycling further reduced the quantity of resources that maintain inside a circular plastics economy (Hundertmark et al., 2018; PlasticsEurope, 2023). Consequently, recycling rates are low, which can be explained by the inefficiency of mechanical and chemical recycling strategies that cannot compete with virgin production from fossil resources. Sustainable and efficient end-of-life solutions must be established to overcome the drawbacks of conventional recycling, thereby increasing the circularity of the plastics economy.

1.4 Towards a sustainable plastics economy

*Parts of this section, in modified form, were previously published in Tiso, T., Winter, B., Wei, R., Hee, J., **de Witt, J.,** Wierckx, N., Quicker, P., Bornscheuer, U., Bardow, A., Nogales, J., Blank, LM., (2022). The metabolic potential of plastics as biotechnological carbon sources – Review and targets for the future. Metabolic Engineering, 71, 77-98. doi:10.1016/j.ymben.2021.12.006*

Today, the plastics economy is predominantly linear following the credo Take-Make-Use-Dispose. This is caused by the inability of current recycling approaches to enable a fully circular plastics economy due to limiting recycling technologies or insufficient economic incentives (Ellis et al., 2021). On the other hand, plastics are predominantly carbon and could be provided as valuable substrate for biotechnological processes (Wierckx et al., 2015). Biological end-of-life solutions for plastics are an emerging and promising strategy to overcome the bottlenecks of mechanical and chemical recycling thereby potentially increasing recycling rates in the future (Figure 1.4-1). Typically, biocatalysts, namely

enzymes and microorganisms, operate at moderate conditions compared to chemical processes, catalyze selective reactions and do not depend on toxic chemicals (Tiso et al., 2021b; Wei et al., 2020). For PET, techno-economic analyses predicted that enzymatic recycling could become cost-competitive with virgin PET production once major cost drivers such as mechanical pre-treatment or enzymatic efficiency are addressed (Singh et al., 2021). Moreover, suitable biocatalysts have the potential to depolymerize and upcycle plastics in an energy-efficient manner providing sustainable end-of-life solutions.

For this, enzymatic depolymerization of plastics is required, which results in the formation of mixed plastic hydrolysates, consisting of various monomers and oligomers. Subsequent microbial funneling of the obtained hydrolysates into the central metabolism of powerful microbial platform strains can be used to avoid the costly and laborious separation of individual building blocks for re-polymerization. Instead, microbial upcycling can be used to produce value-added compounds from plastic-derived hydrolysates (Wierckx et al., 2015). The microbial production of biodegradable plastics is seen as a prime solution with regard to a circular plastics economy (Blank et al., 2020). The following chapters will highlight how enzymatic depolymerization of plastics and their microbial upcycling into value-added products can provide sustainable end-of-life solutions, thereby facilitating the shift to a fully circular plastic economy.

Figure 1.4-1. Biological and circular solutions for plastics. Enzymatic depolymerization can be used as sustainable alternative to chemical depolymerization yielding mixed hydrolysates consisting of monomers and oligomers. The identification and engineering of enzymes is essential to enable efficient depolymerization. Depending on the depolymerized plastics, different mixed hydrolysates are obtained. To avoid costly purification of individual building blocks, biological funneling can be used to channelize the hydrolysate into the central metabolism of suitable microbial hosts. Metabolic engineering is a powerful tool to enable or boost the ability to metabolize plastic hydrolysate by modifying the host's native metabolism. Depending on the microbial host and metabolic engineering, several value-added products can be produced by microbial upcycling. Such can include platform or specialty chemicals, as well as biodegradable materials that can either be reprocessed into virgin plastics or used for other applications, ultimately resulting in mixed hydrolysates at the end of their life.

1.4.1   Enzymatic depolymerization of plastics and coatings

Plastics are relatively new-to-nature, with less than 100 years of history in the environment. However, the natural evolution of novel enzymatic degradation mechanisms usually happens over much longer timescales (Buller et al., 2023). Thus, most enzymes showing depolymerization activities towards plastics are likely still the result of moonlighting activities mainly towards polyesters (Tiso et al., 2021b; Wei and Zimmermann, 2017). Furthermore, physical and chemical properties of plastics, such as high crystallinities, make them more resistant towards enzymatic depolymerization (Chow et al., 2023). Enzyme engineering is a powerful tool to overcome such bottlenecks and to boost the moonlighting activities of wild type enzymes, thereby generating tailored and efficient biocatalysts for plastics depolymerization (Zhu et al., 2022a). In general, two strategies can be applied, namely directed evolution and rational design (Cobb et al., 2013; Lutz, 2010). Directed evolution consists of iterative cycles of mutant library construction using random mutagenesis techniques such as DNA shuffling or error-prone PCR, followed by high-throughput screenings for beneficial variants. Although directed evolution is a more comprehensive strategy of enzyme engineering, it remains under-explored probably due to the lack of suitable high-throughput screenings able to quantify the depolymerization of insoluble plastics (Zhu et al., 2022a). In contrast, rational design relies on understanding the structure-function relationships of enzymes, thereby predicting potential beneficial mutations. Recent advances in precise *in silico* structure predictions by AlphaFold (Jumper et al., 2021) are a promising boost for rational design strategies, but are limited by the understanding of catalytic mechanisms.

In the past years, several hydrolases were discovered that were able to depolymerize PET and thus were designated as PETases. These include, among others, a cutinase from *Thermobifida fusca* (TfH) (Müller et al., 2005), the leaf-branch compost cutinase (LCC) isolated from leaf-branch compost metagenomes (Sulaiman et al., 2012), the *Is*PETase of *Ideonella sakaiensis* (Yoshida et al., 2016), as well as the polyester hydrolase of *Halopseudomonas aestusnigri* (*Haes*_PE-H) (Bollinger et al., 2020b). The exploration of metagenomes greatly increased the number of potential PETase candidates, as this approach provides access to sequences of the vast amount of uncultivable organisms (Danso et al., 2018). A key determinant of the plastic-depolymerizing activities of most wild type enzymes

is their low thermostability. Due to increased thermostabilities, reaction temperatures close to or above the T_g (60-70 °C for PET) can be achieved that facilitate the mobility and flexibility of polymer chains and consequently their accessibility resulting in improved depolymerization efficiency (Wei and Zimmermann, 2017). Enzyme engineering of individual PETases significantly increased their thermostabilities and thus their activities towards PET. For example, semi-rational engineering of LCC resulted in the powerful variant ICCG that featured a T_m of 94.5 °C and a depolymerization rate of approximately 120 mg$_{PET}$ h^{-1} mg$_{enzyme}$$^{-1}$ that was over 2800-fold higher compared to thermostable TfH (Müller et al., 2005; Tournier et al., 2020). In contrast to cutinases such as LCC and its variants, *Is*PETase harbors a flexible Trp185 residues that was revealed to aid polymer binding making it a promising biocatalyst for engineering (Han et al., 2017; Joo et al., 2018). Indeed, several thermostable variants with improved activities towards PET were constructed using rational engineering (Austin et al., 2018; Cui et al., 2021; Ma et al., 2018; Son et al., 2019). Recently, an automated directed evolution platform enabled the construction of the HotPETase variant (T_m=82.5 °C) that depolymerized semi-crystalline PET faster than any other previously reported PETase due to the introduction of an additional disulfide bond (Bell et al., 2022). In addition to increasing the enzyme's thermostability, enzyme engineering can also enhance the interaction between the substrate and the active site. Such strategy was performed for *Haes*-PE-H that resulted in increased activity of the Y250S variant towards not only PET but also Impranil DLN-SD (Bollinger et al., 2020b; Molitor et al., 2020).

Impranil DLN-SD is an anionic aliphatic PEU widely used as coating material within the textile industry to improve and fine-tune the fiber's properties. In addition to PE-H, urethanases are required to fully depolymerize coating materials such as Impranil DLN-SD. In the absence of hydrolyzing the PU regions, exclusively degrading the polyester regions would result in the formation of PU micro- or nanoplastics. However, no enzymes able to degrade polymeric PU substrates are reported in literature except for oxidative enzymes, such as laccases, which depolymerize PU *via* an unspecific oxidation of the polymer backbone (Liu et al., 2021a; Magnin et al., 2021; Wei et al., 2020). Instead, some cutinases and urethanases were revealed to cleave PU oligomers (Akutsu-Shigeno et al., 2006; Branson et al., 2023). Enzyme engineering of such promising candidates and increasing

efforts in library screenings are powerful strategies to enable future depolymerization of high-molecular-weight PU.

Similar to PU, enzymatic depolymerization of synthetic PA, often referred to as nylons, is barely reported in literature (Buchholz et al., 2022; Negoro, 2000). The lack of synthetic PA-depolymerizing enzymes is quite surprising giving the high abundance of natural PA, such as proteins or silk, and their corresponding amidases in nature. This contradiction can be explained by the challenging hydrolysis of amide bonds in synthetic PA, which have limited accessibility due to strong intermolecular hydrogen-bonding networks (Puiggalí, 2021). A manganese peroxidase from a white rot fungus was reported to degrade PA6.6 films but no sequence information was linked to this activity (Deguchi et al., 1998). In contrast, three types of PA6-oligomer hydrolases, designates as nylonases, are biochemically characterized in literature and were identified in *Paenarthrobacter ureafaciens* that was isolated from wastewater of a PA6-manufacturing plant (Kinoshita et al., 1975) (Figure 1.4-2). NylA is a 6-aminohexanoate- (Ahx) cyclic dimer hydrolase that specifically cleaves the cyclic Ahx dimer (Ahx$_2$) into the linear Ahx$_2$ (EC 3.5.2.12) (Kinoshita et al., 1975). The Ahx-oligomer exohydrolase NylB degrades linear Ahx-oligomers via an exo-type cleavage showing decreasing activities towards increasing chain lengths (EC 3.5.1.46) (Kinoshita et al., 1981). In contrast, NylC is an Ahx-oligomer endohydrolase and degrades cyclic as well as linear Ahx-oligomers with a degree of oligomerization greater than three *via* an endo-type cleavage (3.5.1.117) (Negoro et al., 1992). Although, or probably because, nylonases are the only group of enzymes showing activities towards synthetic amides, no activities towards over 70 natural amides was detected (Kinoshita et al., 1977; Kinoshita et al., 1981). Due to the endo-type cleave, NylC, an N-terminal nucleophile (Ntn) hydrolase, is the most promising nylonase for PA depolymerization (Figure 1.4-2). Directed evolution resulted in a thermostable NylC variant (NylC$_{TS}$, T_m=88 °C) that was able to depolymerize PA6 (Negoro et al., 2012). Although further engineering resulted in a variant with 1.9-fold improved turnover frequency (NylC$_{TS}$$^{P27Q/F301L}$) (Puetz et al., 2023), even the best-performing nylonase only hydrolyzed small fractions of PA highlighting the need for future improvements. Moreover, it is essential to increase the diversity of nylonases, thereby identifying the most promising candidates for enzyme engineering. Currently, however, the number of

characterized nylonases is limited to a small set of enzymes with poor activities towards polymeric substrates (Negoro et al., 2021) (Figure 1.4-2).

A) Characterized nylonases

Nylonase	Origin	Substrate	T_m (°C)	Reference
$NylA_{p2}$	*P. ureafaciens*	cyclic Ahx$_2$	n.d.	Kinoshita *et al.*, 1975
$NylB_{p2}$	*P. ureafaciens*	linear Ahx (n = 2-20)	n.d.	Kinoshita *et al.*, 1981
wild-type NylCs				
$NylC_{p2}$	*P. ureafaciens*	linear and cyclic Ahx (n > 3)	52	Negoro *et al.*, 1992
$NylC_A$	*Agromyces* sp. KY5R	linear and cyclic Ahx (n > 3)	60	Yasuhira *et al.*, 2007
$NylC_K$	*Kocuria* sp.	linear and cyclic Ahx (n > 3)	67	Yasuhira *et al.*, 2007
engineered NylC$_{p2}$				
$NylC_{TS}$	*P. ureafaciens*	linear and cyclic Ahx (n > 3), PA6, PA6.6	88	Negoro *et al.*, 2012
$NylC_{TS}^{P27Q/F301L}$	*P. ureafaciens*	linear and cyclic Ahx (n > 3), PA6, PA6.6	85	Puetz *et al.*, 2023

B) Degradation of PA6-oligomers
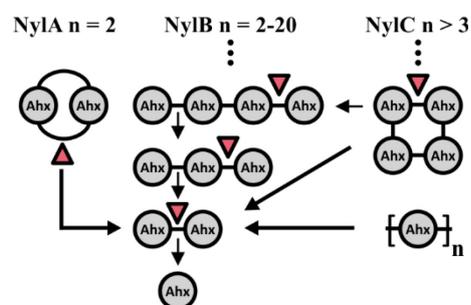
C) Structure of NylC$_{p2}$
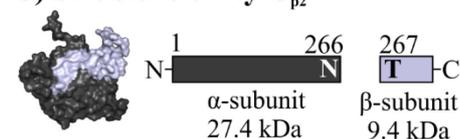
Figure 1.4-2. Characterized nylonases in literature. (A) Three types of nylonases (NylA, NylB, and NylC) are described in literature that display specific activities towards oligomers of PA6. In addition to NylC$_{p2}$, three highly similar NylCs only differing in 5 and 15 amino acids compared to NylC$_{p2}$ are known. Enzyme engineering of NylC$_{p2}$ resulted in two variants with improved thermostabilities that enabled depolymerization of polymeric substrates, albeit with low activities. **(B)** NylA specifically hydrolyzes cyclic Ahx$_2$. NylB performs an exo-cleavage and degrades linear oligomers (n = 2-20), whereas NylC degrades linear and cyclic oligomers (n>3) *via* an endo-cleavage. **(C)** NylCs are members of the Ntn-hydrolase superfamily that perform a posttranslational autocleavage at N266/T267 yielding and α- and β-subunit that form an active NylC after structural re-arrangement. Modified from Negoro (2000) and Negoro et al. (2023).

In contrast to previously described plastics, polyolefins, such as PE and PP, solely consist of C-C bonds preventing specific hydrolysis of any functional groups. Instead, enzymatic depolymerization of polyolefins would require the oxidation of the polymer backbone. Recently, hexamerins belonging to the hemocyanin/phenol oxidase family were discovered in the saliva of *Galleria mellonella* (wax worm) larvae, which were able to oxidize PE backbones (Sanluis-Verdes et al., 2022; Spínola-Amilibia et al., 2023). Moreover, two laccase-like multicopper oxidases were identified in *Rhodococcus opacus* R7 that oxidized untreated PE, as evidenced by the detection of oxidation products (Zampolli et al., 2023). Although the described enzymes showed low activities and act in a random manner, they are promising candidates to lead the way towards enzymatic recycling of polyolefins.

Overall, enzymatic depolymerization of plastics and their coatings is still in its infancy and depolymerization efficiencies greatly depend on the target polymer. For PET, enzymatic recycling is advancing towards commercial implementation, whereas depolymerization of hard-to-access polymers requires intense screenings for promising enzyme candidates that can be optimized by enzyme engineering. The exploitation of metagenomes is a promising strategy to identify potential enzyme candidates of uncultivable organisms (Streit and Schmitz, 2004). Based on recent breakthroughs in artificial intelligence and machine learning, artificial protein design might revolutionize the discoveries of tailored or even entirely artificial enzymes for plastics deconstruction (Ferruz et al., 2022).

1.4.2 Microbial metabolism of plastic monomers and oligomers

The strategies for enzymatic plastics depolymerization described above could become a sustainable method for turning plastic in an accessible feedstock for biotechnology as their size prevents a direct import into microorganisms. Moreover, to establish biological end-of-life solutions for plastics, it is essential to funnel plastic monomers and oligomers into the central metabolism of suitable microbial hosts providing them as substrate for subsequent microbial upcycling. The discovery of plastic-degrading enzymes also resulted in the identification of microorganisms that additionally harbor metabolic routes for the utilization of degradation products such as *I. sakaiensis* (Yoshida et al., 2016). However, the presence of plastic-degrading enzymes, especially those with moonlighting activities, does not consequently imply the ability to metabolize the corresponding monomers and oligomers. While some monomers and oligomers are metabolized *via* native pathways encoding the metabolism of similar substrates, other building blocks require specific routes that are not available ubiquitously. Moreover, specialized metabolic routes are often present in niche-adapted species, which are not suitable for microbial upcycling due to lacking genetic tractability or complex culture conditions. Metabolic engineering is a powerful strategy to overcome the bottlenecks and limitations of native pathways, resulting in the utilization of otherwise inaccessible substrates. In addition, synthetic pathways containing heterologous steps can be designed and transferred into well-established microbial platform strains, providing plastic monomers and oligomers as substrates for microbial upcycling.

In the past decades, several microorganisms have been characterized that metabolized synthetic plastic monomers and oligomers *via* their native metabolic routes. Due to the discovery of *Is*PETase and the ability to metabolize the PET monomers ethylene glycol (EG), terephthalic acid (TA), as well as the PET oligomers mono(2-hydroxylethyl) TA (MHET) and bis(2-hydroxylethyl) TA (BHET), *I. sakaiensis* gained much attention (Yoshida et al., 2016). In addition to PET, *Is*PETase also degraded BHET, whereas MHET was only hydrolyzed by a specific MHETase into EG and TA. In contrast to *I. sakaiensis*, several other microorganisms have been described, which utilized EG and TA as sole carbon source (Fincher and Payne, 1962; Narancic et al., 2021; Trifunović et al., 2016; Wang et al., 1995). EG is metabolized by the sequential oxidation to glyoxylate *via* the intermediates glycolaldehyde and glycolate (Mückschel et al., 2012). Metabolic engineering enabled metabolism of EG in well-established microbial hosts including *Escherichia coli* (Pandit et al., 2021) and *Pseudomonas putida* (Franden et al., 2018a; Li et al., 2019). Microbial degradation of TA occurs *via* ring activation to protocatechuate followed by ring-opening and subsequent degradation to β-ketoadipate (Salvador et al., 2019). The metabolic pathways for TA from *Pseudomonas umsongensis* GO16 were successfully transferred to *P. putida* enabling utilization of TA as sole carbon source (Narancic et al., 2021). Like TA, adipic acid (AA) is another important dicarboxylic acid mainly used for the production of PA and polyesters. Metabolism of AA was discovered in *Acinetobacter baylyi* that occurs *via* β-oxidation. First, AA is imported into the cell (DcaKP), followed by CoA-activation (DcaIJ) and subsequent β-oxidation yielding 3-oxoadipyl-CoA (DcaA, DcaE, DcaH). Lastly, the thiolase DcaF catalyzes the formation of succinyl-CoA and acetyl-CoA that are funneled into the TCA cycle (Parke et al., 2001). Heterologous expression of *dca* genes in *P. putida* coupled with adaptive laboratory evolution (ALE), resulted in a strain able to metabolize AA as sole carbon source (Ackermann et al., 2021).

Like AA, 1,6-hexamethylenediamine (HMDA) is a monomer of PA6.6. Although the biogenic C_4- and C_5-diamines putrescine and cadaverine are metabolized by a variety of microorganisms (Kurihara et al., 2005; Luengo and Olivera, 2020), catabolism of the C_6-diamine HMDA is not reported in literature. Instead, HMDA can be used as nitrogen source as reported for *Taonella mepensis* WT-6 but is not utilized as sole carbon source (Zhou et al., 2021). Since putrescine and cadaverine were revealed to be transaminated, either *via*

direct transamination or *via* γ-glutamylation to their corresponding dicarboxylate, metabolism of HMDA might be possible *via* transamination to AA followed by subsequent β-oxidation (Luengo and Olivera, 2020). In contrast to HMDA, native metabolism of other PA monomers such as Ahx and its lactam, namely ε-caprolactam, is described in literature. In *Pseudomonas jessenii*, metabolism of ε-caprolactam was revealed to occur *via* ring opening to Ahx, catalyzed by a caprolactamase, and subsequent transamination to AA and ultimately degraded *via* β-oxidation (Otzen et al., 2018). In addition to Ahx and ε-caprolactam, *P. ureafaciens* also metabolized oligomers of PA6 due to the activity of previously described nylonases (NylA, NylB, and NylC) that in combination hydrolyze cyclic and linear oligomers of PA6 into Ahx (Negoro, 2000). The discovery of transaminases (NylD) and oxidoreductases (NylE) in *P. ureafaciens* revealed the same metabolic route as described in *P. jessenii* (Takehara et al., 2018).

Overall, native metabolic routes for plastic monomers and oligomers are present in nature but often limited to non-platform strains while also harboring substantial bottlenecks. Using metabolic engineering, native metabolic routes can be leveraged and extended towards a variety of synthetic substrates providing them as feedstock for microbial upcycling.

1.4.3   Microbial upcycling of plastics

Conventional recycling strategies display several disadvantages, such as the need for pure feedstocks and the fact that they result in downcycling of the material. For establishing end-of-life solutions that are both circular and efficient, the product's value needs to be maintained or even increased during recycling. Microbial upcycling is a promising strategy to overcome the bottlenecks of traditional recycling by funneling mixed plastic hydrolysates into the central metabolism of microbial platform strains that are able to produce value-added compounds. This avoids the need for costly separation and purification of individual building blocks and prevents downcycling, thereby facilitating a circular economy for plastics. Depending on the microbial host, several value-added compounds can be considered as products including building blocks for plastics, biosurfactants, or biodegradable polymers (Tiso et al., 2021b; Wierckx et al., 2015).

Due to their versatility, aromatic compounds are essential in modern life and comprise both bulk and specialty chemicals. Since the majority of aromatic compounds is currently produced from fossil resources, microbial upcycling towards this group of chemicals is of increasing interest (Schwanemann et al., 2020). The aromatic nature of TA makes it a suitable substrate for the microbial upcycling towards aromatics without funneling the substrate down to the TCA cycle. Using engineered *E. coli*, microbial upcycling of TA to various aromatics or derived chemicals such as vanillic acid, muconic acid, or gallic acid was achieved (Kim et al., 2019). Sadler and Wallace (2021) combined enzymatic PET depolymerization by LCC with microbial upcycling utilizing engineered *E. coli* and achieved 79 % conversion of TA into vanillic acid.

Besides aromatics, fatty acids and lipids are also relevant target products for microbial upcycling, as they are extensively used in the cosmetic and food industry. Recently, Gregory et al. (2023) combined chemical depolymerization of high-density PE with microbial upcycling using microbial consortia to produce wax esters, which are of high industrial value. The feedstock obtained from chemical depolymerization of PE was mainly hexadecanoic acid and C_{12}-C_{16} alkanols that were converted by the consortia isolated from plastic-contaminated soil. Hexadecanoic acid was also utilized by the deep-sea bacterium *Dietzia maris* As-13-3 for the microbial production of rhamnolipids that are widely used as biosurfactants (Wang et al., 2014).

In terms of circularity, the microbial production of biodegradable polymers from plastic hydrolysates is the ideal strategy as it keeps resources in the plastics economy. Moreover, their production is an emerging field and could fit the scale of fossil-based plastics in the future. Polyhydroxyalkanoates (PHA) are biodegradable polyester that are natively produced by several microorganisms, and thus display valuable products for microbial upcycling. Due to their properties and biocompatibility, PHA can be used for the production of biodegradable plastics or medical devices (Philip et al., 2007; Prieto et al., 2016). Typically, PHA biosynthesis is induced by deficiency conditions such as the limitation of nitrogen, phosphorus, trace elements, or oxygen to store excess carbon intracellularly (Mezzina et al., 2021; Prieto et al., 2016). PHAs are classified into three groups based on the total number of carbon atoms in their (*R*)-3-hydroxyacyl monomers. Polyhydroxybutyrate (PHB) is a

short-chain-length (scl) PHA homopolymer consisting of the C_4-monomer (*R*)-3-hydroxybutyrate, whereas medium-chain-length (mcl) PHA consist of monomers ranging from C_6 to C_{14}. In contrast to scl- and mcl-PHA, long-chain-length (lcl-) PHA composed of $C_{>15}$ monomers are rarely present in nature (Li et al., 2016; Mezzina et al., 2021). Depending on the monomer composition, mechanical and physiochemical properties of the materials differ resulting in different application fields such as packaging or pharmaceutical industry (Li et al., 2016; Mezzina et al., 2021). Several bacteria are known to produce PHB, including the well-characterized *Cupriavidus necator* H16 (Reinecke and Steinbüchel, 2009), but also species of the genus *Bacillus* (López et al., 2012) and *Azotobacter* (Pettinari et al., 2001) produce PHB. Biosynthesis of PHB is encoded by the *phaCAB* operon and starts with the condensation of two molecules of acetyl-CoA yielding acetoacetyl-CoA that is catalyzed by the β-ketothiolase (PhaA). Next, activity of the acetoacetyl-CoA reductase (PhaB) results in the formation of (*R*)-3-hydroxybutyryl-CoA that is incorporated into the growing polymer chain by the PHB synthase (PhaC) (Reinecke and Steinbüchel, 2009). Liu et al. (2021b) used a microbial consortium of a TA-degrading *Pseudomonas stutzeri* isolate expressing *phaCAB* from *C. necator* H16 and the engineered *Yarrowia lipolytica* Po1f secreting *Is*PETase to produce PHB from PET. Unlike PHB, mcl-PHA are mainly produced by the genus *Pseudomonas* that will be reviewed in chapter 1.5.

Despite its promising future, microbial upcycling has certain limitations, depending on the individual process. Such can include low yields due to the release of CO_2, which could bring them close to combustion (Sadler and Wallace, 2021), while simultaneously facilitating the climate change. However, such emissions could also be utilized as additional feedstock for upcycling (Blank et al., 2020). Typically, during microbial upcycling, cultures are co-fed to produce and maintain biomass, thus requiring external carbon and/or energy sources that could reduce the economic viability (Lee et al., 2023). Another critical aspect of microbial upcycling can be the lack of fitting scales between the substrate and product. The production of niche chemicals, such as vanillic acid (Sadler and Wallace, 2021) or biopharmaceutics (Alvarez-Gonzalez et al., 2023), would make a negligible impact on reducing the vast quantities of plastic produced. Instead, the microbial production of biopolymers like PHA aligns better with the magnitude of plastic waste as a substrate, thus potentially facilitating the transition towards a circular plastic economy. Nevertheless, the production of other

value-added compounds that have applications beyond the plastics industry. This serves as proof-of-principle for a sustainable alternative to conventional end-of-life strategies for plastics, and can be linked to higher-volume products.

1.5 *Pseudomonas putida* KT2440 – a biotechnological chassis for plastic upcycling

To establish efficient microbial upcycling strategies for mixed plastic hydrolysates, it is essential to use a suitable biotechnological host. Ideally, such host should possess a versatile metabolism, which can be leveraged and extended by metabolic engineering and is capable of producing value-added compounds.

The genus *Pseudomonas* was first described in 1894, and more than 190 species have been identified since then (Peix et al., 2018). Typically, Pseudomonads are characterized by a versatile metabolism, a high tolerance towards stressors such as solvents or xenobiotic compounds, and their adaptability towards different lifestyles. This is due to their isolation from diverse environments including soils, sediments, plants, or humans in the case of the pathogenic species *Pseudomonas aeruginosa* PAO1 (Peix et al., 2018). The saprophytic soil bacterium *P. putida* KT2440 is one of the best-characterized Pseudomonads and is known for its versatile metabolism, which is encoded within a 6.18 Mb genome (Bagdasarian et al., 1981; Nelson et al., 2002). This strain is often mistakenly designated as Generally Recognized as Safe (GRAS), even within the *Pseudomonas* community (Dvořák and de Lorenzo, 2018; Kampers et al., 2019; Loeschcke and Thies, 2015; Nikel and de Lorenzo, 2018; Wierckx et al., 2015) (and many more). Nevertheless, this strain is classified by the Food and Drug Administration as host–vector system safety level 1, meaning it is safe to work within a biosafety level 1 laboratory (Kampers et al., 2019; National Archives and Records Administration, 1982). Moreover, the safety of this strain is evidenced by the absence of virulence factors (Belda et al., 2016; Dos Santos et al., 2004) and became a well-studied model laboratory species over the last decades. Its robust central carbon metabolism is accompanied with several peripheral pathways for oxidation, enabling the utilization a wide range of carbon and nitrogen sources (Nikel and de Lorenzo, 2018). Another advantage

of *P. putida* KT2440 is its genetic accessibility due to the development of many synthetic biology tools that enable metabolic engineering (Martínez-García and de Lorenzo, 2011; Volke et al., 2022; Zobel et al., 2015). Hence, this strain rapidly became a synthetic biology workhorse for industrial biocatalysis (Nikel and de Lorenzo, 2018).

Metabolic engineering has been extensively used to leverage and extend its versatile metabolism to enable the utilization of a variety of plastic monomers including TA (Narancic et al., 2021), EG (Franden et al., 2018a; Li et al., 2019), AA (Ackermann et al., 2021), or 1,4-butanediol (BDO) (Li et al., 2020) (Figure 1.5-1). Metabolism of EG and BDO was achieved by adaptive laboratory evolution (ALE) that is based on the emergence of natural mutations under specific conditions yielding improved phenotypes (Dragosits and Mattanovich, 2013). In both cases, *P. putida* KT2440 showed poor growth on the substrates. However, after prolonged incubation with regular culture transfer over several weeks, mutants able to metabolize the respective substrate emerged. Whole-genome sequencing (WGS) of isolated mutants and subsequent reverse engineering identified the mutations required for growth. For EG, a mutation within *gclR* was discovered that likely caused disruption of the GclR binding site upstream the PP_4297-4301 cluster, which encodes the glyoxylate metabolism. Characterization of the evolved strains and reverse engineering indicated that EG was metabolized *via* oxidation to glyoxylate, which was further converted to pyruvate encoded by the identified PP_4297-4301 operon (Li et al., 2019) (Figure 1.5-1). As for EG, ALE on BDO also resulted in a mutation within a transcriptional regulator. In this case, a mutation within PP_2046 was identified that affected expression of the downstream operon PP_2047-51 encoding an alcohol dehydrogenase and enzymes involved in β-oxidation. Using proteomics, the hypothetical pathways for BDO metabolism were elucidated. BDO could be subjected to β-oxidation resulting in the formation of glycolyl-CoA and acetyl-CoA and/or directly oxidized to succinate or succinyl-CoA (Li et al., 2020). Both approaches highlight the versatile metabolism of *P. putida* KT2440, as no heterologous enzymes were required for EG and BDO metabolism. Instead, native pathways with side activities for both substrates were present but not expressed in the wild type strain, which was addressed by ALE. A more rational approach was performed by Narancic et al. (2021) to enable metabolism of TA. Heterologous expression of the *tph* operon from *P. umsongensis* GO16 in *P. putida* KT2440 enabled growth on TA *via* protocatechuate,

which was further degraded to succinate and acetyl-CoA (Figure 1.5-1). Finally, a combined approach of ALE and rational strain engineering was performed by Ackermann et al. (2021), in which heterologous expression of the *dcaAKIJP* cluster from *A. baylyi* and subsequent ALE on AA resulted in the utilization of the substrate. The heterologous transporter DcaKP enabled uptake of AA that was subsequently CoA-activated by DcaIJ and subjected to β-oxidation. During ALE, mutations in transcriptional regulators emerged, which induced expression of β-oxidation-encoding genes required for degradation of AA (Figure 1.5-1).

The versatile metabolic repertoire of *P. putida* KT2440 not only allows metabolic funneling of several plastic monomers, but also enables the biosynthesis of a broad range of value-added compounds such as rhamnolipids (Tiso et al., 2020), β-ketoadipate (Werner et al., 2021) or mcl-PHA (Prieto et al., 2016). The combination of metabolic funneling and the biosynthesis of value-added compounds makes *P. putida* an excellent choice for microbial upcycling approaches.

Rhamnolipids are such relevant value-added compounds, as they are extensively used as biosurfactants in the pharmaceutical and cosmetic industry. Biosynthesis starts with the formation of 3-(3-hydroxyalkanoyloxy)alkanoate from two β-hydroxy fatty acids (RhlA) and subsequent attachment of rhamnose units (RhlB, RhlC) (Ochsner et al., 1994). However, the wild type *P. putida* KT2440 is not able to produce rhamnolipids, whereas *P. aeruginosa* PAO1 is one of the best-characterized rhamnolipid-producing strains. Metabolic engineering was used to transfer the rhamnolipid biosynthesis pathway from *P. aeruginosa* PAO1 into *P. putida* KT2440, which yielded a powerful recombinant platform strain for the production of rhamnolipids (Beuker et al., 2016; Tiso et al., 2020; Tiso et al., 2017). Moreover, the newly acquired ability to produce rhamnolipids was combined with the synthetic metabolic pathways for plastic monomer degradation by Utomo et al. (2020). The authors demonstrated the production of rhamnolipids from a mixture containing AA, EG, and BDO using a mixed culture of three engineered strains of *P. putida* KT2440, each able to degrade one monomer.
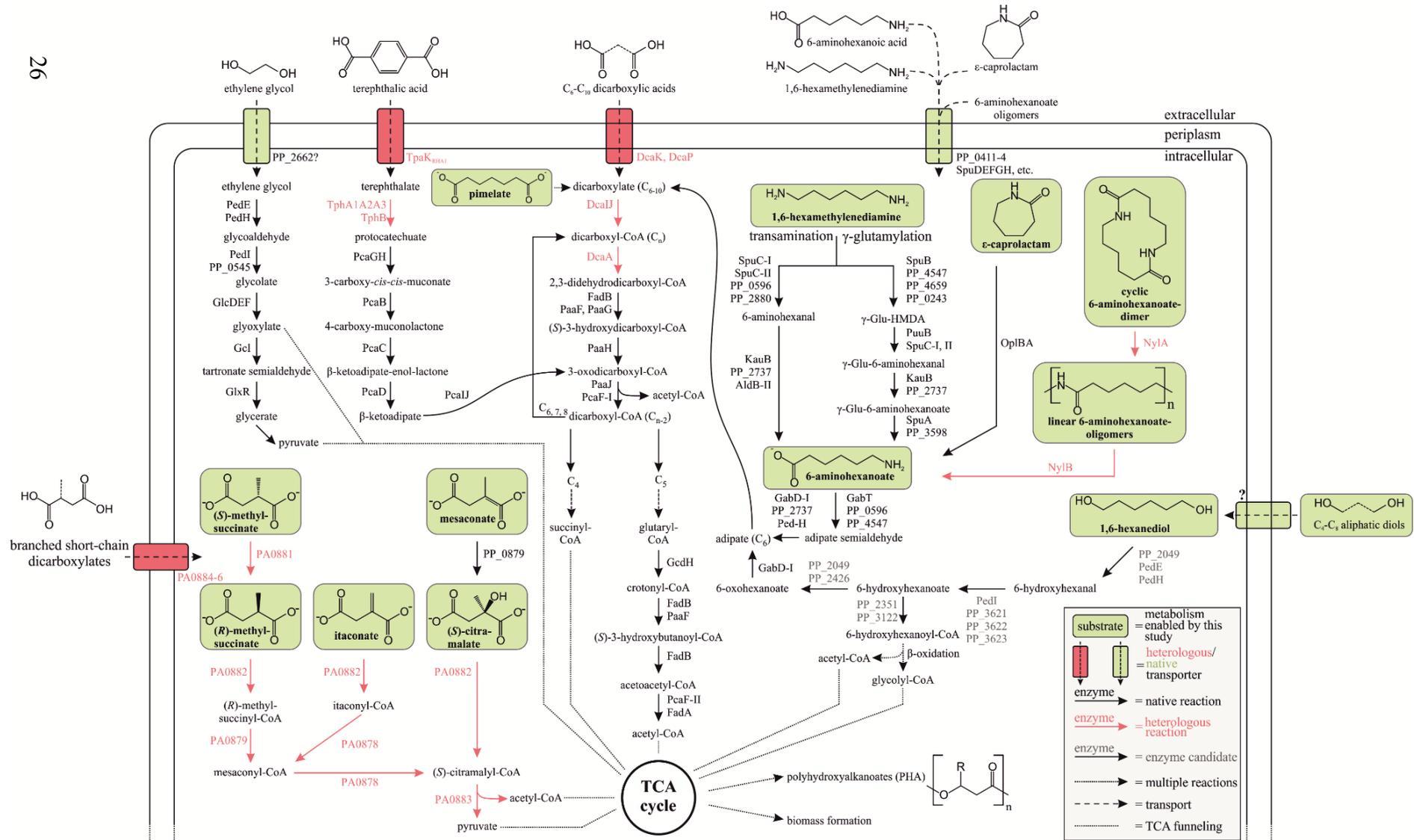
Figure 1.5-1. Metabolism of plastic monomers and oligomers by engineered *P. putida* KT2440. Previous studies implemented metabolism of ethylene glycol (Franden et al., 2018a; Li et al., 2019), terephthalate (Narancic et al., 2021; Sullivan et al., 2022), adipate (Ackermann et al., 2021), and 1,4-butanediol (Li et al., 2020). In this study, the substrate range was greatly extended by prevalent plastic monomers and oligomers highlighted in green using metabolic engineering including: branched short-chain dicarboxylates, pimelate, 1,6-hexamethylenediamine, 6-aminohexanoate, ε-caprolactam, cyclic and linear PA6-oligomers as well as 1,6-hexanediol. Moreover, production of polyhydroxyalkanoates including polyhydroxybutyrate from these substrates was demonstrated in this study.

Besides rhamnolipids, *P. putida* KT2440 can also be utilized for the production of mcl-PHA as biodegradable polyester. Biosynthesis of mcl-PHA is part of a complex global metabolic network and blends activities of fatty acid *de novo* synthesis with fatty acid β-oxidation (Figure 1.5-2). Accumulation of mcl-PHA in strain KT2440 can reach up to 75 % of the cell dry weight (Sun et al., 2007) and metabolic engineering has been applied to increase mcl-PHA production (Prieto et al., 2016; Salvachúa et al., 2020; Wang et al., 2011). Depending on the carbon source, *P. putida* KT2440 has two main routes for PHA biosynthesis. PHA-related substrates, such as fatty acids, are directly channeled into the β-oxidation, providing the (*R*)-3-hydroxyacyl-CoA precursors. In contrast, PHA non-related substrates, such as sugars, are converted to acetyl-CoA that is shunted into fatty acid *de novo* synthesis, which is linked to β-oxidation through the activity of the 3-hydroxyacyl-ACP thioesterase (PhaG) and the mcl-fatty acid-CoA ligase (AlkK) (Figure 1.5-2). The production of mcl-PHA from pure plastic monomers such as AA (Ackermann et al., 2021), BDO (Li et al., 2020), EG (Franden et al., 2018a), and TA (Bao et al., 2023) was demonstrated. Furthermore, PHA production from oxygenated intermediates, such as aliphatic dicarboxylates, obtained from chemical oxidation of PE, PS, and PET, was achieved with engineered *P. putida* KT2440 (Sullivan et al., 2022). In the same study, production of β-ketoadipate from the oxygenated intermediates was achieved. Another tandem chemical deconstruction and microbial upcycling approach using *P. putida* KT2440 was performed by Werner et al. (2021). Deep metabolic engineering enabled full conversion of a PET hydrolysate into β-ketoadipate, which can be used for the production of performance-increased PA.
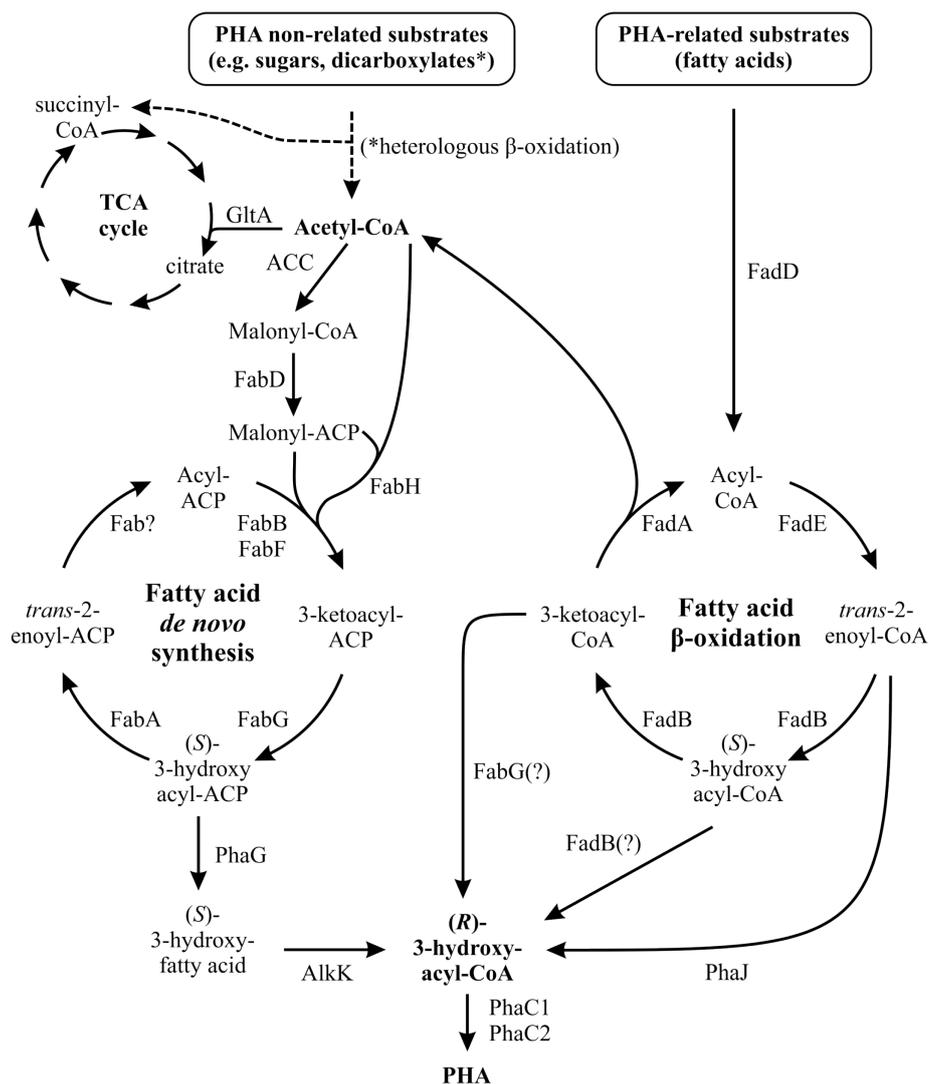
Figure 1.5-2. Biosynthesis pathways of PHA in *P. putida* KT2440. PHA non-related substrates such as sugars or dicarboxylates are degraded into acetyl-CoA that is shunted into fatty acid *de novo* synthesis. Activity of PhaG and AlkK provide (*R*)-3-hydroxyacyl-CoA as precursor for PHA synthesis. PHA-related substrates, namely fatty acids such as octanoate, can be directly converted into (*R*)-3-hydroxyacyl-CoA or further degraded *via* fatty acid β-oxidation. Dicarboxylates are degraded *via* a heterologous β-oxidation (*) and acyl-CoA intermediates cannot be directly converted to (*R*)-3-hydroxyacyl-CoA precursors. Modified from Mezzina et al. (2021).

To summarize, *P. putida* features many beneficial properties making it a biotechnological chassis strain for microbial plastic upcycling. Its native versatile metabolism can be leveraged by metabolic engineering to extend the substrate range by prevalent plastic monomers. Moreover, this strain is a microbial platform for the production of diverse value-added compounds. Especially the ability to accumulate PHA offers the solution to close the gap in the plastics economy, as biodegradable plastics can be produced avoiding the production of virgin fossil-based plastics. Nevertheless, the great potential of *P. putida* KT2440 for plastic upcycling has not yet been fully exploited, as many plastic building blocks cannot be metabolized, until today.

1.6 Aim and scope of the thesis

This thesis aims to develop new biological end-of-life solutions for plastics by combining enzymatic depolymerization with biological funneling and microbial upcycling, using engineered strains of *P. putida* KT2440.

To achieve this, novel enzyme candidates capable of depolymerizing PA should be discovered and characterized, as only a limited number of inefficient nylonases are currently described in the literature. Increasing the diversity of characterized nylonases will broaden the basis for enzyme engineering and facilitate the design of efficient PA-degrading nylonases through future enzyme engineering.

Secondly, this thesis aims to extend the substrate range of the biotechnological workhorse *P. putida* KT2440 by prevalent plastic monomers and oligomers. Although this strain was already engineered to funnel different mixed plastic hydrolysates into its central metabolism, many plastic-derived compounds are still not accessible to its native or previously engineered pathways. Therefore, the main focus will be to employ deep metabolic engineering to enable the metabolism of PA monomers such as 1,6-HMDA, Ahx, and ε-caprolactam as well as mixed PA hydrolysates. Moreover, even and uneven chain-length aliphatic dicarboxylates and diols, which are present in many PUs and polyesters, are targets for synthetic pathway integration. The portfolio should be further extended by branched short-chain dicarboxylates, which gain increasing interest in the polymer industry as they allow cross-linking of polymer chains. Once these compounds can be funneled into the central metabolism, the production of value-added compounds is envisioned. Therefore, mcl-PHA and PHB should be produced from the newly accessible feedstocks, as they can be further processed into biodegradable polyesters.

Finally, the biodegradation of coatings should be investigated as they increase the complexity of plastics and hinder mechanical and chemical recycling. For this, novel bacterial strains capable of degrading PEU coatings should be isolated. The corresponding enzymes and metabolic routes should be revealed, paving the way for sustainable end-of-life solutions for entire plastic materials, including their coatings.

By achieving these objectives, this thesis will make a significant impact on establishing sustainable end-of-life solutions for plastics as well as their coatings. Overall, this thesis will contribute to facilitate the transition from a linear to a circular plastics economy.

2   Publications and manuscripts

This chapter consists of five manuscripts that have either been published, are currently under review or revision, or are to be published in peer-reviewed journals. The presented work results from collaborations with various partners of the EU project Glaukos and other collaborations that have resulted in joint publications. Contributions of the authors to the respective manuscripts are described using the Contributor Roles Taxonomy (CRediT) (Allen et al., 2019).

32

2.1 Microbial upcycling of polyamides using engineered *Pseudomonas putida*

Invitation to revise and resubmit to *Nature Microbiology*.

de Witt, J.[1] Luthe, T.[1], Jensen, K.[2], Polen, T.[1], Wirtz, A.[1], Frunzke, J.,[1], Wynands, B.[1], and Wierckx, N.[1*] (2024).

[1] Institute of Bio- and Geosciences IBG-1: Biotechnology, Forschungszentrum Jülich, Jülich, Germany

[2] Novozymes A/S, Biologiens Vej 2, Kgs. Lyngby DK-2800, Denmark

[*] Corresponding author

CRediT authorship contribution statement:

J. de Witt: Investigation, Data Curation, Formal Analysis, Methodology, Visualization, Validation, Writing – Original Draft Preparation, Writing – Review & Editing.

T. Luthe: Data Curation, Formal Analysis, Writing – Review & Editing.

K. Jensen: Resources, Supervision.

T. Polen: Methodology, Formal Analysis, Data Curation, Writing – Review & Editing.

A. Wirtz: Methodology, Writing – Review & Editing.

J. Frunzke: Resources, Writing – Review & Editing.

B. Wynands: Supervision, Methodology, Writing – Review & Editing.

N. Wierckx: Supervision, Funding Acquisition, Project Administration, Conceptualization, Writing – Review & Editing.

Overall contribution: 75 %

The presented experimental work was conducted by JdW and supported by TL (RNA-seq), AW (HPLC methodology) and TP (genome sequencing). Validation and visualization was done by JdW. The writing of the original draft was done by JdW, which was reviewed and edited by KJ, JF, BW, and NW. Funding for the project was acquired by NW.

2.1.1 Graphical abstract
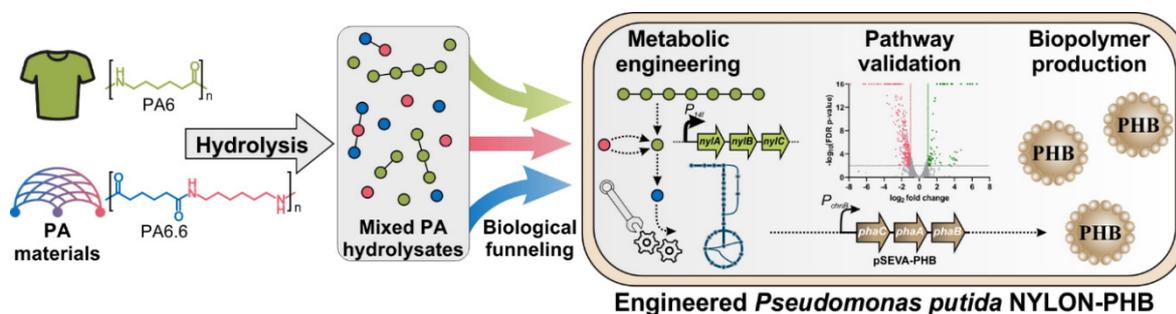
2.1.2 Abstract

Aliphatic polyamides (PA), or nylons, are widely used in the textile and automotive industry due to their high durability and tensile strength, but recycling rates are currently below 5%. Chemical recycling of PA is possible, but typically yields mixtures of monomers and oligomers. Microbial upcycling is a powerful technology to overcome this drawback. In this study, *Pseudomonas putida* KT2440 was engineered for the synthetic metabolism of common C_6-PA monomers such as 6-aminohexanoic acid, ε-caprolactam and 1,6-hexamethylenediamine guided by adaptive laboratory evolution. Heterologous expression of nylonases resulted in a strain able to additionally metabolize linear and cyclic nylon oligomers. RNA sequencing and reverse engineering revealed the metabolic pathways of these non-natural substrates. Moreover, the production of polyhydroxybutyrate (PHB) from C_6-PA monomers and PA6 hydrolysates was demonstrated in media with low carbon:nitrogen ratios. This study provides the first microbial host for the biological conversion of PA monomers and mixed PA hydrolysates to a value-added product. Thereby, we lead the path for establishing sustainable end-of-life solution for millions of tons of fishing nets, clothing, and technical materials per year.

2.1.3 Introduction

Global plastic production is continuously increasing and reached a new all-time high with 390 million tons produced in 2021, thereby amplifying ecological hazards and the need to establish sustainable end-of-life solutions for plastics (PlasticsEurope, 2022). Aliphatic polyamides (PA), or nylons, are a class of synthetic plastics characterized by their high tensile strength and long durability. Hence, PA are used in a variety of application fields, including the textile and fishing gear industry and the automotive sector. PA can be synthesized by polycondensation of dicarboxylic acids and diamines such as adipic acid (AA) and 1,6-hexamethylenediamine (HMDA) to yield PA6.6, or *via* ring-opening polymerization of lactams such as ε-caprolactam (yielding PA6), which is the cyclic form of 6-aminohexanoic acid (Ahx). Global production will soon reach 10 million tons and low recycling rates, such as < 2 % for PA fibers, are urging for sustainable end-of-life solutions (Minor et al., 2023; Textile Exchange, 2022). Currently, most PA materials are landfilled or incinerated since traditional recycling strategies such as chemical or mechanical recycling typically require highly pure PA feedstocks, while resulting in reduced-quality products and using high amounts of energy (Alberti et al., 2019; Pietroluongo et al., 2020). Moreover, chemical recycling through hydrolysis yields mixtures of various monomers and oligomers that need to be separated, making the process uncompetitive (Jehanno et al., 2022; Minor et al., 2023).

Such drawbacks could be overcome by combining chemical hydrolysis with biological catalysis, which allows metabolic funneling of complex hydrolysates and subsequent conversion to value-added products thereby avoiding costly purification steps (Ellis et al., 2021; Sullivan et al., 2022). However, such hybrid strategies have so far mostly been limited to relatively easily recyclable polyesters such as poly(ethylene terephthalate) (Tiso et al., 2021b). Currently, no suitable microbial hosts exist to convert PA-derived hydrolysates into value-added products. Although natural PA are ubiquitous in nature, i.e., in proteins or silk, microbial growth on synthetic PA monomers is barely reported in literature. Metabolism of Ahx or ε-caprolactam was found in some microorganisms, such as *Pseudomonas jessenii* (Otzen et al., 2018) or *Paenarthrobacter ureafaciens* (Takehara et al., 2018). The C_4- and C_5-biogenic amines putrescine and cadaverine are metabolized by a variety of microorganisms (Kurihara et al., 2005; Luengo and Olivera, 2020), but these are very

uncommon as PA building blocks. In contrast there is, to the best of our knowledge, no report on the microbial utilization of the C_6-diamine HMDA as sole carbon source. Instead, HMDA was reported to be only utilized as nitrogen source in microbial conversions(Zhou et al., 2021). The ability to metabolize PA6-oligomers (Ahx-oligomers) was reported for a small number of microorganisms namely *Agromyces* sp. KY5R, *Kocuria* sp. KY2, and *P. ureafaciens* (Yasuhira et al., 2007). Ahx-oligomer degradation is catalyzed by a small group of Ahx-oligomer-hydrolases, called nylonases, that specifically hydrolyze amide bonds within the oligomers. The Ahx-cyclic-dimer hydrolase (NylA) converts cyclic Ahx_2 into linear Ahx_2 (Kinoshita et al., 1975), whereas the Ahx-oligomer exohydrolase (NylB) and Ahx-oligomer endohydrolase (NylC) degrade linear Ahx-oligomers (Kakudo et al., 1993; Kinoshita et al., 1981; Negoro et al., 1992). Nevertheless, nylonase-expressing strains are thus far only used for degradation of Ahx-oligomers, i.e. in wastewater treatment. For microbial upcycling, metabolization of PA-related substrates must be linked to product formation. *Pseudomonas putida* KT2440 has already been engineered to metabolize a variety of plastic monomers including AA, 1,4-butanediol, ethylene glycol, terephthalate, and itaconate (Ackermann et al., 2021; de Witt et al., 2023; Franden et al., 2018b; Li et al., 2020; Li et al., 2019; Narancic et al., 2021). Moreover, *P. putida* KT2440 can produce several value-added compounds such as polyhydroxyalkanoates (PHA) (Tiso et al., 2021a), rhamnolipids (Tiso et al., 2020), or β-ketoadipic acid (Werner et al., 2021) from these plastic monomers. However, *P. putida* is not capable of metabolizing PA-related monomers or oligomers, which prevented their upcycling until now.

In addition to chemical recycling, considerable amounts PA monomers as well as linear and cyclic oligomers are formed as by-products through incomplete polymerization and head-to-tail condensation during PA production, respectively (Ueda et al., 1998). Such by-products can accumulate in the environment (Kinoshita et al., 1975), while simultaneously wasting potential carbon and nitrogen resources for microbial upcycling strategies. To establish sustainable end-of-life solutions for PA and to facilitate the transition towards a circular economy, the construction of powerful microbial hosts allowing biological funneling of PA-related waste streams and their subsequent microbial upcycling is sorely needed.

In this study, we used deep metabolic engineering guided by laboratory evolution to enable metabolism of prevalent PA monomers, namely HMDA, Ahx, and ε-caprolactam, by a single strain of *P. putida* KT2440. RNA-sequencing (RNA-seq) was performed to identify key enzymes and transporters of the engineered metabolic pathways, and heterologous expression of the nylonase-encoding genes *nylA*, *nylB*, and *nylC* from *P. ureafaciens* extended the substrate range to linear and cyclic Ahx-oligomers. The engineered strain fully metabolized hydrolysates of PA6 and was further engineered to convert them into polyhydroxybutyrate (PHB) as value-added product. Thereby, our work provides the first powerful host enabling the microbial upcycling of PA monomers and complex PA6 hydrolysates thereby overcoming the drawbacks of traditional recycling processes leading the path for sustainable end-of-life solutions for synthetic PA.

2.1.4   Results

2.1.4.1   Enabling metabolism of PA monomers

The majority of commercial PA consists of monomers with a chain-length of six carbon atoms (C_6). To enable microbial upcycling of C_6-PA monomers, *P. putida* KT2440 should be engineered to funnel AA, HMDA, Ahx and ε-caprolactam into its central metabolism. Since the aliphatic diamines putrescine (C_4) and cadaverine (C_5) are metabolized *via* sequential transamination to their corresponding dicarboxylate (Luengo and Olivera, 2020), metabolism of HMDA, Ahx and ε-caprolactam was anticipated to occur *via* AA. Hence, *P. putida* KT2440-AA, which was recently engineered to utilize AA and other dicarboxylates (Ackermann et al., 2021), was used as starting strain for further experiments.

Initially, *P. putida* KT2440-AA did not grow on HMDA as sole carbon source (Figure 2.1-1). However, growth of a single replicate was observed after prolonged incubation of 5 days. The ability to metabolize HMDA remained after passage through complex medium indicating the emergence of stable mutations that enabled growth on the substrate. Whole-genome sequencing (WGS) of the isolated HMDA-metabolizing mutant, designated as HMDA-1, revealed an in-frame deletion of 9 bp in PP_2884 encoding a XRE family transcriptional regulator. This led to the absence of three amino acids (F61, F62 and S63) in

the predicted DNA-binding domain of the transcriptional regulator (Figure 2.1-1, Figure S5.1-1). In addition to HMDA, the HMDA-1 mutant also metabolized Ahx and ε-caprolactam as sole carbon source, whereas the initial *P. putida* KT2440-AA could not metabolize any of these substrates (Figure 2.1-1). To analyze the involvement of PP_2884 in C_6-PA monomer metabolism, two knock-out mutants were constructed either lacking the entire PP_2884 gene (ΔPP_2884) or mimicking the 9 bp deletion resulting in the loss of F61, F62, and S63 (PP_2884$^{\Delta 3}$). Both strains metabolized HMDA, Ahx, and ε-caprolactam and showed an identical growth phenotype (Figure 2.1-1). Hence, the transcriptional regulator likely acts as repressor and the deletion of F61, F62, and S63 within the DNA-binding domain might abolish the ability to bind its regulatory targets. When both modifications were introduced into wild type *P. putida* KT2440, none of the C_6-PA monomers were metabolized. Hence, metabolism of the C_6-PA monomers by the ΔPP_2884 and PP_2884$^{\Delta 3}$ mutants occurred *via* AA requiring the previous modifications of the *P. putida* KT2440-AA strain.
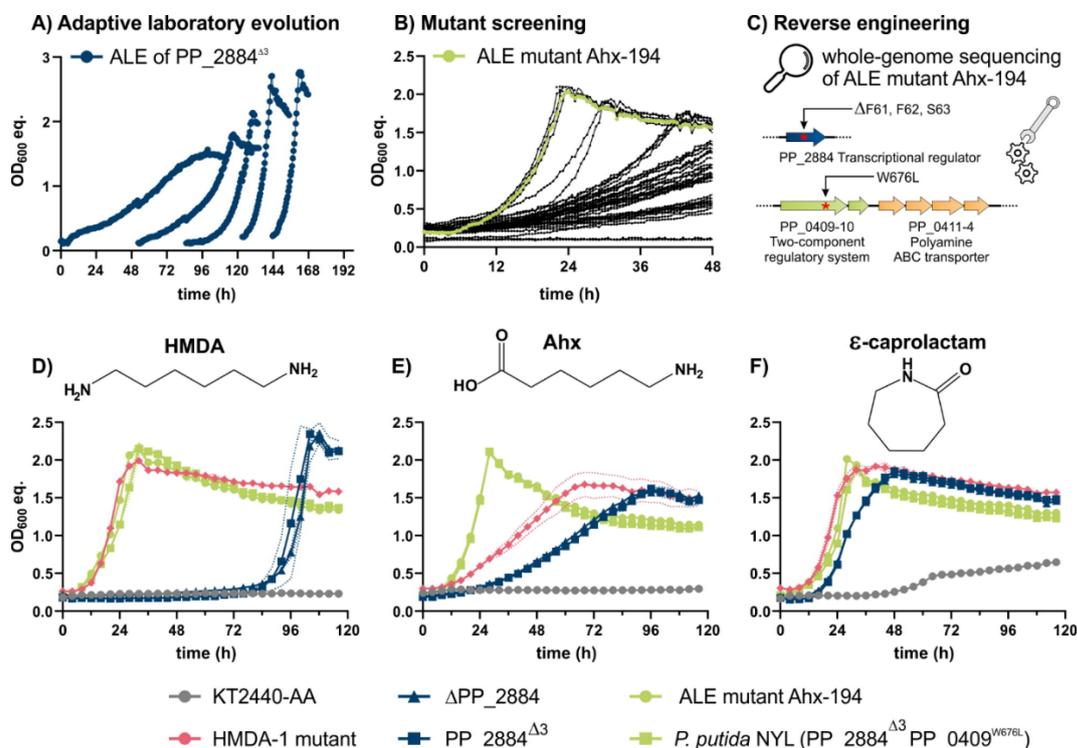
Figure 2.1-1. Engineering growth of *P. putida* on C_6-PA monomers. Strains were cultivated in a Growth Profiler in 96-well microtiter plates with minimal medium containing 15 mM of 1,6-hexamethylenediamine (HMDA), 6-aminohexanoate (Ahx), or ε-caprolactam as sole carbon source. The mean values and standard deviations of three replicates are shown (n=3).

However, both ΔPP_2884 and PP_2884$^{\Delta 3}$ showed longer lag phases and decreased growth rates compared to the HMDA-1 mutant suggesting the presence of further mutations in this strain contributing to the observed phenotype (Figure 2.1-1). Since no further mutations could be found in the genome of HMDA-1, and since growth on Ahx was slower than on HMDA and ε-caprolactam, adaptive laboratory evolution (ALE) of *P. putida* KT2440-AA PP_2884$^{\Delta 3}$ was performed using Ahx as substrate (Figure 2.1-1). After ALE, single mutants were isolated and screened for the ability to metabolize HMDA, Ahx, and ε-caprolactam (Figure 2.1-1, Figure S5.1-2). Among them, ALE mutant Ahx-194 showed fastest growth on all substrates and thus was selected for WGS. Within the genome of ALE mutant Ahx-194, a single nucleotide variant (SNV) was identified in PP_0409, encoding a sensor histidine kinase. This SNV resulted in the exchange of tryptophan to leucine at position 676 (PP_0409^{W676L}) that was located within the predicted histidine kinase domain, which is part of the two-component regulatory system encoded by PP_0409-10 (Figure 2.1-1). To confirm an involvement of this operon in the metabolism of C_6-PA monomers, the PP_0409^{W676L} mutation was introduced into *P. putida* KT2440-AA PP_2884$^{\Delta 3}$. Indeed, the resulting strain (PP_2884$^{\Delta 3}$, PP_0409^{W676L}, designated as *P. putida* NYL) showed identical growth compared to the ALE mutant Ahx-194 with HMDA, Ahx and ε-caprolactam as sole carbon source validating a successful reverse engineering (Figure 2.1-1). In contrast to PP_2884, deletion of PP_0409-10 in *P. putida* KT2440-AA PP_2884$^{\Delta 3}$ resulted in impaired growth on all three substrates, indicating that it acts as transcriptional activator (Figure S5.1-3). Hence, the mutated histidine kinase PP_0409^{W676L} likely resulted in an always-on state of the two-component regulatory system. PP_0409-10 share amino acid sequence identities of 65 % (PP_0409) and 87 % (PP_0410) with AgtS (PA0600) and AgtR (PA0601) of *Pseudomonas aeruginosa* PAO1, respectively. Since AgtSR activates gene expression of the downstream encoded transporter AgtABCD in the presence of γ-aminobutyrate (Chou et al., 2014), PP_0409-10 might also activate expression of the downstream located PP_0411-4 encoding a putative polyamine ABC transporter for C_6-PA monomer import that will be analyzed below.

2.1.4.2 Unraveling metabolism of C_6-PA monomers

Modifications in the two transcriptional regulators encoded by PP_2884 and PP_0409-10 in *P. putida* KT2440-AA enabled rapid growth of *P. putida* NYL on all tested C_6-PA

monomers. The fact that two regulators were identified as bottlenecks suggests that all enzymes and transporters required for C_6-PA monomer metabolism were present in the initial *P. putida* KT2440-AA but their corresponding genes were likely not expressed. To confirm this hypothesis and to identify the targets of both transcriptional regulators, the transcriptomes of *P. putida* KT2440-AA and its two mutants PP_2884$^{\Delta 3}$ and *P. putida* NYL were compared by RNA-seq under AA- or Ahx-metabolizing conditions (Figure 2.1-2).

In total, 81 and 362 genes were significantly (FDR *p*-value < 0.01) up- and down-regulated, respectively, in *P. putida* NYL compared to KT2440-AA growing on AA (Figure 2.1-2, Table S5.1-1). As expected from the PP_0409^{W676L} mutation, the putative polyamine ABC transporter encoded by PP_0411-4 was highly up-regulated in *P. putida* NYL (Figure 2.1-2). Deletion of PP_0411-4 led to reduced growth on HMDA, Ahx, and ε-caprolactam revealing its function as universal C_6-PA monomer transporter (Figure S5.1-4). However, growth of this mutant was not fully abolished, indicating the presence of secondary transport systems for C_6-PA monomers. Such transport systems probably include PuuP (putrescine permease), SpuDEFGH (spermidine ABC transporter), and PotF-I (putrescine-binding protein), whose encoding genes were also up-regulated in *P. putida* NYL (Figure 2.1-2). Additionally, genes likely associated to C_6-PA monomer metabolism were up-regulated including *puuB* (γ-glutamylputrescine oxidase), *spuC-II* (polyamine:pyruvate transaminase), *spuB* (γ-glutamylputrescine oxidase), and *kauB* (4-guanidinobutyraldehyde dehydrogenase). The profile of up-regulated genes indicated that C_6-PA monomers are metabolized *via* two pathways, namely the direct transamination route and the γ-glutamylation pathway (Figure 2.1-2). Moreover, several genes of the so-called *ped* cluster were up-regulated (Table S5.1-1). This cluster encodes alcohol and aldehyde dehydrogenases with relaxed substrate specificity (Wehrmann et al., 2017) and hence likely contributed to metabolism of C_6-PA monomers by oxidizing aldehyde intermediates of the pathways (Figure 2.1-2). In contrast to PP_0409-10, the XRE family regulator encoded by PP_2884 was revealed as transcriptional repressor (Figure 2.1-1). RNA-seq of the PP_2884$^{\Delta 3}$ mutant confirmed the up-regulation of, among others, *ped-H*, *puuP*, *puuB*, and *spuC-II* in PP_2884$^{\Delta 3}$ compared to the unevolved strain revealing them as regulatory targets of PP_2884 (Figure 2.1-2).
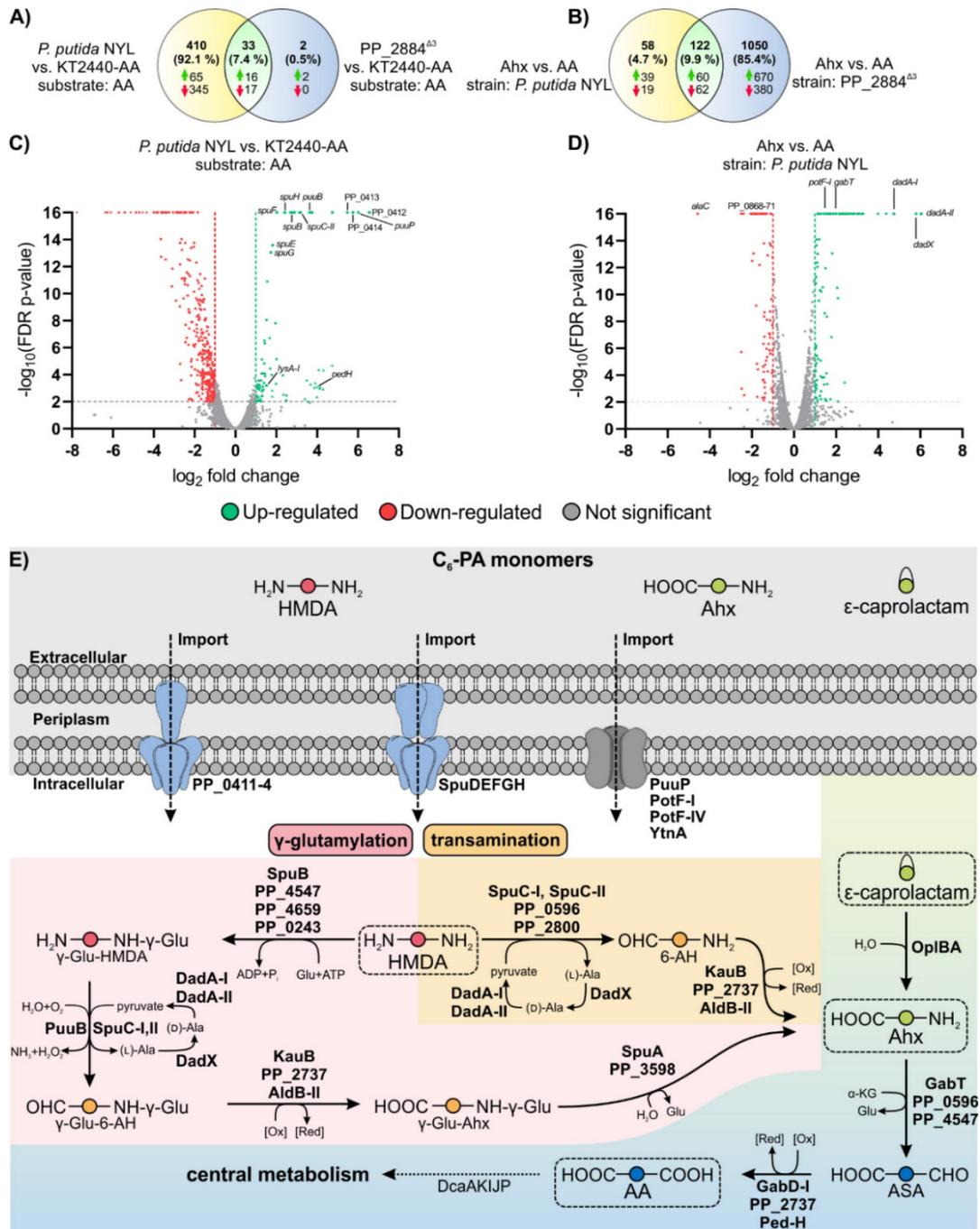
Figure 2.1-2. Metabolism of C$_6$-PA monomers in engineered *P. putida*. A and B) Venn diagrams of differentially expressed genes (DEGs) (FDR-*p*-value < 0.01 and |log$_2$ fold change| > 1) identified by RNA-seq. The numbers of total DEGs (black) and up- (green arrow) or down-regulated (red arrow) genes are displayed. Differential gene expression was compared for the indicated strains using AA or Ahx as substrate. **C and D)** Volcano plots of DEGs. Up- and down-regulated genes are shown in green and red, respectively. Insignificant hits (FDR-*p*-value ≥ 0.01 or |log$_2$ fold change| < 1) are displayed in grey. Thresholds are displayed as dotted lines in their respective color. A full list of significantly up- and down-regulated genes is shown in Table S5.1-1 and Table S5.1-2. **E)** Metabolic pathways for C$_6$-PA monomers. HMDA, Ahx, and ε-caprolactam are imported *via* the universal polyamine ABC transporter PP_0411-4, as well as several other putative secondary transport systems. HMDA can be converted by both γ-glutamylation and transamination *via* 6-aminohexanal (6-AH) or its γ-glutamylated (γ-Glu) form to Ahx that is further transaminated to adipate semialdehyde (ASA) and oxidized to AA. Indicated proteins (bold) were significantly up-regulated.

All genes described so far were up-regulated in the presence of AA, indicating their constitutive expression as no C_6-PA monomer was present during cultivation. Differential gene expression for *P. putida* NYL was therefore also compared on Ahx versus AA (Figure 2.1-2). By this, natively regulated targets within the reverse engineered strain should be identified whose expression is induced by the presence of Ahx. In total, 99 genes were significantly (FDR *p*-value < 0.01) up-regulated under Ahx-metabolizing conditions including several oxidoreductases (*dadA-II*, *dadA-I*, PP_2737, or *gabD-I*), aminotransferases (PP_0596, *gabT*, or PP_4547), and transporters (*ytnA*, PP_0544, or *potF-IV*) likely involved in C_6-PA monomer metabolism (Figure 2.1-2). In strain PP_2884$^{\Delta3}$, expression of *oplB* and *oplA* (PP_3514-5) was significantly (FDR-*p*-value < 0.01) up-regulated (1.9- and 2.4-fold respectively) when the strain was cultivated with Ahx compared to AA. OplBA is a valerolactam hydrolase that also shows activity towards ε-caprolactam although the substrate was not metabolized by the *P. putida* KT2440 wild type (Schmidt et al., 2022; Thompson et al., 2019b). Indeed, deletion of *oplBA* (PP_3514-5) in strain *P. putida* NYL abolished growth on ε-caprolactam confirming OplBA as ε-caprolactamase and thereby revealing another key enzyme for C_6-PA monomer metabolism (Figure S5.1-5). Furthermore, several genes including the *alg*-cluster (PP_1277-1288) were down-regulated in *P. putida* NYL that likely increased growth through reduced biofilm formation (Figure 2.1-2).

Overall, this analysis deciphered that the mutated regulators affect the expression of a wide array of genes, both proximally and distally located on the genome. Moreover, the versatility of *P. putida*'s metabolism towards synthetic compounds was revealed, which enables growth on nylon monomers through exclusively native metabolic enzymes activated by two key mutations affecting transcriptional regulation of a wide variety of genes.

2.1.4.3 Heterologous expression of nylonases pioneer the metabolism of PA6 oligomers

Transcriptomic analysis revealed that uptake systems for polyamines such as spermidine or spermine are involved in C_6-PA monomer metabolism of *P. putida* NYL. Polyamines often share transport systems with natural polyamides (Luengo and Olivera, 2020), suggesting that linear oligomers of PA6 could also be imported and metabolized by *P. putida* NYL. To test

whether these transporters could enable metabolism of linear PA6 oligomers, the Ahx-oligomer exohydrolase (NylB) from *P. ureafaciens* was codon-optimized and constitutively expressed in *P. putida* NYL. NylB catalyzes the exo-cleavage of linear Ahx-oligomers resulting in the sequential release of Ahx (Kinoshita et al., 1981; Negoro, 2000). Indeed, heterologous expression of *nylB* in *P. putida* NYL-P_{14f}-*nylB* enabled slight growth on the linear dimer (Ahx$_2$) and trimer (Ahx$_3$) of PA6 after prolonged cultivation, whereas *P. putida* NYL could not utilize these oligomers (Figure 2.1-3). However, growth with both substrates was extremely slow and thus ALE of *P. putida* NYL-P_{14f}-*nylB* was performed on linear Ahx$_2$. Among the isolated mutants, two ALE strains (Ahx$_2$-322 and Ahx$_2$-323) showed much faster growth on both Ahx$_2$ and Ahx$_3$ (Figure S5.1-6) and were selected for WGS. In total, three putatively promising hotspots of mutations associated with Ahx-oligomer metabolism were identified in both ALE mutants. These include mutations in the substrate-binding protein of the previously identified C$_6$-PA monomer transporter (PP_0412^{V222L} and PP_0412^{T127K}). Furthermore, the two-component regulatory system CbrA/CbrB (PP_4695-6) was mutated in the predicted *Per-Arnt-Sim* (PAS) domain of the sensor kinase (CbrA^{A625T} and CbrA^{A522T}). The third promising mutation was a SNV (C→T) and an insertion (T) in the upstream regions of PP_2176 and PP_2177 both encoding transcriptional regulators. Moreover, PP_2177 is part of an operon (PP_2177-80) encoding the γ-glutamylation pathway of polyamines. Based on the identified mutations in ALE mutant Ahx$_2$-322, reverse engineering of the unevolved *P. putida* NYL-P_{14f}-*nylB* was performed, resulting in strain *P. putida* NYL *P_{14f}-nylB* PP_0412^{V222L} PP_4695^{A625T} $P_{PP_2177}$$^{C→T}$ designated as *P. putida* NYLON-B (NYLon Oligomer metabolism through NylB). Reverse engineering confirmed that all three mutations were required to mimic the fast-growing phenotype of the ALE mutants with linear Ahx$_2$ and Ahx$_3$ (Figure 2.1-3, Figure S5.1-7). Since NylB does not contain a secretion signal peptide, the linear Ahx-oligomers must be imported for subsequent utilization. The mutation in the previously identified transporter PP_0411-4 caused by ALE on Ahx$_2$ suggests an altered affinity towards Ahx-oligomers. Indeed, deletion of PP_0411-4 in *P. putida* NYLON-B resulted in reduced growth with linear Ahx$_2$ and Ahx$_3$ confirming their uptake *via* PP_0411-4 and indicating a relaxed substrate specificity caused by the mutation in the substrate binding domain (PP_0412^{V222L}) (Figure 2.1-3). Since growth of the ΔPP_0411-4 mutant was not abolished (Figure 2.1-3 c, g), additional native transport

systems showing affinity towards Ahx-oligomers must be present in *P. putida* as discussed for C_6-PA monomer transport above. The mutation upstream of PP_2177-80 might cause constitutive expression of the adjacent operon encoding *spuC-I* (Figure S5.1-8) (Schmidt et al., 2022). Although Ahx-oligomers and Ahx cannot be metabolized *via* γ-glutamylation, this mutation was beneficial for growth on Ahx-oligomers. This can be explained by the side activity of SpuC-I towards Ahx (Schmidt et al., 2022) thereby likely reducing the accumulation of Ahx that was identified as putative bottleneck of Ahx-oligomer metabolism (Figure 2.1-3). Although no genes directly associated with Ahx-oligomer metabolism were identified in genetic proximity of CbrA/CbrB, the detected mutation within the PAS domain of CbrA was essential for utilization of Ahx-oligomers. In *P. putida* KT2440, CbrA/CbrB is a global metabolic two-component regulator that regulates carbon-nitrogen balance, amino acid metabolism and hence likely Ahx-oligomer metabolism in the reverse engineered strain (Amador et al., 2010; Valentini et al., 2014; Wirtz et al., 2020). This is supported by the involvement of CbrA/CbrB in regulating the expression of *spuC* in *P. aeruginosa* PAO1 (Lu et al., 2002). Overall, the $CbrA^{A625T}$ mutation might resulted in signal transduction induced by Ahx-oligomers, whereas it could be natively triggered by monomers in *P. putida* NYL.

The ability of *P. putida* NYLON-B to metabolize linear Ahx_2 and Ahx_3 suggested that also larger oligomers (n > 3) might be a substrate for this strain. To obtain such substrates, the soluble fraction of PA6 was extracted from PA6 pellets. Two novel high-performance liquid chromatography (HPLC) methods were developed to quantify the resulting cyclic (Figure 2.1-3 d) and linear (Figure 2.1-3 e) monomers and oligomers of Ahx. The soluble PA6 fraction contained the monomers ε-caprolactam and Ahx but also cyclic (n = 2-6) and linear (n = 2-7) Ahx-oligomers (Figure S5.1-9). Cultivation of *P. putida* NYLON-B on this extract revealed metabolism of all soluble linear Ahx-oligomers (n = 2-7) as sole carbon and nitrogen source highlighting the broad substrate range of this strain (Figure 2.1-3). In contrast, cyclic Ahx-oligomers were not metabolized by *P. putida* NYLON-B, which can be explained by the specificity of NylB towards linear but not cyclic Ahx-oligomers (Negoro, 2000) (Figure 2.1-4).
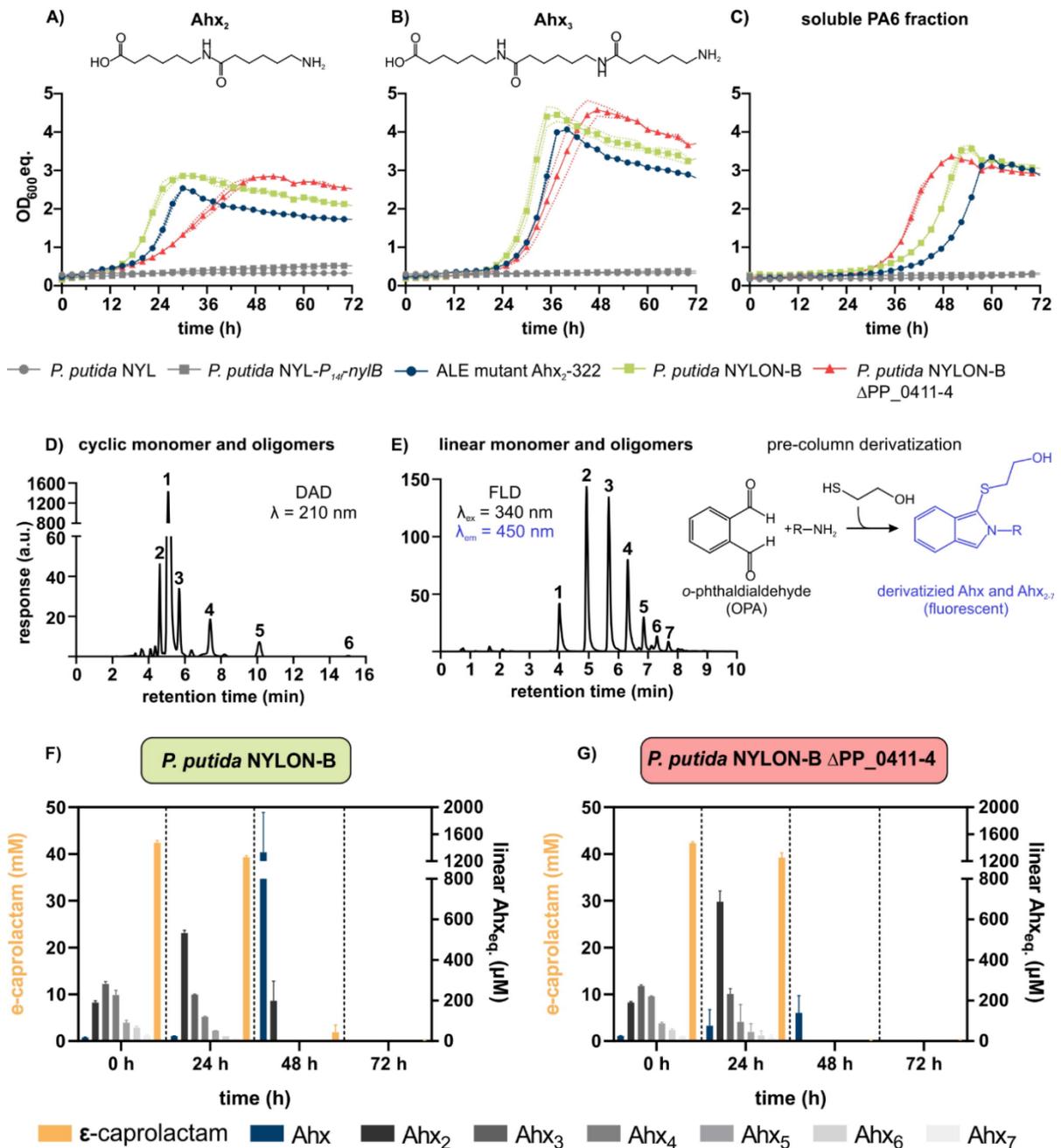
Figure 2.1-3. Metabolism of linear Ahx-oligomers by engineered *P. putida* strains. Strains were grown in MSM with 15 mM Ahx$_2$ **(A)**, Ahx$_3$ **(B)**, or a soluble PA6 fraction containing ε-caprolactam, Ahx, and linear Ahx-oligomers **(C)** as sole carbon and nitrogen source. The composition of the soluble PA6 fraction is shown in Figure S5.1-9. **D)** HPLC chromatogram showing the separation of ε-caprolactam (1) and cyclic Ahx-oligomers (2-6). Peak numbers correspond to the size (n) of the Ahx-oligomers. Compounds were detected with a diode array detector (DAD) at λ = 210 nm. **E)** HPLC chromatogram of Ahx (1) and linear Ahx-oligomers (2-7). Terminal R-NH$_2$ groups were pre-column derivatized using *o*-phthaldialdehyde (OPA). The derivatives were detected with a fluorescence detector (FLD) with excitation λ = 340 nm and emission λ = 450 nm. HPLC analysis of culture supernatants of *P. putida* NYLON-B (**F**) (green) and its ΔPP_0411-4 mutant (**G**) (red) cultivated with the soluble PA6 fraction as sole carbon and nitrogen source. The concentrations of ε-caprolactam and Ahx equivalents (Ahx$_{eq}$) of Ahx and its linear oligomers are shown for indicated cultivation times. Ahx$_{eq}$ were calculated by multiplying the detected Ahx-oligomer concentration with the size (n) of the corresponding oligomer. The mean values and standard deviations of three replicates are shown (n=3).

Although nylon hydrolysates typically only contain linear PA oligomers, considerable amounts of cyclic Ahx-oligomers do form during polymer synthesis by head-to-tail condensation. They therefore also display relevant targets for microbial funneling of nylon synthesis waste streams. To enable their metabolism, the P_{14f}-*nylB* cassette was replaced to express either NylA (*P. putida* NYLON-A), or NylC (*P. putida* NYLON-C), or all three nylonases (*P. putida* NYLON-ABC). NylA specifically catalyzes the hydrolysis of cyclic Ahx_2 into linear Ahx_2 but shows no activity towards larger cyclic Ahx-oligomers (Kinoshita et al., 1975). In contrast to this, the Ahx-oligomer endohydrolase (NylC) hydrolyzes cyclic oligomers with a degree of oligomerization greater than three into their linear forms (Negoro et al., 1992). Hence, the combined activity of NylA, NylB, and NylC is expected to be required for degradation of cyclic Ahx-oligomers. Strain *P. putida* NYLON-ABC was still able to metabolize Ahx and linear Ahx-oligomers confirming activity of NylB. As expected, *P. putida* NYLON-ABC grew on a cyclic Ahx_{2-6} mixture as sole carbon and nitrogen source (Figure 2.1-4 a). HPLC analysis revealed metabolism of cyclic Ahx_2 confirming the activities of NylA and NylB (Figure 2.1-4). Although expression of NylC was targeted, cyclic Ahx-oligomers greater than the dimer were not metabolized by *P. putida* NYLON-ABC. *In vitro* assays using crude extracts of nylonase-expressing strains indicated that NylC might be inactive preventing degradation of larger cyclic oligomers (Figure 2.1-4).

Overall, ALE and metabolic engineering enabled metabolism of prevalent C_6-PA monomers, linear Ahx_{2-7} oligomers, and cyclic Ahx_2, while RNA-seq revealed the corresponding metabolic pathways. Heterologous expression of nylonases enabled the hydrolysis of cyclic Ahx_2 into linear Ahx_2 (NylA) that was further degraded into Ahx (NylB). Moreover, NylB enabled the metabolism of linear Ahx_{2-7} oligomers by the sequential release of Ahx. All C_6-PA monomers, namely HMDA, Ahx, and ε-caprolactam are metabolized *via* AA in the reverse engineered strains (Figure 2.1-5).
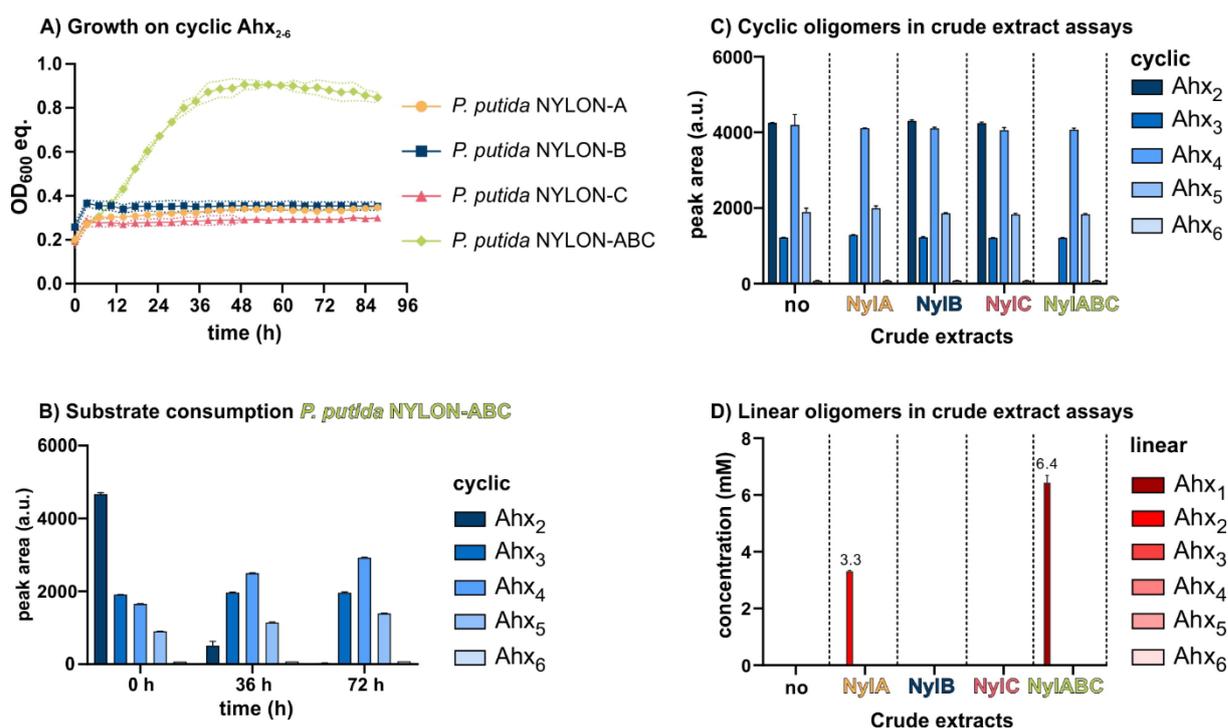
Figure 2.1-4. Metabolism of cyclic Ahx-oligomers. A) Engineered strains of *P. putida* expressing either *nylA*, *nylB*, *nylC*, or *nylABC* were cultivated with cyclic Ahx$_{2-6}$ as sole carbon and nitrogen source. **B)** HPLC analysis was performed to reveal the substrate consumption of *P. putida* NYLON-ABC that was found to only metabolize cyclic Ahx$_2$. Crude extract assays of different nylonase-expressing strains were performed with cyclic Ahx$_{2-6}$ to investigate nylonase activity. The peak area of cyclic Ahx-oligomers **(C)** and concentration of linear Ahx-oligomers **(D)** is shown after a reaction time of 6 h. *P. putida* NYL, not expressing any nylonase (no), was compared as control reaction. For all data sets the mean values and standard deviations of three replicates are shown (n=3).

2.1.4.4   Microbial upcycling of PA6 hydrolysates to PHB

The deep engineering and characterization of *P. putida* KT2440 NYLON-ABC paved the way for enabling microbial upcycling of PA6 materials, thereby providing a novel end-of-life solution for materials such as textiles and fishing gear. As potential upcycling product, *P. putida* KT2440 natively synthesizes PHA. However, typically a carbon to nitrogen ratio (C:N) of 30:1 is used to produce PHA in batch cultivations, while PA6 has a C:N ratio of 6:1, making it unsuitable for native PHA production. To circumvent the need of nitrogen-limiting conditions for PHA production, strain *P. putida* NYLON-ABC was transformed with pSEVA6311::*phaCAB* enabling inducible expression of *phaCAB* from *Cupriavidus necator* H16 for PHB production. In parallel, the PP_5003-6 operon was deleted to avoid a possible depolymerization of PHB by the native PHA depolymerase

(PP_5004). The resulting *P. putida* NYLON-ABC ΔPHA, pSEVA6311::*phaCAB*, designated as *P. putida* NYLON-PHB, was cultivated in mineral salts medium supplemented with HMDA, Ahx or ε-caprolactam as sole carbon and nitrogen sources. Induction of *phaCAB* resulted in the production of PHB from all three C_6-PA monomers. Using HMDA as substrate, PHB was produced to 13.2 ± 1.0 % of the cell dry weight (CDW) (Table 2.1-1). For Ahx and ε-caprolactam, 7.7 ± 0.2 % and 8.2 ± 0.3 % PHB were produced, respectively. The lower growth rate with HMDA ($\mu = 0.080 \pm 0.003$ h^{-1}) compared to Ahx ($\mu = 0.110 \pm 0.005$ h^{-1}) and ε-caprolactam ($\mu = 0.101 \pm 0.002$ h^{-1}) might translate into increased PHB production as it competes with biomass formation. This is also indicated by the lower CDW when HMDA was used as substrate. In order to demonstrate microbial upcycling of nylon into a biodegradable polymer, PHB production from a PA6 hydrolysate was investigated. For this, PA6 was hydrolyzed using acid hydrolysis, resulting in a soluble mixture containing Ahx and linear Ahx_{2-7} (Figure S5.1-10). The PA6 hydrolysate was adjusted to contain concentrations of Ahx and Ahx-oligomers that are C-mol equivalent to 30 mM Ahx. Using this hydrolysate as feedstock, 7.0 ± 0.3 % PHB of the CDW were produced, which is not significantly (*p*-value < 0.05) different from using pure Ahx as substrate. The ability to upcycle nylon monomers and PA6 hydrolysates with equal efficiency highlights the power of the engineered *P. putida* NYLON-PHB for enabling novel sustainable end-of-life solutions for synthetic PA materials. Thereby, microbial upcycling circumvents the need for costly separation and purification steps of Ahx monomer and oligomer fractions by funneling them into the central metabolism and converting them to PHB as sole product (Figure 2.1-5).

Table 2.1-1. Production of PHB by engineered *P. putida* NYLON-PHB from PA-related substrates. The strain was cultivated in 50 mL mineral salts medium supplemented with 30 mM of the indicated substrate. For the PA6 hydrolysate, the total content of Ahx and Ahx-oligomers was adjusted to be equimolar to 30 mM of monomeric Ahx. Cultivations were performed until the optical density at 600 nm remained constant indicating the end of light-scattering PHB production.

substrate	CDW (g L^{-1})	PHB (%)
HMDA	0.67 ± 0.05	13.2 ± 1.0 %
Ahx	1.53 ± 0.16	7.7 ± 0.2 %
ε-caprolactam	1.45 ± 0.13	8.2 ± 0.3 %
PA6 hydrolysate	1.71 ± 0.09	7.0 ± 0.3 %
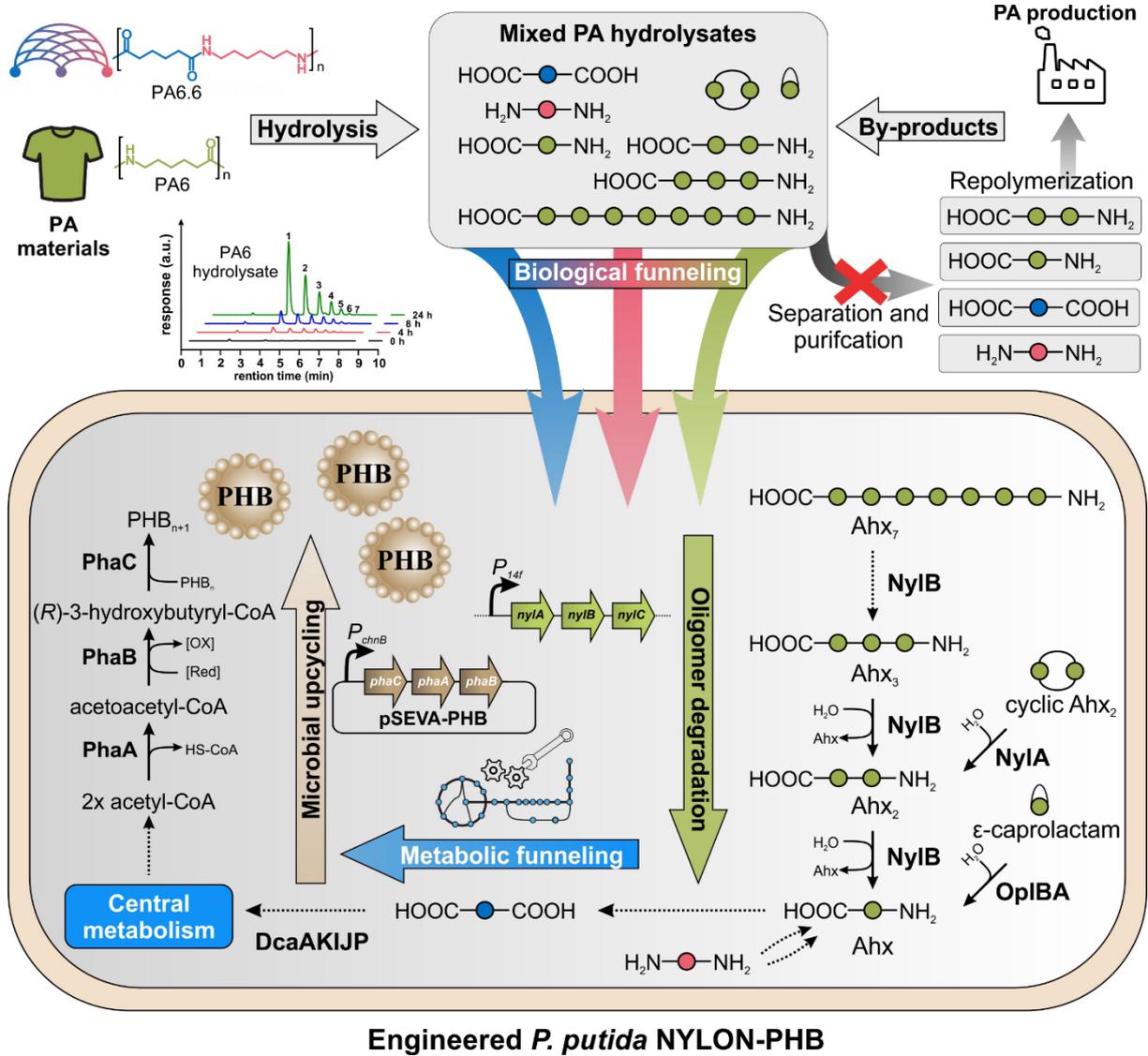
Figure 2.1-5. Microbial upcycling of PA materials to polyhydroxybutyrate. PA materials are depolymerized using acidic hydrolysis. The resulting hydrolysates consists of various monomers and oligomers that are channelized into engineered *P. putida* KT2440 NYLON-PHB and funneled into its central metabolism. Heterologous expression of *phaCAB* enables production of PHB in the presence of excess nitrogen. Using this approach, costly separation and purification steps for traditional recycling strategies can be avoided.

2.1.5 Discussion

In the present study, we used deep metabolic engineering guided by laboratory evolution to establish the synthetic metabolism of PA-related feedstocks in the microbial host *P. putida* KT2440. This yielded the highly engineered strain *P. putida* NYLON-ABC that is able to funnel various PA monomers as well as cyclic and linear oligomers of PA6 into its central metabolism. RNA-seq revealed the synthetic metabolic pathways of HMDA, Ahx, and ε-caprolactam and identified key regulators and transporters required for metabolism of PA-derived feedstocks. Of note, most modifications could be obtained through laboratory evolution, hinting at how natural evolution could occur on nylon pollutants. This highlights the versatile metabolism of *P. putida* KT2440, which is leveraged towards non-natural substrates by metabolic engineering in this study. Synthetic PHB production from C_6-PA monomers and PA6 hydrolysates with a high C:N ratio was successfully demonstrated using *P. putida* NYLON-PHB. Hence, we enable the conversion of PA to a biodegradable polymer, providing a novel end-of-life option for PA wastes such as fishing nets and clothing.

Currently, the vast majority of PA are landfilled or incinerated, as traditional recycling methods are not economically viable (Minor et al., 2023; Textile Exchange, 2022). Mechanical and chemical recycling require highly pure feedstocks while simultaneously yielding reduced-quality products (Alberti et al., 2019; Pietroluongo et al., 2020). Moreover, PA and other plastic materials often contain coatings, plasticizers, dyes and many more additives that increase the complexity of the final material. Such complexity is the key factor that makes current recycling strategies inefficient, as they require laborious and expensive purification and separation steps (Jung et al., 2023). Traditional recycling faces enormous challenges with increasingly complex polymers, blends, composites, and mixed waste streams (Zuin and Kümmerer, 2022). There is therefore an urgent need for feedstock-flexible recycling technologies that can deal better with mixtures of chemicals and materials.

Our strategy of combining chemical hydrolysis with microbial upcycling overcomes the drawbacks of traditional recycling as complex hydrolysates can be funneled into the central metabolism of our engineered microbial host. Thereby, costly separation of monomers can be avoided. In addition, the robustness of Pseudomonads towards solvents and feedstock

contaminants eliminates the need for additional pretreatment steps (Weimer et al., 2020; Wynands et al., 2019). Further engineering of *P. putida* might increase PHB production to maximize the yields of value-added products and to further optimize the overall process. However, the potential of the *P. putida* NYLON strains goes well beyond PHB production. Our results expand the catabolic range of *P. putida* into the realm of polyamides, making them suitable as carbon and nitrogen sources for biotechnological processes. Pseudomonads have been intensively studied for the bio-based production of a wide range of value-added chemicals (Nikel and de Lorenzo, 2018). This vast store of knowledge can be leveraged by our work, which unlocks production of these chemicals from plastic waste by enabling a transition from sugars to PA as feedstock. This further highlights the superiority of microbial upcycling over traditional recycling strategies.

Ideally, future research on nylonases or other, yet unknown amidases, can replace chemical hydrolysis with enzymatic depolymerization of PA. Thereby, a holistic bio-based end-of-life solution for PA could be establish with greatly improved energy and material balances. Such research is currently performed for NylC and yielded a thermostable mutant able to depolymerize PA6 powder (Negoro et al., 2012). Moreover, the recent development of high-throughput screenings for directed evolution of nylonases is a promising advance to establish biodegradation of PA materials (Puetz et al., 2023). Combining such strategies for enzymatic PA degradation with the present breakthrough on microbial upcycling of PA hydrolysates has the huge potential to pioneer sustainable end-of-life solutions for the millions of tons of plastic waste that are currently landfilled and incinerated. Connecting this work with additional synthetic routes to feed other hydrolysates such as of PET (Narancic et al., 2021), PE, or PS (Sullivan et al., 2022) into biological catalysts will revolutionize the end-of-life solutions not only for pure plastics but also polymer blends and mixtures that are currently not amenable to traditional recycling.

2.1.6 Materials and methods

2.1.6.1 Strains and culture conditions

All chemicals used in this study were obtained from Sigma-Aldrich (St. Louis, MO, USA) or Merck (Darmstadt, Germany) unless stated otherwise. All strains used in this study are listed in Table S1. *P. putida* KT2440 strains were cultivated in 4-fold buffered (15.52 g L^{-1} K$_2$HPO$_4$ and 6.52 g L^{-1} NaH$_2$PO$_4$) mineral salt medium (MSM) (Wierckx et al., 2005). Pre-cultures contained 20 mM glucose and 3 mL of culture volume was cultivated in 14 mL culture tubes (Greiner bio-one, Frickenhausen, Germany) in a Multitron shaker (Infors, Bottmingen, Switzerland) at 30 °C and 180 rpm shaking speed. For online growth detection, a Growth Profiler 960 (Enzyscreen, Heemstede, the Netherlands) was used. This instrument uses image analysis to analyze cultures in transparent bottom 96-well microtiter plates. The resulting green values (G-values, based on the number of green pixels) correlate with the optical density of a cell culture. These G-values were converted to OD$_{600}$ equivalents using a calibration curve for *P. putida* KT2440. Main cultures were grown in 96-well plates (CR1496dg) with a volume of 200 μL at 30 °C and 225 rpm shaking speed with an amplitude of 50 mm. Images for growth analysis were taken every 30 minutes. HMDA, Ahx, Ahx$_2$ (Ambeed, USA) Ahx$_3$ (Ambeed, USA), and ε-caprolactam were used in concentrations of 15 mM as pure substrates. For preparing MSM containing the soluble PA6 fraction or cyclic Ahx fraction, 7 mg mL^{-1} of the substrate mixtures were dissolved in 4-fold buffered MSM and filtered through a 0.22 μM PES filter membrane upon growth experiments. For PHB production, 50 mL of 4-fold buffered MSM with 30 mM substrate was used containing 1 mM cyclohexanone as inducer of *phaCAB* expression and 10 μg mL^{-1} gentamycin to maintain pSEVA6311::*phaCAB*.

2.1.6.2 Plasmid cloning and strain engineering

Genomic DNA of *P. putida* KT2440 was isolated using the Monarch® Genomic DNA Purification Kit (New England Biolabs, Ipswich, MA, USA). Primers were purchased as DNA oligonucleotides from Eurofins Genomics (Ebersberg, Germany). DNA fragments were obtained by PCR using the Q5® High-Fidelity 2× master mix as DNA Polymerase (New England Biolabs, Ipswich, MA, USA). Plasmids were assembled by Gibson assembly (Gibson et al., 2009) using the NEBuilder HiFi DNA Assembly Master Mix (New England Biolabs). All plasmids and oligonucleotides used and generated in this study are listed in

Table S2 and Table S3, respectively. For the transformation of assembled DNA fragments and plasmids into competent cells of *E. coli*, a heat shock protocol was used (Hanahan, 1983). The targeted modification, deletion, and integration of genes into the chromosome of *P. putida* KT2440 was achieved by homologous recombination, applying the I-SceI-based system (Martínez-García and de Lorenzo, 2011) according to a streamlined protocol (Wynands et al., 2018). The 500-600 bp up- and downstream flanking regions (TS1 and TS2) of the selected target region were integrated into the suicide delivery vector pEMG. For the integration of codon-optimized nylonase genes from *P. ureafaciens* into *P. putida* KT2440 the intergenic region of PP_0340-1 was chosen as landing pad as the *att*Tn7-site was already occupied due to previous modifications enabling growth on adipate. The sequences of the codon-optimized genes are shown in Table S5.1-3.

2.1.6.3   Whole-genome sequencing

Genomic DNA of selected strains was purified using a Monarch Genomic DNA Purification Kit (NEB) from an overnight LB culture. Afterwards, one microgram of DNA was used for library preparation using the NEBNext® Ultra™ II DNA Library Prep Kit for Illumina® (NEB). The library was evaluated by qPCR using the KAPA library quantification kit (Peqlab, Erlangen, Germany). Afterwards, normalization for pooling was done and paired-end sequencing with a read length of 2×150 bases was performed on a MiSeq (Illumina). The sequencing output (base calls) were received as demultiplexed fastq files. The data (*e.g.* trimming, mapping, coverage extraction) were processed using the CLC Genomic Workbench software (Qiagen Aarhus A/S, Aarhus, Denmark). Reads were mapped against modified versions of the *P. putida* KT2440 genome that included the genomic integrations. The relevance of identified mutations was assessed manually. Sequencing data are stored in the NCBI Sequence Read Archive under BioProject PRJNA1023861.

2.1.6.4   RNA sequencing

Strains of *P. putida* were pre-cultured in MSM with AA or Ahx as described above for 16 h. For RNA sequencing, fresh cultures were inoculated with a starting OD_{600} of 0.1 and cells harvested after entering the mid-exponential phase. Total RNA was isolated using the Quick-RNA^{TM} Microprep Kit (Zymo Research, Irvine, CA, USA). RNA sequencing was performed by Genewiz (Leipzig, Germany). Transcriptome analysis was performed using CLC

genomics workbench v.20 (Qiagen, Germany). Low quality reads (0.05), ambiguous nucleotides, and adapter sequences were trimmed after quality control. Reads were mapped to the genome of *P. putida* KT2440-AA and transcripts per million (TPM) were calculated with costs for mismatch = 2, insertion = 3 and deletion = 3 as well as length and similarity fraction of 0.9 for both strands with a maximum number of hits for a read of 10. 'Differential Expression in Two Groups' of CLC was used for determining differentially expressed genes between strains and conditions tested and for drawing volcano plots. Transcriptomic data were deposited at Gene Expression Omnibus (GEO) of NCBI under accession number GSE244960.

2.1.6.5 High-Performance Liquid Chromatography analysis

Samples were taken from liquid cultivations or *in vitro* assays and were filtered through an AcroPrep™ 96-well filter plate (Pall Corporation, Port Washington, NY, USA) to obtain the analytes for HLPC analysis. HPLC analysis was performed using a 1260 Infinity II HPLC equipped with a fluorescence detector (FLD) and a diode array detector (DAD) (Agilent, Santa Clara, California, USA). To analyze linear substrates harboring one or two primary amines, pre-column derivatization using *o*-phthaldialdehyde (OPA) reagent (Sigma-Aldrich, ready-to-use-mix) was performed. For separation of the derivatized molecules, the Kinetex® 2.6 μm EVO C18 100 Å column (100 x 2.1 mm) (Phenomenex, California, USA) was used. As mobile phase, 10 mM sodium-borate buffer (A) (pH 8.2) and methanol (B) was used (70 % A–30 % B) applying increasing gradients of methanol (70 % B after 10 min, 100 % B after 12 min, 100 % B for 1 min, 30 % B after 14 min, 1 min post-run). The flow was adjusted to 0.4 mL min^{-1} at 40 °C. Derivatized molecules were detected using a FLD with an excitation of $\lambda = 340$ nm and an emission of $\lambda = 450$ nm. Detection of cyclic Ahx-oligomers was performed using the DAD with an absorption of $\lambda = 210$ nm (reference $\lambda = 300$ nm). Cyclic oligomers of Ahx were separated using a Zorbax Eclipse XDB-C8 column (4.6 × 150 mm) with a H_2O_{MilliQ}:MeOH ratio of 60:40 and a constant flow of 0.5 mL min^{-1} at 40 °C. As no analytical standards were available for cyclic Ahx-oligomers, the corresponding peak area was analyzed allowing semi-quantitative analysis.

2.1.6.6 PHB quantification *via* gas chromatography

PHB quantification was performed using acidic methanolysis and gas chromatography (GC) analysis as described in Li *et al.* (2020). For this, cells were harvested by centrifugation at $5000 \times g$ for 10 min and washed with H_2O_{MilliQ}. Prior to analysis, samples were lyophilized overnight in a Christ LT-105 freeze drier (Martin Christ Gefriertrocknungsanlagen, Osterode am Harz, Germany). Five to fifteen milligram of lyophilized cells were mixed with 2 mL acidified methanol (15 % (v/v) H_2SO_4) and 2 mL chloroform containing methyl benzoate as internal standard in a pyrex tube. The tubes were sealed and incubated at 100 °C for 3 h. After cooling the tubes for 2 min, 1 mL of H_2O_{MilliQ} was added and the solution was mixed. The phases were allowed to separate and the organic phase was filtered through cotton wool before further analysis. The 3-hydroxybutanoic acid methyl ester was quantified using an Agilent 7890A Gas Chromatograph equipped with a HP Innowax column (30 m × 0.25 mm × 0.5 µm) and a flame ionization detector (FID). An oven ramp cycle was employed as follows: 120 °C for 5 min, increasing by 3 °C/min to 180 °C, 180 °C for 10 min. A 10:1 split was used with helium as the carrier gas and an inlet temperature of 250 °C. Commercially available 3-hydroxybutanoic acid was methylated as described above and used as standard to quantify PHB monomers.

2.1.6.7 Production of soluble PA fractions

The soluble fraction of PA6 was obtained from PA6 pellets (B4Plastics, Dilsen-Stokkem, Belgium). Soluble oligomers were obtained by stirring 100 g L^{-1} of PA6 material in H_2O_{MilliQ} for 72 h. After that, the sample was filtrated using a bottle top filtration unit (0.22 µM PES membrane). The filtrate was subjected to a rotary evaporator (Rotavapor R-210, Büchi, Flawil, Switzerland) for 4 h at 40 °C and 60 mbar to receive a white, solid fraction of Ahx-oligomers. The cyclic Ahx_{3-6} mixture was prepared from the cyclic Ahx_{2-6} mixture that was kindly donated by Dai-ichiro Kato (Kagoshima University, Japan) (Negoro et al., 2021). To obtain cyclic Ahx_{3-6}, *P. putida* NYLON-ABC was cultivated for 96 h in MSM supplemented with the cyclic Ahx_{2-6} mixture. After that, the mixture was filter-sterilized and HPLC analysis confirmed the absence of cyclic Ahx_2 that was metabolized by the strain. The resulting mixture containing cyclic Ahx_{3-6} was used for screening experiments.

2.1.6.8 *In vitro* assays

Cells of nylonase-expressing strains were harvested during the exponential phase (OD_{600} = 2.0) from an MSM cultivation supplemented with 20 mM glucose. Four milliliter of culture was centrifuged at 21,000 × g at 4 °C for 2 min. The cell pellet was resuspended in 2 mL of 100 mM phosphate buffer (pH 7.5). For cell lysis, ultra-sonication was performed using an UP200S (Hielscher, Teltow, Germany) with an amplitude of 55 and 30 s lysis and chill for three times. To remove cell debris from the crude extracts, samples were centrifuged at 21,000 × g at 4 °C for 10 min. For the final assay, 500 µL of the obtained supernatant was mixed with 500 µL of cyclic Ahx_{2-6} solution (7 mg ml^{-1}) that was filtered through a 0.22 µM PES filter membrane.

2.1.6.9 Preparation of the PA6 hydrolysate

One gram of PA6 pellets was incubated in 10 mL of 50 % (v/v) H_2SO_4 for 24 h at 100 °C using an oil bath. After that, the soluble hydrolysate was filtered through a 0.22 µM PES filter membrane and subsequently diluted 10-fold with H_2O_{MilliQ}. Next, $Ca(OH)_2$ was added under agitation until a pH of 7 was reached. The precipitating $CaSO_4$ was removed by filtration through a 0.22 µM filter paper. For growth experiments, components of MSM were added to this mixture and filtered through a 0.22 µM PES membrane filter to obtain the sterile PA6 hydrolysate for growth and PHB production experiments.

2.1.6.10 In silico tools

Promoters for *P. putida* were predicted using SAPPHIRE (Coppens and Lavigne, 2020). Prediction of protein domains were performed with InterPro (Paysan-Lafosse et al., 2022). Operons were predicted using the Operon Mapper (Taboada et al., 2018). Protein structures were predicted using ColabFold (Mirdita et al., 2021). DNA and protein sequences were aligned to the nucleotide collection (nr/nt) of the NCBI database using BLASTn and BLASTp (Sayers et al., 2022). Gene annotations were performed based on the *Pseudomonas* genome database that can be accessed *via* https://pseudomonas.com/ (Winsor et al., 2016).

2.1.7 Declaration of competing interest

The authors declare no competing interest.

2.1.8 Acknowledgements

2.2 Increasing the diversity of nylonases for polyamide degradation

de Witt, J.[1], Ostheller, M-E.[2], Jensen, K.[3], van Slagmaat C.A.M.R.[4], Polen, T.[1], Wynands, B.[1], and Wierckx, N.[1][*] (2024).

[1] Institute of Bio- and Geosciences IBG-1: Biotechnology, Forschungszentrum Jülich, Jülich, Germany

[2] Aachen-Maastricht Institute for Biobased Materials (AMIBM), Maastricht University, Brightlands Chemelot Campus, Urmonderbaan 22, 6167 RD Geleen, The Netherlands

[3] Novozymes A/S, Biologiens Vej 2, Kgs. Lyngby DK-2800, Denmark

[4] B4Plastics BV, IQ-parklaan 2A, 3650, Dilsen-Stokkem, Belgium

[*] Corresponding author

2.2.1 Abstract

Global production of synthetic polyamides (PA), or nylons, is increasing while recycling rates are currently below 5 % contributing to the global plastics crisis. Enzymatic depolymerization is a powerful strategy to overcome the drawbacks of mechanical and chemical recycling and has the potential to increase PA recycling rates. However, enzymatic depolymerization of PA is currently limited to a small group of nylonases (NylC) that exhibit low activities making them unsuitable for efficient enzymatic recycling. In this study, we extend the diversity of nylonases by library screenings and *in silico* analysis. Six novel nylonase candidates were successfully purified that showed varying sequence identities ranging from 84.2 % to 30.0 % towards the previously characterized $NylC_{p2}$ from *Paenarthrobacter ureafaciens*. Activity of some nylonase candidates towards cyclic PA-oligomers and polymeric substrates was confirmed *via* the detection of soluble degradation products. These nylonases were also active on synthesized poly(ester-amides) (PEA), and this activity was synergistically increased by combination with the cutinase LCC. Overall, our discoveries greatly increase the input of NylC enzymes for future enzyme engineering strategies to boost their activities, and they show the potential of PEA for tuning the biodegradability of performance polymers. Thereby, this study leads the path for developing efficient enzymatic PA and PEA depolymerization processes, revealing significant insights into combining the contrary polymer parameters of performance and biodegradability.

2.2.2 Introduction

Synthetic polyamides (PA), or nylons, are characterized by their durability and high tensile strength, leading to their widespread application in the textile, fishing gear, and automotive industry. PA6 and PA6.6 are the most industrially relevant PA and are obtained by ring-opening polymerization of ε-caprolactam, that is the lactam of 6-aminohexanoate (Ahx), and polycondensation of adipic acid and 1,6-hexamethylenediamine, respectively. Despite an increasing production, PA recycling rates are below 5 % contributing to the global plastics crisis as the majority of post-consumer PA is landfilled (Minor et al., 2023; Textile Exchange, 2022). The mostly linear cradle-to-grave lifespan of PA can be explained by the limitations of traditional recycling strategies. Mechanical recycling, performed by melting and re-extrusion, typically requires highly pure feedstocks while yielding reduced-quality products (Pietroluongo et al., 2020). Consequently, the materials undergo downcycling that ultimately leads to their disposal. Chemical recycling, on the contrary, depolymerizes the material into its monomers and oligomers, which can then be purified and re-polymerized thereby maintaining the material's properties. However, chemical depolymerization, such as for PA6, typically requires high amounts of energy as well as expensive and often non-recyclable catalysts while being sensitive towards feedstock contaminations (Alberti et al., 2019). Contrary to this, enzymatic depolymerization displays a sustainable solution for the breakdown of plastics as enzymes operate at moderate conditions compared to chemical processes, catalyze selective reactions, and avoid toxic chemicals (Ellis et al., 2021). For poly(ethylene terephthalate) (PET), enzymatic recycling is advancing towards commercial implementation due to the design of tailored PETase variants (Bell et al., 2022; Bollinger et al., 2020b; Tournier et al., 2020). Moreover, techno-economic analyses predict that enzymatic recycling could become cost-competitive with virgin PET production if key cost drivers can be reduced (Singh et al., 2021; Uekert et al., 2022). Recent approaches also focused on combining chemical hydrolysis with biological catalysis, which allows metabolic funneling of mixed hydrolysates and subsequent upcycling to value-added products using engineered microorganisms. Such hybrid strategies were successful demonstrated for PET (Sullivan et al., 2022) and PA (de Witt *et al*., manuscript in preparation).

Although natural PAs are ubiquitous in nature, such as in proteins or silk, enzymatic depolymerization of synthetic PAs is rare. In fact, only a small group of Ahx-oligomer

hydrolases, designated as nylonases, is reported to hydrolyze the amide bonds of synthetic PA6 oligomers. The Ahx-cyclic-dimer hydrolase (NylA) specifically converts the cyclic Ahx-dimer (Ahx$_2$) into linear Ahx$_2$ (Kinoshita et al., 1975). NylB acts as Ahx-oligomer exohydrolase and degrades linear Ahx-oligomers by an exo-type mechanism resulting in the sequential release of Ahx (Kinoshita et al., 1981). The third nylonase, NylC, is an Ahx-oligomer endohydrolase and degrades both cyclic and linear Ahx-oligomers with a degree of oligomerization greater than three (Negoro et al., 1992). All three nylonases (NylA$_{p2}$, NylB$_{p2}$, and NylC$_{p2}$) were discovered on plasmid pOAD2 in *Paenarthrobacter ureafaciens* that was isolated from wastewater of a PA-manufacturing plant (Negoro, 2000; Okada et al., 1983). Interestingly, activity of nylonases is limited towards synthetic Ahx-oligomers while no activity was reported to a variety of natural amides (Kinoshita et al., 1977; Kinoshita et al., 1981).

NylC is the most promising nylonase for PA depolymerization due to its endo-cleavage mechanism and specificity for larger Ahx-oligomers. Initially, NylC is expressed as inactive precursor protein. After post-translational auto-cleavage between N266 and T267, which results in the formation of an α- (27.4 kDa) and β-subunit (9.4 kDa), structural re-assembly generates an active NylC enzyme (Kakudo et al., 1993). Based on this characteristic, NylC is classified as a member of the N-terminal nucleophile- (N-tn) hydrolase superfamily. Besides the D308-D306-T267 catalytic triad, NylC also possesses Y146 and K189 as additional catalytic or substrate-binding residues that are required for substrate hydrolysis (Negoro et al., 2023). Enzyme engineering of NylC$_{p2}$ resulted in a quadruple mutant that showed increased thermostability and exhibited catalytic activity towards powdered and thin-layered PA6, PA6.6, and PA6.6-co-6.4 (Nagai et al., 2014; Negoro et al., 2012). Recently, the activity of this mutant was further increased by directed evolution (Puetz et al., 2023). Two highly similar homologs of NylC$_{p2}$ were identified in *Agromyces* sp. KY5R (NylC$_A$) and *Kocuria* sp. (NylC$_K$) that share 98.6 % and 95.8 % sequence identity towards NylC$_{p2}$ (Yasuhira et al., 2007). Until today, only these three highly similar NylCs were characterized in literature highlighting the limited enzymological diversity, which severely limits the potential of enzymatic PA depolymerization.

In this study, we aimed to increase the diversity of characterized NylCs with activities towards PA-related substrates including the emerging group of poly(ester-amides) (PEA). Whereas the majority of consumer products that are traditionally made of tough PA require a high durability in the practical sense, the need for rapid biodegradation of emitted microplastics therefrom into the environment poses a paradoxical issue. Hence, this study aims to provide detailed insights into both enzymatic degradation and strategic polymer design to align material properties with biodegradability. For this, novel NylC candidates should be identified by library screenings and *in silico* analyses. Successfully purified NylC candidates should be subjected to activity assays using Ahx-oligomers as well as polymeric materials as substrates. Thereby, this study greatly increases the enzymological diversity of NylCs for future enzyme engineering, thereby facilitating the development of enzymatic PA recycling processes. In parallel, key insights into polymer design should be revealed that allow the combination of both biodegradability and performance, which often are opposing polymer features. By combining enzymatic degradation and architectural design of PEA, this study facilitates the shift towards a more circular plastics economy.

2.2.3 Results and discussion

2.2.3.1 Screening and expression of novel NylC candidates

To increase the diversity of NylCs, public and internal databases were screened for homologs of $NylC_{p2}$ (Negoro et al., 1992) (UniProt: Q79F77). We also performed enrichment cultures of compost samples using PEA to isolate strains with putative nylonase activities. This led to the isolation of a *Rhodococcus* sp. and a *Gordonia* sp. as revealed by 16S rDNA analysis and subsequent whole-genome sequencing. Since the characterized $NylC_{p2}$, $NylC_A$, and $NylC_K$ are closely related, we screened the obtained datasets *in silico* for NylC candidates with different amino acid sequences towards $NylC_{p2}$ to yield a diverse set of enzyme candidates. Apart from $NylC_{p2}$, six NylC candidates ($NylC_{1-6}$) were successfully expressed and purified, each with varying amino acid sequence identities compared to $NylC_{p2}$ (Table 2.2-1, Figure 2.2-1). Multiple sequence alignments revealed the presence of the typical N/T autocleavage site in all NylC candidates classifying them into the N-tn hydrolase superfamily (Figure 2.2-1). Moreover, the D308-D306-T267 catalytic triad of $NylC_{p2}$ was highly conserved in $NylC_{1-6}$ (Table 2.2-1, Figure 2.2-1). $NylC_{1-4}$ also possessed the two

additional catalytic residues, namely Y148/Y130/Y137/Y120 and K191/K173/K180/K163, required for PA hydrolysis as revealed for $NylC_{p2}$. In $NylC_5$ and $NylC_6$, these additional catalytic residues were less conserved since Y146 was replaced by F130/F129 and no K could be identified by multiple sequence alignments at position K189 of $NylC_{p2}$. Using ColabFold (Mirdita et al., 2021), the structures of $NylC_{1-6}$ were predicted and aligned to $NylC_{p2}$. Structural alignments revealed that K244 of $NylC_6$ and K189 of $NylC_{p2}$ were in close proximity indicating that $NylC_6$ harbors all catalytic residues required for PA hydrolysis. Although $NylC_5$ contained K242, structural alignments indicated an incorrect arrangement of this residue as it was opposed to K189 of $NylC_{p2}$ (Figure 2.2-2). Overall, structural alignments revealed that the catalytic triads are highly conserved in all NylC candidates compared to $NylC_{p2}$ (Figure 2.2-2). Moreover, $NylC_5$ and $NylC_6$ differ from $NylC_{1-4}$, as the additional catalytic residues were less conserved, which might influence their activity towards PA.

Table 2.2-1. Overview of NylC enzymes. The amino acid sequence identity towards $NylC_{p2}$ is shown as well as the predicted molecular weight of the α- and β-subunit upon post-translational autocleavage with C-terminal His_6-tag. Multiple sequence alignments and structural alignments indicated the putative catalytic triads of $NylC_{1-6}$. The melting temperature (T_m) of purified $NylC_{1-6}$ was determined by nano differential scanning fluorimetry. Sequences of $NylC_{1-6}$ are shown in Table S5.2-1.

Protein ID	Donor organism	Sequence identity (%)	Molecular weight (α + β) (kDa)	Putative catalytic triad	T_m (°C)	Reference
$NylC_{p2}$	*Paenarthrobacter ureafaciens*	100	27.4 + 9.4	D308, D306, T267	52	Kinoshita et al. (1981)
$NylC_A$	*Agromyces* sp. KY5R	98.6	27.4 + 9.4	D308, D306, T267	60	Yasuhira et al. (2007)
$NylC_K$	*Kocuria* sp.	95.8	27.4 + 9.4	D308, D306, T267	67	Yasuhira et al. (2007)
$NylC_1$	*Leucobacter chromiiresistens* JG 31	84.2	28.0 + 10.4	D310, D308, T269	58.4	This study
$NylC_2$	*Microbacterium oxydans*	62.5	26.0 + 10.2	D292, D290, T251	67.4	This study
$NylC_3$	*Streptomyces* sp. 63005	61.2	26.4 + 10.2	D298, D296, T257	63.9	This study
$NylC_4$	*Variovorax boronicumulans*	48.4	25.9 + 9.3	D292, D290, T251	82.9	This study
$NylC_5$	*Gordonia* sp.	31.7	24.3 + 12.6	D289, D287, T248	78.1	This study
$NylC_6$	*Rhodococcus* sp.	30.0	25.1 + 11.7	D291, D289, T250	74.9	This study
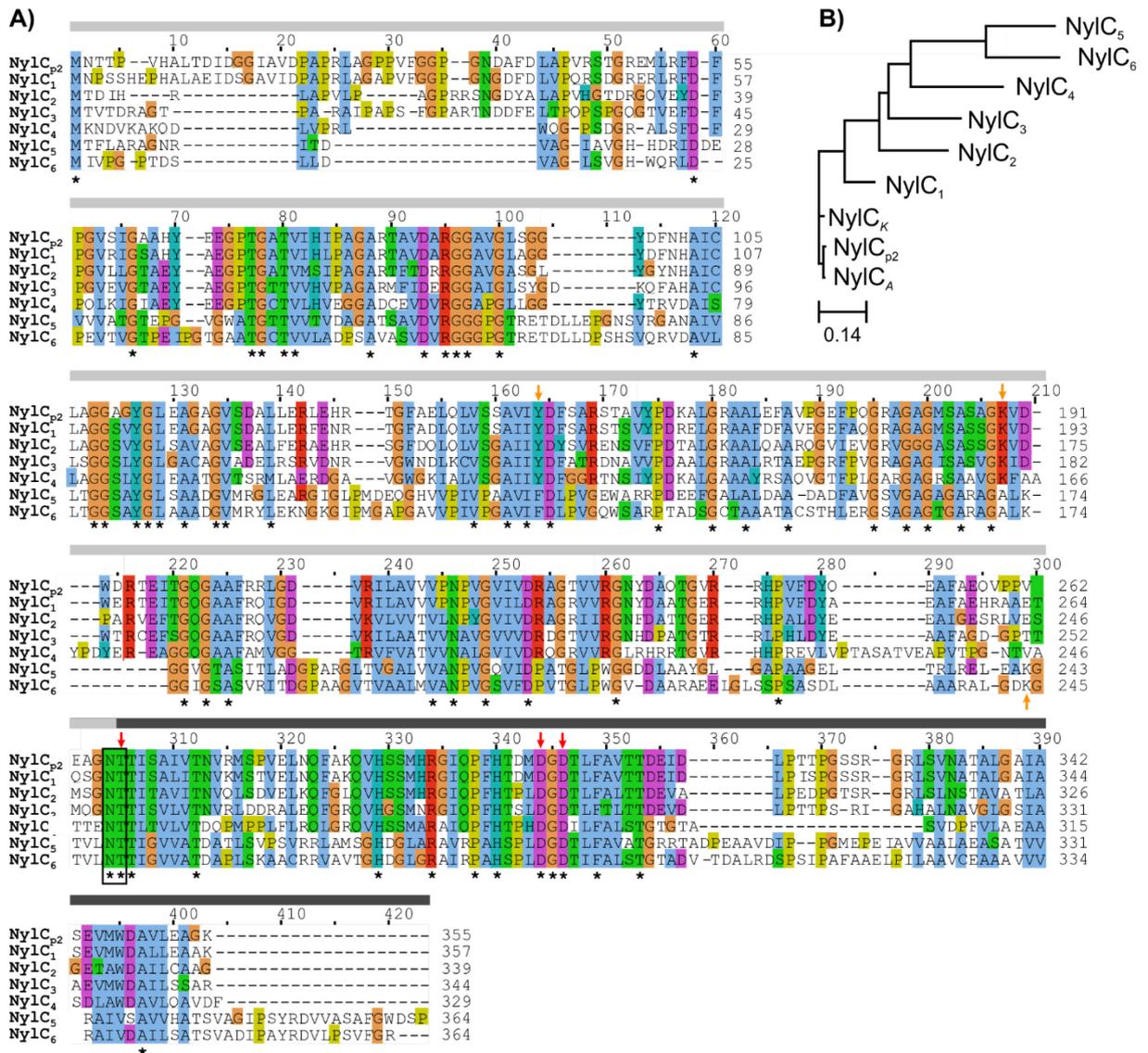
Figure 2.2-1. Multiple sequence alignments and phylogenetic analysis. A) T-Coffee alignment algorithm (Notredame et al., 2000) was used for the multiple sequence alignment using the EMBL-EBI tool (Madeira et al., 2022). Amino acids are colored based on Clustal X 2.0 default coloring (Larkin et al., 2007). Conserved amino acids are indicated with an asterisk (*). The D-D-T catalytic residues (red arrows) and substrate-binding residues (Y/F and K) (orange arrows) are highlighted, while the N/T autocleavage site is enclosed in a black box. The grey and black lines indicate the α- and β-subunits respectively. **B)** Phylogenetic tree of NylCs. The scale bar represents the number of changes per nucleotide.
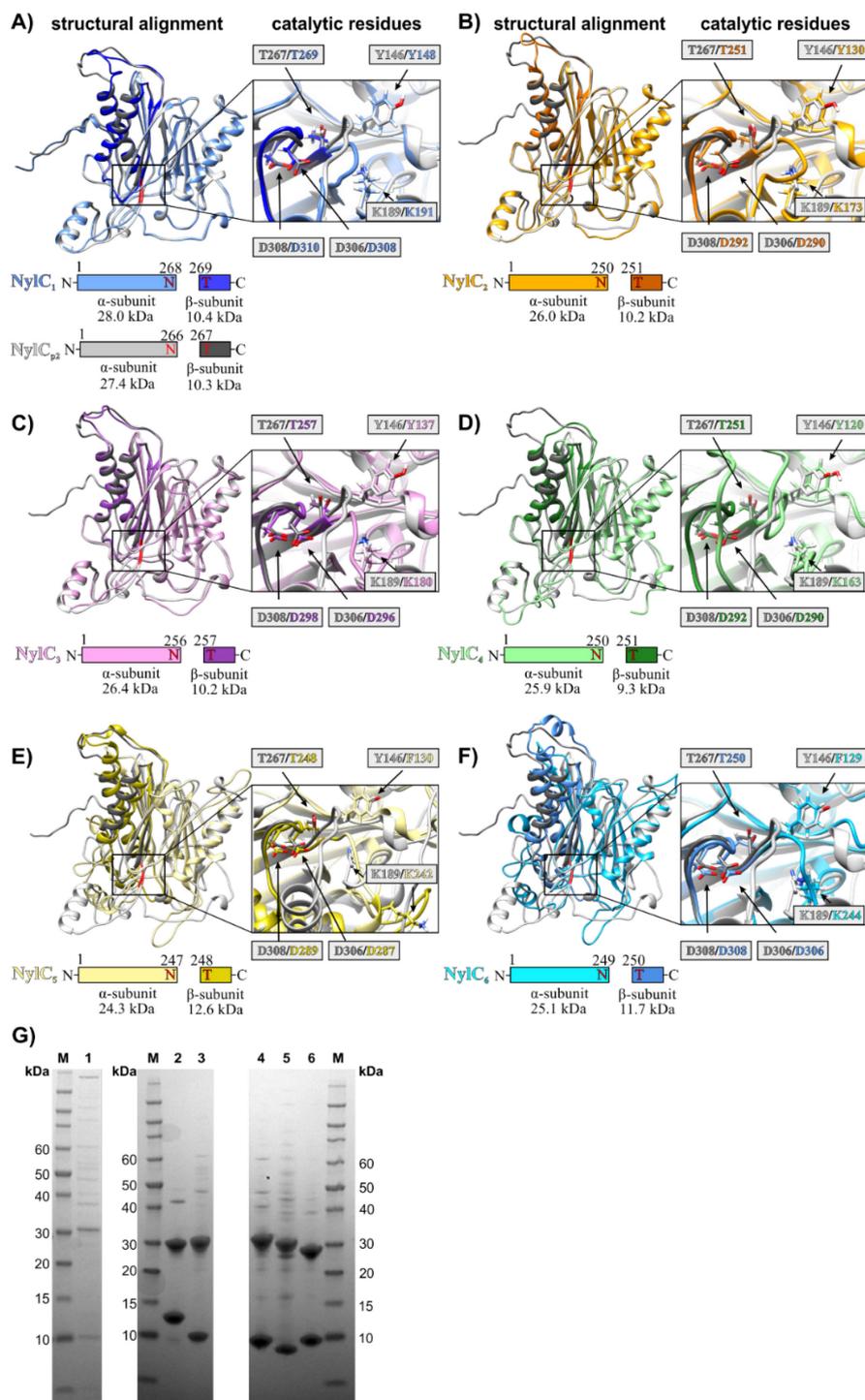
Figure 2.2-2. Structural alignments of NylC$_{p2}$ and NylC$_{1-6}$ and enzyme purification. (A-F) Protein structures of NylC$_{1-6}$ were predicted using ColabFold (Mirdita et al., 2021) and were aligned to NylC$_{p2}$. The holistic structural alignments are shown as well as the alignments of the catalytic residues (box). The N/T-autocleavage site is highlighted in red. **(G)** SDS-PAGE of purified NylC$_{1-6}$. The lanes were loaded as followed: Marker (M), NylC$_1$ (1), NylC$_5$ (2), NylC$_6$ (3), NylC$_3$ (4), NylC$_4$ (5), NylC$_2$ (6). The two bands correspond to the α- and β- subunits.

NylC$_{1-6}$ were expressed with a C-terminal His$_6$-tag allowing their purification. Although the ratio of cleaved (α- and β-subunit) to uncleaved (precursor) NylC$_{p2}$ was reported to increase from approximately 10 % to 100 % within 48 h of incubation after purification (Negoro et al., 2023), SDS-PAGE of purified NylC$_{1-6}$ indicated that no significant amounts of precursor protein was present without prior incubation. Instead, the α- and β-subunits of NylC$_{1-6}$ were detected indicating that their precursor autocleavage might be faster compared to NylC$_{p2}$ (Figure 2.2-2). Moreover, the interaction of α- and β-subunits of NylC$_{1-6}$ were strong enough to allow purification of both subunits with a single C-terminal His$_6$-tag, which was present in the β-subunits. Unfortunately, NylC$_{p2}$ could not be expressed in *Bacillus* sp. and its heterologous expression seems to be limited to *Escherichia coli* until today (Nagai et al., 2014; Puetz et al., 2023). For commercial production of nylonases, however, expression in industrial workhorses such as *Bacillus subtilis*. is a prerequisite requiring further optimization.

Activity of NylC$_{p2}$ towards PA6 was enabled by designing thermostable mutants, as elevated reaction temperatures typically result in increased accessibility of amorphous polymer regions due to increased chain mobility (Nagai et al., 2014; Puetz et al., 2023). To investigate the thermostability and thus evaluate the potential activity towards polymeric substrates, purified NylC$_{1-6}$ were subjected to nano differential scanning fluorimetry (DSF) to determine their melting temperature (T_m). Compared to non-engineered NylC$_{p2}$ ($T_m = 52$ °C) (Negoro et al., 2012), NylC$_{1-6}$ showed higher thermostabilities ranging from $T_m = 58.4$ °C (NylC$_1$) to $T_m = 82.9$ °C (NylC$_4$) (Table 2.2-1). The overall higher thermostability indicates that NylC$_{1-6}$ might be active at higher temperatures, which might facilitate depolymerization above the glass transition temperature (T_g) of PA6 ($T_g \sim 60$ °C). Thermostability is a key factor in enzymatic polymer degradation as extensively shown for PET (Bell et al., 2022; Tournier et al., 2020). Thus, if active, NylC$_{1-6}$ might be promising candidates for enzyme engineering or shuffling to outperform the current thermostability of engineered NylC$_{p2}$ ($T_m = 88$ °C) (Negoro et al., 2012). The broad range of T_m along with varying amino acid sequence identities indicate a successful increase in the diversity of NylC candidates.

2.2.3.2   Activity towards PA6 oligomers

To test whether the $NylC_{1-6}$ candidates are true nylonases, their activities towards cyclic and linear oligomers of PA6, designated as Ahx-oligomers, were tested. Subsequent HPLC analyses were performed to detect degradation products. Although $NylC_{p2}$ was reported to hydrolyze linear and cyclic Ahx-oligomers with a degree of oligomerization greater than three, none of the $NylC_{1-6}$ candidates was active towards soluble linear Ahx oligomers (n=2-7). Instead, activity towards the cyclic Ahx-oligomer fraction (n≥2) (Negoro et al., 2021) was detected for $NylC_1$, $NylC_2$, and $NylC_5$ by the release of linear Ahx-oligomers (Figure 2.2-3). As additional control reaction, the Ahx-cyclic-dimer hydrolase from *P. ureafaciens* ($NylA_{p2}$) (Kinoshita et al., 1975) was incubated with the cyclic Ahx-oligomer fraction. As expected, this resulted in the conversion of cyclic Ahx_2 into linear Ahx_2. Activity of $NylC_1$ and $NylC_2$ on the cyclic Ahx-oligomers resulted in the release of linear Ahx_4 and Ahx_5, whereas $NylC_5$ additionally released linear Ahx_3 (Figure 2.2-3). The linear degradation products were not further hydrolyzed. In contrast to this, $NylC_{p2}$ was reported to further degrade such linear Ahx-oligomers yielding linear Ahx_2 as end-product (Kakudo et al., 1993). Interestingly, none of the soluble cyclic oligomers (n=2-6) that were detected *via* HPLC were hydrolyzed by $NylC_1$, $NylC_2$, and $NylC_5$, even though linear products were detected. This might be due to a limitation in the detection of larger, insoluble oligomers. According to this theory, the release of linear Ahx_{3-5} by the NylCs must originate from the hydrolysis of larger insoluble and thus undetectable cyclic oligomers (n>6). Consequently, $NylC_1$ and $NylC_2$ might be active towards cyclic Ahx_{8-10}, resulting in the initial ring opening to the corresponding linear oligomers, followed by subsequent degradation to linear Ahx_{4-5} by an endo-cleavage. The additional release of linear Ahx_3 by $NylC_5$, while not degrading cyclic Ahx_6, indicates activity towards cyclic Ahx_7 that is degraded to linear Ahx_{3-4} after initial hydrolysis to linear Ahx_7. To confirm the activity towards exclusively insoluble Ahx-oligomers, only the soluble fraction of cyclic Ahx-oligomers (n≤6) was tested as substrate for $NylC_{1-6}$ obtained by filtration (Figure 2.2-3). Indeed, none of the enzymes showed activity towards the soluble cyclic Ahx-oligomers as no linear degradation products were detected, suggesting that the enzymes were exclusively active on insoluble cyclic and linear Ahx-oligomers.

Overall, these results reveal that the activity and substrate specificity of $NylC_1$, $NylC_2$, and $NylC_5$ differ from that of $NylC_{p2}$ as no soluble cyclic or linear oligomers were hydrolyzed by the novel NylC enzymes. Instead, activity towards insoluble oligomers was observed, which might be accompanied by the ability to hydrolyze insoluble linear chains of PA. The inactivity of some NylC candidates highlights the diversity of the N-tn hydrolase superfamily, which complicates the identification of new NylCs based on *in silico* analyses only. The different substrate specificities of the identified NylCs compared to $NylC_{p2}$ and its close homologs indicate a much greater diversity of nylonases in nature than originally anticipated.
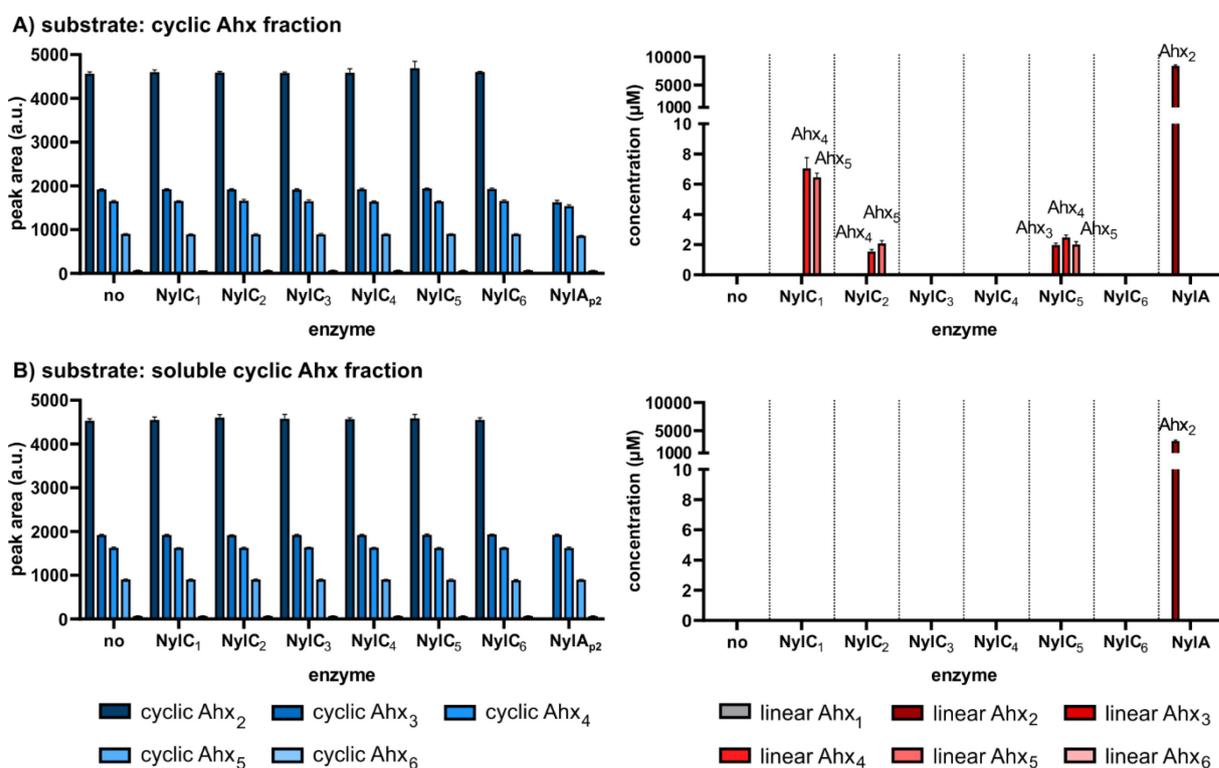
Figure 2.2-3. Activity screenings of $NylC_{1-6}$. Reactions were performed using 4 g L^{-1} cyclic Ahx-oligomers (Aco2) (Negoro et al., 2021) (A) and its soluble fraction that was obtained by filtration (B). Reactions were performed using 500 nM of purified enzyme in 50 mM phosphate buffer, pH 7.3 at 30 °C for 8 h. Cyclic and linear soluble oligomers were detected using HPLC. The mean values and standard deviations (SD) of three replicates are shown (n=3).

The activity of $NylC_1$, $NylC_2$, and $NylC_5$ towards insoluble Ahx-oligomers suggested that they might also be capable of hydrolyzing PA6 of higher molar masses. To test this, each NylC was incubated with powdered PA6 at temperatures between 30 °C and 70 °C in

increments of 10 °C. However, none of the enzymes was active towards PA6 under any of the conditions tested as no soluble oligomers were detected in the supernatants. It has to be noted that the enzymatic activity towards polymeric substrates greatly depends on several factors such as crystallinity and dispersion of the substrate. Moreover Nagai et al. (2014) discovered that even after enzymatic depolymerization of PA6, oligomers were still bound to the polymer chains through hydrogen bonding. Instead, degradation of thin-layered PA-films, which were approximately 1,000-fold thinner than the diameter of powdered PA, resulted in a highly increased reaction rate. The combination of such factors might have contributed to the apparent inactivity of NylC$_{1-6}$ towards PA6. Enzyme engineering might overcome these barriers as performed for NylC$_{p2}$, whose non-engineered version also showed no activity towards PA6 (Nagai et al., 2014).

2.2.3.3 Synthesis and enzymatic degradation of poly(ester-amides)

To demonstrate activity of NylC$_{1-6}$ towards other polymeric substrates, we performed activity assays using PEA. In contrast to well-established PA, PEA are an emerging group of polymers and combine the thermal and mechanical properties of PA with the biodegradability of polyesters (Fonseca et al., 2014; Winnacker and Rieger, 2016). To investigate if NylC$_{1-6}$ are able to depolymerize PEAs, we tested their activities towards powdered PA6.6-, PA6.10-, or PA6.6-*co*-6.10-based PEAs (PEA1-4) that contained aliphatic or branched diols to yield the desired PEAs (Table S5.2-2). Both the weight average molecular weight (Mw) and number average molecular weight (Mn) differed among the synthesized PEA ranging from 1,846-7,371 Da (Mn) and 3,587-13,814 Da (Mw), respectively (Table 2.2-2). While PEA1 displayed the highest Mn and Mw values among the PEA samples (Mn = 7,371 Da and Mw = 13,814 Da), these values still fell significantly below those of PA6 (Mn = 12,220 Da and Mw = 67,860 Da).

The differential scanning calorimetry (DSC) thermograms, showing the heating and cooling curves, revealed crucial thermal properties of PEA1-4 and PA6 (Figure 2.2-4). For PA6, two significantly distinct melting peaks were observed (T_m1 = 213 °C and T_m2 = 220 °C). In contrast, PEA2 and PEA4 showed two similar melting peaks, as both feature the first peak at a temperature of ~173 °C and a second melting peak at 210 °C, which is lower compared to PA6. This phenomenon could be attributed to the characteristic of PEA2 and PEA4

incorporating sebacic acid as a monomer. Notably, the only distinction between PEA2 and PEA4 lies in the ester monomers employed, yet their melting points exhibited similarity. Consequently, it is reasonable to anticipate that the melting point of PEA may be more significantly influenced by the amide regions rather than the ester regions. The existence of two melting peaks may reflect the presence of a secondary crystal structure or the formation of crystals of different sizes, but further investigation is required to define the precise cause. In contrast to PEA2 and PEA4, PEA1 and PEA 3, displayed a less sharp single melting peak at temperatures of 236 °C and 182 °C, respectively. Hence, PEA1 has the highest melting point from all PEA samples. These results suggest that based on the lower melting peaks of the PEA2-4 samples in comparison to PA6, those samples might need to be processed at lower temperatures than PA6, whereas PEA1 might demand a higher processing temperature than PA6.

Table 2.2-2. Polymer characteristics of PEA1-4 and PA6. Weight average molecular weight (Mw), number average molar mass (Mn) and polydispersity index (PDI) values of unprocessed PEA1-4 and PA6 granules are as well as he melting temperatures (T_m1 and T_m2), re-cooling temperature (T_{rc}), and crystallization temperature (T_c). Data means are with standard deviation (n=3).

Polymer	Mn (Da)	Mw (Da)	PDI	T_m1 (°C)	T_m2 (°C)	T_{rc} (°C)	T_c (°C)
PA 6	12220 ± 855	67860 ± 4750	5.55	213 ± 2	220 ± 2	198 ± 2	164 ± 2
PEA1	7371 ± 516	13814 ± 936	1.87	236 ± 3	-	208 ± 3	200 ± 3
PEA2	2099 ± 147	4174 ± 272	1.99	173 ± 2	210 ± 3	188 ± 3	179 ± 1
PEA3	2139 ± 159	4880 ± 341	2.28	182 ± 2	-	160 ± 2	136 ± 2
PEA4	1846 ± 129	3587 ± 231	1.94	173 ± 2	210 ± 3	189 ± 2	181 ± 3

The DSC thermograms of both PA6 and all PEA samples revealed a recrystallization temperature (T_{rc}) around ~198 °C for PA6, ~208 °C for PEA1, ~188 °C for PEA2 and PEA4, and ~160 °C for PEA3. During cooling, variations in crystal size or type, along with potential defects, may arise in the forming crystals. Upon heating, these smaller crystals (and sometimes crystal defects) can melt and recrystallize or merge into larger crystals, which subsequently melt at higher temperatures. This recrystallization peak may also indicate the presence of amorphous polymer chains that gain mobility at elevated temperatures, forming a more ordered crystalline structure, as previously documented. In the cooling curve results, PA6 exhibited a crystallization peak remaining at approximately ~164 °C (Figure 2.2-4,

Table 2.2-2). Conversely, PEA1, PEA2, and PEA4 displayed peaks at higher temperatures compared to PA6, with respective values of ~200 °C, ~179 °C, and ~181 °C. Only PEA3 exhibited a lower crystallization temperature of 136 °C.
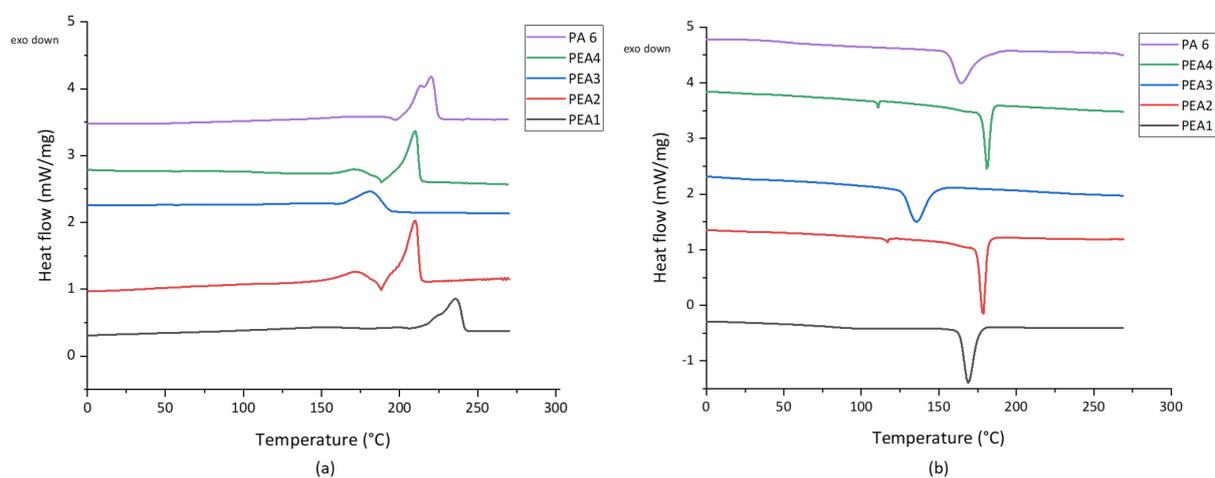
Figure 2.2-4. DSC thermograms of PEA1-4 and PA6 granules. The heating (a) and cooling (b) curves are shown.

After their characterization, the activities of $NylC_{1-6}$ towards PEA1-4 were investigated. $NylC_1$ and $NylC_2$ were active towards PEA1 and PEA3 as the release of linear PA6.6- and PA6.10-oligomers was detected (Figure 2.2-5). $NylC_1$ showed higher activities for both substrates, as it released approximately three fold more linear PA6.6 dimer ($PA6.6_2$) than $NylC_2$. In contrast to this, no or only low activity was detected towards PEA2 or PEA4, respectively, which contained PA6.10 regions (Figure 2.2-5). These results indicate a preference for $NylC_{1-2}$ towards amide bonds within PA6.6 regions compared to PA6.10 regions of PEA compositions. For engineered $NylC_{p2}$, a similar preference for amide bonds consisting of shorter monomers was revealed (PA6.6 and PA6.6-*co*-6.4) and no degradation of PA6.10 has been reported until today (Nagai et al., 2014). Given the different polymer characteristics of PEA1 and PEA3, the varying biodegradability is likely related to the enzymatic specificities of NylCs rather than to the individual polymer properties of the PEA.

To facilitate depolymerization, the well-established leaf and branch compost cutinase (LCC) (Sulaiman et al., 2012), able to hydrolyze various polyester including poly(ester-urethanes) (Schmidt et al., 2017), was used for initial depolymerization of the PEAs. Activity of LCC

was expected to release amide oligomers that might be further degraded by $NylC_1$ and $NylC_2$. Since LCC features a high temperature optimum, initial hydrolysis of PEA1-4 was performed at 70 °C and subsequent treatment with $NylC_{1-2}$ was performed at 30 °C. To track any residual activity of LCC during the subsequent incubation at 30 °C, control reactions with $NylB_{p2}$ were performed. This nylonase was reported to specifically hydrolyze linear PA6-oligomers not showing any activity towards PA6.6, PA6.10, and their corresponding oligomers (Kinoshita et al., 1981; Negoro, 2000). Interestingly, initial treatment of PEA1-4 by LCC resulted in the release of amide oligomers with primary amino groups revealing activity of LCC towards the amide regions (Figure 2.2-5). For PEA1, only containing PA6.6 regions, the release of amide oligomers by LCC was approximately 2.7-fold lower compared to $NylC_1$ (Figure 2.2-5). In contrast to this, LCC treatment of PEA2-4, containing PA6.6-*co*-PA6.10 or PA6.10 regions, resulted in highly increased amounts of amide oligomers compared to $NylC_1$ (Figure 2.2-5). The combination of LCC and $NylC_1$ resulted in a synergistic effect when PEA1 and PEA3 were tested as substrates, yielding approximately 2.2- and 1.3-fold more soluble products compared to the sum of products released by individual LCC or $NylC_1$ treatments. Hence, initial depolymerization of LCC resulted in the release of larger PA6.6-oligomers that were subsequently further degraded by $NylC_1$. In contrast to PA6-oligomers, $NylC_1$ was active towards soluble PA6.6-oligomers, as revealed for $PA6.6_4$, which resulted in the formation of $PA6.6_2$ as the end product of hydrolysis. No synergistic effect was observed when PEA2 and PEA4 were tested confirming low activities of $NylC_1$ towards PA6.10-oligomers. Although the polymer characteristics of PEA2-4 were rather similar, the biodegradability of PEA3 was remarkably higher. This highlights the importance of incorporating PA6.6 regions into PEA, which could function as target hydrolysis sites for nylonases. PEA1, containing pure PA6.6-regions, showed less biodegradability compared to PEA3 (PA6.6-*co*-PA6.10 regions) but featured improved polymer characteristics such as increased Mn and Mw. Hence, it is crucial to design future PEA that align both counteracting parameters, as suggested with PEA1, by focusing on the incorporation of PA6.6 regions and simultaneously boosting the nylonase activities. Overall, $NylC_1$ was revealed as most active nylonase and showed activities towards not only PA6.6 oligomers but also PEA that contain PA6.6-regions.
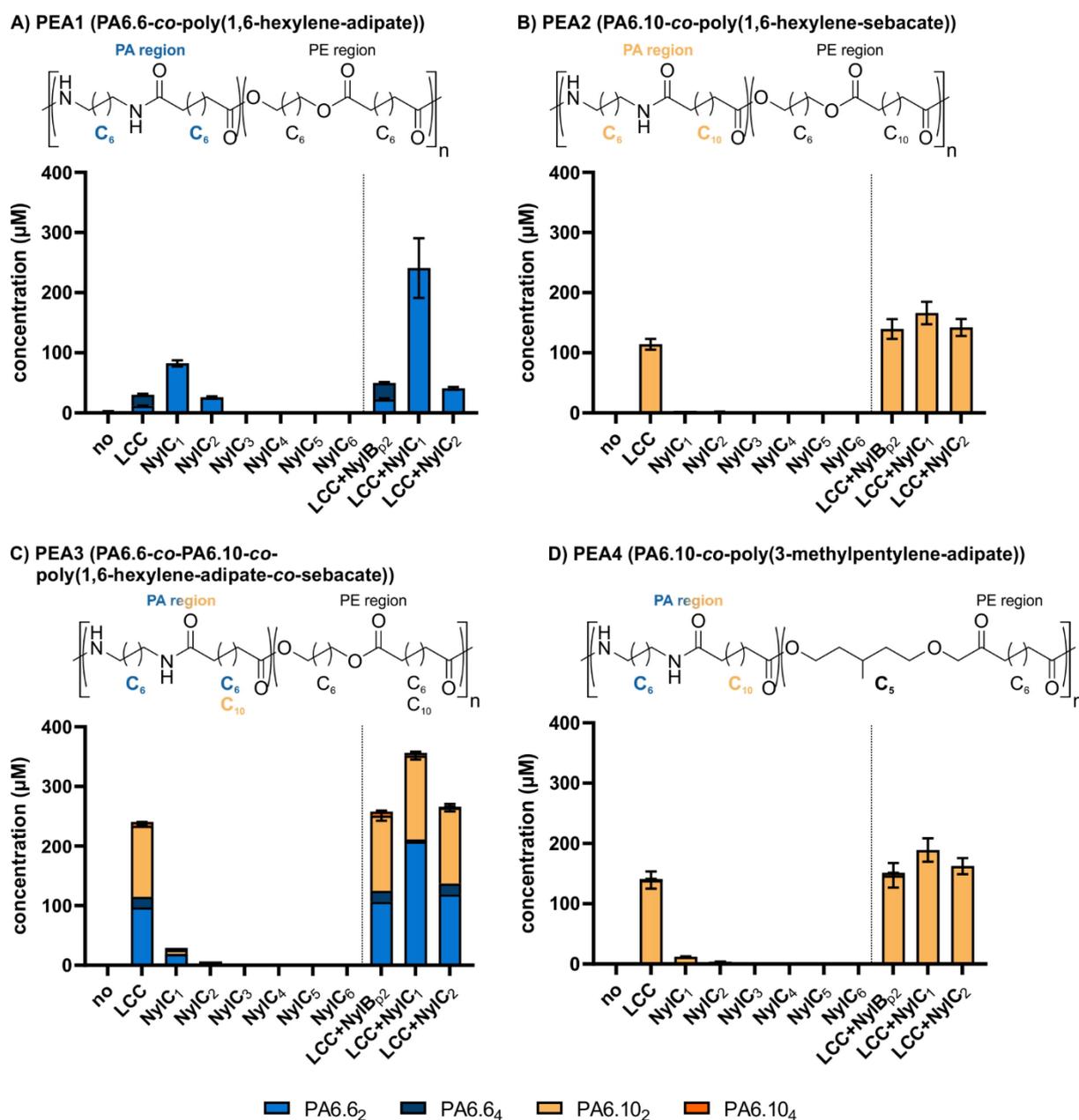
Figure 2.2-5. Enzymatic degradation of PEA by LCC and nylonases. Degradation products containing primary amino groups were detected *via* pre-column derivatization coupled with HPLC analysis. Powdered PEA (10 g/l) were used as substrate for the reactions performed in 50 mM phosphate buffer (pH 7.3) using 500 nM of purified enzyme. Reactions containing a single enzyme were incubated at 70 °C (LCC) or 30 °C (NylC$_{1-6}$) for 24 h. For combined enzymatic reactions, samples were first incubated with LCC (70 °C, 24 h) and subsequently with NylC$_1$, NylC$_2$ or NylB$_{p2}$ (30 °C, 24 h). The mean values and standard deviations (SD) of two replicates are shown (n=2).

2.2.4 Conclusions and outlook

In the present study, we increased the enzymological diversity of NylCs and discovered three novel NylCs that were active towards insoluble cyclic and linear Ahx-oligomers, of which two were active towards polymeric PEA substrates. Overall, we greatly increased the input of NylCs for future enzyme engineering to boost their activities towards PA and PEA. Based on previous engineering of NylC$_{p2}$, rational design can be performed to increase the thermostability of the novel nylonases (Negoro et al., 2012). Moreover, the recently developed high-throughput screening system for directed evolution of nylonases can be applied to identify yet unknown mutations that increase the overall activities (Puetz et al., 2023). Such mutations could for example facilitate the post-translational autocleavage, the structural re-assembly of α- and β-subunits, or the interactions between individual NylC monomers. The extensive engineering of our novel NylC enzymes has the great potential to enable efficient and sustainable enzymatic recycling of PA and PEA materials in the future. Finally, our multi-disciplinal insights offer a promising vantage point for the strategic design of hybrid PEAs that combine the contrary features of material parameters of performance and biodegradability.

2.2.5 Materials and methods

2.2.5.1 In silico tools

Multiple sequence alignments were performed using the EMBL-EBI tool (Madeira et al., 2022) and the T-Coffee alignment algorithm (Notredame et al., 2000) was used chosen. Amino acids were colored based on Clustal X 2.0 default coloring (Larkin et al., 2007). Protein structures were predicted using ColabFold (Mirdita et al., 2021) and structural alignments were performed with UCSF Chimera (Pettersen et al., 2004).

2.2.5.2 Enrichment cultures

Soil samples (10 g L^{-1}) from a compost heap were used to inoculate mineral salts medium (Wierckx et al., 2005) supplemented with 50 g L^{-1} of a poly(ester-amide) consisting of adipic acid, 1,6-hexamethylenediamine, and 1,6-hexanediol. Shake flasks were incubated at 30 °C and 200 rpm for 3 d until they were transferred to fresh medium After five re-inoculations,

enriched strains were isolated on lysogeny broth (LB) agar plates. For cryogenic conservation, strains were cultivated in LB medium for 30 °C for 18 h and 500 µL of cell culture was mixed with 500 µL of 50 % (v/v) glycerol. Glycerol stocks were stored at -80 °C.

2.2.5.3 16S rDNA sequencing

Genomic DNA was isolated from cells obtained from LB cultures using the Monarch gDNA Purification Kit (NEB). The 16S rDNA sequence was amplified from the isolated gDNA by PCR using Q5 High-Fidelity 2×Master Mix (NEB) and the primer FD1/2 (5′-3′ AGAGTTTGATCMTGGCTCAG) and RP1/2 (5′-3′ ACGGYTACCTTGTTACGACTT) (Weisburg et al., 1991). PCR products were purified using a Monarch PCR Cleanup Kit (NEB) and sequenced by Eurofins Genomics (Ebersberg, Germany). The obtained sequencing results were aligned to the nucleotide collection (nr/nt) of the NCBI database using BLASTn (Sayers et al., 2022).

2.2.5.4 Whole-genome sequencing

One microgram of genomic DNA was used for library preparation using the NEBNext Ultra™ II DNA Library Prep Kit for Illumina (NEB). The library was evaluated by qPCR using the KAPA library quantification kit (Peqlab, Erlangen, Germany). Afterwards, normalization for pooling was done and paired-end sequencing with a read length of 2×150 bases was performed on a MiSeq (Illumina). The reads of demultiplexed fastq files as the sequencing output (base calls) were trimmed and quality-filtered using the CLC Genomic Workbench software (Qiagen Aarhus A/S, Aarhus, Denmark). The filtered reads were used for de novo assembly using the CLC Genomic Workbench software.

2.2.5.5 Molecular cloning

Codon-optimized genes encoding the nylonases were chromosomally integrated and expressed in *Bacillus subtilis* using a similar setup as described previously (Jensen et al., 2010) with the following modifications. A 21 bp sequence was added at the terminal gene sequences encoding a C-terminal histidine tag (His$_6$-tag) and harboring the stop codon. Cells were made competent according to Yasbin et al. (1975).

2.2.5.6 Enzyme purification

Cells of nylonase-expressing *B. subtilis* were cultivated in Cal18 medium (4 % Yeast extract, 0.13 % MgSO$_4$×7 H$_2$O, 5 % Maltodextrin, 2 % Na$_2$HPO$_4$×12 H$_2$O, 0.67 % Na$_2$MoO$_4$ trace metal solution and 0.01 % Dowfax 63N10) (Jensen et al., 2010) or terrific broth (TB) medium (Cold Spring Harbor Laboratories, 2010) for 48-72 h at 30 °C. Cell cultures were centrifuged at 7,000 × *g* for 15 min and the supernatant was used for immobilized-metal affinity chromatography using His SpinTrap^{TM} columns (Cytivia). After that, enzymes were desalted with HiTrap$^{®}$ desalting columns (Cytivia) using 50 mM HEPES buffer (pH 7.3). Purified samples were analyzed by SDS-PAGE analysis using Criterion^{TM} Precast Gels.

2.2.5.7 Nano differential scanning fluorimetry

The melting temperature (T_m) of the studied enzymes was analyzed by nano differential scanning fluorimetry (nanoDSF) using a Prometheus NT.48 (NanoTemper). For this, the enzymes were diluted to a concentration of 2 mg ml^{-1} in 50 mM HEPES buffer (pH 7.3). The thermal stability was tested with a heating scan range from 20 to 90 °C at a scan rate of 3 °C min^{-1}. Data analyzes and determination of the T_m was performed using the PR ThermControl software (NanoTemper).

2.2.5.8 Activity assays

All enzymatic reactions were performed at 30 °C in 50 mM phosphate buffer, pH 7.3 using 500 nM of purified enzyme. The cyclic Ahx-oligomer fraction Aco2 (n≥2) (Negoro et al., 2021) was used at concentrations of 4 g L^{-1} resulting in a turbid reaction sample due to insoluble Ahx-oligomers. For investigating the soluble cyclic Ahx-oligomers as substrate, this mixture was filtered through a 0.22 µm PES filter membrane to remove insoluble oligomers. For degradation experiments with polymeric substrates, 10 g L^{-1} of powdered PEA was used as substrate. Initial treatment with nylonases was performed at 30 °C, whereas LCC treatment was performed at 70 °C. Combined enzymatic degradation was initially performed at 70 °C (LCC) and subsequently at 30 °C after the addition of nylonases.

2.2.5.9   High-Performance Liquid Chromatography analysis

Samples obtained from activity assays were filtered through an AcroPrep™ 96-well filter plate (Pall Corporation, Port Washington, NY, USA) to remove any particles prior to HLPC analysis. HPLC analysis was performed using a 1260 Infinity II HPLC equipped with a fluorescence detector (FLD) and a diode array detector (DAD) (Agilent, Santa Clara, California, USA). To analyze linear PA-oligomers harboring primary amine groups, pre-column derivatization using *o*-phthaldialdehyde (OPA) reagent (Sigma-Aldrich, ready-to-use-mix) was performed. For separation of the derivatized molecules, the Kinetex® 2.6 μm EVO C_{18} 100 Å column (100 x 2.1 mm) (Phenomenex, California, USA) was used. As mobile phase, 10 mM sodium-borate buffer (A) (pH 8.2) and methanol (B) was used with an initial ratio of 70:30 (A:B). This ratio was gradually increased to 30:70 after 10 min and 0:100 after 12 min followed by 1 min of 0:100. After that, the ratio was switched to 70:30 after 14 min and 1 min post-run was performed. The flow was adjusted to 0.4 mL min^{-1} at and the oven temperature was set to 40 °C. Derivatized molecules were detected using a FLD using an excitation of $\lambda = 340$ nm and an emission of $\lambda = 450$ nm. Detection of cyclic Ahx-oligomers was performed using the DAD with an absorption of $\lambda = 210$ nm (reference $\lambda = 300$ nm). Cyclic oligomers of Ahx were separated using a Zorbax Eclipse XDB-C8 column (4.6 × 150 mm) with a H_2O_{MilliQ}:MeOH ratio of 60:40 and a constant flow of 0.5 mL min^{-1} at 40 °C. As no analytical standards were available for cyclic Ahx-oligomers, the corresponding peak area was analyzed allowing semi-quantitative analysis.

2.2.5.10 Polymer synthesis

In a typical polycondensation procedure, the syntheses of PEA were conducted solvent-free and under an inert atmosphere on approximately a 0.15 – 0.35 kg scale in a glass polymerization reactor (500 mL size; Glasblazerij Janssen B.V.). Mechanical stirring was applied using an overhead stirrer (Heidolph, hei-TORQUE Expert) connected to a magnet stirring coupling piece with a torque restriction of 20 MPa·cm^{-1} (Premex Glenfiz), and a 2D-round-shaped stainless steel stirring anchor. Vacuum was applied using a membrane pump (Pfeiffer MVP-15) in conjunction with a manually operated vacuum controller (Vacuubrand, Vacuu-Select). Stoichiometrically correct amounts of reagents (*i.e.* $m_{diacid} = m_{diamine} + m_{diol}$) were weighed into the reactor along with 0.1 wt% catalyst and 0.1 wt% antioxidant. The

setup was sealed and carefully purged with five vacuum/nitrogen cycles, and subsequently set at P = 900 mbar. The reaction was initiated by heating using a silicone oil bath to reach 220°C within 45 minutes under stirring at 50 rpm, upon which the reaction mixture turned into a viscous yellow liquid and profuse water distillation took place. Whenever the water distillation was observed to cease, all reaction conditions were gradually driven more stringent – toward 100 mbar, 240°C, and stirring at 300 rpm – over the course of two hours. Intermediately, the reactor was filled with nitrogen gas and the flask with aqueous condensate was quickly replaced by an empty one under an outflow of nitrogen gas. The reaction was proceeded for another 3 hours at 240°C and stirring at 300 rpm but now the vacuum was gradually decreased to 1 mbar to afford substantial buildup of polymer chains, as observed by the thickening of the reaction mixture and the gradual increase of monitored torque on the overhead stirrer. Ultimately, the vacuum was released by nitrogen filling into the reactor, and the polymeric product was cast into a silicone tray while still hot and molten.

2.2.5.11 Polymer characterization

Differential scanning calorimetry was carried out using the Q2000 device (TA Instruments, Asse, Belgium). We focused on the melting temperature (T_m), the recrystallization temperature (T_{rc}), and the crystallization temperature (T_c) within the different PEA in comparison to PA6. All samples were tested at a heating rate of 10 °C/min, using a temperature range of 0 to 275 °C with a sample size of ~5 mg. For each sample, we made three measurements and the mean values are presented.

The molecular weight of the samples was determined by gel permeation chromatography (GPC) using a 1260 Infinity System (Agilent Technologies, Santa Clara, CA, USA). We used hexafluor-2-isopropanol (HFIP) containing 0.19% sodium trifluoroacetate as the mobile phase, flowing at a rate of 0.33 mL/min. GPC was used to compare the PEA samples to the polymer PA6. Solutions were prepared by dissolving 3 mg samples in HFIP for ~3 h before passing through a 0.2-µm polytetrafluoroethylene filter and injecting them into a modified silica column filled with 7 µm particles (Polymer Standards Service, Mainz, Germany). The relative molecular weight (Mw), number average molar mass (Mn), and polydispersity index (PDI) were determined using refractive index detectors calibrated with

a standard polymethyl methacrylate polymer (1.0×105 g mol^{-1}). We performed GPC analysis three times with each sample and presented the mean values for comparison.

2.2.6   Declaration of competing interest

The authors declare no competing interest.

2.2.7   Acknowledgements

2.3 Bio-upcycling of even and uneven medium-chain-length diols and dicarboxylates using engineered *Pseudomonas putida*

Published as:

Ackermann Y. S.[1†], **de Witt J.** [1†]**,** Mezzina M. P.[2], Schroth C[1]., Polen T[1]., Nickel, P. I.[2], Wynands B.[1], and Wierckx N.[1*] (2024). Bio-upcycling of even and uneven medium-chain-length diols and dicarboxylates using engineered *Pseudomonas putida*. *Microb. Cell Factories – in press*, doi:10.1186/s12934-024-02310-7

[1] Institute of Bio- and Geosciences IBG-1: Biotechnology, Forschungszentrum Jülich, Jülich, Germany
[2] The Novo Nordisk Foundation Center for Biosustainability, Technical University of Denmark, Kongens Lyngby, Denmark
[†] these authors contributed equally to this study.
[*] Corresponding author

CRediT Author contributions
Y. S. Ackermann: Methodology, Investigation, Validation, Formal analysis, Data curation, Writing-original draft, Writing-review and editing, Visualization.
J. de Witt: Methodology, Investigation, Validation, Formal analysis, Data curation, Writing-original draft, Writing-review and editing, Visualization.
M. Mezzina: Investigation, Writing-review and editing,
C. Schroth: Investigation, Writing-review and editing.
T. Polen: Methodology, Formal analysis, Data curation, Writing-review and editing.
P. I. Nikel: Resources, Writing-review and editing, Supervision, Funding acquisition.
B. Wynands: Methodology, Writing-review and editing, Supervision.
N. Wierckx: Conceptualization, Resources, Data curation, Writing-original draft, Writing-review and editing, Visualization, Supervision, Project administration, Funding acquisition.

Overall contribution: 42 %

The presented experimental work was conducted by JDW and CS (diol part and PHA/PHB analysis) and YSA (dicarboxylic acid part). MPM and PIN performed the construction of pS6311·PHB and genome sequencing was performed by TP. Validation was done by YSA, JdW, TP, BW and NW. Visualization of all data was performed by YSA and JdW. The writing of the original draft was done by YSA and JdW, which was reviewed and edited by NW and all co-authors. Funding for the project was acquired by NW.

2.3.1 Graphical abstract
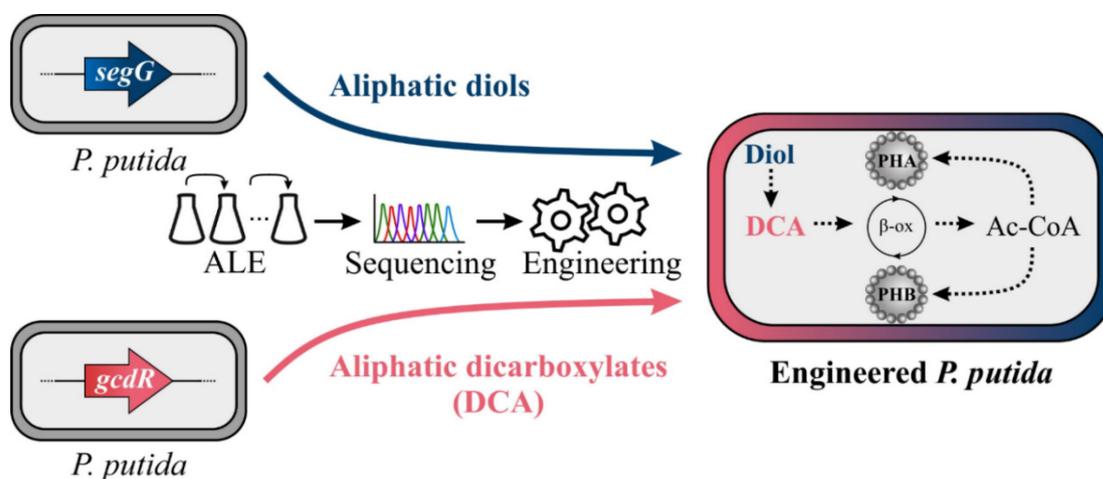
2.3.2 Abstract

Bio-upcycling of plastics is an emerging alternative process that focuses on extracting value from a wide range of plastic waste streams. Such streams are typically too contaminated to be effectively processed using traditional recycling technologies. Medium-chain-length (mcl) diols and dicarboxylates (DCA) are major products of chemically or enzymatically depolymerized plastics, such as polyesters or polyethers. In this study, we enabled the efficient metabolism of mcl-diols and -DCA in engineered *Pseudomonas putida* as a prerequisite for subsequent bio-upcycling. We identified the transcriptional regulator GcdR as target for enabling metabolism of uneven mcl-DCA such as pimelate, and uncovered amino acid substitutions that lead to an increased coupling between the heterologous β-oxidation of mcl-DCA and the native degradation of short-chain-length DCA. Adaptive laboratory evolution and subsequent reverse engineering unraveled two distinct pathways for mcl-diol metabolism in *P. putida,* namely *via* the hydroxy acid and subsequent native β-oxidation or *via* full oxidation to the dicarboxylic acid that is further metabolized by heterologous β-oxidation. Furthermore, we demonstrated the production of polyhydroxyalkanoates from mcl-diols and -DCA by a single strain combining all required metabolic features. Overall, this study provides a powerful platform strain for the bio-upcycling of complex plastic hydrolysates to polyhydroxyalkanoates and leads the path for future yield optimizations.

2.3.3 Introduction

The plastic crisis is a pressing environmental issue facilitated by an increasing plastic production that reached about 390 million metric tons in 2021, of which 90 % was based on fossil raw materials. More than half of the plastics produced are polyolefins such as polypropylene, low- or high-density polyethylene, and polyesters like PET (PlasticsEurope, 2022). Especially mixed plastics are a major challenge for mechanical and chemical recycling as they typically require pure feedstocks or the costly purification of individual building blocks (Ellis et al., 2021; Idumah and Nwuzor, 2019; Wei et al., 2020).

Bio-upcycling is a promising strategy to overcome the drawbacks of conventional end-of-life solutions (Tiso et al., 2021b) . This describes the process of biologically converting plastic waste into valuable products or materials through (bio-)depolymerization and subsequent microbial cultivation. Such conversion could provide better end-of-life options for hard-to-recycle polymers and composites because biology is uniquely capable to work with complex mixtures and materials (Wierckx et al., 2015). Furthermore, significant efforts were invested in the past to combine enzymatic or chemical depolymerization with microbial metabolization by using genetic and metabolic engineering (Ellis et al., 2021). For example, pyrolysis was used to produce hydrocarbon wax from PE polymers, which was subsequently oxidized to a mixture of fatty acids. This mixture could then serve as substrate for polyhydroxyalkanoate (PHA) production in *Pseudomonas* (Guzik et al., 2021). Furthermore, Sullivan *et al.* combined a chemical auto-oxidation step to break down the carbon bonds of high-density PE or PET with a microbial bioconversion step to further metabolize the resulted monomers into new compounds (Sullivan et al., 2022). Unfortunately, both chemical and enzymatic degradation processes sometimes lead to unfavorable by-products such as toxic monomers or require harmful solvents (Magnin et al., 2020). Although in some cases it is possible to separate toxic compounds, such as aromatic diamines (Eberz et al., 2023; Utomo et al., 2020), this will not always be economically feasible. Therefore, it is important to use robust microbial hosts. One promising candidate is the widely used biotechnological host *Pseudomonas putida* KT2440 (Bitzenhofer et al., 2021; Schwanemann et al., 2020). Besides a high tolerance to chemical stress and rapid growth, in previous studies *P. putida* was already enabled to grow on different plastic monomers such as 1,4-butanediol (BDO), adipic acid (AA), ethylene glycol, or itaconate (Ackermann et al., 2021; de Witt et

al., 2023; Franden et al., 2018b; Li et al., 2020; Utomo et al., 2020). Moreover, *P. putida* KT2440 was engineered to serve as platform organism for the production of several value-added molecules including aromatic compounds (Schwanemann et al., 2020), rhamnolipids (Tiso et al., 2020), and medium-chain-length (mcl) polyhydroxyalkanoates (PHA), consisting of C_6-C_{12} monomers (Dalton et al., 2022; Mezzina et al., 2021; Prieto et al., 2016).

Mcl-aliphatic diols, such as BDO and 1,6-hexanediol (HDO), are prevalent monomers of polyurethanes or polyesters. Previous studies enhanced metabolism of BDO in *P. putida* KT2440 (Li et al., 2020). A mutation in a transcriptional regulator, encoded by PP_2046, activated the downstream operon PP_2047-51, thereby greatly enhancing the rate of BDO metabolism. Since this operon encodes enzymes involved in β-oxidation, it is likely that BDO is converted to glycolyl-CoA and acetyl-CoA, although direct oxidation to succinate could not be excluded. A relevant group of intermediates within this pathway are the partly oxidized hydroxy acids (HA) such as 6-hydroxyhexanoate which is the monomer of polycaprolactone. The production of PHA from BDO by *P. putida* was successfully shown (Li et al., 2020). Nevertheless, several other mcl-diols including HDO can currently not be funneled into the central metabolism of *P. putida* for bio-upcycling.

Together with mcl-aliphatic diols, mcl-dicarboxylates (DCA) are mainly used for the synthesis of polyesters but also to produce polyamides and polyurethanes. Furthermore, mcl-DCA are products from chemical oxidation of longer polyolefins (Sullivan et al., 2022). Growth on single mcl-DCA was already achieved with the engineered *P. putida* KT2440ge ΔP_{paaF}-*paaYX*::P_{14g} Δ*psrA* (KT2440-AA) strain expressing the heterologous *dcaAKIJP* cluster from *Acinetobacter baylyi* (Ackermann et al., 2021). However, metabolism of especially uneven-chain-length (ucl) DCA is still rather inefficient, especially in the case of pimelate (C_7). An exception to this is glutarate (C_5), which is a favorable native carbon source for *P. putida* and is metabolized through two independent pathways. One is regulated by the GntR family regulator CsiR, which induces a CoA-independent pathway with glutarate hydroxylase (CsiD) and L-2-hydroxyglutarate oxidase (LhgO) as key enzymes (Zhang et al., 2018). Furthermore, *P. putida* contains a CoA-dependent pathway, in which glutarate is activated by a CoA-transferase (PP_0159) to glutaryl-CoA and then further decarboxylated by glutaryl-CoA dehydrogenase (GcdH) to crotonyl-CoA (Zhang et al.,

2019). Crotonyl-CoA can then be converted *via* acetoacetyl-CoA into two acetyl-CoA molecules.

In this study, we aimed to extend the substrate range of *P. putida* KT2440 with prevalent polyethylene and polyester hydrolysate constituents, namely mcl-diols and –DCA, using metabolic engineering and laboratory evolution. Especially metabolism of substrates of uneven chain-length is limited and needs to be addressed. The combination of unravelled pathways should result in a mutant that is able to funnel a complex polyester mock hydrolysate into its central metabolism providing it as substrate for bio-upcycling. To demonstrate such an approach, PHA and poly(3-hydroxybutyrate) (PHB) production from mcl-diols and -DCA as pure substrates and in a mock hydrolysate is envisioned. Altogether, this study leads the path for future bio-upcycling of mixed plastic hydrolysates that currently are a burden to conventional recycling.

2.3.4   Results and discussion

2.3.4.1   Engineering metabolism of aliphatic diols

Aliphatic mcl-diols are prevalent monomers in a variety of polymers such as polyesters or polyurethanes. In previous work, *P. putida* KT2440 was engineered to metabolize BDO as sole carbon source (Li et al., 2020). The metabolic pathway for BDO was predicted to occur *via* its partial oxidation to 4-hydroxybutyrate followed either by CoA-activation and subsequent β-oxidation resulting in acetyl-CoA and glycolyl-CoA, or by full oxidation to succinate. In contrast to succinate, longer chain-length DCA and thus the corresponding diols cannot be directly funneled into the central metabolism but require the heterologous β-oxidation for DCA (Ackermann et al., 2021). Consequently, two different pathways might enable metabolism of aliphatic diols, in which either the partly oxidized HA (HA-CoA-activating) or the further oxidized DCA is CoA-activated (DCA-CoA-activating) (Figure 2.3-1). As the wild type strain is not capable of metabolizing mcl-DCAs, engineering its background might only enable degradation *via* the HA-CoA-activating pathway. In contrast, engineering of *P. putida* KT2440-AA, which is able to metabolize mcl-DCA, could lead to degradation *via* both pathways.

To enable growth on HDO *via* the HA-CoA-activating pathway, adaptive laboratory evolution (ALE) of the *P. putida* KT2440 wild type was performed on HDO (Figure S5.3-1). Subsequent whole-genome sequencing of ALE mutants and reverse engineering resulted in the triple mutant PP_2046^{A257T}, PP_2790^{A220V}, *ttgG*$^{\Delta4bp}$ that metabolized HDO and 1,8-octanediol (ODO) but not 1,7-heptanediol (Figure 2.3-1). Interestingly, the transcriptional activator encoded by PP_2046 that was already involved in BDO metabolism, was revealed to be involved in HDO metabolism as well. Hence, HDO was likely metabolized by the HA-CoA-activating pathway encoded by PP_2047-51. Additionally, a mutation within a second regulator, more specifically a sigma factor 54-dependent sensory box protein encoded by PP_2790, was found to be involved in HDO metabolism. This regulator might activate expression of orthologs of this pathway with higher affinities for HDO than BDO. Moreover, a frameshift mutation within *ttgB* (PP_1385) encoding an efflux pump membrane protein increased growth on HDO. Possibly, the intact TtgABC efflux pump reduces intracellular HDO concentrations thereby hindering its metabolism.

In addition to the HA-CoA-activating pathway, HDO might also be metabolized by the DCA-CoA-activating pathway *via* adipate (AA). Therefore, *P. putida* KT2440-AA that was recently engineered to metabolize AA and other even chain-length DCA was chosen as a starting point for enabling mcl-diol metabolism. Although this strain was not able to grow on HDO as sole carbon source (Figure 2.3-1). ALE resulted in the isolation of mutants able to metabolize 15 mM HDO within 24 h (Figure S5.3-1). Whole-genome sequencing of the fastest-growing ALE mutant revealed two single nucleotide variants (SNV). The first SNV occurred in PP_5423 encoding a putative membrane protein causing arginine 29 to be replaced by proline (PP_5423^{R29P}). The second mutation caused the exchange of glycine 70 to arginine in the protein translocase subunit SecG encoded by PP_5706 (*secG*^{G70R}). Both positions are highly conserved among Pseudomonads. Reverse engineering of the unevolved *P. putida* KT2440-AA revealed that the *secG*^{G70R} mutation alone could reproduce the growth phenotype of the isolated ALE mutant. Reverse engineering of the PP_5423^{R29P} mutation enabled growth on HDO, albeit much slower and with a long lag phase. Combination of both *secG*^{G70R} and PP_5423^{R29P} in one strain did not further enhance growth compared to the *secG*^{G70R} mutant (Figure S5.3-2), indicating the mutated SecG protein as most important for HDO metabolism. SecG is an auxiliary protein that recognizes pre-protein signal sequences

and builds the core of the protein translocation apparatus SecABCDEFGY (Crane and Randall, 2017). Deletion of *secG* in the unevolved *P. putida* KT2440-AA mimicked the phenotype of the *secG*^{G70R} mutant on HDO as sole carbon source indicating that the SNV likely caused a loss of function (Figure S5.3-3). We speculate that this mutation could affect the subcellular localization of oxidoreductases, thereby influencing the transport of HDO and/or its intermediates into the cytoplasm. However, global effects on other proteins, such as transporters, or signaling pathways are also conceivable but further investigations are required to unravel the exact mechanisms. Because the metabolism of 6-hydroxyhexanoate was found to not require the *secG*^{G70R} mutation, we conclude that this mutation affects the first oxidation steps of the diol to the HA (Figure S5.3-4). In addition to DCA-CoA-activating pathway, 6-hydroxyhexanoate was also metabolized *via* the HA-CoA-activating pathway in the reverse engineered KT2440 wild type-based strain. Hence, 6-hydroxyhexanoate can be directed into the central metabolism *via* both pathways enabling future bio-upcycling processes of polycaprolactone hydrolysates.

In addition to HDO, the reverse engineered *secG*^{G70R} mutant was also able to utilize ODO as sole carbon source, whereas 1,7-heptanediol was poorly metabolized by the strain (Figure 2.3-1). These results are in agreement with the ability of the parent strain *P. putida* KT2440-AA to metabolize the corresponding dicarboxylate suberate (C_8) much better than pimelate (C_7) (Ackermann et al., 2021). To test whether HDO and ODO were metabolized *via* the DCA-CoA-activating pathway, the *dcaAKIJP* operon, enabling growth on mcl-DCA, was deleted in *P. putida* KT2440-AA *secG*^{G70R}. Indeed, the *secG*^{G70R} Δ*dcaAKIJP* mutant showed decreased growth with HDO and ODO indicating that both substrates were metabolized *via* their mcl-DCA (Figure 2.3-1). However, this indicated that the HA-CoA-activating pathway was also active in the *P. putida* KT2440-AA-based strain. Although the *secG*^{G70R} Δ*dcaAKIJP* mutant showed an increased lag-phase with ODO compared to HDO, the observed growth indicated that ODO is the favored substrate for the HA-CoA-activating pathway. Deletion of PP_2051 encoding a 3-ketoacyl-CoA thiolase that is involved in the degradation of BDO, did not alter the phenotypes of the *secG*^{G70R} Δ*dcaAKIJP* mutant with HDO and ODO, likely due to the presence of isozymes (Liu et al., 2023) (Figure S5.3-3). Hence, both pathways can be used to metabolize mcl-diols but they result in different central metabolites as end products namely acetyl-CoA and glycolyl-CoA for the HA-CoA-

activating or acetyl-CoA and succinyl-CoA for the DCA-CoA-activating pathway (Figure 2.3-1). In contrast to succinyl-CoA, the metabolic route for glycolyl-CoA is unknown, but a conversion to glyoxylate is likely. This can be funneled into the glyoxylate shunt (Li et al., 2019), or it might also be metabolized *via* tartronate semialdehyde yielding 2-phosphoglycerate that is an intermediate of glycolysis (Franden et al., 2018b). Since degradation of glycolyl-CoA can be associated with the release of CO_2 and consumption of NAD(P)H, the HA-CoA-activating pathway might be energetically inferior compared to the DCA-CoA-activating pathway. In addition to this, the deletion of *dcaAKIJP* within the DCA-CoA-activating pathway might enable the consolidation of a mixture containing diols and DCA to a single group of monomers. Such bioconversion using a Δ*dcaAKIJP* mutant would enhance the economic viability of monomer recycling from PE hydrolysates as not a heterogeneous mixture of monomers but only a single type of building blocks needs to be purified from the hydrolysate.
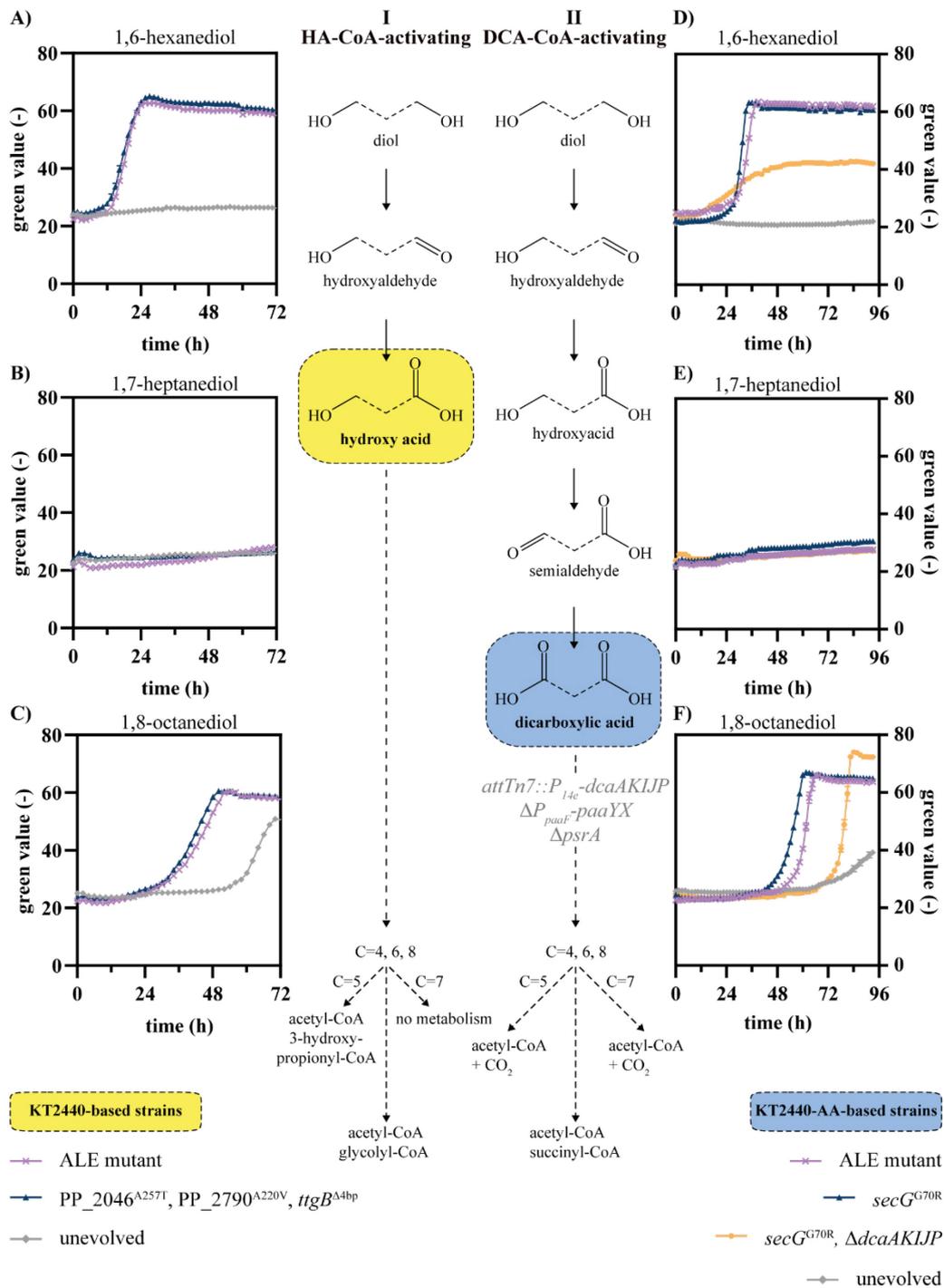
Figure 2.3-1. Metabolic pathways of aliphatic diols in engineered *P. putida* KT2440. *P. putida* KT2440 wild type-based strains (A-C) and *P. putida* KT2440-AA-based strains (D-F) were cultivated in mineral salts medium (MSM) supplemented with 1,6-hexanediol, 1,7-heptanediol, or 1,8-octanediol in concentrations that are C-mol equivalent to 30 mM 1,6-hexanediol. Depending on the background strain, the mcl-diols are either metabolized via the HA-CoA-activating (I) or DCA-CoA-activating (II) pathway which required the expression of the heterologous *dcaAKIJP* cluster in *P. putida* KT2440-AA (genomic modifications in grey). Depending on the chain-length of the diol (dashed lines), namely C=4 (1,4-butanediol), C=5 (1,5-pentanediol), C=6 (1,6-hexanediol), C=7 (1,7-heptanediol), and C=8 (1,8-octanediol) and the respective pathway, different central metabolites are obtained. The results of single mutant cultivation are shown in Figure S5.3-2. Growth was monitored using a Growth Profiler. Error bars indicate the standard error of the mean (n=3).

2.3.4.2   Engineering metabolism of ucl-DCA

Given that *P. putida* KT2440-AA grows very poorly on ucl-DCA, the inability of the *secG*^{G70R} mutant to metabolize ucl-diols likely stems from this downstream limitation. Hence, the next step was to optimize catabolism of ucl-DCA. Sullivan *et al.* demonstrated the upcycling of a DCA mixture from plastic waste containing polyesters (Sullivan et al., 2022). Even when growth was enabled on the mixture containing C_4-C_{17} DCA and all substrates were degraded over time, growth inhibition was observed on the single monomers with uneven-chain-length, especially pimelate (C_7). This suggested a further misregulation of connecting metabolic pathways, possibly at the point of glutaryl-CoA, resulting from β-oxidation of these DCA (Harrison and Harwood, 2005). Since it is known that pimelate cannot act as an inducer of GcdR, the absence of glutarate could explain the difference in growth between a monomer mixture and pimelate as sole carbon source (Thompson et al., 2019a). To further investigate this misregulation, an evolution experiment was performed. *P. putida* KT2440-AA and the corresponding evolved strains *P. putida* A12.p and A12.1ge (Ackermann et al., 2021), were cultivated in MSM containing pimelate as sole carbon source to provoke stable mutations. After 70-80 hours of cultivation, weak growth was detectable (Figure 2.3-2). The cultures of all replicates were spread on LB agar plates and single colonies were re-inoculated in MSM containing pimelate as sole carbon source. This re-inoculation resulted in a significantly shorter lag phase and better growth, suggesting that stable mutations had occurred.

Whole-genome sequencing of two of the *P. putida* A12.1ge strains re-inoculated on pimelate revealed mutations in the regulator *gcdR*. One strain (PA1.2) contained a C→T mutation in *gcdR* resulting in a G148D substitution, while the other strain (PA1.1) contained a C→T mutation, resulting in a G154D substitution. Among Pseudomonads, both positions are highly conserved and the emerged amino acid exchanges are located in the substrate binding domain of GcdR. This LysR family regulator governs the expression of *gcdH*, encoding a glutaryl-CoA dehydrogenase, and PP_0159, encoding a family III CoA-transferase (Madhuri Indurthi et al., 2016; Zhang et al., 2019). Glutarate is the effector of GcdR (Thompson et al., 2019a; Zhang et al., 2019), but since pimelate is degraded *via* glutaryl-CoA and not glutarate, the reason for the poor growth is likely the lack of induction of *gcdH*.

We hypothesized that the mutations found in *gcdR* ameliorate this lack of induction, hence enhancing growth on longer- ucl-DCA.
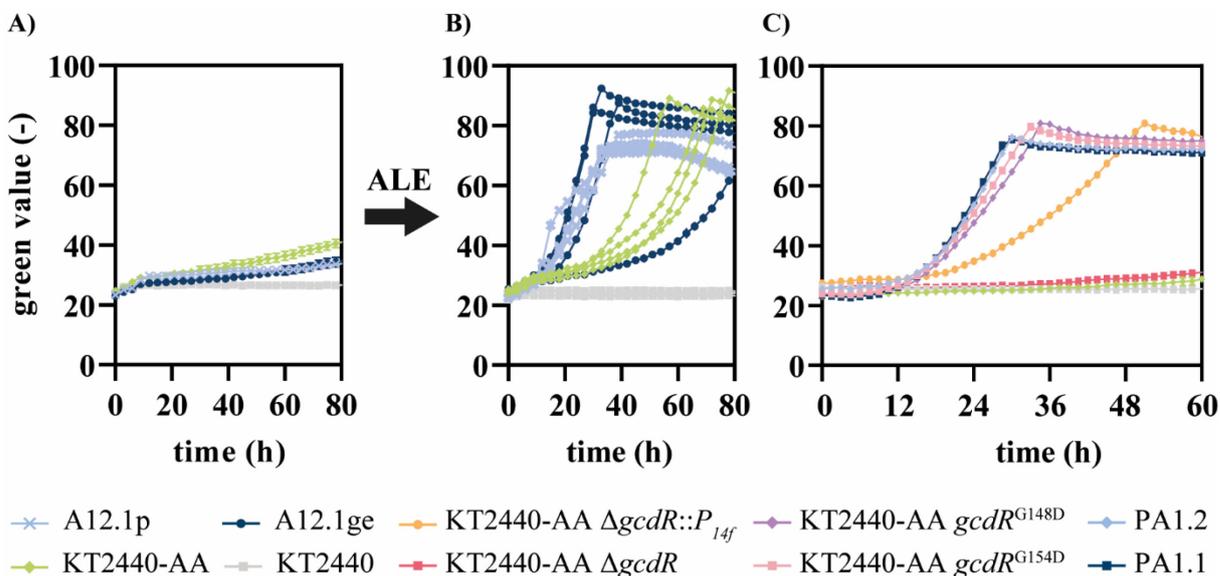
Figure 2.3-2. Adaptive laboratory evolution and reverse engineering for growth on pimelate. All strains were cultivated in three-fold buffered MSM containing 25.7 mM pimelate as sole carbon source. (A) Long-term cultivation of strains that are not able to grow on pimelate to induce adaptive mutations. (B) Growth of single strains which were isolated on LB agar plates after 80 h from the experiment shown in A. (C) Growth of reverse engineered strains based on mutations found after whole-genome sequencing of evolved *P. putida* A12.1ge strains. Growth was monitored using a Growth Profiler. Error bars indicate the standard error of the mean, but errors are sometimes so small that they are not visible behind the lines (n=3).

To investigate the impact of the regulator GcdR on the degradation of ucl-DCA, a *gcdR* knockout strain was compared to a strain harboring the synthetic promoter *P₁₄f* for constitutive expression of *gcdH*-PP_0159 (Figure 2.3-2). Since *P. putida* KT2440-AA Δ*gcdR* was not able to grow on pimelate as sole carbon source, it is likely that GcdR activates the transcription of *gcdH*-PP_0159. Growth on glutarate was not decreased by the deletion of *gcdR* probably due to the second CoA-independent degradation pathway of *P. putida* (Figure S5.3-5). In contrast, constitutive expression of *gcdH*-PP_0159 enabled growth on pimelate, but at a lower rate than in the two evolved strains, indicating that activation of the native promoter mediated by the mutated GcdR is stronger than the expression obtained using a constitutive synthetic promoter. This was confirmed by genomic insertion of the mutations encoding the amino acid exchanges found in the evolved strains. Growth of these

reverse engineered strains was much better compared to the constitutive P_{14f} expression, almost completely mimicking the growth phenotype of the evolved strains (Figure 2.3-2).

2.3.4.3 SNVs in *gcdR* may cause changes in ligand binding

To comprehend the effects of the G148D and G154D mutations on GcdR, RT-qPCR experiments were performed to analyze expressions levels of *gcdH* in the *gcdR* mutants on different ucl-DCA and on glucose (Figure 2.3-3). In the GcdR^{G154D} mutant, the expression levels of *gcdH* are the same on all substrates. Hence, this mutation likely led to a strong constitutive activation, at a level similar to the wild type induced by glutarate. In contrast, in the GcdR^{G148D} mutant, expression levels of *gcdH* are much higher on glutarate and pimelate than on glucose or azelate, indicating that this mutant is induced by both ucl-DCA, in contrast to the wild type regulator which is only induced by glutarate. This indicates that the G148D mutation increased the spectrum of possible ligands of GcdR. ColabFold protein structure simulations and YASARA docking studies (Krieger and Vriend, 2014; Mirdita et al., 2021) indicate a structural impact of G148D and G154D on the effector binding pocket of GcdR (Figure 2.3-3, Figure S5.3-6). The G148D substitution is more distal from the pocket, which appears to be larger compared to the wild type. The G154D mutation is closer to the pocket, where the negatively charged aspartic acid might lead to a conformational change that is not easily modelled by this *in silico* method. This would support the RT-qPCR results, although these are only simulations that need further confirmation. The expression levels of *gcdH* with the wild type regulator induced by glutarate, the G148D mutant induced by glutarate or azelate, and the constitutive G154D mutant, are similarly high, significantly exceeding that of the constitutive P_{14f} promoter exchange strain. This supports that the slow growth of the latter strain was caused by the relatively weak expression driven by the promoter exchange.
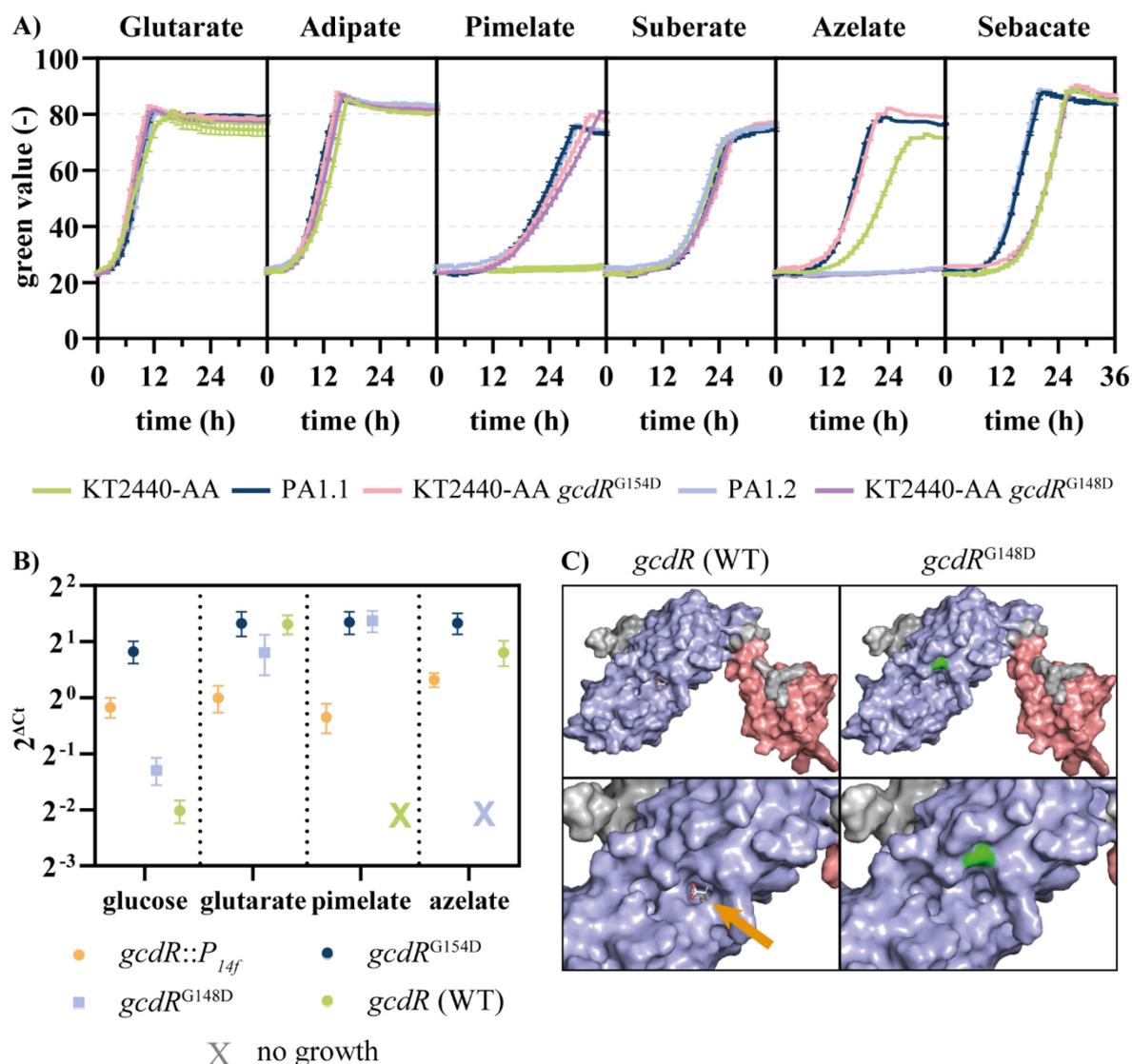
Figure 2.3-3. Characterization of growth of engineered and evolved strains of *P. putida* on dicarboxylic acids of varying chain lengths. (A) All strains were cultured in MSM containing the specified carbon source that are C-mol equivalent to 30 mM adipate. The growth was monitored using a Growth Profiler. Error bars indicate the standard error of the mean (n=3). (B) Relative expression levels of gcdH in cells of *P. putida* with wild type or mutated versions of the regulator GcdR on different C-sources were determined by RT-qPCR. The C_t values were normalized to the C_t of *rpoD*. Standard errors of the means were calculated using three technical replicates of two biological replicates. Expression levels in cells that did not grow on certain substrates were set equal to unexpressed values and are indicated with "X". (C) Three-dimensional structures were predicted with ColabFold and visualized with PyMOL. Docking of glutaric acid in the wild type regulator was calculated using YASARA (orange arrow). The mutated amino acid (D148) is marked in green. The blue surface color indicates the effector binding domain and the red surface color indicates the DNA binding domain. The visualization of the mutant *gcdR*^{G154D} is shown in Figure S5.3-6.

With this knowledge, the strains containing the SNVs were compared to *P. putida* KT2440-AA in terms of growth on different mcl-DCA. This confirmed the improvement of growth of the GcdR^{G154D} strain on ucl-DCA compared to the starting strain (Figure 2.3-3). The most conspicuous difference can be seen on azelate. The parent strain with wild type *gcdR* grew reasonably well on this C_9-DCA, possibly as a result of the two acetyl-CoA released from β-oxidation of this longer chain length. However, growth on azelate was enhanced by the G154D mutation but inhibited by G148D. This indicated that the G148D mutation altered the effector binding pocket such that pimelate causes induction, while azelate causes repression.

2.3.4.4   Enabling growth on ucl 1,7-heptanediol

P. putida KT2440-AA *secG*^{G70R} metabolized diols of even chain-length *via* the DCA-CoA-activating pathway, whereas the ucl 1,7-heptanediol was poorly metabolized by this strain due to its inability to utilize pimelate. Since introducing the *gcdR*^{G154D} mutation into *P. putida* KT2440-AA enabled metabolism of pimelate as sole carbon source, it was introduced into *P. putida* KT2440-AA *secG*^{G70R}. Indeed, the resulting *secG*^{G70R}, *gcdR*^{G154D} mutant metabolized 1,7-heptanediol and deletion of the *dcaAKIJP* cluster confirmed its metabolism *via* the DCA-CoA-activating pathway (Figure 2.3-4). The *gcdR*^{G154D} mutation was also introduced into the wild type-based *ttgG*^{Δ4bp}, PP_2046^{A257T}, PP_2790^{A220V} mutant that metabolized HDO and ODO *via* the HA-CoA-activating pathway. However, the resulting mutant was not able to metabolize 1,7-heptanediol (data not shown). This highlights the DCA-CoA-activating pathway as most suitable pathway for funneling aliphatic even and uneven mcl-DCA and -diols into the central metabolism of the engineered *P. putida* KT2440-AA *secG*^{G70R}, *gcdR*^{G154D}. A mixture consisting of C_6-C_{10} DCA and C_6-C_8 diols was fully consumed by this strain confirming the successful funneling of all substrates from a complex mixture into the central metabolism (Figure 2.3-4).
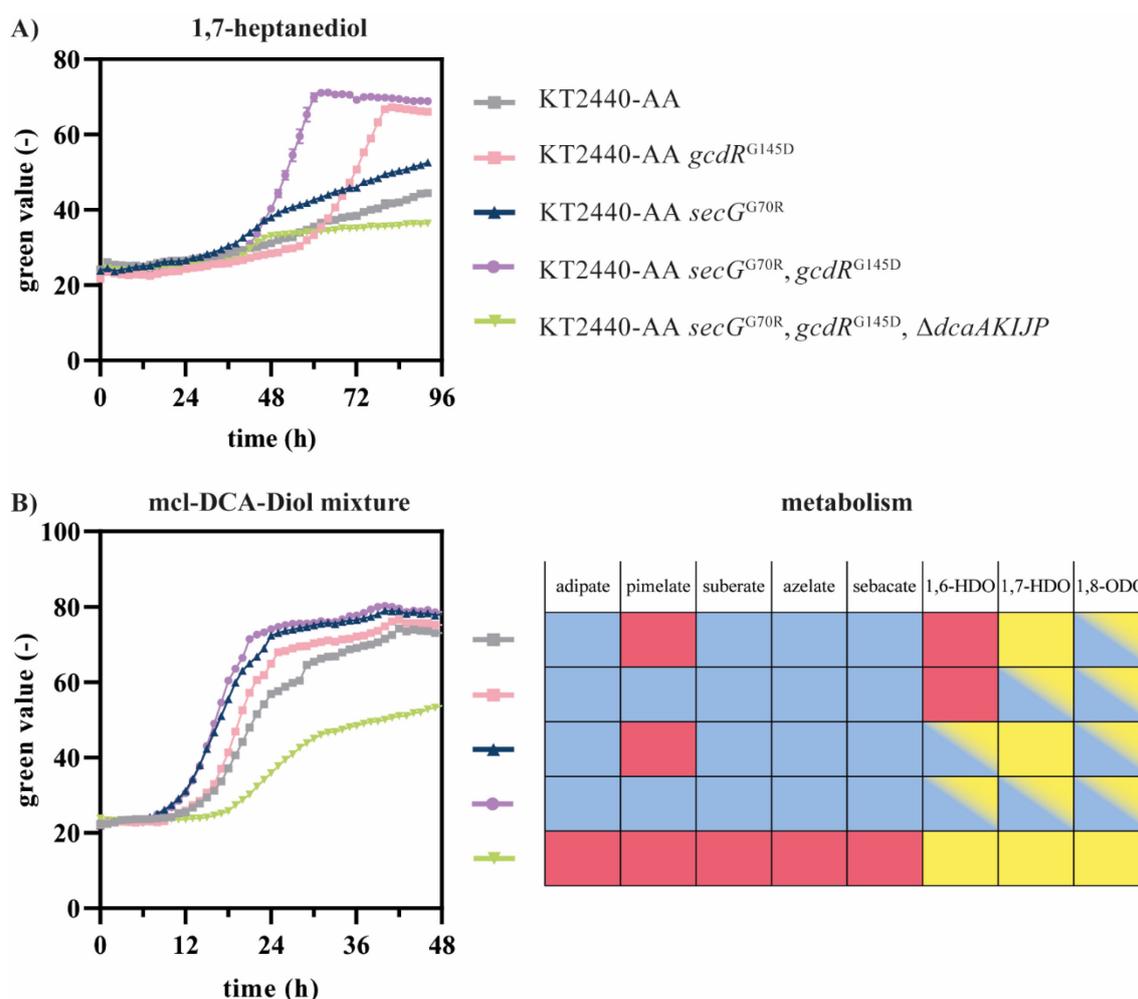
Figure 2.3-4. Growth of KT2440-AA strains on 1,7-heptanediol and on a mcl-DCA -diol mixture. All strains were cultivated in MSM containing 25.7 mM 1,7-heptanediol (A) or a mixture consisted of adipate, pimelate, suberate, azelate, sebacate, 1,6-hexanediol (HDO), 1,7-heptanediol, and 1,8-octanediol (ODO) with concentrations of 3 mM each (B). Red indicates the inability of the strain to metabolize the substrate. Yellow indicates metabolism via the HA-CoA-activating pathway, whereas blue indicates that the substrate was metabolized via the DCA-CoA-activating pathway. Potential activity of both pathways is indicated as color gradient. All mutations shown are in the KT2440-AA strain. Error bars indicate the standard error of the mean (n=3).

2.3.4.5 Towards bio-upcycling of complex aliphatic mixtures

Although growth on single monomers is useful to elucidate the genetic and biochemical basis of mcl-DCA metabolism, for bio-upcycling purposes it is necessary to metabolize mixtures of complex plastic hydrolysates. For example, auto-oxidation of high-density polyethylene (HDPE) yields a mixture of C_4-C_{22} dicarboxylic acids (Sullivan et al., 2022). This mixture was successfully degraded by Sullivan *et al.* by strain AW162 comparable to

P. putida KT24440-AA described above (Sullivan et al., 2022). Strain AW162 lacks the mutations in *gcdR* and is not able to grow on pimelate as sole carbon source (Sullivan et al., 2022). However, AW162 was able to metabolize ucl-DCA in a mixture, likely due to the presence of glutarate to induce *gcdH*-PP_0159. We hypothesized that the relatively low concentration of glutarate might lead to sub-optimal expression that might be ameliorated by the *gcdR* mutation. Indeed, comparison of growth of our reverse engineered strain with and without *gcdR*^{G154D} on a mixture of C_4-C_{10} DCA reveals a much better growth for the strain harboring the mutation (Figure 2.3-5). This was the case for mixtures with and without glutarate.
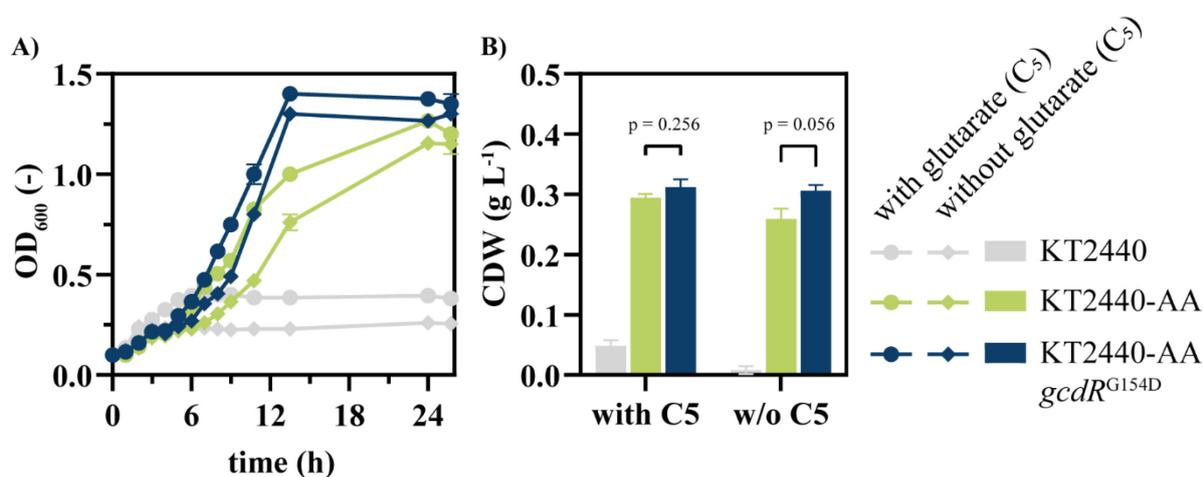
Figure 2.3-5. Growth of strains on a mixture of various (mcl)-dicarboxylic acids. All strains were cultivated in three-fold buffered MSM containing 1 mM of each DCA (C_4-C_{10}) with and without glutarate to compare the influence of inducer. For offline growth measurements, samples were taken at several time points (A). Final consumption of all monomers was confirmed by HPLC (data not shown). After 26 hours sample were taken for final cell dry weight determination (B). Error bars indicate the standard error of the mean (n=2).

The successful funneling of DCA and diols of even and uneven chain lengths into the central metabolism of our engineered *P. putida* KT2440-AA *secG*^{G70R}, *gcdR*^{G154D} paves the way for investigating their bio-upcycling. As target product, polyhydroxyalkanoates (PHA) were selected that are biodegradable polyesters with increasing industrial applications (Blanco et al., 2021; Dalton et al., 2022). In nitrogen-limited media, *P. putida* KT2440 natively produces mcl-PHA providing (*R*)-3-hydroxyacyl-CoA, the primary precursor, *via* two pathways (Liu et al., 2023). By this, related substrates such as fatty acids are converted to (*R*)-3-hydroxyacyl-CoA *via* β-oxidation, whereas unrelated substrates such as glucose are

funneled *via* malonyl-CoA into fatty acid *de novo* synthesis resulting in the production of the precursor. To test if the engineered *P. putida* KT2440-AA *secG*[G70R], *gcdR*[G154D] is able to produce mcl-PHA from mcl-DCA and -diols, the strain was cultivated in nitrogen-limited medium with a C:N ratio of 30:1 using substrate concentrations that are C-mol equivalent to 30 mM adipate. Although all mcl-DCA are metabolized *via* the *dcaAKIJP*-encoded β-oxidation, PHA production was clearly dependent on the chain-length of the substrate (Table 2.3-1). Using adipate as substrate, mcl-PHA were produced to 15.7 ± 1.0 % of the cell dry weight (CDW) with 3-hydroxydecanoic acid as the dominant monomer (57.8 ± 3.2 %). In contrast to this, only 3.3 ± 0.1 % mcl-PHA were produced from pimelate and less than 1 % mcl-PHA were produced from suberate, azelate, and sebacate. The same trend was observed when different mcl-diols were tested for mcl-PHA production. In total, 10.0 ± 0.6 % mcl-PHA were produced from HDO and 4.3 ± 0.1 % from 1,7-heptanediol. As observed for suberate, mcl-PHA production from ODO was below 1 %. Although the relative monomer composition of adipate and pimelate compared to HDO and 1,7-heptanediol was similar, the total amount of mcl-PHA was higher when the mcl-DCA were used as substrates (Table 2.3-1). This can be explained by the presence of the HA-CoA-activating pathway for mcl-diol metabolism in the Δ*dcaAKIJP* mutants. Hence, less carbon was likely funneled from the diols into the DCA-CoA-activating pathway yielding less favorable precursors for mcl-PHA production. When a mock hydrolysate consisting of C_6-C_{10}-DCA and C_6-C_{10}-diols with 5 mM each was used as substrate, 0.3 ± 0.0 % mcl-PHA were produced. This low yield can be explained by the relative high amount of C_8-C_{10} substrates that were identified to be barely suitable for mcl-PHA production. Our results fit into the observations of Sullivan *et al.* that reported a yield of 11.8 ± 2.9 % mcl-PHA from a mixture containing benzoate, acetate, and C_4-C_{17}-mcl-DCA (Sullivan et al., 2022). When a polystyrene hydrolysate was tested, only 0.8 ± 0.2 % mcl-PHA were produced indicating that only fractions of complex mixtures can be used to produce PHA. In contrast to C_8-C_{10}-fatty acids that are well-suited for mcl-PHA production in *P. putida* KT2440 (Prieto et al., 2016), C_8-C_{10}-DCA were not appropriate for mcl-PHA production. This likely results from the fact that mcl-DCA such as adipate and pimelate are metabolized *via* β-oxidation, but unlike fatty acids they are not directly used as PHA precursors. Rather they are broken down to acetyl-CoA, and then shunted back into fatty acid *de novo* synthesis, which is linked back to β-oxidation through the action of PhaG.

Possibly, the longer-chain DCA, which match the typical PHA monomer chain length, induce components of β-oxidation that interfere with PHA synthesis by degrading the hydroxyacyl-CoA precursor. Moreover, the ratio between succinyl-CoA and acetyl-CoA increases with increasing chain-length using C-molar equivalent concentrations of the substrate. The changing ratio might influence PHA production (Figure 2.3-6). This could also be an explanation for the variation in CDWs when different substrates are metabolized (Table 2.3-1).

Table 2.3-1. Production of mcl-PHA by engineered P. putida KT2440-AA *secG*^{G70R}, *gcdR*^{G154D} from different substrates. The CDW, PHA content, and relative monomer composition of mcl-PHA are shown. The strain was cultivated in MSM supplemented with C-mol equimolar concentrations to 30 mM of adipate using a C:N ratio of 30:1. The mock hydrolysate consisted of 5 mM of each individual substrate. Error values are calculated as standard deviations (n=2). Exemplary GC chromatograms are shown in Figure S5.3-7.

substrate	CDW (g L^{-1})	PHA (%)	C$_6$ (%)	C$_8$ (%)	C$_{10}$ (%)	C$_{12}$ (%)
adipate	0.62 ± 0.05	15.7 ± 1.05	14.3 ± 3.2	24.1 ± 0.2	57.8 ± 3.2	3.8 ± 0.2
pimelate	0.62 ± 0.02	4.3 ± 0.12	14.2 ± 0.2	32.3 ± 0.3	47.9 ± 0.2	5.6 ± 0.0
suberate	0.47 ± 0.00	0.4 ± 0.01	n. d.	5.0 ± 1.1	48.4 ± 1.6	46.6 ± 3.4
azelate	0.47 ± 0.01	0.4 ± 0.02	n. d.	n. d.	48.8 ± 3.4	51.2 ± 3.4
sebacate	0.52 ± 0.03	0.6 ± 0.01	n. d.	9.9 ± 0.2	55.8 ± 0.7	34.3 ± 0.4
1,6-hexanediol	0.57 ± 0.03	10.0 ± 0.6	10.0 ± 0.5	33.4 ± 0.2	52.9 ± 0.1	3.8 ± 0.2
1,7-heptanediol	0.57 ± 0.01	3.4 ± 0.01	12.8 ± 0.7	30.0 ± 0.0	49.7 ± 0.2	7.5 ± 0.5
1,8-octanediol	0.43 ± 0.01	0.5 ± 0.00	4.7 ± 0.5	7.2 ± 0.1	49.1 ± 2.8	39.0 ± 2.0
mock hydrolysate	0.89 ± 0.02	0.3 ± 0.01	n. d.	n. d.	60.9 ± 1.1	39.1 ± 1.1

To avoid the abovementioned hypothesized conflict, we investigated whether PHB might be a favored product for the bio-upcycling of the described substrates. This short-chain polymer is produced from acetoacetyl-CoA, which is converted to (*R*)-3-hydroxybutyryl-CoA as substrate for PHB synthesis. To produce PHB in *P. putida* KT2440, the ability to produce mcl-PHA was abolished by deleting the PP_5003-6 gene cluster including the PHA (de-)polymerases. Since *P. putida* KT2440 is not a natural PHB producer, a PHB biosynthesis pathway from *C. necator* H16 was expressed in the KT2440-AA *secG*^{G70R} *gcdR*^{G154D} mutant. The synthetic pathway comprises *phaCAB*, encoding (i) PhaA, a thiolase that condenses two acetyl- CoA moieties into acetoacetyl-CoA, (ii) PhaB, a reductase that converts acetoacetyl-

CoA into (*R*)-3-hydroxybutyryl-CoA and (iii) PhaC, a short-chain-length (scl)-PHA synthase that polymerizes 3-hydroxybutyryl-CoA monomers (C$_4$) to yield PHB. We constructed a synthetic operon with these genes under the transcriptional control of the ChnR/P$_{chnB}$ expression system, inducible by cyclohexanone (Benedetti et al., 2016), and a synthetic ribosome binding site (5'-AGG AGG AAA AAC AT-3') upstream of each gene. This construct was assembled in the pSEVA631 vector by USER cloning, resulting in plasmid pS6311·PHB.

Heterologous expression of the *phaCAB* cluster indeed enabled production of PHB by *P. putida* KT2440-AA *secG*^{G70R}, *gcdR*^{G154D} carrying pS6311·PHB under nitrogen-sufficient conditions (Table 2.3-2). In contrast to native mcl-PHA production, uneven substrates such as pimelate (15.14 ± 0.05 %) and 1,7-heptanediol (21.86 ± 2.77 %) were preferred for PHB accumulation. This can be explained by the formation of acetoacetyl-CoA as intermediate that is directly used for PHB synthesis. Hence less carbon is available for biomass formation yielding lower CDWs (Table 2.3-2). When azelate was used as substrate, less PHB (6.53 ± 0.92 %) was produced compared to pimelate likely caused by the formation of an additional molecule of acetyl-CoA that was used for the production of biomass as indicated by the CDW.
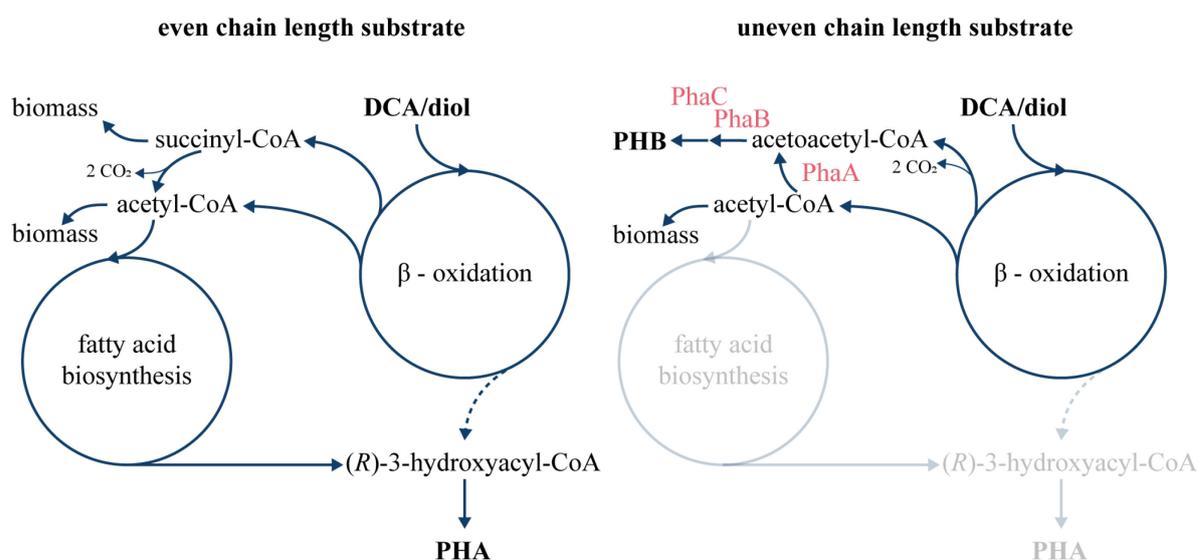
Figure 2.3-6. Comparison between PHA and PHB synthesis from even- and uneven-chain aliphatic diols and dicarboxylates. The heterologous enzymes from *C. necator* responsible for PHB production are shown in red.

Although mcl-PHA were produced from adipate, this substrate as well as suberate and sebacate were not suited for the production of PHB as acetyl-CoA was likely used for biomass formation (Table 2.3-2). Moreover, HDO and ODO also resulted in lower amounts of PHB. In all, these results indicate that the produced PHB was mainly derived from acetoacetyl-CoA as intermediate of ucl-DCA or -diol metabolism. Consequently, our results indicate that acetyl-CoA from substrates with even chain length are predominantly utilized for the production of biomass rather than converted to acetoacetyl-CoA for PHB synthesis. To enable efficient upcycling of substrates with even and uneven chain lengths present in mixed hydrolysates, future studies could investigate the combination of scl- with mcl-PHA synthesis pathways in a single strain. By this both mcl- and ucl-substrates can be converted to scl-co-mcl-PHA that features enhanced physical properties compared to homopolymeric PHAs (Wang et al., 2023).

Table 2.3-2. Production of PHB by engineered *P. putida* KT2440-AA *secG*^{G70R}, *gcdR*^{G154D} carrying plasmid pS6311·PHB from different substrates. The CDW and PHB content are shown. The strain was cultivated in MSM supplemented with C-equimolar concentrations of pure substrates and 1 mM cyclohexanone as inducer for phaCAB expression. The strain was cultivated in MSM supplemented with C-mol equimolar concentrations to 30 mM of adipate using a C:N ratio of 30:1. The mock hydrolysate consisted of 5 mM of each individual substrate. Error values are calculated as standard deviations (n=2). Exemplary GC chromatograms are shown in Figure S5.3-7.

substrate	CDW (g L^{-1})	PHB (%)
adipate	1.52 ± 0.05	1.16 ± 0.06
pimelate	0.23 ± 0.01	15.14 ± 0.05
suberate	1.52 ± 0.04	1.56 ± 0.19
azelate	1.47 ± 0.01	6.53 ± 0.92
sebacate	1.52 ± 0.02	2.35 ± 0.07
1,6-hexanediol	1.29 ± 0.14	3.59 ± 0.01
1,7-heptanediol	0.26 ± 0.01	21.86 ± 2.77
1,8-octanediol	0.56 ± 0.01	2.20 ± 0.76
mock hydrolysate	1.16 ± 0.01	3.59 ± 0.01

2.3.5 Conclusions

Bio-upcycling of complex monomer mixtures, either from a single polymer or from mixed plastic waste streams, is a promising approach for the establishment of a circular economy. In order to achieve an efficient bio-upcycling approach, the funneling of different monomers into the value-added products is crucial. We successfully engineered the combined degradation of diols and dicarboxylic acids in a single platform strain of *P. putida* KT2440. Using this strain, we demonstrated the conversion of monomer mixtures into different PHA, which are of increasing interest in the polymer industry. Although PHA yields are currently relatively low ($\pm\,0.03$ g_{PHA} $g_{substrate}^{-1}$), our study provides fundamental insights into the different metabolic pathways available for aliphatic α,ω-functionalized molecules and how their central metabolic products affect product formation. This leads the path for future PHA yield optimizations and increased the range of potential substrates for PHA production.

2.3.6 Materials and methods

2.3.6.1 Strains and culture conditions

The chemicals used in this work were obtained from Carl Roth (Karlsruhe, Germany), Sigma-Aldrich (St. Louis, MO, USA), or Merck (Darmstadt, Germany) unless stated otherwise. All bacterial strains used in this work are listed in Table S1. Unless otherwise stated, *P. putida* KT2440 strains were cultivated for quantitative microbiology experiments in three-fold buffered (11.64 g L^{-1} K_2HPO_4, 4.89 g L^{-1} NaH_2PO_4) MSM. Pre-cultures contained 20 mM glucose. For cultivation experiments, the final concentrations of diols or dicarboxylates were C-molar equivalent to 30 mM adipate. For online growth measurements cultures were grown and analyzed with the Growth Profiler® 960 (Enzyscreen, Heemstede, The Netherlands) by image analysis. Main cultures were cultivated in transparent bottom 96-well microtiter plates (CR1496dg) with a volume of 200 µL at 30 °C and 225 rpm shaking speed.

Adaptive laboratory evolution (ALE) on HDO was performed in 96-well microtiter plates by iterative inoculation of fresh medium after the stationary phase was reached. For *P. putida* KT2440-AA, 30 mM HDO was used as sole carbon source. Since *P. putida* KT2440 did not

grow with HDO as sole carbon source at the start of the ALE, 15 mM HDO and 15 mM BDO were used for the first two batches of the ALE. This concentration was shifted to 20 mM HDO and 10 mM BDO (batches 3-5), and to 30 mM HDO (batches 6-14). After ALE, single clones were isolated on LB agar plates and screened for growth on HDO as sole carbon source. The best growing strains were selected for whole genome sequencing.

Liquid cultivations with additional analysis were incubated at 30 °C, with a shaking speed of 200 rpm and an amplitude of 50 mm using Climo-Shaker ISF1-X (Kuhner Shaker, Birsfelden, Switzerland) in 500 mL non-baffled Erlenmeyer flasks with metal caps, containing 50 mL culture volume. For PHA production experiments, cells were cultivated in three-fold buffered and nitrogen-limited MSM. For this, a C:N ratio of 30:1 was used. PHB production was carried out in three-fold buffered MSM with 1 mM of cyclohexanone as inducer and 10 µg mL^{-1} gentamicin to maintain the pS6311·PHB plasmid. Cultivations were performed in 500 mL shake flasks with 50 mL of culture volume at 30 °C and 200 rpm until the stationary phase was reached.

2.3.6.2 Plasmid cloning and strain engineering

Cloning primers were ordered as unmodified DNA oligonucleotides from Eurofins Genomics (Ebersberg, Germany) and are listed in Table S3. The Q5 High-Fidelity 2× Master Mix (New-England Biolabs, Ipswich, MA, USA) was used for the amplification of cloning fragments, while the One*Taq* Quick-Load 2× Master Mix (New-England Biolabs, Ipswich, MA, USA) was used for screening together with a pre-lysis step in alkaline PEG200 (Chomczynski and Rymaszewski, 2006). Plasmids used in this study were assembled by Gibson assembly (Gibson et al., 2009) using the NEBuilder HiFi DNA assembly Master Mix (New-England Biolabs, Ipswich, MA, USA) or USER cloning (Cavaleiro et al., 2015) and are listed with more details in Table S2. In order to bestow PHB biosynthesis to *P. putida* strains, plasmid pS6311·PHB was constructed as follows. First, plasmid pS648::(sRBS)*phaCAB* was constructed in order to introduce synthetic RBSs upstream of each gene comprising the PHB operon. Such sRBSs sequences were introduced in the USER primers and *phaCAB* from *Cupriavidus necator* H16 was amplified from pS341·PHA (Durante-Rodríguez et al., 2018). The resulting plasmid, bearing sRBSs upstream of each of the three genes comprising the *pha* operon, was then used as template for the amplification

of this construction. Lastly, pSEVA2311 (Silva-Rocha et al., 2013) was used as template for PCR amplification of the ChnR/P*chnB* expression system. These two USER fragments were used to assemble plasmid pS6311·PHB.

Transformation of *E. coli* with assembled DNA and purified plasmids was performed by a heat chock protocol (Hanahan, 1983). Transformation of *P. putida* was performed by electroporation or conjugational transfer of mobilized plasmids by patch mating as described by Wynands et al. (2018). Knockouts, promoter exchanges and point mutations were obtained using either a modified pSNW2 system from Volke et al. (2020) based on the pEMG system described by Martínez-García and de Lorenzo (2011) or the original system with a modified protocol described by Wynands et al. (2018). Antibiotics were added to the medium as needed to support plasmid maintenance and to select for genomic recombination events (final concentration: Kanamycin sulfate 50 mg L^{-1}; Gentamicin 25 mg L^{-1}). Plasmids, gene deletions and point mutations were confirmed by Sanger sequencing performed by Eurofins Genomics (Ebersberg, Germany).

2.3.6.3 RT-qPCR

To analyze gene expression levels, RT-qPCR was performed. Therefore, pre-cultures of *P. putida* strains were used to inoculate 50 mL shake flask main cultures in three-fold buffered MSM containing either glutarate (36 mM), pimelate (25.7 mM), azelate (20 mM) or glucose (20 mM) as sole carbon source to an initial OD$_{600}$ of 0.1. After incubation to mid-exponential growth phase, cells were harvested from 2 mL of cell culture by centrifugation (21,000 × *g* for 2 min) and immediately resuspended in 1 mL RNAlater. (Thermo Fisher Scientific, Massachusetts, USA) and stored at -20 °C until further analysis. RNA extraction was performed using the Quick-RNA Miniprep Kit (Zymo Research, Irvine, CA, USA) and cDNA was prepared from the purified RNA using the LunaScript RT superMix Kit (New England Biolabs, Ipswich, MA, USA). The expression levels of target genes were analyzed using primers designed by qPCR assay design tool from Eurofins Genomics and listed in Table S2 (*gcdH*) or in Otto et al. (2019) (*rpoD*). Quantitative RT-PCR was performed using Luna Universal qPCR Master Mix (New England Biolabs, Ipswich, MA, USA) in 96-well plates by the qTOWER 2.2 (Analytik Jena, Jena, Germany). The reaction conditions were used as described in the manufacturer's instructions. Experiments were performed in

technical triplicates of biological duplicates. Gene expression levels were evaluated by comparing the Ct values of the housekeeping gene *rpoD* (Wang and Nomura, 2010) with the Ct value of *gcdH* using the following equation: Gene expression level $= 2^{\text{Ct}(rpoD)\text{-Ct(target)}}$

2.3.6.4 Genome sequencing

Genomic DNA from selected strains was purified using a Monarch Genomic DNA Purification Kit (NEB) from an overnight LB culture. Afterwards, 1 µg of DNA was used for library preparation using the NEBNext® Ultra™ II DNA Library Prep Kit for Illumina® (New England Biolabs, Ipswich, MA, USA). The library was evaluated by qPCR using the KAPA library quantification kit (Peqlab, Erlangen, Germany). Afterwards, normalization for pooling was done and paired-end sequencing with a read length of 2 × 150 bases was performed on a MiSeq (Illumina, San Diego, CA, USA). The sequencing output (base calls) were received as demultiplexed fastq files. The data (e.g. trimming, mapping, coverage extraction) were processed using the CLC Genomic Workbench software (Qiagen Aarhus A/S, Aarhus, Denmark). For each sample, the output was mapped to the GenBank accession AE015451.2 as the *P. putida* KT2440 reference genome with further modifications for previous genetic engineering (Ackermann et al., 2021). Sequencing data are deposited in the NCBI Sequence Read Archive under BioProject number PRJNA987418.

2.3.6.5 Analytical methods

In shake flask experiments, bacterial growth was monitored as optical density at a wavelength of 600 nm (OD_{600}) with an Ultrospec 10 cell Density Meter (Ge Healthcare, Little Chalfront, Buckinghamshire, United Kingdom). Online analysis of growth was measured by the Growth Profiler and analyzed using the Growth Profiler Control software V2_0_0. The corresponding green values are derived from image analysis of the image taken from the bottom of microtiter plates.

For measuring extracellular mcl-diols and DCA metabolites, samples were harvested from liquid cultivation by centrifugation (21,000 × *g* for 2 min) and the supernatant was analysed using a 1260 Infinity II HPLC equipped with a 1260 Infinity II Refractive Index Detector (Agilent, Santa Clara, California, USA). Analytes were eluted using a 150 x 7.80 mm organic acid resin column (Rezex ROA – organic acid H+ (8%), Phenomenex, Torrance, CA, USA)

together with a 40 × 8 mm organic acid resin pre-column with 5 mM H_2SO_4 as mobile phase at a flow rate of 0.7 mL min^{-1} at 80 °C. Metabolites were quantified using HPLC-grade chemicals.

2.3.6.6 PHA and PHB analysis *via* gas chromatography

PHA and PHB quantification was performed using acidic methanolysis and gas chromatography (GC) analysis as described in Li et al. (2020). For this, cells were harvested by centrifugation at 5000 × g for 10 min and washed with H_2O. Prior to analysis, samples were lyophilized overnight in a Christ LT-105 freeze drier (Martin Christ Gefriertrocknungsanlagen, Osterode am Harz, Germany). Next, 5-15 mg of lyophilized cells were mixed with 2 mL acidified methanol (15 % (v/v) H_2SO_4) and 2 mL chloroform containing methyl benzoate as internal standard in a 15 mL Pyrex tube. The tube was sealed and incubated at 100 °C for 3 h. After cooling the tubes on ice for 2 min, 1 mL of H_2O_{MilliQ} was added to each tube and the solution was mixed by vortexing. The phases were allowed to separate and the organic phase (lower phase) was filtered through cotton wool before further analysis.

The 3-hydroxyalkanoic acid methyl ester were quantified using an Agilent 7890A Gas Chromatograph equipped with a HP Innowax column (30 m × 0.25 mm × 0.5 μm) and a flame ionization detector (FID). An oven ramp cycle was employed as follows: 120 °C for 5 min, increasing by 3 °C/min to 180 °C, 180 °C for 10 min. A 10:1 split was used with helium as the carrier gas and an inlet temperature of 250 °C. Commercially available 3-hydroxyalkanoic acids (C_4-C_{12}) were methylated as described above and used as standards to quantify PHA monomers.

2.3.7 Availability of data and materials

All data generated or analysed during the study are included in this published article and its supplementary informations. Sequencing data are deposited in the NCBI Sequence Read Archive under BioProject number PRJNA987418.

2.3.8 Competing interests

The authors declare that they have no competing interest.

2.3.9 Acknowledgements

2.4 Characterization and engineering of branched short-chain dicarboxylate metabolism in *Pseudomonas* reveals resistance to fungal 2-hydroxyparaconate

Published as:

de Witt, J.[1], Ernst, P.[1], Gätgens, J.[1], Noack, S.[1], Hiller, D.[2], Wynands, B.[1], Wierckx, N.[1*], (2023). Characterization and engineering of the branched short-chain dicarboxylate metabolism of *Pseudomonas* reveals resistance to fungal 2-hydroxyparaconate. *Metabolic Engineering*, 75, 205-216. doi:10.1016/j.ymben.2022.12.008

[1] Institute of Bio- and Geosciences IBG-1: Biotechnology, Forschungszentrum Jülich, Jülich, Germany

[2] Institut für Mikrobiologie, Technische Universität Braunschweig, Germany

[*] Corresponding author

CRediT authorship contribution statement:
J. de Witt: Methodology, Investigation, Validation, Formal analysis, Data curation, Writing – original draft, Writing – review and editing, Visualization.
P. Ernst: Investigation
J. Gätgens: Investigation, Resources
S. Noack: Resources, Writing – review and editing
D. Hiller: Investigation
B. Wynands: Conceptualization, Writing – Review & Editing
N. Wierckx: Conceptualization, Funding acquisition, Supervision, Writing – Review & Editing

Overall contribution: 70 %

The presented experimental work was conducted by JdW and partly by PE (*U. cynodontis* cultivation), JG (GC-ToF-MS analysis), DH (*C. albicans* cultivation). Validation was done by JdW. Visualization of all data was performed by JdW. The writing of the original draft was done by JdW, which was reviewed and edited by SN, BW, and NW and all co-authors. Funding for the project was acquired by NW.

Additional data related to this publication are shown in the addendum to this chapter (2.4.10).

2.4.1 Highlights

- Engineered branched short-chain dicarboxylate (BSCD) metabolism in *P. putida*
- Characterized transport and substrate range of BSCD pathway from *P. aeruginosa*
- Revealed a link to fungal secondary metabolite resistance to 2-hydroxyparaconate
- Engineered *P. putida* enables bio-upcycling of BSCD-containing polymer hydrolysates

2.4.2 Graphical abstract
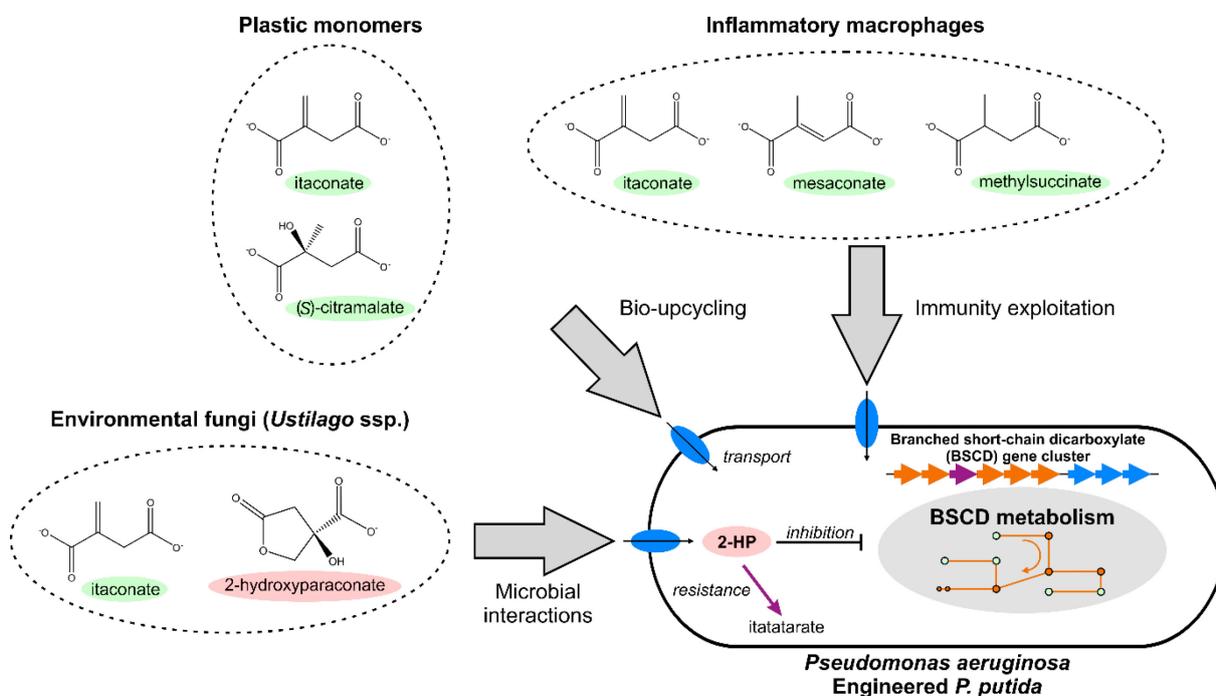
2.4.3   Abstract

In recent years branched short-chain dicarboxylates (BSCD) such as itaconic acid gained increasing interest in both medicine and biotechnology. Their use as building blocks for plastics urges for developing microbial upcycling strategies to provide sustainable end-of-life solutions. Furthermore, many BSCD exhibit anti-bacterial properties or exert immunomodulatory effects in macrophages, indicating a medical relevance for this group of molecules. For both of these applications, a detailed understanding of the microbial metabolism of these compounds is essential. In this study, the metabolic pathway of BSCD degradation from *Pseudomonas aeruginosa* PAO1 was studied in detail by heterologously transferring it to *Pseudomonas putida*. Heterologous expression of the PA0878-0886 itaconate metabolism gene cluster enabled *P. putida* KT2440 to metabolize itaconate, (*S*)- and (*R*)-methylsuccinate, (*S*)-citramalate, and mesaconate. The functions of the so far uncharacterized genes PA0879 and PA0881 were revealed and proven to extend the substrate range of the core degradation pathway. Furthermore, the uncharacterized gene PA0880 was discovered to encode a 2-hydroxyparaconate (2-HP) lactonase that catalyzes the cleavage of the itaconate derivative 2-HP to itatartarate. Interestingly, 2-HP was found to inhibit growth of the engineered *P. putida* on itaconate. All in all, this study extends the substrate range of *P. putida* to include BSCD for bio-upcycling of high-performance polymers, and also identifies 2-HP as promising candidate for anti-microbial applications.

2.4.4 Introduction

The global plastic crisis urges us to redesign the entire life cycle of polymers. Nearly 400 Mt of plastics were produced in 2020 (Hundertmark et al., 2018), and estimated 90 Mt of plastic waste is predicted to enter the aquatic ecosystems by 2030 (Borrelle et al., 2020). This underlines the need for a more sustainable plastics life cycle. Ideally, polymers should be designed to be both bio-based and biodegradable to show a high degree of sustainability while also reducing the environmental burden (Wei et al., 2020). In recent years, major progress was achieved in the (bio-) catalytic depolymerization of plastics including polyesters, polyurethanes, and polyamides (Ellis et al., 2021; Magnin et al., 2020; Negoro et al., 2018; Tournier et al., 2020). Due to the heterogenic composition of many plastic products, their depolymerization results in a diverse mixture of monomeric building blocks. To close the life cycle of these plastics, the obtained mixed plastic hydrolysates need to be re- or upcycled. For the latter, microbial upcycling can be a powerful tool enabling the conversion of mixed plastic hydrolysates to value-added compounds (Tiso et al., 2021b; Wierckx et al., 2015). Microbial upcycling requires efficient funneling of plastic monomers into the central metabolism of suitable microorganisms. *Pseudomonas putida* KT2440 and related species are well known in this respect, and strains have been isolated or engineered to funnel prevalent plastic monomers such as ethylene glycol (Franden et al., 2018b; Li et al., 2019), 1,4-butanediol (Li et al., 2020), adipate (Ackermann et al., 2021), terephthalate (Narancic et al., 2021), and 2,4-toluenediamide (Puiggené et al., 2022) into their central metabolism. Furthermore, non-pathogenic Pseudomonads enable safe and practical research and were also engineered to produce a variety of value-added compounds, including polyhydroxyalkanoates (PHA) (Dalton et al., 2022; Mezzina et al., 2021), aromatic compounds (Schwanemann et al., 2020) as well as rhamnolipids (Tiso et al., 2020). The direct upcycling of plastic monomers to such products was also achieved by engineering non-pathogenic Pseudomonads (Kenny et al., 2012; Werner et al., 2021). Recently, a two-stage chemical oxidation and biological funneling approach using engineered *P. putida* was developed enabling upcycling of various plastics (Sullivan et al., 2022). Application of this method on polypropylene (PP) would result in the release of branched short-chain dicarboxylates (BSCD).

Aliphatic dicarboxylates are widely used for the synthesis of polyesters, polyamides and polyurethanes. In the past years, the subgroup of BSCD, gained importance as bio-based platform chemicals (Klement and Büchs, 2013; Saha, 2017; Üzüm and Karadağ, 2006; Wu et al., 2021b; Xie et al., 2014). Especially their use as bio-based monomers for plastics is of great interest, as certain branches allow cross-linking of polymer chains and polymer properties can be tuned (Little et al., 2020; Voit and Lederer, 2009; Xie et al., 2014). Among BSCD, itaconic acid is the most prominent platform chemical as it can be used for plastic production, water decontamination, controlled drug delivery systems and many more (Okabe et al., 2009; Steiger et al., 2017; Willke and Vorlop, 2001). Besides its use as bio-based platform chemical, itaconate was revealed as mammalian metabolite synthesized by the product of the immunoresponsive gene 1 (*irg1*) upon macrophage activation (Michelucci et al., 2013; Strelko et al., 2011). Itaconate not only triggers anti-inflammatory cascades (Mills et al., 2018) but also possesses anti-bacterial properties by inhibiting the isocitrate lyase that is the key enzyme of the glyoxylate cycle (Hillier and Charnetzky, 1981; Höner Zu Bentrup et al., 1999). Since the glyoxylate cycle is essential for pathogenic bacteria to survive in the host environment, itaconate inhibits growth of pathogens (Hillier and Charnetzky, 1981). Nowadays, itaconate can be produced by fermentation processes from renewable feedstocks using *Aspergillus terreus* and species of the genus *Ustilaginaceae* such as *Ustilago maydis* and *Ustilago cynodontis* (Becker et al., 2021; Geiser et al., 2014; Guevarra and Tabuchi, 1990; Okabe et al., 2009; Wierckx et al., 2020). Besides itaconate, species of the genus *Ustilago* also produce two derivatives, namely its chiral lactone 2-hydroxyparaconate (2-HP) and itatartarate (ITT) (Guevarra and Tabuchi, 1990). In *U. maydis*, itaconate is converted to 2-HP by the cytochrome P450 monooxygenase Cyp3 (Geiser et al., 2016a). It is anticipated that a putative ring-cleaving dioxygenase (Rdo1) converts 2-HP to ITT, although this function could thus far not be confirmed (Geiser et al., 2018; Geiser et al., 2016a). Both molecules, 2-HP and ITT, cannot be synthesized as pure compounds yet and are not commercially available, but they might exhibit interesting physiological properties due to their metabolic linkage to itaconate.

Many pathogens such as *Salmonella typhimurium*, *Yersinia pestis*, or *Pseudomonas aeruginosa* PAO1 have acquired an itaconate degradation pathway to overcome the anti-bacterial effects of itaconate (Martin et al., 1961; Sasikaran et al., 2014) (Figure 2.4-3). Most

itaconate-degrading pathogens such as *Y. pestis* contain an operon only encoding an itaconyl-CoA transferase (Ict), itaconyl-CoA isomerase/mesaconyl-C_4-CoA hydratase (Ich), and (*S*)-citramalyl-CoA lyase (Ccl) (Sasikaran et al., 2014). In contrast, in the genome of *P. aeruginosa* PAO1 these enzymes are encoded in the PA0878-PA0883 operon which contains three additional genes of thus far unknown functions. The combination of these three genes is relatively specific to *P. aeruginosa*, although some species contain one or two similar genes (Sasikaran et al., 2014).

The interest in BSCD as bio-based polymer building blocks is rising. Furthermore, oxidative depolymerization of prevalent plastics such as PP results in the formation of BSCD (Partenheimer, 2003; Sullivan et al., 2022). To close the life cycle of such plastics, microbial upcycling using *P. putida* KT2440 could be applied. So far, itaconate degradation seems to be limited to pathogenic species that are not suitable for biotechnological applications (Sasikaran et al., 2014). Furthermore, the degradation of other BSCD such as (*S*)-(*R*)-methylsuccinate is not fully unraveled yet. Besides their usage as bio-based building blocks, many BSCD such as itaconate, mesaconate or citraconate were recently identified as anti-bacterial and immunomodulatory compound (Bernard, 2022; Chen et al., 2022; He et al., 2022; McGettrick and O'Neill, 2022). Hence, the identification and characterization of bacterial metabolic pathways of BSCD is also of great importance to combat pathogenic and multidrug-resistant species.

In this study, the metabolic pathways for itaconate and other BSCD from *P. aeruginosa* PAO1 were characterized through their heterologous expression in the non-pathogenic *P. putida* KT2440. Peripheral degradation pathways for various BSCD were elucidated and a general BSCD uptake transporter was identified. Metabolic engineering enabled efficient growth of *P. putida* KT2440 on 20 mM of different BSCD within 16 h. Hence, a metabolic pathway of notable medical relevance was characterized, and at the same time, the range of upcyclable plastic monomers by *P. putida* KT2440 is extended. Furthermore, the functions of three so-far uncharacterized genes from the PA0878-0883 itaconate degradation cluster were explored and linked to the degradation of the itaconate derivatives 2-HP and ITT which have anti-bacterial and anti-fungal properties and interfere with the ability of bacteria to grow on itaconate.

2.4.5   Results and discussion

2.4.5.1   Degradation and transport of BSCD by engineered *P. putida* KT2440

In vitro studies indicated that degradation of itaconate requires the enzymes Ict, Ich, and Ccl that are encoded in the PA0878-PA0883 gene cluster of *P. aeruginosa* PAO1 (Sasikaran et al., 2014). Homologs of the encoding genes occur almost exclusively in pathogenic bacteria, whereas non-pathogenic strains such as *P. putida* KT2440 lack these genes. This highlights the importance of itaconate degradation by pathogens to survive in the host environment (Cordes and Metallo, 2021). Since Ict of *P. aeruginosa* PAO1 showed activity not only towards itaconate but also (*S*)-citramalate and methylsuccinate (Sasikaran et al., 2014), the PA0878-PA0883 gene cluster might encode degradation pathways for further BSCD. Especially the uncharacterized genes PA0879, PA0880, and PA0881 might be relevant for funneling additional BSCD into the pathway.

To investigate the metabolic functions of the PA0878-PA0883 gene cluster from *P. aeruginosa* PAO1, it was fused to the strong constitutive P_{14f} promoter (Zobel et al., 2015) and chromosomally integrated into the *Tn7* attachment site in the genome of *P. putida* KT2440 (Figure 2.4-1 a). Additional genes (PA0884-PA0886) encoding a putative dicarboxylate transporter were identified 112 bp downstream of PA0883. Using the operon-mapper (Taboada et al., 2018), it was predicted that both gene clusters are encoded in a single PA0878-PA0886 operon. To test whether the putative transporter is involved in the degradation of BSCD, a second construct with the entire PA0878-PA0886 gene cluster fused to P_{14f} was integrated as well (Figure 2.4-1). The resulting strains were grown in minimal medium supplemented with 20 mM of the following BSCD as sole carbon source: itaconate, (*S*)-citramalate, (*R*)-citramalate, mesaconate, citraconate, and racemic (*S*)-(*R*)-methylsuccinate.

A)
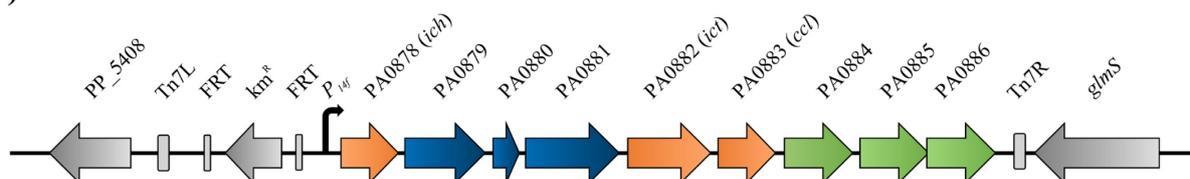
B)

strains										
P_{14f}-PA0878-0883								-	-	-
P_{14f}-PA0878-0886										
ΔPA0878 (*ich*)	Δ									
ΔPA0879-81		Δ	Δ	Δ						
ΔPA0879		Δ								
ΔPA0880			Δ							
ΔPA0881				Δ						
ΔPA0882 (*ict*)						Δ				
ΔPA0883 (*ccl*)							Δ			

Figure 2.4-1. Heterologous expression of the PA0878-0886 cluster in *P. putida* KT2440. (A) The PA0878-PA0883 and PA0878-PA0886 clusters of *P. aeruginosa* PAO1 were fused to the strong constitutive P_{14f} promoter and integrated into the *attTn7* site of *P. putida* KT2440. PA0878 (*ich*), PA0882 (*ict*) and PA0883 (*ccl*) (orange) are involved in itaconate degradation. PA0879, PA0880 and PA0881 encode a putative acyl-CoA dehydrogenase, a putative ring-cleaving dioxygenase and an MmgE/PrpD family protein (blue). A putative BSCD transporter is encoded by PA0884-PA0886 (green). **(B)** Overview of investigated strains in this study. Grey indicates the presence of a gene, whereas absent and deleted genes are marked with a "-" and "Δ", respectively. *Modified from de Witt et al. (2023).*

Wild type *P. putida* KT2440 was not able to utilize any of the tested substrates (Figure 2.4-2). Integration of the PA0878-PA0883 cluster enabled *P. putida* KT2440 to grow on itaconate, (*S*)-citramalate, mesaconate, and (*S*)-(*R*)-methylsuccinate as sole carbon source, whereas (*R*)-citramalate and citraconate were not metabolized. However, growth on most BSCD was relatively slow (ranging from 0.11 ± 0.00 h^{-1} for itaconate to 0.01 ± 0.00 h^{-1} for citramalate) compared to typical growth on glucose or other plastic monomers (Ackermann et al., 2021; Li et al., 2020). Inclusion of the putative transporter-encoding genes in the P_{14f}-PA0878-PA0886 construct enabled much faster growth rates around 0.4 h^{-1} (Figure 2.4-2, Table S5.4-1). Thus, PA0884-PA0886 likely encodes a BSCD transporter importing itaconate, mesaconate, (*S*)-citramalate, and (*S*)-(*R*)-methylsuccinate, making it a dedicated uptake system for these compounds in *P. aeruginosa*. Furthermore, these results indicate the presence of a native transporter in *P. putida* KT2440 that facilitates uptake of itaconate at a moderate rate, and uptake of (*S*)-citramalate, mesaconate and (*S*)-(*R*)-methylsuccinate at a minor rate. Homologs of the BSCD transporter were identified in several *Pseudomonas*

species that harbor a homologous six-gene itaconate metabolism cluster. Thus, the identified transporter might be a potential drug target for treatment of these pathogens using transport inhibitors. Interestingly, no homologous transporter system was identified in genetic vicinity of the three-gene operons of other pathogens such as *Y. pestis* and *Mycobacterium tuberculosis.* Instead, transporters with low similarities to PA0884-0886 were found in these strains, not associated with the itaconate metabolic operon (sequence identity < 35 %, query coverage < 40 %, E-value cutoff e^{-20}). Hence, itaconate uptake within these species could be investigated in future studies to identify alternative transporters.
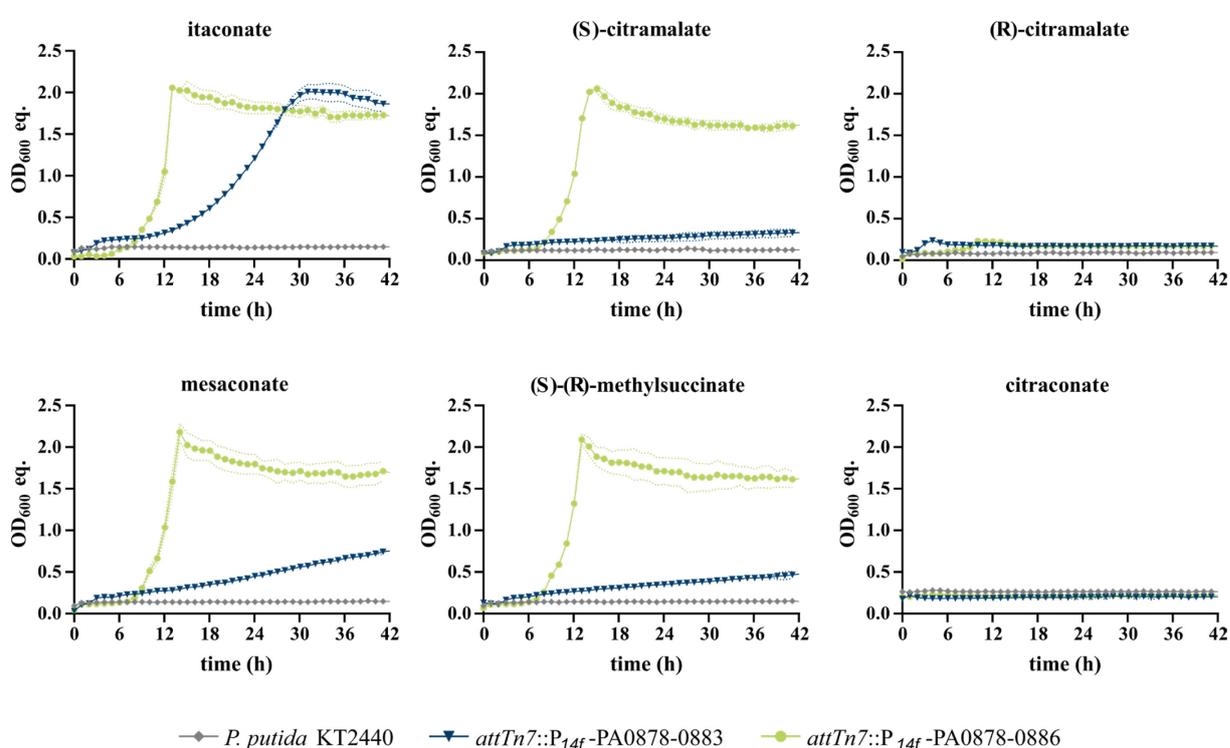
Figure 2.4-2. Substrate range of *P. putida* KT2440 strains harboring the PA0878-0883 cluster and effect of the PA0884-0886 BSCD transporter. *P. putida* KT2440 wild type and the two strains *attTn7*::P_{14f}-PA0878-0883 and *attTn7*::P_{14f}-PA0878-0886 were grown in a Growth Profiler in 96-well microtiter plates with minimal medium containing 20 mM of the indicated BSCD as sole carbon source. OD_{600} equivalents (OD_{600} eq.) were derived from green-values obtained from the Growth Profiler using a calibration curve. Growth rates are shown in Table S5.4-1. The mean values with standard deviation (SD) of three replicates are shown. *Modified from de Witt et al. (2023).*

2.4.5.2 Characterization of peripheral BSCD pathways

To further investigate the individual degradation pathways for each BSCD, different mutants were designed based on *P. putida* KT2440 *attTn7*::P_{14f}-PA0878-PA0886 lacking individual

genes of the expression cassette (Figure 2.4-1). These constructs also allow to study a putative involvement of the uncharacterized genes PA0879, PA0880, and PA0881 encoding a putative acyl-CoA dehydrogenase, a probable ring-cleaving dioxygenase and an MmgE/PrpD family protein, in these pathways.

Efficient growth on itaconate required the expression of *ich*, *ict*, and *ccl* whereas it was not affected by the deletion of PA0879, PA0880, and PA0881 (Figure 2.4-3 a). Although strain ΔPA0882 (Δ*ict*) could grow on itaconate, this growth was delayed, and slower ($\mu = 0.11 \pm 0.00$ h^{-1}) compared to the strain expressing the full operon, which is likely due to the moonlighting activity of succinyl-CoA synthetase (SucCD) towards itaconate (Sasikaran et al., 2014). These results verify the previously proposed degradation pathway of itaconate based on *in vitro* assays *via* CoA-activation (by Ict) followed by isomerization/hydration (by Ich), and cleavage into acetyl-CoA and pyruvate (by Ccl) (Sasikaran et al., 2014) and *P. aeruginosa* PAO1 Δ*ict* experiments (Riquelme et al., 2020) (Figure 2.4-3 b).

In contrast to growth on itaconate, the absence of Ict abolished growth on (*S*)-citramalate, suggesting that this substrate is not recognized by SucCD. Degradation of (*S*)-citramalate only required the expression of *ict* and *ccl*, indicating the direct conversion of (*S*)-citramalate to (*S*)-citramalyl-CoA followed by cleavage to acetyl-CoA and pyruvate (Figure 2.4-3 b). In contrast, (*R*)-citramalate was not metabolized. These results support the previously described stereoselectivity of Ict (Sasikaran et al., 2014).

Degradation of mesaconate also required the presence of Ict and Ccl, indicating a similar degradation pathway as for (*S*)-citramalate (Figure 2.4-3 a). Neither Ich, nor any of the uncharacterized proteins were required for mesaconate degradation. Thus, mesaconate is likely not directly CoA-activated by Ict to mesaconyl-C$_4$-CoA, since that would require Ich for further degradation. In *Burkholderia xenovorans*, Bxe_A3136 encodes a class I fumarase catalyzing the hydration of mesaconate to (*S*)-citramalate, thus enabling growth on mesaconate *via* Ict and Ccl (Kronen et al., 2015). The PP_0897 enzyme encoded in the genome of *P. putida* KT2440 shares a sequence identity of 75 % with Bxe_A3136 at the protein level, making it a likely homolog. This was confirmed by deletion of PP_0897 in *P. putida* KT2440 *attTn7*::*P$_{14f}$*-PA0878-PA0886, which abolished growth on mesaconate (Figure 2.4-3 a, Figure S5.4-1). Furthermore, (*S*)-citramalate accumulated in culture supernatants when the Δ*ict* mutant was grown with mesaconate and glucose as mixed

116

substrates (Figure S5.4-2).Thus, PP_0897 was revealed as mesaconase hydrating mesaconate to (*S*)-citramalate, which is further metabolized as described above (Figure 2.4-3 b). Furthermore, the ΔPP_0897 mutant showed reduced growth on acetate (data not shown), indicating a role as fumarase of the encoded enzyme in the TCA cycle hydrating fumarate to (*S*)-malate.

Besides Ict, Ich, and Ccl, growth on (*S*)-(*R*)-methylsuccinate also required the presence of the PA0879 gene, indicating that the corresponding product has methylsuccinyl-CoA dehydrogenase activity (Figure 2.4-3 a). Interestingly, the absence of the MmgE/PrpD family protein encoded by PA0881 led to reduced growth with the racemic substrate (μ = $0.18 \pm 0.00\,h^{-1}$) (Figure 2.4-3 a). Since half of the optical density was reached for the ΔPA0881 mutant (Figure S5.4-1), PA0881 is likely involved in the metabolism of one enantiomeric form of methylsuccinate. To elucidate which enantiomer is degraded *via* the MmgE/PrpD family protein, growth was analyzed with either (*S*)- or (*R*)-methylsuccinate as pure substrate. Indeed, (*R*)-methylsuccinate was degraded in the absence of PA0881, whereas degradation of the (*S*)-enantiomer required the presence of PA0881 (Figure 2.4-3 a). Based on these results it can be concluded that (*R*)-methylsuccinate is CoA-activated by Ict to (*R*)-methylsuccinyl-CoA, which is further converted to mesaconyl-C_4-CoA by the identified methylsuccinyl-CoA dehydrogenase (Mch) encoded by PA0879. Formation of mesaconyl-C_4-CoA as intermediate is highly likely to occur, because the presence of Ich is still required for (*R*)-methylsuccinate metabolism. Utilization of (*S*)-methylsuccinate additionally required the presence of PA0881 indicating that at least one enzyme of the (*R*)-methylsuccinate degradation pathway is enantioselective for the (*R*)-enantiomer. Ict was previously revealed to be enantioselective towards (*S*)-citramalate and not (*R*)-citramalate (Sasikaran et al., 2014). Thus, activity of Ict might also be limited towards (*R*)-methylsuccinate. This is supported by the fact that the spatial position of the methyl group in relation to the C_4 atom, where the CoA-activation takes place, is the same for (*S*)-citramalate and (*R*)-methylsuccinate (Figure 2.4-3 b). Thus, the PA0881-encoded MmgE/PrpD family protein likely acts as an (*S*)-(*R*)-methylsuccinate isomerase converting the (*S*)- to the (*R*)-enantiomer. Alternatively, PA0881 might also be an (*S*)-(*R*)-methylsuccinyl-CoA isomerase. Since Mch acts near the chiral center of (*R*)-methylsuccinyl-CoA this enzyme could in principle also be enantioselective for (*R*)-

methylsuccinyl-CoA. For human very long-, long- and medium-chain acyl-CoA dehydrogenases an enantioselectivity was revealed as they only acted on the respective (*S*)-2-methylacyl-CoA-enantiomer (Battaile et al., 1998). In contrast to this, a human short/branched-chain acyl-CoA dehydrogenase was found to be active on both (*S*)- and (*R*)-2-methylbutyryl-CoA despite showing a preference for the (*S*)-enantiomer (Korman et al., 2005; Vockley et al., 2000).

A)

strain	substrate					
	itaconate	(S)-citramalate	mesaconate	(S)-(R)-methylsuccinate	(R)-methylsuccinate	(S)-methylsuccinate
P$_{14f}$-PA0878-0886	++	++	++	++	++	++
ΔPA0878 (ich)	-	++	++	-	-	-
ΔPA0879-0881	++	++	++	-	-	-
ΔPA0879	++	++	++	-	-	-
ΔPA0880	++	++	++	++	++	++
ΔPA0881	++	++	++	+	++	-
ΔPA0882 (ict)	±	-	-	-	-	-
ΔPA0883 (ccl)	-	-	-	-	-	-
ΔPP_0897	++	++	-	++	++	++

B)

Figure 2.4-3. Proposed degradation pathways of BSCD encoded by the PA0878-0886 gene cluster. (A) *P. putida* KT2440 *attTn7::P$_{14f}$-PA0878-0886* and its deletion mutants were grown on the indicated BSCD as sole carbon source. Growth of the mutants was classified into the following categories: Final OD$_{600}$ of > 1.5 is reached within16 h (++), final OD$_{600}$ of < 1.5 reached within 16 h (+), final OD$_{600}$ of > 1 reached after 36 h (±), and no growth (-). Associated growth curves are shown in Figure S5.4-1 and growth rates are displayed in Table S5.4-1. **(B)** Degradation pathways of the five BSCD (dashed boxes). *Modified from de Witt et al. (2023).*

The MmgE/PrpD family (IPR005656) is a rather heterogeneous family with members exhibiting diverse metabolic functions. Most members of this family are annotated as 2-methylcitrate dehydratase (EC 4.2.1.79) (PrpD) that are involved in propionate catabolism, catalyzing the third step of the 2-methylcitric acid cycle (Rocco et al., 2017). Moreover, members of the MmgE/PrpD family share high sequence identities with *cis*-aconitate decarboxylases (CAD) that convert *cis*-aconitate into itaconate (EC 4.1.1.6) (Chun et al., 2020b). However, no dehydration or decarboxylation step is required for funneling (*S*)-methylsuccinate into the revealed pathway for its (*R*)-enantiomer. A unique function within the MmgE/PrpD family was revealed for an iminodisuccinate (IDS) epimerase from *Agrobacterium tumefaciens* BY6. This enzyme catalyzes the epimerization of (*R*),(*R*)-, (*S*),(*S*)- and (*R*),(*S*)-IDS and represents the only isomerase within the MmgE/PrpD family, so far (Lohkamp et al., 2006). To gain a detailed insight and to locate the PA0881-encoded protein in this functionally diverse protein family, ColabFold was used to predict its protein structure (Mirdita et al., 2021) (Figure S5.4-3). Distance Matrix Alignment (DALI) was used to align the predicted structure to entries of the Protein Data Bank (PDB) to perform a structure-based identity search (Holm, 2020). Using this approach, it was revealed that the PA0881-encoded MmgE/PrpD family protein shared the highest structure identity with the IDS epimerase from *A. tumefaciens* BY6 (Table S5.4-2). Taken together, the structural similarity to the IDS epimerase, the probable enantioselectivity of Ict towards (*R*)-methylsuccinate, the fact that most well-studied MmgE/PrpD family proteins act on non-CoA-activated molecules, and the experimental results, all strongly indicate that the PA0881 MmgE/PrpD family protein acts as (*S*)-(*R*)-methylsuccinate isomerase to enable growth on (*S*)-methylsuccinate.

2.4.5.3 Degradation of itaconate in the presence of its derivatives (*S*)-2-hydroxyparaconate and itatartarate

The putative ring-cleaving dioxygenase encoded by PA0880 (hence named Rdo_{PA}) is the last protein with unknown function encoded within the PA0878-0886 operon. With a size of 127 amino acids, Rdo_{PA} is a relatively small protein. Interestingly, Rdo_{PA} has a protein sequence identity of 59.7 % compared to the Rdo1 putative ring-cleaving dioxygenase encoded in the

itaconate production gene cluster of *U. maydis* (Geiser et al., 2016b). In *U. maydis* itaconate is further converted to its chiral lactone (*S*)-2-hydroxyparaconate (2-HP) by the cytochrome P450 monooxygenase Cyp3 (Geiser et al., 2016a). Permeabilized cells of *U. cynodontis* convert 2-HP to itatartarate (ITT) (Guevarra and Tabuchi, 1990), and it is anticipated that Rdo1 catalyzes this conversion although this could thus far not be confirmed (Geiser et al., 2018; Geiser et al., 2016a). Both compounds might exhibit interesting physiological properties due to their metabolic linkage to itaconate, and we hypothesized that Rdo_{PA} could be involved in their degradation due to the sequence similar to Rdo1. Since 2-HP and ITT are not commercially available, the engineered *Ustilago cynodontis* NRBC 9727 Δ*fuz7* (Hosseinpour Tehrani et al., 2019), was used to produce a mixture of itaconate, 2-HP, and ITT. The obtained mixture was diluted to contain 20 mM of itaconate, adjusted to pH of 6.7, and was used to investigate the degradation of itaconate in the presence of 2-HP and ITT as well as the putative function of Rdo_{PA} as 2-HP lactonase.

Growth of *P. putida* KT2440 *attTn7*::P_{14f}-PA0879-0886 with the itaconate/2-HP/ITT mixture containing 20 mM itaconate reached a similar final optical density compared to when 20 mM itaconate was used as sole carbon source but growth was slower with a rate of 0.15 ± 0.01 h^{-1} on the mixture, compared to 0.39 ± 0.02 h^{-1} on pure itaconate (Figure 2.4-3 a, Figure 2.4-4 a). Hence, 2-HP and ITT were likely not assimilated by this strain. The absence of Ich and Ccl abolished growth with the mixture, which is in agreement with the results obtained when itaconate was used as sole carbon source (Figure 2.4-3 a, Figure 2.4-4 a). However, growth of the Δ*ict* mutant (μ= 0.01 ± 0.00 h^{-1}) with the itaconate/2-HP/ITT mixture was more impaired compared to growth on itaconate as sole substrate (μ = 0.11 ± 0.00 h^{-1}) (Figure S5.4-1). This might indicate inhibition of SucCD by ITT, given its structural similarity to itaconate.

The most prominent effect was caused by the absence of Rdo_{PA}, which entirely abolished growth on itaconate in the presence of 2-HP and ITT (Figure 2.4-4 a). In contrast, pure itaconate was metabolized by the ΔPA0880 mutant (μ = 0.38 ± 0.02 h^{-1}) (Figure 2.4-3A). HPLC analysis of the samples from the *P. putida* KT2440 *attTn7*::P_{14f}-PA0879-0886 culture grown with the mixture confirmed the degradation of 2-HP, whereas the Δ*rdo*$_{PA}$ mutant did not degrade 2HP, verifying that this reaction is catalyzed by Rdo_{PA} (Figure

2.4-4 b). Hence, 2-HP inhibited itaconate metabolism, and Rdo$_{PA}$ was found to abolish this inhibition by converting 2-HP into ITT.

The detection of two HPLC peaks near the retention time of ITT led to the assumption that other products accumulated during 2-HP degradation, which were not further metabolized (Figure 2.4-4 b). Growth experiments with *P. aeruginosa* PAO1 revealed accumulation of the same degradation products (Figure 2.4-4 b). Gas chromatography time-of-flight mass spectrometry (GC-ToF-MS) was used to identify the unknown dead-end metabolites by comparing samples of *P. putida* KT2440 *attTn7*::*P$_{14f}$*-PA0879-0886 and the Δ*rdo$_{PA}$* mutant. A detailed list of all detected molecules is summarized in Table S5.4-3. This analysis revealed the accumulation of ITT in the sample expressing the PA0878-0886 operon (Figure 2.4-4 c, Table S5.4-3). The increased ITT concentration probably caused the observed peak shift of ITT during HPLC analysis (Figure 2.4-4 b, c). No 2-HP was detected in this sample, confirming its entire conversion to ITT. Since the accumulation of ITT by *P. putida* KT2440 *attTn7*::*P$_{14f}$*-PA0879-0886 did not affect growth, 2-HP alone, and not ITT, likely inhibited growth of the Δ*rdo$_{PA}$* mutant on itaconate. In both samples, a compound exhibiting the identical mass and a similar MS-spectrum but a different retention time as 2-HP was detected by GC-ToF-MS (Figure 2.4-4 c, Figure S5.4-4, Table S5.4-3). Since 2-HP is a chiral molecule, this compound might be the enantiomeric form of 2-HP that was found to be not degraded by Rdo$_{PA}$. This theory is confirmed by residual peaks detected by HPLC that showed the same retention time as 2-HP in samples that expressed *rdo$_{PA}$* (Figure 2.4-4 b, c). According to Guevarra and Tabuchi, (*S*)-2-HP is produced from itaconate by *U. cynodontis* (Guevarra and Tabuchi, 1990) that would reveal Rdo$_{PA}$ to act enantioselective on the (*S*)-form.

The only other major peak detected by GC-ToF-MS was 2,4-dihydroxybutyrate (2,4-DHB), which emerged in the sample that expressed *rdo$_{PA}$*, suggesting it as a product of a dead-end pathway of 2-HP degradation (Figure 2.4-4 d). 2,4-DHB was also identified in metabolomics analysis of *P. putida* DOT-T1E (Sayqal et al., 2016) as well as in human blood (Hoffmann et al., 1993) and urine (Bouatra et al., 2013) without indications for a specific function. Interestingly, 2,4-DHB was identified as an inhibitor of the eukaryotic malic enzyme that catalyzes the oxidative decarboxylation of malate to pyruvate, which is a relevant reaction for a wide range of metabolic pathways (Rognstad and Katz, 1979; Schimerlik and Cleland,

1977). So far, no native bacterial pathway is known for the production of 2,4-DHB, although a synthetic pathway was recently described from malate *via* malyl-4-phosphate and malate-4-semialdehyde (Zhu et al., 2022b). Given the circumstances, it is more likely that 2,4-DHB is produced from ITT (Figure 2.4-4 d), but a mechanism of this conversion remains to be elucidated. Based on the structural similarity of ITT to citrate, we speculate that ITT could be first dehydrogenated by an aconitase-like hydratase to 2-(hydroxymethyl)fumaric acid. Subsequent decarboxylation by a CAD-like enzyme followed by hydration would result in the production of 2,4-DHB (Figure S5.4-5).
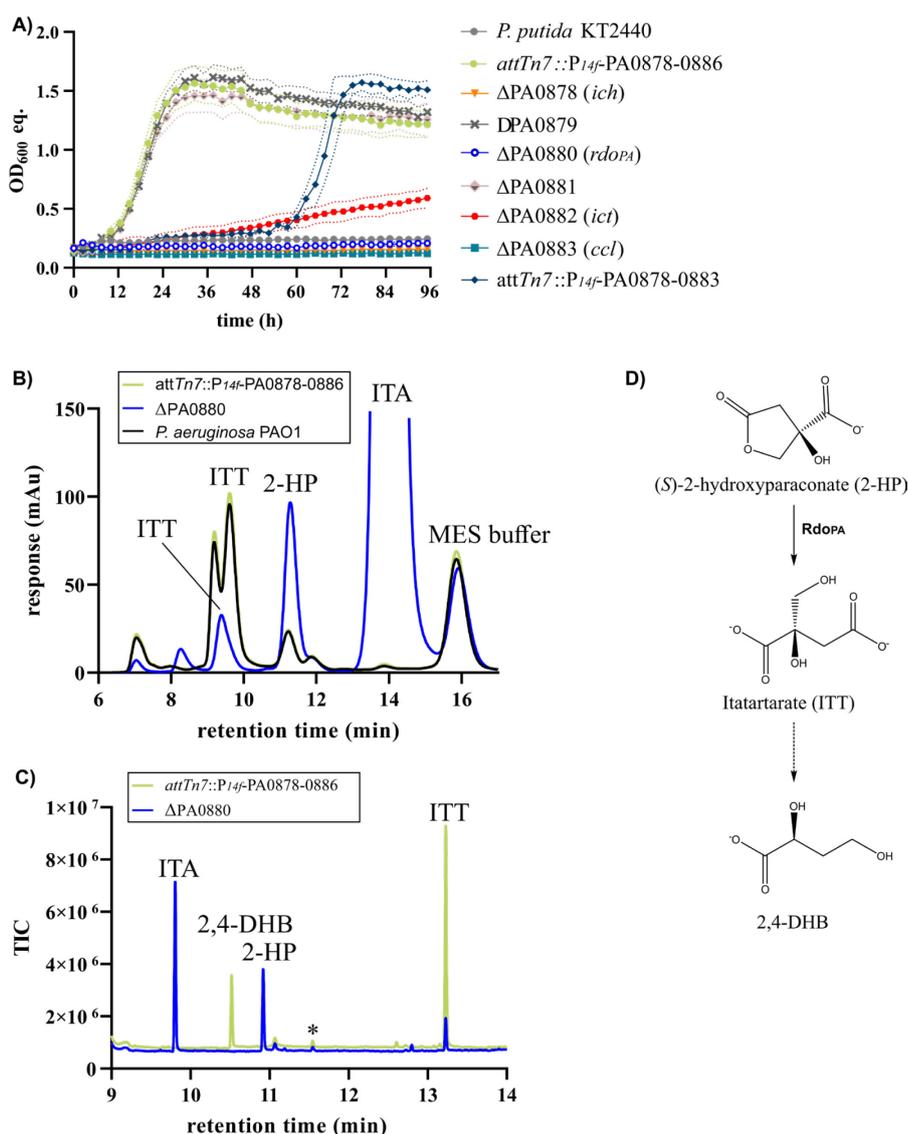
Figure 2.4-4. Effects of 2-HP and ITT on itaconate metabolism. (A) Strains of *P. putida* KT2440 were grown in a Growth Profiler in 96-well microtiter plates with minimal medium containing a mixture of itaconate, 2-hydroxyparaconate (2-HP) and itatartarate (ITT). The mixture was diluted to contain 20 mM of itaconate, whereas concentrations of 2-HP and ITT were approximately 32 mM and 17 mM. OD_{600} equivalents (OD_{600} eq.) were derived from green-values obtained from the Growth Profiler using a calibration curve. Growth rates are shown in Table S5.4-1. The mean and standard deviation (SD) of three replicates is shown. **(B)** HPLC chromatogram of samples obtained from cultivation of indicated strains with the itaconate/2-HP/ITT mixture after 72 h. Response of the DAD signal (λ=210 nm) is shown in arbitrary units (mAu). The peak shift of ITT was probably caused by the increase in ITT concentration. The asterisk indicates a peak exhibiting the same retention time as 2-HP. **(C)** GC-ToF-MS chromatogram of samples obtained from cultivation of indicated strains with the itaconate/ITT/2-HP mixture. Total ion current (TIC) is shown. The asterisk marks an unknown molecule that exhibited the same mass and MS-spectrum as 2-HP but showed a different retention time. This compound was probably detected *via* HPLC, showing the same retention time as 2-HP. **(D)** Proposed dead-end pathway for 2-HP and ITT in *P. putida* KT2440 *attTn7*::P_{14f}-PA0879-0886 and *P. aeruginosa* PAO1. Rdo_{PA}, encoded by PA0880, converted 2-HP to ITT. Accumulation of ITT might have caused its partial conversion to 2,4-dihydroxybutyrate (2,4-DHB), methylated ITT (Figure S5.4-6), 3-hydroxy-3-methylbutyrate, and other unknown compounds detected by GC-ToF-MS. A detailed pathway from ITT to 2.4-DHB is shown in Figure S5.4-5. *Modified from de Witt et al. (2023).*

2.4.5.4   Effects of (*S*)-2-hydroxyparaconate and itatartarate on microbial metabolism

The observed inhibitory effect of 2-HP on itaconate metabolism led to the question if growth with itaconate was specifically inhibited or if 2-HP is a general inhibitor of microbial metabolism. To test these hypotheses, strains were grown with a mixture containing approximately 33 mM of 2-HP and 20 mM of ITT, but no itaconate, in the presence of glucose or acetate as substrates. This mixture was produced with the engineered *Ustilago cynodontis* NBRC9727 Δfuz[7] *cyp3 P_{etef}-mttA P_{ria1} ria1 P_{etef}-cyp3* that was optimized for production of the itaconate derivatives (Ernst *et al.*, manuscript in preparation).

Growth of *P. putida* KT2440 *attTn7::P_{14f}* -PA0879-0886 and its mutant strains in the presence of the 2-HP/ITT mixture without the addition of glucose or acetate did not result in growth (Figure 2.4-5). Hence none of the itaconate derivatives was metabolized as carbon source. Surprisingly, the engineered strain harboring the *attTn7::P_{14f}*-PA0879-0886 expression cassette grew lower on glucose in the presence of 2-HP and ITT ($\mu = 0.23 \pm 0.00$ h^{-1}), compared to the wild type strain ($\mu = 0.32 \pm 0.00$ h^{-1}), and also showed a longer lag-phase (Figure 2.4-5 b).

Growth of the Δ*rdo_{PA}* mutant was even further impaired with a lag-phase of approximately 24 h and a growth rate of 0.20 ± 0.01 h^{-1}. Since Rdo$_{PA}$ was revealed to convert 2-HP into ITT, these results indicate an inhibitory effect of 2-HP under the tested conditions. Although Rdo$_{PA}$ was not present in the Δ*rdo_{PA}* mutant and no homolog was identified in this strain, the mutant was still able to grow with glucose after approximately 24 h. Hence, 2-HP might be partly degraded *via* an abiotic or unspecific route, decreasing the 2-HP concentration below a critical level.

Interestingly, the *attTn7::P_{14f}*-PA0879-0883 mutant, lacking the BSCD transporter, grew faster ($\mu = 0.38$ h ± 0.01 h^{-1}) than the *attTn7::P_{14f}*-PA0879-0886 strain ($\mu = 0.23 \pm 0.00$ h^{-1}). This indicates that 2-HP and ITT are probably also imported *via* PA0884-0886, facilitating the observed inhibition of growth. Additionally, the *attTn7::P_{14f}*-PA0879-0883 mutant grew slightly faster than the wild type strain (0.32 ± 0.00 h^{-1}) although both strains lacked the BSCD transporter. Assuming an unspecific or leaky transport of 2-HP and ITT, as revealed for itaconate and other BSCD, the presence of Rdo$_{PA}$ in the *attTn7::P_{14f}*-PA0879-0883

mutant facilitated growth on glucose in the presence of 2-HP and ITT. Since degradation of 2-HP by Rdo_{PA} led to the accumulation of ITT, these results indicate an inhibitory effect of 2-HP during growth under the tested conditions, whereas ITT seemed not to affect growth.

Growth of all mutants that expressed the BSCD transporter was slower compared to wild type and the *attTn7*::P_{14f}-PA0879-0883 mutant indicating that 2-HP and ITT are also imported by PA0884-0886. Among the mutants that expressed the BSCD-transporter, ΔPA0882 (*ict*) showed the fastest growth (μ= 0.31 h ± 0.00 h^{-1}). This effect might be explained by the production of toxic CoA-intermediates of 2-HP and/or ITT catalyzed by Ict. Due to the activity of Ict towards many BSCD, this enzyme might also catalyze the CoA-activation of 2-HP and/or ITT. Such CoA-activated forms cannot be further degraded as no strain was able to grow with the 2-HP/ITT mixture, thus inhibiting growth by sequestration of coenzyme A. The absence of Ict in the ΔPA0882 (*ict*) mutant prevents production of such expected CoA-intermediates resulting in faster growth. Toxic effects of CoA-activated intermediates of the itaconate degradation pathway were indicated based on knockout mutants (Figure S5.4-7). Since 2-HP and ITT might be CoA-activated by Ict, the previously proposed pathway for 2,4-DHB production from ITT (Figure S5.4-5) could also be encoded by the PA0878-0883 cluster operating with the CoA-activated forms starting with ITT-CoA. In contrast to 2-HP and ITT, none of the other BSCD inhibited growth of the tested strains with glucose as carbon source (Figure S5.4-8).

The presence of 2-HP and ITT also affected growth of the investigated strains when acetate was added as carbon source (Figure 2.4-5 c). Again, the *attTn7*::P_{14f}-PA0879-0883 mutant lacking the BSCD transporter showed fastest growth with a rate of 0.32 ± 0.01 h^{-1}. Since a significantly longer lag-phase was revealed for the wild type strain (0.22 ± 0.01 h^{-1}), also lacking the BSCD transporter, the presence of the PA0878-0883 cluster and thus Rdo_{PA} facilitated growth. Hence, the inhibitory effect of 2-HP on bacterial growth was likely stronger under acetate-degrading conditions compared to when glucose was used as carbon source. In addition to this, the Δrdo_{PA} mutant did not grow with acetate after incubation of 96 h, confirming the strong inhibitory effect of 2-HP. The inhibitory effect of 2-HP under acetate-degrading conditions could also be confirmed for the pathogenic yeast *Candida albicans* that does not harbor an Rdo_{PA}/Rdo1 homolog. When the 2-HP and ITT

mixture was added to the yeast nitrogen base (YNB) medium supplemented with acetate as carbon source, growth of *C. albicans* was inhibited for at least 72 h (Figure 2.4-5 d). In addition to 2-HP, several other BSCD also showed varying inhibitory effects on the investigated strains under acetate-degrading conditions (Figure S5.4-8). Addition of 20 mM mesaconate or citraconate most strongly inhibit the growth, while itaconate at this concentration has little effect. The expression of the PA0884-0886 transporter increased the inhibitory effect of mesaconate and citraconate, as was observed for 2-HP. Interestingly, immunoregulatory effects were recently described for both mesaconate and citraconate (McGettrick and O'Neill, 2023).

Overall, the data on BSCD and 2-HP metabolism indicate an evolutionary arms race between (pathogenic) microorganisms and their host, or competing species in ecological microbial niches. The production of itaconate was found to inhibit the glyoxylate shunt that is essential for pathogenic bacteria to survive in the host environment (Hillier and Charnetzky, 1981). Adaption of pathogenic or competing species to itaconate inhibition through its metabolism might have led to the emergence of the novel itaconate-derived compounds inhibiting growth of the adapted bacteria. Production of 2-HP by *Ustilago* ssp. might be a strategy to combat species capable of metabolizing itaconate. However, the exact mechanism of action of the discovered anti-bacterial and anti-fungal properties of 2-HP still needs to be identified. Currently, the production of 2-HP and ITT as pure compounds is investigated that will enable such studies.
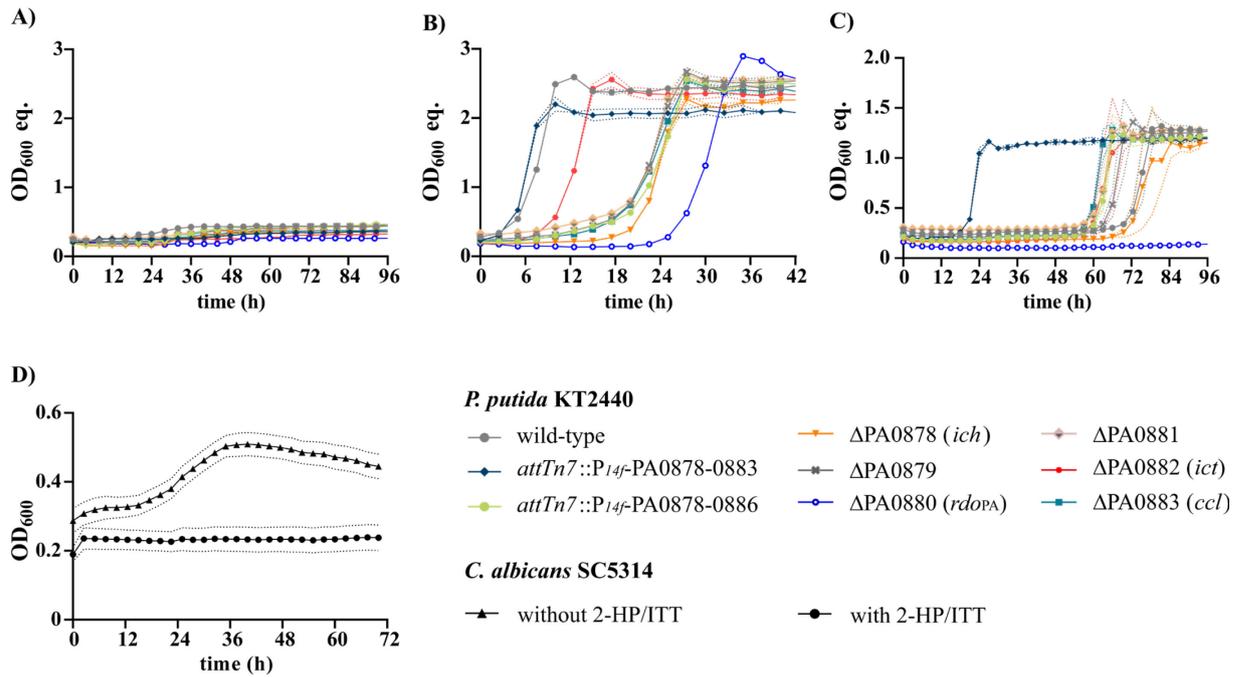
Figure 2.4-5. Inhibitory effect of 2-hydroxyparaconate and/or itatartarate on engineered *P. putida* strains and *C. albicans*. (A) *Pseudomonas* strains were cultivated in a Growth Profiler in 96-well microtiter plates with minimal medium containing a 2-HP/ITT mixture with approximately 33 mM 2-HP and 20 mM ITT, (B) supplemented with 15 mM glucose, (C) or 60 mM acetate. OD_{600} equivalents (OD_{600} eq.) were derived from green-values obtained from the Growth Profiler using a calibration curve. Growth rates are shown in Table S5.4-1.The mean and standard deviation (SD) of three replicates is shown. (D) *C. albicans* SC5314 was grown in a Tecan plate reader in YNB medium supplemented with 244 mM acetate as sole carbon source without (triangle) and with the same mixture of 2-HP and ITT (circle). The mean values and standard error of the mean (SEM) of five replicates is shown. *Modified from de Witt et al. (2023).*

2.4.6 Conclusion and outlook

Bio-upcycling of BSCD is of great importance as their usage as bio-based building blocks for plastics production is increasing. To enable bio-upcycling, funneling of these compounds into the central metabolism of suitable upcycling strains is required. Heterologous expression of the PA0878-0886 cluster resulted in an engineered strain of *P. putida* KT2440 able to rapidly metabolize a variety of BSCD. Besides native PHA production, future implementations of biosynthetic pathways in the constructed strain will potentially enable production of further value-added compounds from polymers containing BSCD as building blocks and thus allow bio-upcycling of plastic waste.

Besides their use as plastic monomers, many BSDC such as itaconate or mesaconate, exhibit anti-bacterial properties or trigger immunomodulatory effects in macrophages. The characterization of the PA0878-0886 gene cluster revealed the metabolic pathways of such relevant BSCD. The profound knowledge on the metabolic pathways gained in this study is a basis for upcoming research to identify potential drug targets against pathogenic species. Additionally, this study revealed a link of BSCD metabolism to fungal secondary metabolite resistance stressing the versatile lifestyle of *Pseudomonas* as both environmental and pathogenic organism, and highlighting the potential of 2-HP as drug candidate.

All in all, this study extends knowledge on BSCD metabolism in *P. aeruginosa*, it uncovers an intriguing link to fungal interactions of this bacterium in the environment, and provides an engineered strain of *P. putida* enabling the bio-upcycling of BSCD-based plastics. It further expands the solution space of catalytic and transport activities that can be exploited and engineered for synthetic pathway development.

2.4.7 Materials and methods

2.4.7.1 Strains and culture conditions

All chemicals used in this study were obtained from Sigma-Aldrich (St. Louis, MO, USA), Carl Roth (Karlsruhe, Germany), or Merck (Darmstadt, Germany) unless stated otherwise. All bacterial strains used in this study are listed in Table S1. *P. putida* KT2440 strains and *P. aeruginosa* PAO1 were cultivated in 5-fold buffered (19.40 g L^{-1} K_2HPO_4 and 8.15 g L^{-1} NaH_2PO_4) mineral salt medium (MSM) (Wierckx et al., 2005). Pre-cultures contained 20 mM glucose and 2 mL of culture volume was cultivated in 14 mL culture tubes (Greiner bio-one, Frickenhausen, Germany) in a Multitron shaker (Infors, Bottmingen, Switzerland) at 30 °C and 180 rpm shaking speed. For cultivations with dicarboxylates as substrates, stock solutions of 500 mM itaconic acid, (*S*)-citramalic acid, (*R*)-citramalic acid, (*S*)-methylsuccinic acid (Ambeed, Arlington Hts, IL, USA), (*R*)-methylsuccinic acid, and citraconic acid were diluted in MSM to reach a final concentration of 20 mM. Due to the lower solubility of mesaconic acid, a 200 mM stock solution was prepared for the substrate that was diluted in MSM to reach a final concentration of 20 mM. For online growth detection, a Growth Profiler 960 (Enzyscreen, Heemstede, The Netherlands) was used. This device analyses cultures in microtiter plates with transparent bottoms by image analysis. The resulting green-values (G-values, based on green pixel counts) correlate with the optical density of a cell culture. These G-values were converted into OD_{600} equivalents using a calibration curve for *P. putida*. Main cultures were cultivated in 96-well plates (CR1496dg) with a volume of 200 μL at 30 °C and 225 rpm shaking speed with an amplitude of 50 mm. Pictures for growth analysis were taken every 30 min.

For production of the itaconate, 2-HP, and ITT mixture, *Ustilago cynodontis* NRBC 9727 Δ*fuz*[7] was used (Hosseinpour Tehrani et al., 2019). A further modified strain was used for the production of the 2-HP and ITT mixture not containing itaconate anymore (Ernst *et al.*, manuscript in preparation). For producing the mixtures, pre-cultures of the *U. cynodontis* strains were grown in yeast extract (20 g L^{-1}) peptone (20 g L^{-1}) sucrose (20 g L^{-1}) (YEPS) medium at 30 °C and 250 rpm for 48 h. Main cultures were performed in modified Tabuchi medium (MTM) according to Geiser *et al.* (Geiser et al., 2014). The final MTM contained 100 mM 2-(N-morpholino)ethanesulfonic acid (MES; pH adjusted to 6.5 with NaOH), 0.8 g L^{-1} NH_4Cl, 0.2 g L^{-1} $MgSO_4·7H_2O$, 0.01 g L^{-1} $FeSO_4·7H_2O$, 0.5 g L^{-1} KH_2PO_4, 1 mL L^{-1}

vitamin solution, and 1 mL L^{-1} trace element solution. The vitamin solution contained (per liter) 0.05 g D-biotin, 1 g D-calcium panthotenate, 1 g nicotinic acid, 25 g myo-inositol, 1 g thiamine hydrochloride, 1 g pyridoxol hydrochloride, and 0.2 g *para*-aminobenzoic acid. The trace element solution contained (per liter) 1.5 g EDTA, 0.45 g $ZnSO_4 \cdot 7H_2O$, 0.10 g $MnCl_2 \cdot 4H_2O$, 0.03 g $CoCl_2 \cdot 6H_2O$, 0.03 g $CuSO_4 \cdot 5H_2O$, 0.04 g $Na_2MoO_4 \cdot 2H_2O$, 0.45 g $CaCl_2 \cdot 2H_2O$, 0.3 g $FeSO_4 \cdot 7H_2O$, 0.10 g H_3BO_3, and 0.01 g KI. Shaking cultures were performed in 500 mL shake flasks with a filling volume of 50 mL and were cultivated at 30 °C and 250 rpm with a humidity of 80 % for 5 days. After that, cells were harvested for 20 min at $7000 \times g$. The supernatant was diluted 2-fold with ultrapure H_2O and the pH was adjusted to pH 6.7 using NaOH. After that, the mixture was filtered through a 0.22 μm PES syringe filter and all components for 5-fold buffered MSM were added, resulting in the final growth medium. When indicated, 15 mM glucose or 60 mM acetate were added as additional carbon sources to this mixture. *C. albicans* SC5314 (wild type strain) was grown in yeast nitrogen base (YNB) medium supplemented with 244 mM acetate. For testing the inhibitory effects of 2-HP and ITT, the mixture was diluted to contain the same 2-HP and ITT concentrations as for experiments with *P. putida* KT2440, i.e., approximately 33 mM of 2-HP and 20 mM ITT. *C. albicans* SC5314 was grown in YNB medium and a final acetate concentration of 244 mM as carbon source was used. Measurements were performed in a Tecan infinite M plex reader and the optical density at 600 nm was analyzed.

2.4.7.2 Plasmid cloning and strain engineering

Genomic DNA of *P. aeruginosa* PAO1 was isolated using the Monarch® Genomic DNA Purification Kit (New England Biolabs, Ipswich, MA, USA). Primers were ordered as unmodified DNA oligonucleotides from Eurofins Genomics (Ebersberg, Germany). DNA fragments were obtained by PCR using the Q5® High-Fidelity 2× master mix as DNA Polymerase (New England Biolabs, Ipswich, MA, USA). Plasmids were assembled by Gibson assembly (Gibson et al., 2009) using the NEBuilder HiFi DNA Assembly Master Mix (New England Biolabs). Detailed information about the plasmids and oligonucleotides used in this study are listed in Table S2 and Table S3, respectively. For the transformation of assembled DNA fragments and plasmids into competent *E. coli* cells, a heat shock protocol was used (Hanahan, 1983). The integration of heterologous constructs from *P. aeruginosa* PAO1 into the *attTn7*-site of *P. putida* KT2440 was performed by patch

mating. For this, the *E. coli* PIR2 donor strain holding the respective pBG14f_FRT_Kan plasmid, the helper strain *E. coli* HB101 pRK2013, the transposase-providing *E. coli* HD5α λpir pTNS1, and the recipient *P. putida* KT2440 were used. For the generating the ΔPP_0897 mutant of *P. putida* KT2440 *attTn7*::*P₁₄f* –PA0878-0886 the I-SceI-based system (Martínez-García and de Lorenzo, 2011) was used according to the streamlined protocol (Wynands et al., 2018). The 500-600 bp up- and downstream flanking regions (TS1 and TS2) of PP_0897 were integrated into the suicide delivery vector pSEVA512S. Positive clones were iteratively inoculated in LB medium to cure the strain from pSW-2.

2.4.7.3   HPLC analysis

For analyzing the mixtures of itaconate, 2-HP, and ITT, samples were taken from liquid cultivations and were filtered through an AcroPrep™ 96-well filter plate (Pall Corporation, Port Washington, NY, USA) to obtain the analytes for High-Performance Liquid Chromatography (HLPC) analysis. HPLC analysis was performed using a 1260 Infinity II HPLC equipped with a refractive index detector (RID) and a diode array detector (DAD) (Agilent, Santa Clara, California, USA). Itaconate, 2-HP, and ITT were detected using the DAD at 210 nm. Analytes were eluted using a 300 × 8 mm organic acid resin column (Metab-AAC, Isera, Düren, Germany) together with a 40 × 8 mm organic acid resin pre-column with 5 mM H_2SO_4 as mobile phase at a constant flow rate of 0.6 mL min^{-1} at 40 °C.

2.4.7.4   GC-ToF-MS analysis

For sample preparation, cultures were filtered through an AcroPrep™ 96-well filter plate to obtain cell-free filtrates (Pall Corporation, Port Washington, NY, USA). Aliquots of 130 μL were shock frozen in liquid nitrogen and stored at -20 °C. Prior to analysis, samples were lyophilized overnight in a Christ LT-105 freeze drier (Martin Christ Gefriertrocknungsanlagen, Osterode am Harz, Germany). Two-step derivatization of the samples and GC-ToF-MS analysis was performed as described before by Paczia et al. (2012) using a L-PAL3-S15 liquid auto sampler coupled to a LECO GCxGC HRT+ 4D high resolution time of flight mass spectrometer (LECO, Mönchengladbach, Germany). To identify known metabolites a baseline noise corrected fragmentation pattern together with the corresponding current RI value (Retention time Index) was compared to our in-house accurate m/z database JuPoD, and the commercial nominal m/z database NIST20 (National

Institute of Standards and Technology, USA). Unknown peaks were identified by a virtual reconstruction of the derivatized metabolite structure *via* the measured baseline noise corrected accurate mass m/z fragment pattern in comparison to an accurate m/z fragment register inside the JuPoD main library and were subsequently verified by virtual derivatization and fragmentation of the predicted structure.

2.4.7.5 *In silico* tools

For the prediction of operons the operon-mapper was used and "predicted operons" was set as output option (Taboada et al., 2018). Protein structures were predicted using ColabFold (Mirdita et al., 2021). ColabFold is an optimized version of AlphaFold2 (Jumper et al., 2021) using MMseqs2 allowing faster predictions of protein structures maintaining a high accuracy of the predictions. The platform is accessible *via* Google Colaboratory. Structure-based identity searches of predicted protein structures were performed using Distance Matrix Alignment (DALI) that aligned the predicted structure to entries of the Protein Data Bank (PDB) (Holm, 2020). The structures were aligned to all entries of the PDB.

2.4.8 Declaration of competing interests

The authors declare no competing interest.

2.4.9 Acknowledgements

2.4.10 Addendum

The following data are associated with the publication

de Witt, J.[1]*, Ernst, P.*[1]*, Gätgens, J.*[1]*, Noack, S.*[1]*, Hiller, D.*[2]*, Wynands, B.*[1]*, Wierckx, N.*[1*]*, (2023). Characterization and engineering of the branched short-chain dicarboxylate metabolism of Pseudomonas reveals resistance to fungal 2-hydroxyparaconate. Metab. Eng., 75, 205-216. doi:*10.1016/j.ymben.2022.12.008

but have not been peer reviewed or published.

All data were collected and analyzed by **de Witt, J.**[1]*, who also wrote the following chapter*

[1] Institute of Bio- and Geosciences IBG-1: Biotechnology, Forschungszentrum Jülich, Jülich, Germany

Overall contribution: 100 %

2.4.10.1 Microbial upcycling of BSCD

The deep understanding of the PA0878-0886-encoded metabolic pathway from *P. aeruginosa* PAO1 and its heterologous expression in *P. putida* KT2440 enabled metabolism of various BSCD (chapter 2.4) (de Witt et al., 2023). As BSCD are an emerging group of polymer building blocks and can also emerge from oxidative hydrolysis of prevalent plastics (Sullivan et al., 2022), their upcycling to value-added compounds is of great interest. To demonstrate microbial upcycling, the engineered *P. putida* KT2440 *attTn7::P$_{14f}$*-PA0878-0886 was cultivated with different BSCD in nitrogen-limited mineral salts medium (C:N = 30:1) and production of PHA was analyzed. Overall, PHA was produced to approximately 20 % of the CDW with itaconate, mesaconate, and racemic methylsuccinate (Table 2.4-1). The relative monomer composition was similar to the one of PHA produced from mcl-DCA and -diols (chapter 2.3.4.5). Compared to octanoic acid (mcl-fatty acid) (0.50 g_{PHA} g_{CDW}^{-1} ± 0.02), which is a PHA-related substrate and therefore particularly suitable for PHA production (Prieto et al., 2016), the production of PHA from BSCD was significantly less (0.07-0.13 g_{PHA} g_{CDW}^{-1}). Nevertheless, considerable amounts of PHA were produced from BSCD confirming their microbial upcycling at proof-of-principle scale. Deletion of the PP_5003-6 operon in *P. putida* KT2440 *attTn7::P$_{14f}$*-PA0878-0886, encoding the native PHA polymerases (PP_5003, PP_5005), completely abolished production of PHA from BSCD (data not shown).

Table 2.4-1. PHA production from BSCD using *P. putida* KT2440 *attTn7::P$_{14f}$*-PA0878-0886. Cell dry weight, relative PHA content, and monomer composition are shown. Cultures were performed in mineral salts medium supplemented with 30 mM of the indicated BSCD or 18.75 mM octanoate as control substrate. The mineral salts medium was modified to contain a C:N ratio of 30:1. Error values are calculated as standard deviations (n=2).

substrate	CDW (g L^{-1})	PHA (%)	g_{PHA} g_{CDW}^{-1}	C$_6$ (%)	C$_8$ (%)	C$_{10}$ (%)	C$_{12}$ (%)
itaconate	0.40 ± 0.16	20.3 ± 0.7	0.08 ± 0.01	6.8 ± 2.0	28.5 ± 0.2	60.3 ± 1.5	4.3 ± 0.6
mesaconate	0.67 ± 0.14	18.7 ± 0.8	0.13 ± 0.06	9.8 ± 4.9	29.2 ± 0.1	56.9 ± 4.1	4.1 ± 0.8
(*S*)-(*R*)-methylsuccinate	0.35 ± 0.05	19.0 ± 0.4	0.07 ± 0.01	10.6 ± 0.0	28.7 ± 0.0	57.0 ± 0.1	3.8 ± 0.1
octanoate	1.19 ± 0.02	41.9 ± 2.2	0.50 ± 0.02	14.5 ± 0.1	81.8 ± 0.1	3.8 ± 0.1	n. d.

In addition to PHA, production of PHB from BSCD was also investigated. For this, the *P. putida* KT2440 *attTn7::P₁₄f*–PA0878-0886 ΔPP_5003-6 deletion mutant was transformed with pS6311·PHB harboring the *phaCAB* genes from *C. necator*, which are required for heterologous PHB synthesis (chapter 2.3.4.5). The ΔPP_5003-6 mutant was chosen in order to prevent a possible depolymerization of PHB by the native PHA depolymerase (PP_5004). The resulting strain was cultivated under non-nitrogen-limiting conditions and induction of *phaCAB* genes resulted in the production of PHB from all tested BSCD (Table 2.4-2). Except for (*S*)-(*R*)-methylsuccinate, the relative PHB content of the CDW was lower compared to when PHA was produced. This was accompanied by a more than two-fold increase in the CDW. Consequently, compared to PHA production, the total amount of PHB produced (0.14-0.34 g_{PHB} g_{CDW}^{-1}) was higher. Hence, acetyl-CoA originating from BSCD metabolism was more effectively funneled into the *phaCAB*-encoding PHB synthesis pathway compared to the native *de novo* fatty acid biosynthesis. It is of note that pyruvate, which is the second degradation product of BSCD metabolism, might affect both routes as observed for succinyl-CoA emerging from mcl-DCA and -diol metabolism (chapter 2.3.4.5). The varying growth of *P. putida* KT2440 *attTn7::P₁₄f*-PA0878-0886 ΔPP_5003-6 pS6311·PHB with different BSCD might explain the observed differences in PHB production. The negative control, lacking pS6311·PHB, did not produce any PHB (data not shown) verifying heterologous production *via* the *phaCAB*-encoded heterologous pathway.

Table 2.4-2. PHB production from BSCD using *P. putida* KT2440 *attTn7::P₁₄f*-PA0878-0886 ΔPP_5003-6 pS6311·PHB. Cell dry weight and relative PHB content are shown. The strain was cultivated with 30 mM of the indicated BSCD or 18.75 mM octanoate in mineral salts medium. Error values are calculated as standard deviations (n=2).

substrate	CDW (g L^{-1})	PHB (%)	g_{PHB} g_{CDW}^{-1}
itaconate	1.14 ± 0.09	12.0 ± 0.4	0.14 ± 0.01
mesaconate	1.29 ± 0.11	17.0 ± 1.0	0.22 ± 0.02
(*S*)-(*R*)-methylsuccinate	1.03 ± 0.17	32.6 ± 0.3	0.34 ± 0.06
octanoate	1.61 ± 0.12	36.3 ± 2.3	0.58 ± 0.06

Overall, production of PHA and PHB from BSCD was successfully demonstrated thereby extending the range of upcyclable polymer building blocks using engineered strains of *P. putida* KT2440. Future studies could perform further metabolic engineering to optimize the yields of PHA and PHB production, which are still low compared to PHA-related substrates such as octanoic acid. Moreover, the combination of PHA- and PHB-producing pathways could be envisioned to obtain a scl-co-mcl-PHA polymer that features improved physical properties compared to its individual homopolymers (Wang et al., 2023).

2.4.10.2 Materials and methods

Deletion mutants were constructed as described in chapter 2.4.7.2. Transformation of *P. putida* KT2440 with pS6311·PHB was performed *via* electroporation as described by Choi et al. (2006). Production of PHA and PHB was performed using a C:N ratio of 30:1 and induction of *phaCAB* by 1 mM cyclohexanone, respectively as described in chapter 2.3.6.2. For this, 30 mM of the indicated BSCD or 18.75 mM octanoic acid were used as carbon source. Production of PHA and PHB was quantified *via* GC as described in chapter 2.3.6.6.

2.5 Biodegradation of poly(ester-urethane) coatings by *Halopseudomonas formosensis*

Published as:

de Witt, J.[1], Molitor, R.[2], Gätgens, J.[1], Ortmann de Percin Northumberland, C.[3], Kruse, L.[2], Polen, T.[1], Wynands, B.[1], van Goethem, K.[4], Thies, S.[2], Jaeger, K-E.[1,2], Wierckx, N.[1], (2023). Biodegradation of poly(ester-urethane) coatings by *Halopseudomonas formosensis*. *Microbial Biotechnology*, 17, e14362. doi:10.1111/1751-7915.1436

[1] Institute of Bio- and Geosciences IBG-1: Biotechnology, Forschungszentrum Jülich, Jülich, Germany
[2] Institute of Molecular Enzyme Technology, Heinrich-Heine-University Düsseldorf, Forschungszentrum Jülich, Jülich, Germany
[3] Ernst Ruska-Centre for Microscopy and Spectroscopy with Electrons: ER-C-3: Structural Biology, Forschungszentrum Jülich, Jülich, Germany
[4] I-COATS N.V. 2600 Antwerp, Belgium
[*] Corresponding author

CRediT authorship contribution statement:
J. de Witt: Methodology, Investigation, Validation, Formal analysis, Data curation, Writing – original draft, Writing – review and editing, Visualization.
R. Molitor: Investigation, Writing – Original Draft Preparation
J. Gätgens: Investigation, Resources
C. Ortmann de Percin Northumberland: Investigation, Resources
L. Kruse: Resources
T. Polen: Investigation, Resources
B. Wynands: Writing – Review & Editing
K. van Goethem: Resources
S. Thies: Conceptualization, Supervision, Writing – Review & Editing
K-E. Jaeger: Supervision, Writing – Review & Editing,
N. Wierckx: Conceptualization, Funding acquisition, Supervision, Writing – Review & Editing

Overall contribution: 55 %

The presented experimental work was conducted by JdW (microbiology) and partly by RM (enzyme characterization), JG (GC-ToF-MS), COdPN (TEM microscopy), and TP (genome sequencing). Validation was done by JdW and RM. Visualization of all data was performed by JdW. KvG provided ICO-coatings and LK provided *Halopseudomonas* sp. strains. The writing of the original draft was done by JdW supported by RM and ST, which was reviewed and edited by ST, NW, K-EJ and all co-authors. Funding for the project was acquired by NW and K-EJ.

2.5.1 Graphical abstract
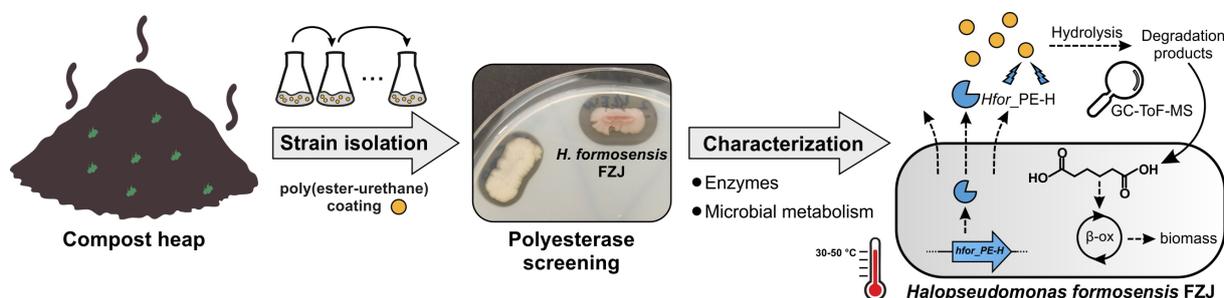
2.5.2 Abstract

Impranil® DLN-SD is a poly(ester-urethane) (PEU) that is widely used as coating material for textiles to fine-tune and improve their properties. Since coatings increase the complexity of such plastic materials, they can pose a hindrance for sustainable end-of-life solutions of plastics using enzymes or microorganisms. In this study, we isolated *Halopseudomonas formosensis* FZJ due to its ability to grow on Impranil DLN-SD and other PEUs as sole carbon sources. The isolated strain was exceptionally thermotolerant as it could degrade Impranil DLN-SD at up to 50 °C. We identified several putative extracellular hydrolases of which the polyester hydrolase *Hfor*_PE-H showed substrate degradation of Impranil DLN-SD and thus was purified and characterized in detail. *Hfor*_PE-H showed moderate temperature stability (T_m = 53.9 °C) and exhibited activity towards Impranil DLN-SD as well as polyethylene terephthalate. Moreover, we revealed the enzymatic release of monomers from Impranil DLN-SD by *Hfor*_PE-H using GC-ToF-MS and could decipher the associated metabolic pathways in *H. formosensis* FZJ. Overall, this study provides detailed insights into the microbial and enzymatic degradation of PEU coatings, thereby deepening our understanding of microbial coating degradation in both contained and natural environments. Moreover, the study highlights the relevance of the genus *Halopseudomonas* and especially the novel isolate and its enzymes for future bio-upcycling processes of coated plastic materials.

2.5.3   Introduction

Coatings are thin layers of polymers that are applied to the surface of materials to improve their appearance or properties. They are used in a wide range of industries, including fishery, automotive, aerospace, medical, and leisure. Many coatings consist of poly(ester-urethane)s (PEUs) that are known for their excellent mechanical properties, including high strength, good fatigue resistance, and high abrasion resistance (Hojabri et al., 2012; Quienne et al., 2020; Ye et al., 2020). Hence, PEUs are used in a variety of coating applications to improve the durability and chemical and biological resistance of these materials. Depending on the chemical composition, coatings can also be used to tune the biodegradability of a material. However, coatings also add to the complexity of a material by increasing the number of polymers it is composed of, and consequently the number of molecular building blocks. PEUs thus currently pose a hindrance for the mechanical and chemical recycling of coated plastics. This makes bio-upcycling a promising sustainable end-of-life solution for PEUs, because this technology is potentially suitable for complex polymer and monomer mixtures (Ballerstedt et al., 2021; Sullivan et al., 2022). In this envisioned approach, biological processes depolymerize the entire plastic product including its coating followed by either bio-recycling or bio-upcycling. For this, enzymes and microorganisms able to depolymerize and metabolize PEUs are essential. In addition, many coatings, for instance on fishing nets, are subject to mechanical abrasion which releases them into nature, making the design and understanding of polymer biodegradability of high environmental importance. Thus, PEU coatings are disseminated into the environment and may hinder the recycling of plastics. However, they also have the potential to increase the application range of biodegradable polymers by protecting sensitive materials and tuning surface properties like lubrication, hydrophobicity, and abrasion resistance. Hence, it is of great interest to establish sustainable end-of-life solutions of such products by identifying microorganism and enzymes able to depolymerize coatings consisting of PEUs.

One of the best-researched industrial PEU is Impranil® DLN-SD, an anionic aliphatic PEU used for the formulation of textile coatings. Several bacterial and fungal species have been described to degrade Impranil DLN-SD including species of *Pseudomonas* and *Cladosporium* (Álvarez-Barragán et al., 2016; Biffinger et al., 2015; Howard and Blake, 1998; Howard et al., 2001; Russell et al., 2011). Enzymes of such microorganisms were

often rashly designated as "polyurethane-degrading enzyme" or "polyurethanase" without confirmation that the urethane (carbamate) bond was hydrolyzed. Instead, these enzymes only showed polyester hydrolase activity, solubilizing the polymer by cleaving the ester bonds present in the PEU but leaving the urethane bond intact. Hence, these enzymes should be classified as extracellular esterases or lipases. So far, no enzymes with true polyurethane depolymerizing activities are scientifically described (Liu et al., 2021a; Wei et al., 2020). Instead, certain urethanases and cutinases are known to cleave only PU oligomers (Akutsu-Shigeno et al., 2006; Branson et al., 2023). Nonetheless, oxidative enzymes exist that are capable of depolymerizing PU, but in an unspecific mode (Magnin et al., 2021). Most enzymes known to depolymerize the ester bonds of Impranil DLN-SD were originally identified as polyethylene terephthalate (PET) hydrolases, including cutinases such as the leaf and branch compost cutinase (LCC), *Thermobifida fusca* cutinase (TfCut2) (Schmidt et al., 2017), lipases (Rowe and Howard, 2002; Schöne et al., 2016), or general esterases (Magnin et al., 2020). Recently, it was shown that members of the niche-adapted genus *Halopseudomonas* possess extracellular type IIa PET-hydrolases (PE-H) that are able to hydrolyze Impranil DLN-SD (Molitor et al., 2020). Furthermore, the PE-H of *Halopseudomonas aestusnigri* (*Haes*-PE-H) and *Halopseudomonas bauzanensis* were shown to be active towards PET (Bollinger et al., 2020b) (Avilan et al., 2023). However, bacterial growth of *Halopseudomonas* spp. with Impranil DLN-SD as sole carbon source has not been investigated and the metabolic pathways of Impranil DLN-SD degradation remain unknown, until now. The lack of established tools for genetic engineering of this genus further complicates the process of investigating the metabolic routes in detail.

In this study, we aimed to identify and characterize novel microorganisms and enzymes for PEU degradation. For this, we performed enrichment cultures that led to the isolation of the Impranil DLN-SD-metabolizing bacterium *Halopseudomonas formosensis* FZJ. The characterization of this strain and its extracellular hydrolases highlights their potential for biodegradation of several PEUs and gives insights into the corresponding metabolic pathways. Moreover, this study reports the first genetic modification within the genus *Halopseudomonas* leading the path for exploring this niche-adapted and biotechnologically relevant genus.

2.5.4 Results and discussion

2.5.4.1 Isolation of poly(ester-urethane)-degrading *Halopseudomonas formosensis FZJ*

PEU-degrading bacteria were isolated from soil samples obtained from a composting facility. For this, enrichment cultures were grown in mineral salts medium (MSM) supplemented with 1 % (v/v) Impranil DLN-SD as sole carbon source at 30 °C. After repetitive inoculation for two weeks, the enriched organisms were isolated on lysogeny broth (LB) agar plates containing 1 % (v/v) Impranil DLN-SD. Two isolated strains showed remarkable halo formation indicating the secretion of PEU-degrading enzymes (Figure 2.5-1 a). 16S rDNA sequencing of the isolates classified them as a *Bacillus* sp. and *Halopseudomonas formosensis.* The 16S rDNA of the latter shares a sequence identity of 99.92 % to that of *H. formosensis* CC-CY503[T] (Lin et al., 2013). This genus was recently re-classified from *Pseudomonas* into the novel *Halopseudomonas* lineage (Bollinger et al., 2020b; Peix et al., 2018; Rudra and Gupta, 2021). Many Halopseudomonads harbor a PE-H, among them *H. aestusnigri* (*Haes*-PE-H) degrading not only Impranil DLN-SD but also PET (Bollinger et al., 2020b; Molitor et al., 2020). Since halo formation and growth on Impranil DLN-SD of the isolated *H. formosensis* strain, designated as *H. formosensis* FZJ, was stronger compared to that of the *Bacillus* sp. isolate (Figure 2.5-1 a, b), whole genome sequencing (WGS) of *H. formosensis* FZJ was performed to screen for putative hydrolases. Genome analysis led to the identification of a PE-H homolog in *H. formosensis* FZJ (*Hfor*_PE-H) that shared a protein sequence identity of 99.7 % with the putative PE-H from *H. formosensis* CC-CY503[T] and of 80.3 % with the characterized PET-degrading *Haes*_PE-H. Including *Hfor*_PE-H, a total number of 24 hydrolases were identified of which 14 were predicted to contain a signal peptide (Table S5.5-1). Such secreted hydrolases may be well suited to extracellularly break down the polymer into monomers and oligomers that are imported and metabolized by *H. formosensis* FZJ.

The presence of a secreted PE-H and the ability to grow on LB agar plates containing Impranil DLN-SD indicated that *H. formosensis* FZJ is able to metabolize the PEU. Growth experiments with Impranil DLN-SD as sole carbon source confirmed the ability of the isolate to metabolize Impranil DLN-SD (Figure 2.5-1 b). Since the turbidity of Impranil DLN-SD interfered with the optical density (OD_{600}) that is usually used as parameter for monitoring

growth, the consumption of NH_4^+ was utilized to quantify bacterial growth using a colorimetric assay (Willis et al., 1996). Moreover, the increase in colony forming units during the cultivation with Impranil DLN-SD as sole carbon source confirmed growth of *H. formosensis* FZJ with the polymeric substrate (Figure S5.5-1). *H. formosensis* FZJ was unable to grow on Impranil DLN-SD when no NH_4^+ was present in the medium, indicating that Impranil was not utilized as nitrogen source. Hence, no urethanase is likely present in this strain resulting in intact carbamate bonds within the polymer

To investigate whether *Hfor*_PE-H was responsible for Impranil DLN-SD degradation, we aimed to delete *Hfor*_PE-H (Δ*Hfor*_PE-H) to test its effect on growth on the polymer. However, members of the genus *Halopseudomonas* were thus far not genetically accessible. Hence, we adapted the streamlined I-SceI-based system that is well established for engineering the genus *Pseudomonas* (Martínez-García and de Lorenzo, 2011; Wynands et al., 2018). Since *ori*RK2 of traditional *sce-I* expression plasmids, such as pSW-2, was not recognized by *H. formosensis* FZJ, we enabled expression of *sce-I* by constructing pQT8-*sce-I* that harbored the pRO1600 origin of replication. Indeed, pQT8-*sce-I* was able to replicate in *H. formosensis* FZJ and thus enabled deletion of the target gene resulting in the Δ*Hfor*_PE-H mutant. This mutant showed impaired growth on Impranil DLN-SD, thus confirming its activity towards the polymer (Figure 2.5-1 b). Since growth of the Δ*Hfor*_PE-H mutant was not entirely abolished, at least one of the remaining 13 putative secreted hydrolases must also possess an activity towards Impranil. Moreover, a synergistic effect of *Hfor*_PE-H with further secreted hydrolases is conceivable as the polymer consists of various ester and urethane bonds that might be favored by different hydrolases. Hence, cleavage of oligomers might be favored by other hydrolases than *Hfor*_PE-H analogous to the synergy of PET- and MHETases during PET depolymerization (Yoshida et al., 2016).

Light microscopy confirmed the breakdown of refractive Impranil DLN-SD by *H. formosensis* FZJ into smaller particles (Figure 2.5-1 e-h). Moreover, cells of *H. formosensis* FZJ seemed to be attached to the polymer suggesting that membrane-bound hydrolases may contribute to polymer degradation (Figure 2.5-1 f-h). Using Transmission Electron Microscopy (TEM), the size of *H. formosensis* FZJ was detected to be approximately 1 μm × 0.5 μm (Figure 2.5-1 g).
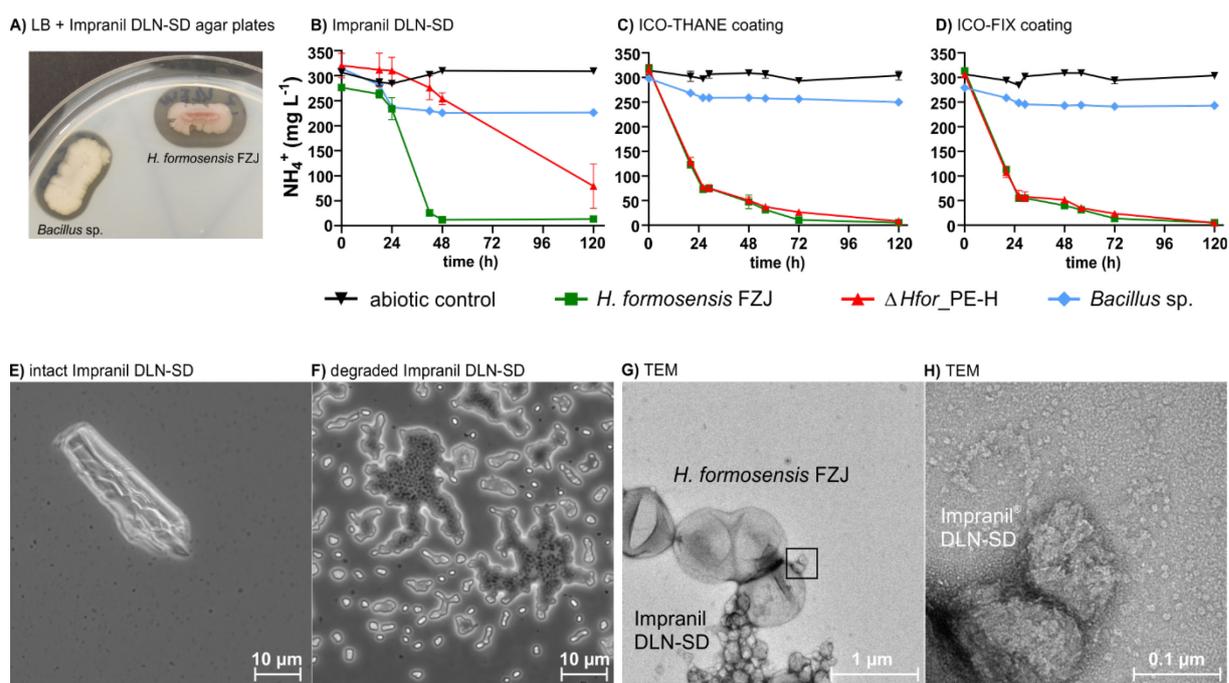
Figure 2.5-1. Growth of *H. formosensis* FZJ with different PEUs. Halo formation of the two isolated strains on LB agar plates containing 1 % (v/v) Impranil DLN-SD (**A**). The wild type *H. formosensis* FZJ, its knock-out mutant of *Hfor*_PE-H (Δ*Hfor*_PE-H), and the *Bacillus* sp. isolate were cultivated at 30 °C in mineral salts medium (MSM) supplemented with 1 % (v/v) Impranil DLN-SD (**B**), 1 % (w/v) ICO-THANE coating (**C**), or 1 % (w/v) ICO-FIX coating (**D**) as sole carbon source. An abiotic control lacking a bacterial isolate was included. Impranil DLN-SD was added as dispersion and the ICO-THANE and ICO-FIX coatings were added in powdered form. Growth was analyzed by measuring the consumption of ammonium (NH$_4^+$). The mean values and standard deviation (SD) of three replicates are displayed. Light microscopy of MSM cultures supplemented with 1 % (v/v) Impranil DLN-SD without (**E**) and with (**F**) *H. formosensis* FZJ was performed after 72 h. The same *H. formosensis* FZJ culture was analyzed by transmission electron microscopy (TEM) with negative straining (**G** and **H**). The presence of *H. formosensis* FZJ and Impranil DLN-SD is indicated as well as the image section that was zoomed into for figure H ((**G**), black square).

Besides Impranil DLN-SD, two solid coatings provided by I-COATS N.V (Antwerp, Belgium) were also metabolized by *H. formosensis* FZJ (Figure 2.5-1 c, d), showing the versatile applicability of this strain for coating degradation. These two commercial bio-based PEU coatings find application in the textile and fishing gear industry, and belong to the ICO-THANE and ICO-FIX family coatings, respectively. To simulate realistic biodegradation conditions, they were applied to a surface, removed, and micronized before inoculation. Interestingly, the Δ*Hfor*_PE-H mutant showed no growth defects compared to the wild type when cultivated with these coatings. This could be explained by the presence of triacylglycerides in these materials. Other secreted hydrolases might degrade these compounds and thus circumvent the need of *Hfor*_PE-H when degrading the ICO-THANE

and ICO-FIX coating. After 72 h of cultivation, both ICO-THANE and ICO-FIX coatings were completely depolymerized into the soluble fraction as no solid particles were observed.

The majority of Halopseudomonads grow at temperatures between 4 - 37 °C (Bollinger et al., 2020a), whereas *H. formosensis* CC-CY503[T] was reported to grow in a range of 20 - 50 °C (Lin et al., 2013). To compare the Impranil DLN-SD-degrading activities within this genus at different temperatures, various strains were cultivated on LB and MSM agar plates containing 1 % (v/v) Impranil DLN-SD. Halo formation on LB indicates the ability to secrete PEU-degrading enzymes, while growth and/or halo formation on MSM indicates the use of Impranil DLN-SD as sole carbon source. On LB agar plates all tested were able to degrade Impranil at 30 °C (Figure 2.5-2 a). However, only *H. formosensis* FZJ degraded the polymer at 40 °C and 50 °C. On MSM agar plates, *H. formosensis* FZJ showed the strongest halo formation at 30 °C among the tested strains (Figure 2.5-2 b). When the temperature was increased to 40 °C, *H. formosensis* FZJ was the only strain still able to grow on Impranil. However, no growth or halo formation was detected when *H. formosensis* FZJ was cultivated on MSM agar plates containing Impranil at 50 °C. Overall, these results reveal *H. formosensis* FZJ as thermo-tolerant strain able to secrete enzymes and degrade Impranil at higher temperatures compared to other Halopseudomonads. As *H. formosensis* FZJ features a relatively high GC content of 62.8 % compared to the other tested strains of this genus (58.5-60.5 %) this might be a potential factor contributing to its increased thermotolerance. Moreover, the increased thermotolerance of *H. formosensis* FZJ likely originates from the compost environment from which it was isolated, which usually encounters higher temperatures than the environment of other Halopseudomonads such as the ocean or soil (Bollinger et al., 2020a). Thermostable enzymes and microorganisms are favored for depolymerization due to the increased polymer chain mobility at elevated temperatures increasing the bioavailability and thus biodegradability of polymers (Sullivan et al., 2022; Tokiwa et al., 2009; Tsuji and Miyauchi, 2001). Although *H. formosensis* FZJ is not a thermophilic organism, its thermotolerance compared to other Halopseudomonads and Impranil-degrading species can contribute to increased biodegradability of PEU coatings.
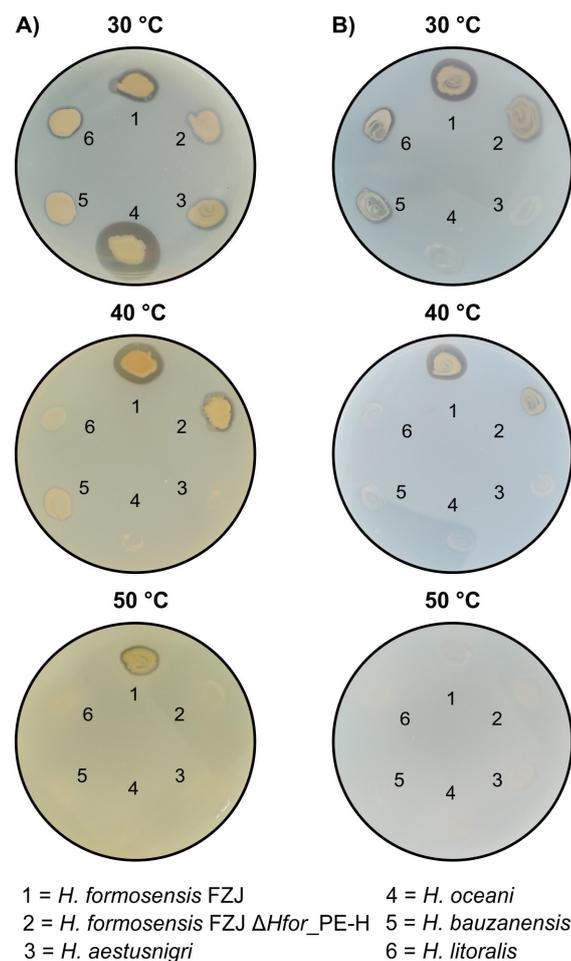
Figure 2.5-2. Temperature-dependent growth of *Halopseudomonas* spp. on Impranil DLN-SD agar plates. Strains were cultivated on lysogeny broth (LB) agar plates (A) or mineral salts medium (MSM) agar plates (B) containing 1 % (v/v) Impranil DLN-SD at the indicated temperature for 4 days. *Modified from de Witt et al. (2023)*.

2.5.4.2 Biochemical characterization of *Hfor*_PE-H

Given that *H. formosensis* FZJ is able to grow on Impranil DLN-SD at higher temperatures than other Halopseudomonads, we aimed to characterize *Hfor*_PE-H in comparison to other related enzymes in this regard. Therefore, *Hfor*_PE-H as well as the closely related *Haes*_PE-H (Bollinger et al., 2020b) and the well-known PETase from *Ideonella sakainensis* (*Is*PETase) (Yoshida et al., 2016) were heterologously expressed and purified for *in vitro* studies. The temperature stabilities were assessed using a Prometheus NanoTemper with a gradient from 20 to 99 °C. In this analysis *Hfor*_PE-H (T_m = 53.9 °C) did not show exceptionally high temperature stability compared to *Haes*_PE-H (55.6 °C) (Figure 2.5-3 a),

indicating that the superior performance at higher temperature results from the thermotolerance of *H. formosensis* FZJ on the cellular level as compared to *H. aestusnigri*.
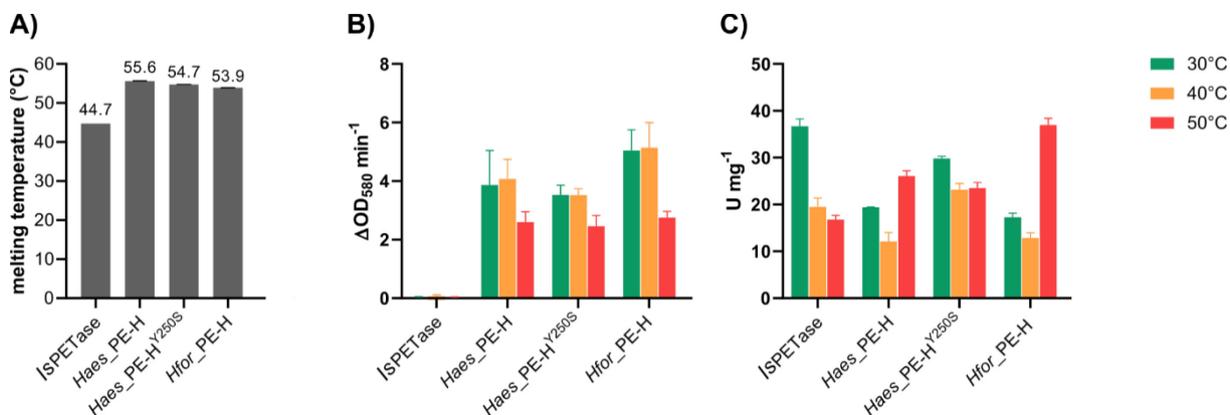
Figure 2.5-3. Temperature-dependent activity of *Hfor*_PE-H. (A) Melting temperatures of the *Hfor*_PE-H in comparison with *Is*PETase and *Haes*_PE-H. All *Halopseudomonas*-derived PE-Hs showed increased structural melting temperatures indicating thermostability. **(B)** Activity of *Hfor*_PE-H and other hydrolases towards Impranil DLN-SD at different temperatures over 10 min with enzyme concentrations of 50 nM. The activity is shown as the absolute decrease of turbidity determined as absorption at a wavelength of 580 nm per minute. As Impranil DLN-SD is a suspension, a reaction time of 10 min was sufficient to observe polymer degradation. Exemplary plots of turbidity decrease over time are displayed in Figure S5.5-2. **(C)** Activity of *Hfor*_PE-H and other hydrolases towards 4-nitrophenyl hexanoate. The activity was measured over the course of 10 min. Error bars indicate the standard deviation (SD) of two replicates.

As indicated by the Δ*Hfor*_PE-H mutant, *Hfor*_PE-H showed polyester-degrading activities that were further analyzed *in vitro*. For this, the decrease of Impranil DLN-SD turbidity was measured over time that corresponds to the hydrolytic activity and depolymerization of the substrate. *Hfor*_PE-H showed similar activities at 30 °C and 40 °C whereas the activity decreased approximately two-fold at 50 °C (Figure 2.5-3 b). Compared to *Haes*_PE-H, *Hfor*_PE-H showed a slightly higher activity at all tested temperatures. Notably, Impranil DLN-SD incubated with *Is*PETase underwent a visible change in appearance that did not result in a decrease of turbidity measured at 580 nm. It might be speculated that this enzyme catalyzed transesterification reactions under the applied assay condition. Interestingly, with the model substrate 4-nitrophenyl hexanoate (4-NPH), *Hfor*_PE-H showed a remarkable increase in activity at 50 °C (Figure 2.5-3 c). This might be explained by temperature-dependent substrate properties that could affect the activity of *Hfor*_PE-H.

Since *H. formosensis* FZJ showed growth on different polyesters, we also tested whether *Hfor*_PE-H can degrade PET. For this, *Hfor*_PE-H was incubated for 168 h at 30 °C with either an amorphous PET film or an amorphous PET foil that was ground to a powder. For the ground PET powder, *Hfor*_PE-H released minor amounts of PET monomers MHET and terephthalate (TA) (Figure 2.5-4 a), while almost no activity was detected with the less accessible PET foil (Figure 2.5-4 b). Overall, *Hfor*_PE-H showed a higher activity towards Impranil DLN-SD but lower activities towards 4-NPH and PET compared to *Is*PETase and *Haes*_PE-H. This is in line with the fact that *H. formosensis* FZJ was isolated by selection for growth on Impranil DLN-SD.
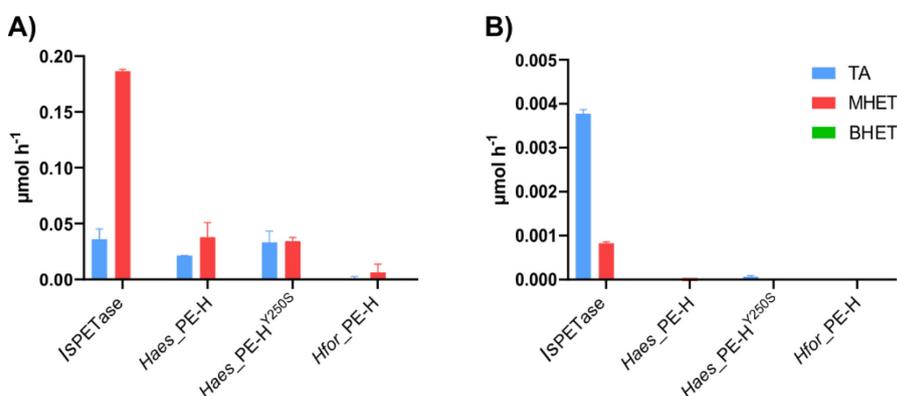
Figure 2.5-4. Activity of *Hfor*_PE-H towards PET substrates. Release of the monomers terephthalate (TA), mono-(2-hydroxyethyl)terephthalate (MHET), and bis-(2-hydroxyethyl)terephthalate (BHET) after incubation with (A) powdered amorphous PET foil or (B) an amorphous PET film for 168 h at 30 °C.

2.5.4.3 Microbial metabolism of poly(ester-urethanes)

The extracellular cleavage of Impranil DLN-SD by *Hfor*_PE-H and the ability to grow on the polymer indicated the release of low molecular weight compounds that were metabolized by *H. formosensis* FZJ. Although the exact composition of Impranil DLN-SD is unknown, Howard *et al.* proposed that it is made of poly hexane/neopentyl adipate polyester and hexamethylene diisocyanate (Howard et al., 2012). To investigate whether *H. formosensis* FZJ metabolizes these putative monomers of Impranil DLN-SD, the strain was cultivated in MSM supplemented with various aliphatic dicarboxylates, diamines, and diols as sole carbon source. None of the investigated diols or diamines with chain-lengths from C_4 to C_8 were metabolized (Figure 2.5-5 a). In contrast to this, dicarboxylates with a chain length of six or higher were metabolized by *H. formosensis* FZJ with a preference for the long-chain

C$_8$-, C$_9$-, and C$_{10}$-dicarboxylates (Figure 2.5-5 b). These results suggested that *H. formosensis* FZJ mainly metabolizes long-chain dicarboxylates that might originate from Impranil DLN-SD hydrolyzed by *Hfor*_PE-H. A protein homology search of the genome of *H. formosensis* FZJ identified genes encoding homologs to the dicarboxylic acid (Dca) metabolic proteins from *Acinetobacter baylyi* ADP1 involved in the metabolism of aliphatic dicarboxylates (Ackermann et al., 2021; Parke et al., 2001). The identified Dca homologs were encoded in a nine-gene and a two-gene operon in *H. formosensis* FZJ (Figure 2.5-5 c). Due to the additional presence of a CoA-carboxylase and a hydroxymethylglutaryl-CoA lyase within the identified nine-gene operon, it is likely that the encoded pathway enables the metabolism of acyclic terpenes but it might show side activities for long-chain dicarboxylate substrates (Jurado et al., 2015). Additionally, a putative transporter, encoded by RED13_001611, was identified that could import such dicarboxylates. The transporter showed a protein sequence identity of 25.8 % towards the *cis,cis*-muconate transport protein (MucK) from *A. baylyi* ADP1 that imports a variety of dicarboxylic acids including muconate and terephthalate (Pardo et al., 2020; Parke et al., 2001). Due to the broad substrate spectrum of MucK and the fact that no homolog of the dicarboxylate transport system DcaKP was discovered in the genome of *H. formosensis* FZJ, the identified transporter likely contributed to the import of C$_6$- to C$_{10}$-dicarboxylates. Future studies will be needed to investigate the role of the identified Dca homologs and the putative dicarboxylate transporter to confirm their role in Impranil DLN-SD metabolism.

A)

substrate	C-atoms	growth
glutaric acid	5	-
adipic acid	6	+
pimelic acid	7	+
suberic acid	8	++
azelaic acid	9	++
sebacic acid	10	++
putrescine	4	-
cadaverine	5	-
1,6-diaminohexane	6	-
1,7-diaminoheptane	7	-
1,8-diaminooctane	8	-
neopentyl glycol	5	-
1,4-butanediol	4	-
1,5-pentanediol	5	-
1,6-hexanediol	6	-
1,7-heptanediol	7	-
1,8-octanediol	8	-
glucose	6	-
acetate	2	+

B)

- C_5 - glutaric acid
- C_6 - adipic acid
- C_7 - pimelic acid
- C_8 - suberic acid
- C_9 - azelaic acid
- C_{10} - sebacic acid

C)

DcaA (34.2 %)   DcaE (28.2 %)   DcaI (45.5 %) DcaJ (47.3 %) DcaF (36.0 %)   DcaH (47.8 %) DcaF (64.2 %)

1 - LysR regulator
2 - oxidoreductase
3 - isovaleryl-CoA dehydrogenase (RED13_002911)
4 - methylcrotonyl-CoA carboxylase subunit β
5 - γ-carboxylgeranoyl-CoA hydratase (RED13_002909)
6 - methylcrotonyl-CoA carboxylase subunit α

7 - hydroxymehtylglutaryl-CoA lyase
8 - CoA transferase A (RED13_002906)
9 - CoA transferase B (RED13_002905)
10 - acetyl-CoA acetyltransferase (RED13_002904)
11 - 3-hydroxyacyl-CoA dehydrogenase (RED13_002860)
12 - acetyl-CoA acetyltransferase (RED13_002859)

Figure 2.5-5. Substrate range of *H. formosensis* FZJ. The strain was cultivated in a Growth Profiler 960 in 96-well microtiter plates in mineral salts medium (MSM) supplemented with the indicated substrate at concentrations that were the C-mol equivalent of 30 mM adipic acid. **(A)** Overview of the investigated substrates. Growth time needed to reach the stationary phase within 18 h (++), 48 h (+), or no growth (-). **(B)** Growth of *H. formosensis* FZJ in MSM with aliphatic dicarboxylic acids as sole carbon source. The mean values and standard deviations (SD) of three replicates are shown. **(C)** Putative gene clusters encoding enzymes for the metabolism of dicarboxylic acids in *H. formosensis* FZJ. Homologous genes of the *dca* cluster from *Acinetobacter baylyi* ADP1 are shown in green with their corresponding protein sequence identity. Orange indicates a putative regulator of this cluster. Genes are numbered according to the indicated gene products and locus tags of the respective genes are displayed in brackets.

To further unravel the metabolic pathways for growth on Impranil DLN-SD by *H. formosensis* FZJ, gas chromatography time-of-flight mass spectrometry (GC-ToF-MS) was performed on supernatants of both *in vivo* cultures and *in vitro Hfor*_PE-H assays. *In vitro* depolymerization of Impranil DLN-SD by *Hfor*_PE-H resulted in the release of four monomers, namely neopentyl glycol, 1,6-hexanediol, adipic acid, and an unknown

compound designated as M_162 (Figure 2.5-6 a, Figure 2.5-7). These results match the structure of Impranil DLN-SD proposed by Howard *et al.*, with the polyester region of the polymer consisting of poly hexane diol/neopentyl adipate polyester. The absence of (di-) amines after enzymatic hydrolysis confirms the inability of *Hfor*_PE-H to hydrolyze the urethane bonds within the polymer. Growth of *H. formosensis* FZJ with Impranil DLN-SD resulted in the accumulation of neopentyl glycol that is in agreement with the inability of the strain to metabolize this monomer (Figure 2.5-5 a, Figure 2.5-6 b). Although adipic acid was metabolized by *H. formosensis* FZJ, it was still present in the culture supernatant, indicating that it was released by *Hfor*_PE-H faster than it could be metabolized (Figure 2.5-7). Moreover, 1,6-hexanediol was detected and, indeed, this compound could not be metabolized by *H. formosensis* FZJ as sole carbon source (Figure 2.5-5 a, Figure 2.5-6 a). 4-Hydroxybutyrate was detected in the culture supernatant, but not in the enzymatically treated sample. This hydroxylated acid is thus unlikely to be a constituent of Impranil DLN-SD, rather, it is a possible intermediate of aliphatic diol metabolism (Li et al., 2020), indicating that *H. formosensis* FZJ can partially oxidize the diols (Figure 2.5-7). The fact that the putative precursor 1,4-butanediol was not detected in any sample suggests that the 4-hydroxybutyrate originates from partial β-oxidation of 1,6-hexanediol. An unknown compound (M_162) was also detected in the culture supernatant of *H. formosensis* FZJ. Mass spectral analysis of M_162 revealed the chemical formula $C_7H_{14}O_4$ and the detected fragmentation pattern indicates that this compound could be a dimer of neopentyl glycol and glycolic acid namely 3-hydroxy-2,2-dimethylpropyl 2-hydroxyacetate (Figure S5.5-1). The presence of such a dimer in the culture supernatant supports our theory that hydrolases other than *Hfor*_PE-H might degrade the released oligomers. However, it can only be speculated whether 3-hydroxy-2,2-dimethylpropyl 2-hydroxyacetate is cleaved extracellularly or imported into the cell for subsequent metabolism (Figure 2.5-7). The absence of glycolic acid in the culture supernatant might indicate that the oligomer is directly imported without prior cleavage into neopentyl glycol and glycolic acid. The presence of many genes encoding intracellular hydrolases in *H. formosensis* FZJ supports the theory of oligomer import and intracellular cleavage of them (Table S5.5-1).

A) Enzymatic degradation

peak	compound	R. T. (min)	no Impranil® DLN-SD TIC area (%)	+ Impranil® DLN-SD TIC area (%)
1	neopentyl gylcol	6.65	n. d.	0.1
3	1,6-hexanediol	9.84	n. d.	1.4
4	adipic acid	11.56	n. d.	6.6
5	M_162	15.30	n. d.	0.8

— no Impranil DLN-SD

— + Impranil DLN-SD

B) Microbial degradation

peak	compound	R. T. (min)	abiotic control TIC area (%)	*H. formosensis* FZJ TIC area (%)
1	neopentyl gylcol	6.65	n. d.	2.6
2	4-hydroxybutyrate	8.85	n. d.	0.8
3	1,6-hexanediol	9.84	n. d.	0.2
4	adipic acid	11.56	n. d.	0.2
5	M_162	15.30	n. d.	0.2

— abiotic control

— *H. formosensis* FZJ

Figure 2.5-6. GC-ToF-MS analysis of Impranil DLN-SD degradation. (A) Chromatogram of *in vitro* depolymerized Impranil DLN-SD (orange) and its negative control not containing the polymer (black) showing the analytical ion current (AIC) over the time. Peaks of released monomers are labelled and summarized in the corresponding table with their annotation, retention time (R. T.) and relative area of the total ion current (TIC). Mass spectral analysis indicated that M_162 might be 3-hydroxy-2,2-dimethylpropyl 2-hydroxyacetate (Figure S5.5-1). Compounds that were not detected in a sample are labelled with "n. d." and P indicates the dominant phosphate peak. Samples were incubated with *Hfor*_PE-H in 100 mM potassium phosphate buffer (pH 7.2) containing 100 mM NaCl with or without 1 % (v/v) Impranil DLN-SD at 30 °C for 1 h. **(B)** Chromatogram of *in vivo* depolymerized Impranil DLN-SD by *H. formosensis* FZJ (green) and its abiotic control (black). Samples were incubated in mineral salts medium supplemented with 1 % (v/v) Impranil DLN-SD at 30 °C for 72 h. A full list of all detected compounds is shown in Table S5.5-2.

Overall, our results unraveled the metabolic pathway for Impranil DLN-SD in *H. formosensis* FZJ. First, *Hfor*_PE-H and putatively other hydrolases are secreted for initial polymer degradation. Enzymatic degradation of the ester segments results in the release of neopentyl glycol, adipate, and 1,6-hexanediol of which only adipate was metabolized by the strain *via* the identified β-oxidation pathway. Moreover, short oligomers such as 3-hydroxy-2,2-dimethylpropyl 2-hydroxyacetate are likely imported into the cell and might be substrates for intracellular hydrolases (Figure 2.5-7). Future genetic engineering of *H. formosensis* FZJ could expand its metabolism by heterologous expression of urethanases and implementation of metabolic routes for monomers such as 1,6-hexanediol or neopentyl glycol (Branson et al., 2023). Considering these modifications, *H. formosensis* FZJ has the great potential to function as platform strain for bio-upcycling of PEU coatings with increasing genetic accessibility of Halopseudomonads.
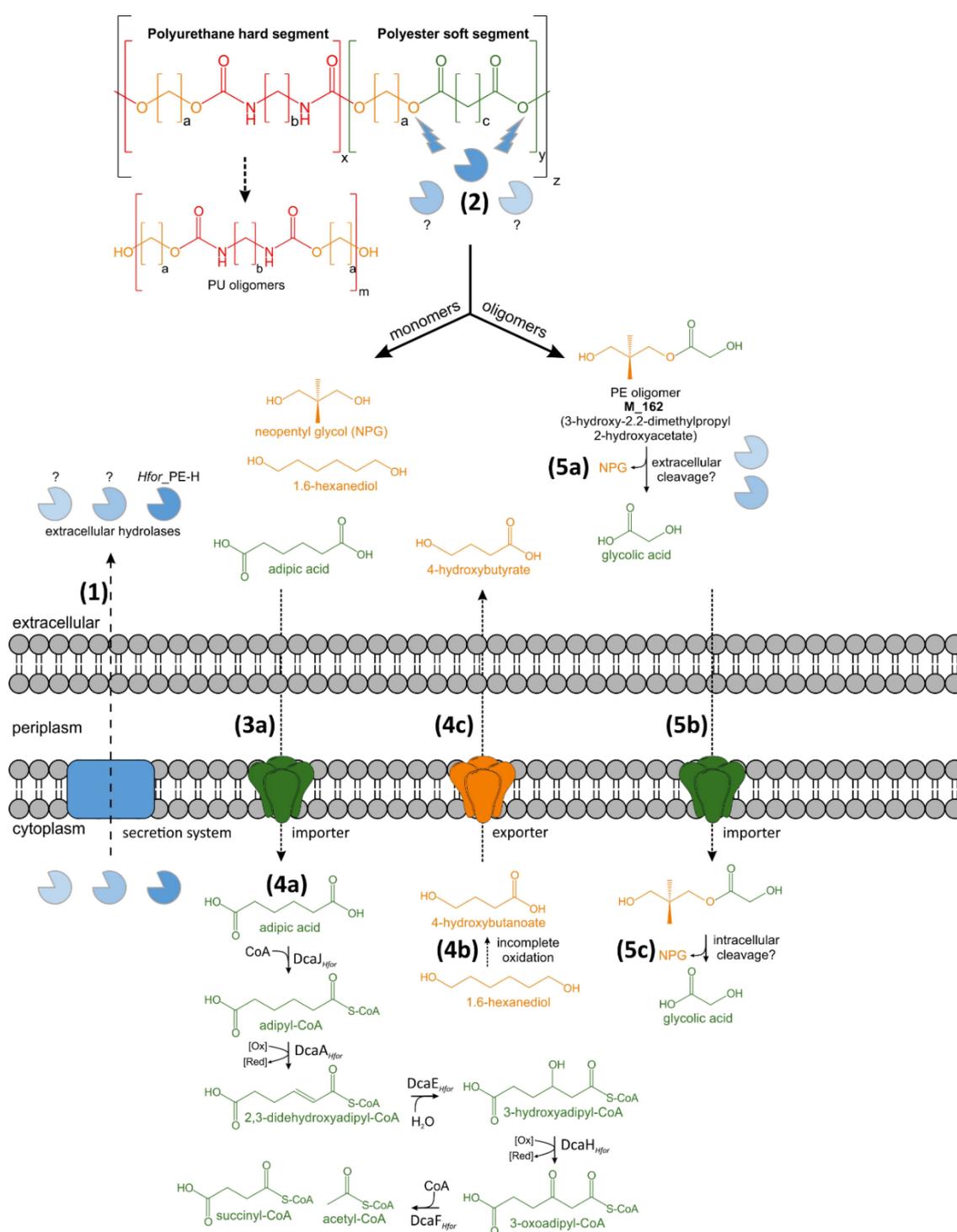
Figure 2.5-7. Proposed metabolic pathways for Impranil DLN-SD degradation by *H. formosensis* FZJ.
(1) Secretion of extracellular hydrolases including *Hfor*-PE-H *via* the Sec protein translocation system. **(2)** Enzymatic hydrolysis of ester bonds within the polyester segment by *Hfor*_PE-H and other extracellular hydrolases. Enzymatic hydrolysis releases large oligomers of polyurethane (PU) as well as monomers and oligomers that were detected *via* GC-ToF-MS. **(3a)** Import of monomers and subsequent metabolism of adipic acid *via* β-oxidation **(4a)**. **(4b)** Incomplete oxidation of 1,6-hexanediol and export of the dead-end product 4-hydroxybutyrate **(4c)**. 3-hydroxy-2.2-dimethylpropyl 2-hydroxyacetate (M_162) was identified as polyester (PE) oligomer released upon *in vivo* degradation of *H. formosensis* FZJ. It is conceivable that this compound is cleaved extracellularly **(5a)** or imported into the cell **(5b)** for intracellular cleavage by hydrolases **(5c)**.

2.5.5 Conclusion and outlook

PEU coatings, such as Impranil DLN-SD, are indispensable for tuning and improving the properties of the plastic materials they are applied on. However, they pose a hindrance for chemical or mechanical recycling. Biodegradation of such coatings is a powerful strategy to overcome these hurdles by using enzymes or microorganisms capable of depolymerizing the protective coating layer. In this study, *H. formosensis* FZJ was isolated for its ability to grow on Impranil DLN-SD and was also able to metabolize ICO-THANE and ICO-FIX PEU coatings as sole carbon source. In contrast to other Halopseudomonads, *H. formosensis* FZJ showed an outstanding temperature tolerance and was able to depolymerize Impranil DLN-SD at up to 50 °C making it a promising candidate for industrial processes. The identified *Hfor*_PE-H showed higher activity towards Impranil DLN-SD compared to its homologs within the phylogenetic lineage. Deletion of the corresponding gene led to impaired growth on Impranil DLN-SD and constitutes the first report of a genetic modification of a *Halopseudomonas* bacterium. Overall, the detailed characterization of Impranil DLN-SD metabolism indicated rapid degradation, but only partial metabolization of the PEU coating by *H. formosensis* FZJ. The profound knowledge on both microorganism and enzymes in thus study contributes to understanding the interaction of microbes with synthetic polymers. Hence, this study leads the path for future bio-recycling strategies aiming for recycling entire plastic materials including their coatings.

2.5.6 Materials and methods

2.5.6.1 Strain isolation and cultivation

H. formosensis FZJ was isolated from a mesophilic compost heap in Würselen, Germany (50.8351551, 6.1411361). For the initial enrichment, mineral salts medium (MSM) (Wierckx et al., 2005) was inoculated with 10 g L^{-1} of compost material and 1 % (v/v) Impranil DLN-SD (Covestro AG, Leverkusen, Germany). Shake flasks were incubated at 30 °C and 200 rpm shaking speed. After 3 days, the flasks were re-inoculated into fresh MSM medium supplemented with 1 % (v/v) Impranil DLN-SD. After five re-inoculations, different species were isolated on lysogeny broth (LB) agar plates containing 1 % (v/v) Impranil DLN-SD. The isolate exhibiting the strongest halo formation was selected for this

study and in the following termed *Halopseudomonas formosensis* FZJ. Strains of *Escherichia coli* were cultivated in LB medium with appropriate antibiotics if necessary. For cultivation of *H. formosensis* FZJ, 10 mM of suberic acid was added to LB medium to facilitate growth. All strains used in this study are shown in Table S1.

2.5.6.2 16S rDNA sequencing

For preliminary identification of the isolated strain, 16S rDNA sequencing was performed. Genomic DNA was purified using a Monarch Genomic DNA Purification Kit (NEB) from an overnight LB culture of single colonies. The 16S rDNA sequence was amplified by PCR using Q5 High-Fidelity 2× Master Mix (NEB) as DNA polymerase and the primers FD1/2 (5'-3'   AGAGTTTGATCMTGGCTCAG)   and   RP1/2   (5'-3' ACGGYTACCTTGTTACGACTT) (Weisburg et al., 1991). PCR products were purified with a Monarch PCR and DNA Cleanup Kit (NEB) and sequenced by Eurofins Genomics (Ebersberg, Germany). The resulting sequences were aligned to the nucleotide collection (nr/nt) of the NCBI database using BLASTn and hits with the highest sequence identities were compared. (Sayers et al., 2022).

2.5.6.3 Whole genome sequencing

Genomic DNA from strains of interest was purified using a Monarch Genomic DNA Purification Kit (NEB) from an overnight LB culture. Afterwards, 1 μg of DNA was used for library preparation using the NEBNext Ultra™ II DNA Library Prep Kit for Illumina (NEB). The library was evaluated by qPCR using the KAPA library quantification kit (Peqlab, Erlangen, Germany). Afterwards, normalization for pooling was done and paired-end sequencing with a read length of 2 × 150 bases was performed on a MiSeq (Illumina). The reads of demultiplexed fastq files as the sequencing output (base calls) were trimmed and quality-filtered using the CLC Genomic Workbench software (Qiagen Aarhus A/S, Aarhus, Denmark). Then, the filtered reads were used for *de novo* assembly using the CLC Genomic Workbench software. Sequencing data are stored in the NCBI Sequence Read Archive under the BioProject number PRJNA987411 under accession number SRR25019772. The annotated genome of *H. formosensis* FZJ can be accessed *via* the accession number SAMN35980280.

2.5.6.4   Quantification of NH$_4^+$ consumption

The turbidity of Impranil DLN-SD in aqueous media prevented to analyze bacterial growth *via* the optical density (OD$_{600}$). Hence, the consumption of NH$_4^+$ was chosen as suitable parameter as it correlates with bacterial growth. For quantifying the NH$_4^+$ consumption, a colorimetric assay was adapted from Willis et al. (1996). The NH$_4^+$ concentration was reduced to 300 mg L^{-1} in the MSM for cultivation. Samples from liquid cultivations were filtered through an AcroPrep™ 96-well filter plate (Pall Corporation, Port Washington, NY, USA) to obtain the analytes for the assay. In a 96-well plate, 10 µL of analytes (0.5 – 50 mg L^{-1} NH$_4^+$) was mixed with 200 µL of reagent A (32 g L^{-1} Na-salicylate, 40 g L^{-1} Na$_3$PO$_4$ × 12 H$_2$O, and 0.5 g L^{-1} sodium nitroprusside (Na$_2$[Fe(CN)$_5$NO] × 2 H$_2$O)). After that, 50 µL of reagent B (0.25 % (v/v) NaClO) was added and mixed. Samples were incubated at room temperature for 20 min and subsequently the absorbance was detected at λ = 685 nm using a Tecan infinite M nano plate reader (Tecan Group, Männerdorf, Schweiz).

2.5.6.5   Genetic engineering

The mutant Δ*Hfor*_PE-H derived from *H. formosensis* FZJ was constructed using the I-SceI-based system (Martínez-García and de Lorenzo, 2011) according to the streamlined protocol (Wynands et al., 2018) and further optimized to allow genetic engineering of *H. formosensis* FZJ. The 500-600 bp up- and downstream flanking regions (TS1 and TS2) of the *Hfor*_PE-H encoding gene were integrated into the suicide delivery vector pEMG. The integration of the suicide vector into *H. formosensis* FZJ was performed by patch mating for 24 h on LB agar plates. For this, the *E. coli* PIR2 donor strain holding the pEMG-Δ*Hfor*_PE-H plasmid, the helper strain *E. coli* HB101 pRK2013, and the recipient *H. formosensis* FZJ were used. To enable expression of *sce-I*, we constructed pQT8-*sce-I* that was recognized by *H. formosensis* FZJ after electroporation. For this, the strain was cultivated in LB medium supplemented with 10 mM suberic acid at 30 °C overnight. Next, the cells were harvested by centrifugation at 16,000 *g* for 1 min. The cell pellet was resuspended in half of the initial volume with 300 mM sucrose. After two additional washing steps, cells were resuspended in 2 % of the initial volume in 300 mM sucrose. Next, 1 µg of pQT8-*sce-I* was added to 50 µL of cells and electroporation was performed using DEVICE X (0.2 cm cuvette, 2.5 kV, 25 µF, and 200 Ω). After the electroporation, 950 µL of LB medium supplemented with 10 mM suberic acid was added and cells were regenerated at 30 °C for 5 h. Transformed cells were

selected on LB agar plates containing 20 mg L^{-1} gentamicin. The successful knock-out of *Hfor*_PE-H was confirmed by DNA sequencing.

2.5.6.6 Microscopic analysis

Light microscopy pictures were taken on an AxioImager M2 equipped with a Zeiss AxioCam MRm camera and an C Plan-Neofluar 100×/1.3 Oil Ph3 objective (Carl Zeiss, Germany). Images were analyzed using the AxioVision 4.8 software (Carl Zeiss). For Transmission Electron Microscopy, *H. formosensis* FZJ was cultivated with Impranil in MSM for 72 h and was adsorbed on CF300-Cu grids (Electron microscopy services) and negatively stained with 2 % uranyl acetate. Staining procedure by side blotting was carried out as described in Ohi et al. (2004). TEM images were acquired on a Talos L120C G2 transmission electron microscope (Thermo Fisher Scientific) operated at 120 keV with a 4k x 4k Ceta 16M CEMOS camera.

2.5.6.7 GC-ToF-MS analysis

For sample preparation, cultures were filtered through an AcroPrep™ 96-well filter plate to obtain cell-free filtrates (Pall Corporation, Port Washington, NY, USA). Aliquots of 130 µL were shock-frozen in liquid nitrogen and stored at -20 °C. Prior to analysis, samples were lyophilized overnight in a Christ LT-105 freeze drier (Martin Christ Gefriertrocknungsanlagen, Osterode am Harz, Germany). Two-step derivatization of the samples and GC-ToF-MS analysis was performed as described before by Paczia et al. (2012) using a L-PAL3-S15 liquid auto sampler coupled to a LECO GCxGC HRT+ 4D high resolution time of flight mass spectrometer (LECO, Mönchengladbach, Germany). To identify known metabolites, a baseline noise-corrected fragmentation pattern together with the corresponding current RI value (Retention time Index) was compared to our in-house accurate m/z database JuPoD, and the commercial nominal m/z database NIST20 (National Institute of Standards and Technology, USA). Unknown peaks were identified by a virtual reconstruction of the derivatized metabolite structure *via* the measured baseline noise corrected accurate mass m/z fragment pattern in comparison to an accurate m/z fragment register inside the JuPoD main library and were subsequently verified by virtual derivatization and fragmentation of the predicted structure.

2.5.6.8 Enzyme production and purification

The expression plasmids including the enzyme-encoding genes were codon-optimized for *E. coli* and ordered from Twist Bioscience, USA and subsequently rehydrated according to the manufacturer protocol. Protein production and purification was carried out according to Bollinger et al. (2020b) with minor changes. For heterologous expression, the *E. coli* strain LOBSTR was used (Andersen et al., 2013). For this, a pre culture was cultivated with 0.5 % (w/v) glucose for 24 h at 37 °C. From this, the main culture was inoculated with a starting OD_{580} of 0.05 and incubated at 30 °C for 24 h under agitation of 160 rpm. The cells were then harvested and purified according to Bollinger et al. (2020b).

2.5.6.9 Biochemical characterization

Esterase activity was measured using 4-nitrophenyl hexanoate as substrate. The substrate solution was prepared from a stock solution of 20 mM 4-nitrophenyl hexanoate in acetonitrile mixed 1/20 with 100 mM potassium-phosphate buffer with 100 mM NaCl (pH 7.2). Ten microliter of the enzyme solution was mixed with 190 µl of the substrate solution in a microtiter plate and immediately measured at 30 °C/40 °C/50 °C in Tecan Infinite M1000Pro (Tecan Traiding AG, Switzerland) or Molecular Devices SpectraMax iD3 (Molecular Devices, USA) photometers at 410 nm for 10 min with a measurement every 22 sec. The volumetric esterase activity was calculated using the formula $\frac{\Delta OD_{410}\,[min^{-1}]*vol.in\,MTP\,[ml]*dillution\,factor}{d\,[cm]*\varepsilon\,[mM^{-1}*cm^{-1}]*sample\,volume\,[ml]} * enzyme\,concentration[\frac{mg}{ml}] = \frac{U}{mg}$ (Nolasco-Soria et al., 2018).

2.5.6.10 Determination of protein thermal melting point

The melting curves of the proteins were measured using nano differential scanning fluorimetry (nanoDSF) using a Prometheus device (NanoTemper Technologies, Inc.). The NanoTemper capillaries were loaded with purified enzyme at a concentration of about 1 mg mL^{-1} in 100 mM potassium phosphate buffer with 100 mM NaCl (pH 7.2). The melting temperature was scanned in a range between 20 and 99 °C at a rate of 1 °C per minute.

2.5.6.11 Enzymatic hydrolysis of PET and quantification of reaction products

The hydrolysis of PET films and powder, was determined as described by Bollinger et al. (2020b) with minor modifications. The reaction mixture in a total volume of 200 µl was

composed of 1 mg mL^{-1} purified enzyme in 100 mM potassium phosphate buffer with 100 mM NaCl (pH 7.2) with 20% (v/v) dimethyl sulfoxide (DMSO) and a circular piece of PET film (6 mm diameter, Goodfellow Cambridge, Ltd.) or 5 mg of powdered amorphous PET film. The reaction mixtures were incubated in centrifugal filters with a cutoff (MWCO) of 10,000 Da (VWR International GmbH) for a total of 96 h at 30 °C. Every 24 h 50 µL of the solution was harvested by centrifugation at 15,000 rpm for 30 sec and frozen at -20 °C until use. The reaction filtrates were analyzed with an UPLC system (Acquity UPLC, Waters GmbH) equipped with an Acquity UPLC BEH C18 column (1.7 µm particle size) using the published method by (Bollinger et al., 2020b). For terephthalic acid (TA) and BHET, commercially available standards were used to calculate amounts from calibration curves. For MHET, standards were used generated by the de Winde lab of the University of Leiden (The Netherlands) and kindly made available to us.

2.5.6.12 Enzymatic hydrolysis of Impranil DLN-SD

Degradation of Impranil DLN-SD was determined by measuring the decrease in optical density at 580 nm (Islam *et. al.* 2019). Ten microliter of enzyme solution were mixed with 190 µL of substrate solution consisting of 100 mM potassium phosphate buffer with 100 mM NaCl (pH 7.2) and 1 % (v/v) Impranil DLN-SD. The final enzyme concentration used in the assays was 50 nM. The loss of turbidity was then measured in a Tecan Infinite M1000Pro (Tecan Traiding AG, Switzerland) or Molecular Devices SpectraMax iD3 (Molecular Devices, USA) photometer at a wavelength of 580 nm for 10 min at 30 °C, 40 °C, and 50 °C with measurement intervals every 22 s. The absolute value of the calculated slope was used as a measure of activity.

2.5.7 Conflict of interest statement

I-COATS is the producer and purveyor of ICO-THANE and ICO-FIX. The authors declare that there are no further conflicts of interest.

2.5.8 Data availability statement

Data will be made available upon request. Sequencing data are stored in the NCBI Sequence Read Archive under the BioProject number PRJNA987411 under accession number

SRR25019772. The annotated genome of *H. formosensis* FZJ is stored under accession number SAMN35980280.

2.5.9 Acknowledgements

3   General discussion and outlook

Plastics are inevitable in our daily life as they offer many advantages over other materials such as glass, paper, or metals in terms of elasticity, lightness, and durability. A total ban on plastics is therefore inconceivable in modern society, and in fact their production is increasing annually (Wei et al., 2020). However, the increasing environmental pollution urges for finding both sustainable and efficient end-of-life solutions to overcome the global plastic crisis. Biological end-of-life solutions are such emerging technologies, which could facilitate the transition towards a circular plastics economy. Furthermore, rethinking the plastics economy requires a paradigm shift in which plastic waste is considered as a valuable resource within a circular economy. This requires suitable biocatalysts, namely engineered enzymes and microorganisms, to which the research in this thesis contributes.

3.1   Plastic-degrading enzymes – big steps ahead

Enzymatic depolymerization of plastics offers many advantages over chemical depolymerization strategies, including their operation at moderate conditions (temperature, pressure, and pH), a high selectivity and catalytic power, as well as a low environmental impact (Ellis et al., 2021; Tournier et al., 2023). In the past decade, many plastic-degrading enzymes were discovered and enzyme engineering resulted in the design of highly optimized biocatalysts such as HotPETase (Bell et al., 2022), ICCG (Tournier et al., 2020) and many more. However, enzymatic depolymerization has only been successfully demonstrated for relatively easy-to-hydrolyze polyester such PET or PLA. Enzymatic recycling of PET bottles is already approaching industrial-scale and is a prime example for a circular process due to its "infinite recycling" technology developed by Carbios (Tournier et al., 2020). Nevertheless, the goal of Carbios to build the world's first industrial-scale PET bio-recycling plant with a capacity of 50,000 tons per year (Carbios, 2023) is just a drop in the ocean compared to European PET production of approximately 3 million tons (PlasticsEurope, 2023). Therefore, the future up-scaling of such technologies is essential to make significant contributions to a circular plastics economy.

In contrast to polyester, enzymatic hydrolysis of PA and PU remains a challenge. The discovery of nylonases capable of hydrolyzing PA-oligomers paved the way for enzymatic PA depolymerization (Kinoshita et al., 1977; Kinoshita et al., 1981; Negoro et al., 1992). Although enzyme engineering resulted in thermostable NylC variants able to partially hydrolyze PA6 and PA6.6, the overall extent of depolymerization was greatly limited (Nagai et al., 2014; Puetz et al., 2023). Enzyme activities and substrate ranges must be increased to efficiently depolymerize real-world PA materials like fishing nets and textiles. This will likely require extensive enzyme engineering, which is facilitated by the increased diversity of nylonase sequences uncovered in chapter 2.2. The additional exploitation of metagenomic datasets for novel nylonase candidates could further increase the number of enzymes available to enzyme engineering, as already successfully performed for the discovery of novel PETase candidates (Danso et al., 2018). Alternatively, peroxidases could be used for oxidative pre-treatment of PA (Deguchi et al., 1998) that could increase the subsequent activities of engineered nylonases. Although enzymatic depolymerization of PA is still inefficient today, it is a promising alternative or supporting technology to chemical recycling that typically operates at harsh conditions and requires non-recyclable as well as toxic catalysts (Alberti et al., 2019). Hybrid strategies consisting of a chemical pretreatment and subsequent enzymatic recycling could be the key for efficient PA recycling processes. Such hybrid processes paved the way for bio-chemical recycling of lignocellulosic biomass, in which chemical pretreatment resulted in the accessibility of cellulose for subsequent enzymatic depolymerization (Lynd et al., 2022; Sheng et al., 2021).

Similar to PA, enzymatic depolymerization of PU is not yet well established. Their chemical diversity, often cross-linked networks, and rigid segments complicate enzymatic hydrolysis. Although urethanases with characterized activities towards low-molecular-weight urethane oligomers are known (Branson et al., 2023; Patel et al., 2003), no efficient enzyme is characterized that can directly hydrolyze urethane bonds in polymers. Due to their chemical complexity, the design of specific enzymes is required for the hydrolysis of each specific PU (Tournier et al., 2023). In other words, the development of a universal enzymatic PU recycling process is rather improbable. Instead, the combination of chemical hydrolysis and enzymatic catalysis is most promising to establish PU recycling processes. Such hybrid chemoenzymatic process was already successfully demonstrated for polyether-PU foam, in

which chemical hydrolysis released low-molecular-weight dicarbamates that were further hydrolyzed by an urethanase (Branson et al., 2023)

Furthermore, PU are often present in PEU that are widely used as coating materials in the textile and fishing gear industry. Due to the presence of soft polyester regions, the biodegradability of PEU is greatly increased compared to PU. The isolation of *H. formosensis* FZJ and the characterization of the PEU-hydrolyzing *Hfor*_PE-H in this thesis (chapter 2.5) demonstrates the biological depolymerization of PEU. However, it was also discovered that the PU bonds were not degraded by the novel isolate. Consequently, micro- and even nanoplastics of PU can emerge from biological degradation of PEU that must be avoided at all costs to reduce the environmental pollution. Therefore, this study provides guiding insights for the design of coatings with enhanced biodegradability to prevent the environmental release of micro- and nanoplastics during natural wear of coatings. In managed recycling environments, it is imperative to combine the action of PEU-degrading enzymes and microorganisms, which specifically hydrolyze the polyester regions, with the activities of urethanases capable of hydrolyzing the resulting PU degradation products. This integrated approach is crucial to prevent the release of micro- and nanoplastics during the recycling process. Heterologous expression of urethanases in *H. formosensis* FZJ or a combined enzymatic reaction of *Hfor*_PE-H and urethanases could be potential strategies. Regulatory guidelines for the design of PEU could facilitate this synergy by stipulating the incorporation of easy-to-hydrolyze PU segments.

In the past decades, very limited success was achieved for the efficient enzymatic depolymerization of plastics with pure C–C backbones, namely polyolefins (such as PE and PP), PVC, and PS (Chow et al., 2023). However, these plastics represent about two-thirds of the global plastics production indicating the enormous efforts for establishing a fully circular plastics economy (PlasticsEurope, 2023). Recently, the discovery of PE-degrading oxidases has attracted much attention, despite their low activities (Sanluis-Verdes et al., 2022; Spínola-Amilibia et al., 2023), although some criticize the lack of evidence for true enzymatic degradation (Tournier et al., 2023). Only time will tell if the latest discoveries are a breakthrough or if other, yet unknown, enzymes may be suitable for the efficient deconstruction C–C-bonded polymers. However, 'time' is limited due to the expanding

plastic crisis that could ultimately urge to ban production of polyolefins and other C–C-bonded polymers for certain applications that could be replaced by alternatives. Concerning a circular economy, such alternatives ideally would be both bio-based and biodegradable plastics. On the other hand, chemical hydrolysis of C–C-bonded polymers has already been achieved and was successfully combined with subsequent microbial upcycling (Sullivan et al., 2022). Therefore, chemical hydrolysis might be superior to enzymatic hydrolysis for challenging plastic degradation scenarios and would provide a more timely response to the escalating plastic crisis.

3.2 Metabolic engineering enables biological funneling of plastic hydrolysates by *P. putida* KT2440

Depolymerization of plastic waste results in mixed hydrolysates consisting of various monomers and oligomers. Subsequent chemical recycling would require laborious and costly purification of the individual building blocks, which is often an economic burden and results in low recycling rates (Bucknall, 2020; Ellis et al., 2021). Microbial catalysis provides a promising alternative by funneling complex hydrolysates into the central metabolism of suitable hosts to produce value-added compounds. This proves particularly beneficial for hydrolysates derived from low-value or poorly recyclable waste streams, such as contaminated mixed streams. *P. putida* KT2440 is such a powerful microbe for microbial upcycling as it is equipped with a versatile metabolism. Using metabolic engineering, the native metabolism was leveraged and extended, enabling the utilization of plastic monomers including TA (Narancic et al., 2021), EG (Franden et al., 2018a; Li et al., 2019), AA (Ackermann et al., 2021), and BDO (Li et al., 2020). However, many plastic-derived compounds are still not accessible to native or synthetic pathways of this strain, such as from PA, PU, or polyester, preventing their biological funneling and thus their microbial upcycling, until now.

This thesis has made significant contributions to overcoming the limitations of biological funneling by greatly extending the substrate range of *P. putida* KT2440 by several plastic-derived monomers and oligomers. In particular, metabolism of the PA monomers ε-caprolactam, Ahx, and HMDA was enabled and heterologous expression of nylonases coupled with deep metabolic engineering further extended the substrate range by cyclic and linear oligomers of PA6 (chapter 2.1). Although parts of the required metabolic pathways were present in rather niche organisms (Otzen et al., 2018; Takehara et al., 2018), these synthetic compounds were not accessible as substrates to biotechnological workhorses. Growth of the engineered strains on real PA hydrolysates, mainly consisting of linear oligomers, was demonstrated. The metabolization of linear oligomers (n=2-7) by *P. putida* KT2440 is a milestone for biological catalysis as such oligomers are the dominant fraction of PA6 hydrolysates (Minor et al., 2023). The ability to also degrade cyclic PA6 dimers might be promising for wastewater treatment as cyclic oligomers are typical by-products of PA-manufacturing plants that easily accumulate in the environment (Danso et al., 2019). However, future research must be conducted to transfer the activity of NylC in *P. putida* KT2440. Thereby, larger cyclic oligomers obtained during polymer synthesis could be metabolized. Overall, this thesis provides mixed PA hydrolysates as feedstocks for biotechnology creating the connection between synthetic metabolism and product formation in the biotechnological workhorse *P. putida* KT2440.

Moreover, metabolism of even and uneven mcl-DCA and -diols was established in *P. putida* KT2440 (chapter 2.3). These are prevalent monomers of polyester but also of PA and PU, respectively. Hence, hydrolysates of even complex and thus hard-to-recycle plastics can be channelized into its central metabolism and used for the production of value-added compounds. Additionally, mcl- and lcl-DCA can emerge from the chemical oxidation of polyolefins such as PE (Sullivan et al., 2022). Since the vast majority of virgin plastics are polyolefins, the broad substrate spectrum of the engineered strain is a promising opportunity to establish more sustainable end-of-life solutions for this dominant group of plastics. To further improve such a process for PE or PP, process parameters such as the choice of catalyst, reaction temperature, or time can be modified to obtain predominantly mcl-DCA, including even and uneven chain lengths (Bäckström et al., 2017). Besides aliphatic DCA, BSCD could also be released upon chemical oxidation of polyolefins such as PP. Moreover,

they gained increasing interest as building blocks for PA and polyester, as their branches allow cross-linking of polymer chains and enable fine-tuning of polymer properties (Little et al., 2020; Voit and Lederer, 2009). In this thesis, metabolism of five prevalent C_5-BSCD, including itaconate and mesaconate, was established in *P. putida* KT2440 (chapter 2.4). Thereby, this work contributes to developing sustainable end-of-life solutions for the increasing amounts of BSCD-based plastics that would otherwise intensify the efforts of traditional recycling yielding further environmental pollution. Nevertheless, it has to be investigated if the synthetic metabolism for BSCD in *P. putida* KT2440 can also funnel DCA with other branches than methyl-branches into the central metabolism. Further metabolic engineering might be required to extend the substrate range for BSCD with various other branches that might be of future interest for the plastic industry.

This thesis demonstrates the promising approach of using metabolic engineering to provide abundant plastic waste as valuable resource for biotechnology. This opens the possibility for pioneering sustainable end-of-life solutions for the millions of tons of plastic waste that are currently landfilled or incinerated. The metabolic diversity and genetic accessibility of *P. putida* KT2440 make it an outstanding platform strain for future implementations of biological funneling of mixed plastic hydrolysates.

3.3 The future of microbial upcycling: A sustainable approach to plastic waste management

Microbial upcycling provides a promising alternative to chemical or mechanical recycling as it utilizes mixed plastic hydrolysates as feedstocks for the production of value-added compounds. The power of microbial upcycling especially becomes apparent for hard-to-recycle plastics, whose deconstruction yield complex hydrolysates, such as PU, polyolefins, or multilayer plastics (Ellis et al., 2021). With regard to a circular economy, however, it is important to maintain or even increase the product's value during microbial upcycling and to match the scales between substrate and product.

In this thesis, microbial upcycling of several plastic monomers and oligomers to scl- and mcl-PHA was demonstrated using engineered strains of *P. putida* KT2440 (chapters 2.1, 2.3, 2.4). A key finding was that the yield of scl- and mcl-PHA differed greatly depending on the substrate and its metabolic route linked to the central metabolism. For example, considerable production of mcl-PHA was achieved for AA and HDO (both C_6), whereas DCA or diols with a chain-length greater than six were not suited for mcl-PHA production (discussed in chapter 2.3). Instead, highest PHB production was observed for pimelic acid and 1,7-heptanediol (both C_7), as metabolism of both substrates yielded acetoacetyl-CoA that is a direct precursor for PHB synthesis. Moreover, production of PHB from PA6-hydrolysates was achieved in the presence of nitrogen, demonstrating the conversion of nylon to PHB through hydrolysis and microbial catalysis. Hence, this thesis demonstrated a proof-of-principle of microbial upcycling of various plastic hydrolysates. However, further optimizations will be required to make these processes economically and ecologically viable. One major limitation can be the low yield of some of processes, leading to significant carbon losses as CO_2. Again, metabolic engineering can be applied to tackle this challenge by also improving the anabolic routes for product synthesis. However, the metabolic and regulatory network for mcl-PHA production in *P. putida* KT2440 is rather complex, but several approaches resulted in engineered strains showing increased PHA production (Cai et al., 2009; Salvachúa et al., 2020; Zhang et al., 2021). Moreover, the heterologous production of scl-*co*-mcl-PHA copolymers or the incorporation of specific monomers, such as unsaturated or nitrogen-containing monomers, can be envisioned to increase the physiochemical properties and thus the value of the final product (Mezzina et al., 2021). Thereby, PHA have the great potential to substitute fossil-based thermoplastics such as PE, PP or PVC, while being biodegradable. The production of biodegradable alternatives from renewable resources or waste streams facilitates the shift towards a circular plastics economy. Overall, metabolic funneling of non-related PHA substrates must be aligned with subsequent upcycling pathways to ensure an efficient carbon flux from the substrate to the product instead of being utilized for the formation of biomass or CO_2 *via* respiration.

Depending on the PHA biosynthesis efficiency from mixed plastic hydrolysates, the production of other value-added compounds might be of interest. Due to its versatile metabolism, *P. putida* KT2440 can also be used for the production of rhamnolipids (Tiso et

al., 2020; Tiso et al., 2017) or platform chemicals such as β-ketoadipate (Sullivan et al., 2022; Werner et al., 2021). Of course, production of such value-added compounds must be improved, and cost-effective large-scale industrial applications must be developed to ensure the economic viability of microbial upcycling. A key challenge for this will be to overcome the lack of fitting scales between substrate and product. Considering the million tons of plastic waste produced annually, only a small fraction could be upcycled to niche chemicals such as vanillic acid, for which the global demand is in the tens of thousands tons (Xu et al., 2024). In contrast, the microbial production of PHA has the potential to more closely match the scale of plastic waste as a potential substrate. Therefore, it could facilitate the transition to a more circular plastics economy, provided that the process can be made efficient enough to unlock low-cost bulk applications. Moreover, future regulations, shortages, or other external factors may create a demand for other value-added products with matching scales to plastic waste. These could include the production of biofuels for which *P. putida* KT2440 could be engineered in the future.

Obviously, establishing sustainable end-of-life solutions for plastics requires the combination of suitable processes for depolymerization, biological funneling, and microbial upcycling. Current methods for chemical depolymerization operate outside of biological boundary conditions and thus depolymerization and microbial upcycling are performed separately, today (Sullivan et al., 2022; Werner et al., 2021). The future development of one-pot processes with simultaneous deconstruction and microbial upcycling would have several advantages as product inhibition or toxicity can be avoided as well as the costly addition of acid and base (Ellis et al., 2021). Breakthroughs in chemical depolymerization and strain engineering could lead to a harmonization of both disciplines. On the other hand, future enzyme engineering could yield suitable biocatalysts for the deconstruction of even C–C-bonded polymers. Such enzymes could be heterologously expressed and secreted by engineered strains of *P. putida* KT2440 combining enzymatic depolymerization with biological funneling and upcycling in a single cell consolidated bioprocess.

Lastly, the successful implementation of microbial upcycling is a multifaceted endeavor, requiring interdisciplinary collaborations but also regulatory support and public engagement. As advancements continue, microbial upcycling has great potential to revolutionize the

plastic industry, paving the way for a circular and sustainable plastic economy. Nevertheless, overcoming the key limitations including low yields and the lack of fitting scales between substrates and products remains crucial for its widespread success. This thesis has contributed to the future success of microbial upcycling by extending the substrate range of the biotechnological workhorse *P. putida* KT2440 with prevalent plastic hydrolysates and enabling the production of PHA from them. With future optimization of the processes and the range of applications, a more sustainable and efficient approach to manage the global plastic crisis can become a reality.

4 References

Achilias, D. S., Roupakias, C., Megalokonomos, P., Lappas, A. A., Antonakou, E. V., 2007. Chemical recycling of plastic wastes made from polyethylene (LDPE and HDPE) and polypropylene (PP). *J. Hazard. Mater*. 149**,** 536-542. 10.1016/j.jhazmat.2007.06.076.

Ackermann, Y. S., Li, W. J., Op de Hipt, L., Niehoff, P. J., Casey, W., Polen, T., Köbbing, S., Ballerstedt, H., Wynands, B., O'Connor, K., Blank, L. M., Wierckx, N., 2021. Engineering adipic acid metabolism in *Pseudomonas putida*. *Metab. Eng.* 67**,** 29-40. 10.1016/j.ymben.2021.05.001.

Akiba, M., Hashim, A. S., 1997. Vulcanization and crosslinking in elastomers. *Prog. Polym. Sci*. 22**,** 475-521. 10.1016/S0079-6700(96)00015-9.

Akutsu-Shigeno, Y., Adachi, Y., Yamada, C., Toyoshima, K., Nomura, N., Uchiyama, H., Nakajima-Kambe, T., 2006. Isolation of a bacterium that degrades urethane compounds and characterization of its urethane hydrolase. *Appl. Microbiol. Biotechnol*. 70**,** 422-429. 10.1007/s00253-005-0071-1.

Alauddin, M., Choudhury, I. A., El Baradie, M. A., Hashmi, M. S. J., 1995. Plastics and their machining: A review. *J. Mater. Process. Technol*. 54**,** 40-46. 10.1016/0924-0136(95)01917-0.

Alberti, C., Figueira, R., Hofmann, M., Koschke, S., Enthaler, S., 2019. Chemical Recycling of End-of-Life Polyamide 6 via Ring Closing Depolymerization. *ChemistrySelect*. 4**,** 12638-12642. 10.1002/slct.201903970.

Allen, L., O'Connell, A., Kiermer, V., 2019. How can we ensure visibility and diversity in research contributions? How the Contributor Role Taxonomy (CRediT) is helping the shift from authorship to contributorship. *Learn. Publ*. 32**,** 71-74. https://doi.org/10.1002/leap.1210.

Allen, S., Allen, D., Baladima, F., Phoenix, V. R., Thomas, J. L., Le Roux, G., Sonke, J. E., 2021. Evidence of free tropospheric and long-range transport of microplastic at Pic du Midi Observatory. *Nat. Commu*. 12**,** 7242. 10.1038/s41467-021-27454-7.

Álvarez-Barragán, J., Domínguez-Malfavón, L., Vargas-Suárez, M., González-Hernández, R., Aguilar-Osorio, G., Loza-Tavera, H., 2016. Biodegradative Activities of Selected Environmental Fungi on a Polyester Polyurethane Varnish and Polyether Polyurethane Foams. *AEM*. 82**,** 5225-5235. doi:10.1128/AEM.01344-16.

Alvarez-Gonzalez, G., Chacón, M., Berepiki, A., Fisher, K., Dixon, N., 2023. Degradation and bioconversion of complex municipal solid waste streams into human biotherapeutics and biopolymers. *bioRxiv*. 2023.02.13.528311. 10.1101/2023.02.13.528311

Amador, C. I., Canosa, I., Govantes, F., Santero, E., 2010. Lack of CbrB in *Pseudomonas putida* affects not only amino acids metabolism but also different stress responses and biofilm development. *Environ. Microbiol.* 12**,** 1748-1761. 10.1111/j.1462-2920.2010.02254.x.

American Chemical Society National Historic Chemical Landmarks. Bakelite: The World's First Synthetic Plastic. http://www.acs.org/content/acs/en/education/whatischemistry/landmarks/bakelite.ht ml (accessed 31.01.2024).

Andersen, K. R., Leksa, N. C., Schwartz, T. U., 2013. Optimized *E. coli* expression strain LOBSTR eliminates common contaminants from His-tag purification. *Proteins*. 81**,** 1857-61. 10.1002/prot.24364.

Angiolillo, M., Fortibuoni, T., 2020. Impacts of Marine Litter on Mediterranean Reef Systems: From Shallow to Deep Waters. *Front. Mar. Sci.* 7. 10.3389/fmars.2020.581966.

Austin, H. P., Allen, M. D., Donohoe, B. S., Rorrer, N. A., Kearns, F. L., Silveira, R. L., Pollard, B. C., Dominick, G., Duman, R., El Omari, K., Mykhaylyk, V., Wagner, A., Michener, W. E., Amore, A., Skaf, M. S., Crowley, M. F., Thorne, A. W., Johnson, C. W., Woodcock, H. L., McGeehan, J. E., Beckham, G. T., 2018. Characterization and engineering of a plastic-degrading aromatic polyesterase. *Proc Natl Acad Sci U S A*. 115**,** E4350-e4357. 10.1073/pnas.1718804115.

Avilan, L., Lichtenstein, B. R., König, G., Zahn, M., Allen, M. D., Oliveira, L., Clark, M., Bemmer, V., Graham, R., Austin, H. P., Dominick, G., Johnson, C. W., Beckham, G. T., McGeehan, J. E., Pickford, A. R., 2023. Concentration-Dependent Inhibition of Mesophilic PETases on Poly(ethylene terephthalate) Can Be Eliminated by Enzyme Engineering. *ChemSusChem*. 16**,** e202202277. 10.1002/cssc.202202277.

Bäckström, E., Odelius, K., Hakkarainen, M., 2017. Trash to Treasure: Microwave-Assisted Conversion of Polyethylene to Functional Chemicals. *Ind. Eng. Chem. Res*. 56**,** 14814-14821. 10.1021/acs.iecr.7b04091.

Bagdasarian, M., Lurz, R., Rückert, B., Franklin, F. C. H., Bagdasarian, M. M., Frey, J., Timmis, K. N., 1981. Specific-purpose plasmid cloning vectors II. Broad host range, high copy number, RSF 1010-derived vectors, and a host-vector system for gene cloning in *Pseudomonas*. *Gene*. 16**,** 237-247. 10.1016/0378-1119(81)90080-9.

Ballerstedt, H., Tiso, T., Wierckx, N., Wei, R., Averous, L., Bornscheuer, U., O'Connor, K., Floehr, T., Jupke, A., Klankermayer, J., Liu, L., de Lorenzo, V., Narancic, T., Nogales, J., Perrin, R., Pollet, E., Prieto, A., Casey, W., Haarmann, T., Sarbu, A., Schwaneberg, U., Xin, F., Dong, W., Xing, J., Chen, G.-Q., Tan, T., Jiang, M., Blank, L. M., 2021. MIXed plastics biodegradation and UPcycling using microbial communities: EU Horizon 2020 project MIX-UP started January 2020. *Environ. Sci. Eur*. 33**,** 99. 10.1186/s12302-021-00536-5.

Bao, T., Qian, Y., Xin, Y., Collins, J. J., Lu, T., 2023. Engineering microbial division of labor for plastic upcycling. *Nat. Commun.* 14**,** 5712. 10.1038/s41467-023-40777-x.

Barnes, D. K. A., 2002. Invasions by marine life on plastic debris. *Nature*. 416**,** 808-809. 10.1038/416808a.

Barnes, S. J., 2019. Out of sight, out of mind: Plastic waste exports, psychological distance and consumer plastic purchasing. *Glob. Environ. Change*. 58**,** 101943. 10.1016/j.gloenvcha.2019.101943.

Battaile, K. P., McBurney, M., Van Veldhoven, P. P., Vockley, J., 1998. Human long chain, very long chain and medium chain acyl-CoA dehydrogenases are specific for the *S*-enantiomer of 2- methylpentadecanoyl-CoA. *Biochim. Biophys. Acta. Mol. Cell. Biol. Lipids.* 1390**,** 333-338. 10.1016/S0005-2760(97)00185-9.

Becker, J., Hosseinpour Tehrani, H., Ernst, P., Blank, L. M., Wierckx, N., 2021. An Optimized *Ustilago maydis* for Itaconic Acid Production at Maximal Theoretical Yield. *J. Fungi.* 7**,** 20.

Beghetto, V., Sole, R., Buranello, C., Al-Abkal, M., Facchin, M., 2021. Recent Advancements in Plastic Packaging Recycling: A Mini-Review. *Materials*. 14**,** 4782.

Belda, E., van Heck, R. G., José Lopez-Sanchez, M., Cruveiller, S., Barbe, V., Fraser, C., Klenk, H. P., Petersen, J., Morgat, A., Nikel, P. I., Vallenet, D., Rouy, Z., Sekowska, A., Martins Dos Santos, V. A., de Lorenzo, V., Danchin, A., Médigue, C., 2016. The revisited genome of *Pseudomonas putida* KT2440 enlightens its value as a robust metabolic chassis. *Environ. Microbiol*. 18**,** 3403-3424. 10.1111/1462-2920.13230.

Bell, E. L., Smithson, R., Kilbride, S., Foster, J., Hardy, F. J., Ramachandran, S., Tedstone, A. A., Haigh, S. J., Garforth, A. A., Day, P. J. R., Levy, C., Shaver, M. P., Green, A. P., 2022. Directed evolution of an efficient and thermostable PET depolymerase. *Nat. Catal*. 5**,** 673-681. 10.1038/s41929-022-00821-3.

Benedetti, I., de Lorenzo, V., Nikel, P. I., 2016. Genetic programming of catalytic *Pseudomonas putida* biofilms for boosting biodegradation of haloalkanes. *Metab. Eng*. 33**,** 109-118. 10.1016/j.ymben.2015.11.004.

Benyathiar, P., Kumar, P., Carpenter, G., Brace, J., Mishra, D. K., 2022. Polyethylene Terephthalate (PET) Bottle-to-Bottle Recycling for the Beverage Industry: A Review. *Polymers*. 14**,** 2366.

Bergmann, M., Collard, F., Fabres, J., Gabrielsen, G. W., Provencher, J. F., Rochman, C. M., van Sebille, E., Tekman, M. B., 2022. Plastic pollution in the Arctic. *Nat. Rev. Earth Environ*. 3**,** 323-337. 10.1038/s43017-022-00279-8.

Bernard, N. J., 2022. Itaconate isomers add complexity. *Nat. Immunol.* 10.1038/s41590-022-01258-3.

Besseling, E., Redondo-Hasselerharm, P., Foekema, E. M., Koelmans, A. A., 2019. Quantifying ecological risks of aquatic micro- and nanoplastic. *Crit. Rev. Environ. Sci. Technol*. 49**,** 32-80. 10.1080/10643389.2018.1531688.

Beuker, J., Barth, T., Steier, A., Wittgens, A., Rosenau, F., Henkel, M., Hausmann, R., 2016. High titer heterologous rhamnolipid production. *AMB Express*. 6**,** 124. 10.1186/s13568-016-0298-5.

Biffinger, J. C., Barlow, D. E., Cockrell, A. L., Cusick, K. D., Hervey, W. J., Fitzgerald, L. A., Nadeau, L. J., Hung, C. S., Crookes-Goodson, W. J., Russell, J. N., 2015. The applicability of Impranil®DLN for gauging the biodegradation of polyurethanes. *Polym. Degrad. Stab*. 120**,** 178-185. 10.1016/j.polymdegradstab.2015.06.020.

Bitzenhofer, Nora L., Kruse, L., Thies, S., Wynands, B., Lechtenberg, T., Rönitz, J., Kozaeva, E., Wirth, Nicolas T., Eberlein, C., Jaeger, K.-E., Nikel, Pablo I., Heipieper, Hermann J., Wierckx, N., Loeschcke, A., 2021. Towards robust *Pseudomonas* cell factories to harbour novel biosynthetic pathways. *Essays Biochem.* 65, 319-336. 10.1042/ebc20200173.

Blanco, F. G., Hernández, N., Rivero-Buceta, V., Maestro, B., Sanz, J. M., Mato, A., Hernández-Arriaga, A. M., Prieto, M. A., 2021. From Residues to Added-Value Bacterial Biopolymers as Nanomaterials for Biomedical Applications. *Nanomaterials (Basel).* 11. 10.3390/nano11061492.

Blank, L. M., Narancic, T., Mampel, J., Tiso, T., O'Connor, K., 2020. Biotechnological upcycling of plastic waste and other non-conventional feedstocks in a circular economy. *Curr. Opin. Biotechnol.* 62, 212-219. 10.1016/j.copbio.2019.11.011.

Bollinger, A., Thies, S., Katzke, N., Jaeger, K.-E., 2020a. The biotechnological potential of marine bacteria in the novel lineage of *Pseudomonas pertucinogena. Microb. Biotechnol.* 13, 19-31. 10.1111/1751-7915.13288.

Bollinger, A., Thies, S., Knieps-Grünhagen, E., Gertzen, C., Kobus, S., Höppner, A., Ferrer, M., Gohlke, H., Smits, S. H. J., Jaeger, K.-E., 2020b. A Novel Polyester Hydrolase From the Marine Bacterium *Pseudomonas aestusnigri* – Structural and Functional Insights. *Front. Microbiol.* 11. 10.3389/fmicb.2020.00114.

Borrelle, S. B., Ringma, J., Law Kara, L., Monnahan Cole, C., Lebreton, L., McGivern, A., Murphy, E., Jambeck, J., Leonard George, H., Hilleary Michelle, A., Eriksen, M., Possingham Hugh, P., De Frond, H., Gerber Leah, R., Polidoro, B., Tahir, A., Bernard, M., Mallos, N., Barnes, M., Rochman Chelsea, M., 2020. Predicted growth in plastic waste exceeds efforts to mitigate plastic pollution. *Science.* 369, 1515-1518. 10.1126/science.aba3656.

Bouatra, S., Aziat, F., Mandal, R., Guo, A. C., Wilson, M. R., Knox, C., Bjorndahl, T. C., Krishnamurthy, R., Saleem, F., Liu, P., Dame, Z. T., Poelzer, J., Huynh, J., Yallou, F. S., Psychogios, N., Dong, E., Bogumil, R., Roehring, C., Wishart, D. S., 2013. The human urine metabolome. *PLoS One.* 8, e73076. 10.1371/journal.pone.0073076.

Boyer, H. W., Roulland-Dussoix, D., 1969. A complementation analysis of the restriction and modification of DNA in *Escherichia coli. J. Mol. Biol.* 41, 459-72. 10.1016/0022-2836(69)90288-5.

Brahney, J., Hallerud, M., Heim, E., Hahnenberger, M., Sukumaran, S., 2020. Plastic rain in protected areas of the United States. *Science.* 368, 1257-1260. 10.1126/science.aaz5819.

Branson, Y., Söltl, S., Buchmann, C., Wei, R., Schaffert, L., Badenhorst, C. P. S., Reisky, L., Jäger, G., Bornscheuer, U. T., 2023. Urethanases for the Enzymatic Hydrolysis of Low Molecular Weight Carbamates and the Recycling of Polyurethanes. *Angew. Chem., Int. Ed.* 62, e202216220. https://doi.org/10.1002/anie.202216220.

British Plastics Federation, 2014. A History of Plastics. https://www.bpf.co.uk/plastipedia/plastics_history/Default.aspx (accessed 31.01.2024).

Buchholz, P. C. F., Feuerriegel, G., Zhang, H., Perez-Garcia, P., Nover, L.-L., Chow, J., Streit, W. R., Pleiss, J., 2022. Plastics degradation by hydrolytic enzymes: The plastics-active enzymes database—PAZy. *Proteins*. 90**,** 1443-1456. 10.1002/prot.26325.

Bucknall, D. G., 2020. Plastics as a materials system in a circular economy. *Philos. Trans. Royal Soc. A* 378**,** 20190268. doi:10.1098/rsta.2019.0268.

Buller, R., Lutz, S., Kazlauskas, R. J., Snajdrova, R., Moore, J. C., Bornscheuer, U. T., 2023. From nature to industry: Harnessing enzymes for biocatalysis. *Science*. 382**,** eadh8615. doi:10.1126/science.adh8615.

Cai, L., Yuan, M. Q., Liu, F., Jian, J., Chen, G. Q., 2009. Enhanced production of medium-chain-length polyhydroxyalkanoates (PHA) by PHA depolymerase knockout mutant of *Pseudomonas putida* KT2442. *Bioresour. Technol*. 100**,** 2265-70. 10.1016/j.biortech.2008.11.020.

Cantor, K. M., Watts, P., 2011. 1 - Plastics Materials. In: Kutz, M., (Ed.), Applied Plastics Engineering Handbook. William Andrew Publishing, Oxford, pp. 3-5.

Carbios, 2023. Carbios obtains building and operating permits, in line with announced schedule, for world's first PET biorecycling plant in Longlaville. https://www.carbios.com/en/carbios-obtains-building-and-operating-permits/ (accessed 31.01.2024).

Cavaleiro, A. M., Kim, S. H., Seppälä, S., Nielsen, M. T., Nørholm, M. H. H., 2015. Accurate DNA Assembly and Genome Engineering with Optimized Uracil Excision Cloning. *ACS Synt. Biol*. 4**,** 1042-1046. 10.1021/acssynbio.5b00113.

Chen, F., Elgaher, W. A. M., Winterhoff, M., Büssow, K., Waqas, F. H., Graner, E., Pires-Afonso, Y., Casares Perez, L., de la Vega, L., Sahini, N., Czichon, L., Zobl, W., Zillinger, T., Shehata, M., Pleschka, S., Bähre, H., Falk, C., Michelucci, A., Schuchardt, S., Blankenfeldt, W., Hirsch, A. K. H., Pessler, F., 2022. Citraconate inhibits ACOD1 (IRG1) catalysis, reduces interferon responses and oxidative stress, and modulates inflammation and cell metabolism. *Nat. Metab.* 4**,** 534-546. 10.1038/s42255-022-00577-x.

Chen, F., Lukat, P., Iqbal, A. A., Saile, K., Kaever, V., Heuvel, J. v. d., Blankenfeldt, W., Büssow, K., Pessler, F., 2019. Crystal structure of *cis*-aconitate decarboxylase reveals the impact of naturally occurring human mutations on itaconate synthesis. *Proc. Natl. Acad. Sci.* 116**,** 20644-20654. doi:10.1073/pnas.1908770116.

Chen, G., Feng, Q., Wang, J., 2020. Mini-review of microplastics in the atmosphere and their risks to humans. *Sci Total Environ*. 703**,** 135504. 10.1016/j.scitotenv.2019.135504.

Choi, K.-H., Kumar, A., Schweizer, H. P., 2006. A 10-min method for preparation of highly electrocompetent *Pseudomonas aeruginosa* cells: Application for DNA fragment transfer between chromosomes and plasmid transformation. *J. Microbiol. Methods*. 64**,** 391-397. 10.1016/j.mimet.2005.06.001.

Chomczynski, P., Rymaszewski, M., 2006. Alkaline polyethylene glycol-based method for direct PCR from bacteria, eukaryotic tissue samples, and whole blood. *Biotechniques*. 40**,** 454, 456, 458. 10.2144/000112149.

Chou, H. T., Li, J.-Y., Lu, C.-D., 2014. Functional Characterization of the *agtABCD* and *agtSR* Operons for 4-Aminobutyrate and 5-Aminovalerate Uptake and Regulation in *Pseudomonas aeruginosa* PAO1. *Curr. Microbiol*. 68**,** 59-63. 10.1007/s00284-013-0446-y.

Chow, J., Perez-Garcia, P., Dierkes, R., Streit, W. R., 2023. Microbial enzymes will offer limited solutions to the global plastic pollution crisis. *Microbl Biotechnol*. 16**,** 195-217. 10.1111/1751-7915.14135.

Chun, H. L., Lee, S. Y., Kim, K.-H., Lee, C. S., Oh, T.-J., Park, H. H., 2020a. The crystal structure of mouse IRG1 suggests that *cis*-aconitate decarboxylase has an open and closed conformation. *PLoS One*. 15**,** e0242383. 10.1371/journal.pone.0242383.

Chun, H. L., Lee, S. Y., Lee, S. H., Lee, C. S., Park, H. H., 2020b. Enzymatic reaction mechanism of cis-aconitate decarboxylase based on the crystal structure of IRG1 from *Bacillus subtilis*. *Sci Rep*. 10**,** 11305. 10.1038/s41598-020-68419-y.

Cobb, R. E., Chao, R., Zhao, H., 2013. Directed Evolution: Past, Present and Future. *AIChE J*. 59**,** 1432-1440. 10.1002/aic.13995.

Cold Spring Harbor Laboratories, 2010. Terric broth (TB) medium. *Cold Spring Harbor Protoc*. 10.1101/pdb.rec085894.

Coppens, L., Lavigne, R., 2020. SAPPHIRE: a neural network based classifier for σ70 promoter prediction in *Pseudomonas*. *BMC Bioinformatics*. 21**,** 415. 10.1186/s12859-020-03730-z.

Cordes, T., Metallo, C. M., 2021. Exploring the evolutionary roots and physiological function of itaconate. *Curr. Opin. Biotechnol*. 68**,** 144-150. 10.1016/j.copbio.2020.11.005.

Crane, J. M., Randall, L. L., 2017. The Sec System: Protein Export in *Escherichia coli*. *EcoSal Plus*. 7. doi:10.1128/ecosalplus.ESP-0002-2017.

Cui, Y., Chen, Y., Liu, X., Dong, S., Tian, Y. e., Qiao, Y., Mitra, R., Han, J., Li, C., Han, X., Liu, W., Chen, Q., Wei, W., Wang, X., Du, W., Tang, S., Xiang, H., Liu, H., Liang, Y., Houk, K. N., Wu, B., 2021. Computational Redesign of a PETase for Plastic Biodegradation under Ambient Condition by the GRAPE Strategy. *ACS Catal*. 11**,** 1340-1350. 10.1021/acscatal.0c05126.

Dalton, B., Bhagabati, P., De Micco, J., Padamati, R. B., O'Connor, K., 2022. A Review on Biological Synthesis of the Biodegradable Polymers Polyhydroxyalkanoates and the Development of Multiple Applications. *Catalysts*. 12**,** 319.

Damer, B., Deamer, D., 2020. The Hot Spring Hypothesis for an Origin of Life. *Astrobiology*. 20**,** 429-452. 10.1089/ast.2019.2045.

Danso, D., Chow, J., Streit, W. R., 2019. Plastics: Environmental and Biotechnological Perspectives on Microbial Degradation. *AEM*. 85**,** e01095-19. 10.1128/aem.01095-19.

Danso, D., Schmeisser, C., Chow, J., Zimmermann, W., Wei, R., Leggewie, C., Li, X., Hazen, T., Streit, W. R., 2018. New Insights into the Function and Global Distribution of Polyethylene Terephthalate (PET)-Degrading Bacteria and Enzymes in Marine and Terrestrial Metagenomes. *AEM*. 84, e02773-17. doi:10.1128/AEM.02773-17.

de Witt, J., Ernst, P., Gätgens, J., Noack, S., Hiller, D., Wynands, B., Wierckx, N., 2023. Characterization and engineering of branched short-chain dicarboxylate metabolism in *Pseudomonas* reveals resistance to fungal 2-hydroxyparaconate. *Metab. Eng.* 75, 205-216. 10.1016/j.ymben.2022.12.008.

de Witt, J., Molitor, R., Gätgens, J., Ortmann de Percin Northumberland, C., Kruse, L., Polen, T., Wynands, B., van Goethem, K., Thies, S., Jaeger, K.-E., Wierckx, N., 2023. Biodegradation of poly(ester-urethane) coatings by *Halopseudomonas formosensis*. *Microb Biotechnol*. 17, e14362. 10.1111/1751-7915.14362.

Deguchi, T., Kitaoka, Y., Kakezawa, M., Nishida, T., 1998. Purification and Characterization of a Nylon-Degrading Enzyme. *AEM*. 64, 1366-1371. 10.1128/aem.64.4.1366-1371.1998.

Dos Santos, V. A., Heim, S., Moore, E. R., Strätz, M., Timmis, K. N., 2004. Insights into the genomic basis of niche specificity of *Pseudomonas putida* KT2440. *Environ Microbiol*. 6, 1264-86. 10.1111/j.1462-2920.2004.00734.x.

Dragosits, M., Mattanovich, D., 2013. Adaptive laboratory evolution – principles and applications for biotechnology. *Microb. Cell Factories*. 12, 64. 10.1186/1475-2859-12-64.

Durante-Rodríguez, G., de Lorenzo, V., Nikel, P. I., 2018. A Post-translational Metabolic Switch Enables Complete Decoupling of Bacterial Growth from Biopolymer Production in Engineered *Escherichia coli*. *ACS Synth Biol*. 7, 2686-2697. 10.1021/acssynbio.8b00345.

Dvořák, P., de Lorenzo, V., 2018. Refactoring the upper sugar metabolism of *Pseudomonas putida* for co-utilization of cellobiose, xylose, and glucose. *Metab Eng*. 48, 94-108. 10.1016/j.ymben.2018.05.019.

Eberz, J., Doeker, M., Ackermann, Y. S., Schaffeld, D., Wierckx, N., Jupke, A., 2023. Selective Separation of 4,4'-Methylenedianiline, Isophoronediamine and 2,4-Toluenediamine from Enzymatic Hydrolysis Solutions of Polyurethane. *Solvent Extr. Ion Exch*. 41, 358-373. 10.1080/07366299.2023.2193229.

Ellis, L. D., Rorrer, N. A., Sullivan, K. P., Otto, M., McGeehan, J. E., Román-Leshkov, Y., Wierckx, N., Beckham, G. T., 2021. Chemical and biological catalysis for plastics recycling and upcycling. *Nat. Catal.* 4, 539-556. 10.1038/s41929-021-00648-4.

Eriksen, M. K., Christiansen, J. D., Daugaard, A. E., Astrup, T. F., 2019. Closing the loop for PET, PE and PP waste from households: Influence of material properties and product design for plastic recycling. *Waste Manage.* 96, 75-85. 10.1016/j.wasman.2019.07.005.

Ferruz, N., Schmidt, S., Höcker, B., 2022. ProtGPT2 is a deep unsupervised language model for protein design. *Nat Commun*. 13, 4348. 10.1038/s41467-022-32007-7.

Figurski, D. H., Helinski, D. R., 1979. Replication of an origin-containing derivative of plasmid RK2 dependent on a plasmid function provided in *trans*. *Proc. Natl. Acad. Sci.* 76**,** 1648-1652. 10.1073/pnas.76.4.1648.

Fincher, E. L., Payne, W. J., 1962. Bacterial Utilization of Ether Glycols. *Appl. Microbiol.* 10**,** 542-547. doi:10.1128/am.10.6.542-547.1962.

Fonseca, A. C., Gil, M. H., Simões, P. N., 2014. Biodegradable poly(ester amide)s – A remarkable opportunity for the biomedical area: Review on the synthesis, characterization and applications. *Prog. Polym. Sci.* 39**,** 1291-1311. 10.1016/j.progpolymsci.2013.11.007.

Franden, M. A., Jayakody, L. N., Li, W. J., Wagner, N. J., Cleveland, N. S., Michener, W. E., Hauer, B., Blank, L. M., Wierckx, N., Klebensberger, J., Beckham, G. T., 2018b. Engineering *Pseudomonas putida* KT2440 for efficient ethylene glycol utilization. *Metab Eng.* 48**,** 197-207. 10.1016/j.ymben.2018.06.003.

Geiser, E., Hosseinpour Tehrani, H., Meyer, S., Blank, L. M., Wierckx, N., 2018. Evolutionary freedom in the regulation of the conserved itaconate cluster by Ria1 in related *Ustilaginaceae. Fungal Biol. Biotechnol.* 5**,** 14. 10.1186/s40694-018-0058-1.

Geiser, E., Przybilla, S. K., Engel, M., Kleineberg, W., Büttner, L., Sarikaya, E., Hartog, T. d., Klankermayer, J., Leitner, W., Bölker, M., Blank, L. M., Wierckx, N., 2016a. Genetic and biochemical insights into the itaconate pathway of *Ustilago maydis* enable enhanced production. *Metab. Eng.* 38**,** 427-435. 10.1016/j.ymben.2016.10.006.

Geiser, E., Przybilla, S. K., Friedrich, A., Buckel, W., Wierckx, N., Blank, L. M., Bölker, M., 2016b. *Ustilago maydis* produces itaconic acid *via* the unusual intermediate *trans*-aconitate. *Microb. Biotechnol.* 9**,** 116-126. 10.1111/1751-7915.12329.

Geiser, E., Wiebach, V., Wierckx, N., Blank, L. M., 2014. Prospecting the biodiversity of the fungal family *Ustilaginaceae* for the production of value-added chemicals. *Fungal Biol. Biotechnol.* 1**,** 2. 10.1186/s40694-014-0002-y.

Geyer, R., Jambeck, J. R., Law, K. L., 2017. Production, use, and fate of all plastics ever made. *Sci. Adv.* 3**,** e1700782. 10.1126/sciadv.1700782.

Gibson, D. G., Young, L., Chuang, R.-Y., Venter, J. C., Hutchison, C. A., Smith, H. O., 2009. Enzymatic assembly of DNA molecules up to several hundred kilobases. *Nat. Methods*. 6**,** 343-345. 10.1038/nmeth.1318.

Gilman, E., Musyl, M., Suuronen, P., Chaloupka, M., Gorgin, S., Wilson, J., Kuczenski, B., 2021. Highest risk abandoned, lost and discarded fishing gear. *Sci. Reports.* 11**,** 7195. 10.1038/s41598-021-86123-3.

Gregory, G. J., Wang, C., Sadula, S., Koval, S., Lobo, R. F., Vlachos, D. G., Papoutsakis, E. T., 2023. Polyethylene Valorization by Combined Chemical Catalysis with Bioconversion by Plastic-Enriched Microbial Consortia. *ACS Sustain. Chem. Eng.* 11**,** 3494-3505. 10.1021/acssuschemeng.2c07461.

Guevarra, E. D., Tabuchi, T., 1990. Accumulation of Itaconic, 2-Hydroxyparaconic, Itatartaric, and Malic Acids by Strains of the Genus *Ustilago. Agric. Biol. Chem.* 54**,** 2353-2358. 10.1271/bbb1961.54.2353.

Guzik, M. W., Nitkiewicz, T., Wojnarowska, M., Sołtysik, M., Kenny, S. T., Babu, R. P., Best, M., O'Connor, K. E., 2021. Robust process for high yield conversion of non-degradable polyethylene to a biodegradable plastic using a chemo-biotechnological approach. *Waste Manag.* 135**,** 60-69. 10.1016/j.wasman.2021.08.030.

Hackler, R. A., Lamb, J. V., Peczak, I. L., Kennedy, R. M., Kanbur, U., LaPointe, A. M., Poeppelmeier, K. R., Sadow, A. D., Delferro, M., 2022. Effect of Macro- and Microstructures on Catalytic Hydrogenolysis of Polyolefins. *Macromolecules.* 55**,** 6801-6810. 10.1021/acs.macromol.2c00805.

Hale, R. C., Seeley, M. E., La Guardia, M. J., Mai, L., Zeng, E. Y., 2020. A Global Perspective on Microplastics. *Journal Geophys. Res. Oceans.* 125**,** e2018JC014719. 10.1029/2018JC014719.

Han, X., Liu, W., Huang, J. W., Ma, J., Zheng, Y., Ko, T. P., Xu, L., Cheng, Y. S., Chen, C. C., Guo, R. T., 2017. Structural insight into catalytic mechanism of PET hydrolase. *Nat Commun.* 8**,** 2106. 10.1038/s41467-017-02255-z.

Hanahan, D., 1983. Studies on transformation of *Escherichia coli* with plasmids. *J. Mol. Biol.* 166**,** 557-580. 10.1016/S0022-2836(83)80284-8.

Harrison, F. H., Harwood, C. S., 2005. The *pimFABCDE* operon from *Rhodopseudomonas palustris* mediates dicarboxylic acid degradation and participates in anaerobic benzoate degradation. *Microbiology (Reading).* 151, 727-736. 10.1099/mic.0.27731-0.

Hartmann, N. B., Hüffer, T., Thompson, R. C., Hassellöv, M., Verschoor, A., Daugaard, A. E., Rist, S., Karlsson, T., Brennholt, N., Cole, M., Herrling, M. P., Hess, M. C., Ivleva, N. P., Lusher, A. L., Wagner, M., 2019. Are We Speaking the Same Language? Recommendations for a Definition and Categorization Framework for Plastic Debris. *Environ. Sci. Technol.* 53**,** 1039-1047. 10.1021/acs.est.8b05297.

He, W., Henne, A., Lauterbach, M., Geißmar, E., Nikolka, F., Kho, C., Heinz, A., Dostert, C., Grusdat, M., Cordes, T., Härm, J., Goldmann, O., Ewen, A., Verschueren, C., Blay-Cadanet, J., Geffers, R., Garritsen, H., Kneiling, M., Holm, C. K., Metallo, C. M., Medina, E., Abdullah, Z., Latz, E., Brenner, D., Hiller, K., 2022. Mesaconate is synthesized from itaconate and exerts immunomodulatory effects in macrophages. *Nat. Metab.* 4**,** 524-533. 10.1038/s42255-022-00565-1.

Hillier, S., Charnetzky, W. T., 1981. Glyoxylate bypass enzymes in *Yersinia* species and multiple forms of isocitrate lyase in *Yersinia pestis. J. Bacteriol.* 145**,** 452-458. 10.1128/jb.145.1.452-458.1981.

Hoffmann, G. F., Meier-Augenstein, W., Stöckler, S., Surtees, R., Rating, D., Nyhan, W. L., 1993. Physiology and pathophysiology of organic acids in cerebrospinal fluid. *J. Inherit. Metab. Dis.* 16**,** 648-69. 10.1007/bf00711898.

Hojabri, L., Jose, J., Leao, A. L., Bouzidi, L., Narine, S. S., 2012. Synthesis and physical properties of lipid-based poly(ester-urethane)s, I: Effect of varying polyester segment length. *Polymer.* 53**,** 3762-3771. 10.1016/j.polymer.2012.06.011.

Holloway, B. W., Krishnapillai, V., Morgan, A. F., 1979. Chromosomal genetics of *Pseudomonas. Microbiol. Rev.* 43**,** 73-102. 10.1128/mr.43.1.73-102.1979.

Holm, L., 2020. Using Dali for Protein Structure Comparison. In: Gáspári, Z., (Ed.), Structural Bioinformatics: Methods and Protocols. Springer US, New York, NY, pp. 29-42.

Höner Zu Bentrup, K., Miczak, A., Swenson, D. L., Russell, D. G., 1999. Characterization of activity and expression of isocitrate lyase in *Mycobacterium avium* and *Mycobacterium tuberculosis*. *J. Bacteriol.* 181**,** 7161-7167. 10.1128/JB.181.23.7161-7167.1999.

Hosseinpour Tehrani, H., Tharmasothirajan, A., Track, E., Blank, L. M., Wierckx, N., 2019. Engineering the morphology and metabolism of pH tolerant *Ustilago cynodontis* for efficient itaconic acid production. *Metab. Eng.* 54**,** 293-300. 10.1016/j.ymben.2019.05.004.

Howard, G. T., Blake, R. C., 1998. Growth of Pseudomonas fluorescens on a polyester–polyurethane and the purification and characterization of a polyurethanase–protease enzyme. *Int. Biodeterior Biodegradation.* 42**,** 213-220. 10.1016/S0964-8305(98)00051-1.

Howard, G. T., Crother, B., Vicknair, J., 2001. Cloning, nucleotide sequencing and characterization of a polyurethanase gene (*pueB*) from *Pseudomonas chlororaphis*. *Int. Biodeterior. Biodegradation.* 47**,** 141-149. 10.1016/S0964-8305(01)00042-7.

Howard, G. T., Norton, W. N., Burks, T., 2012. Growth of *Acinetobacter gerneri* P7 on polyurethane and the purification and characterization of a polyurethanase enzyme. *Biodegradation.* 23**,** 561-573. 10.1007/s10532-011-9533-6.

Hundertmark, T., Mayer, M., McNally, C., Simons, T. J., Witte, C., 2018. How plastics-waste recycling could transform the chemical industry. *McKinsey*.

Hurley, R., Horton, A., Lusher, A., Nizzetto, L., 2020. Chapter 7 - Plastic waste in the terrestrial environment. In: Letcher, T. M., (Ed.), Plastic Waste and Recycling. Academic Press, pp. 163-193.

Idumah, C. I., Nwuzor, I. C., 2019. Novel trends in plastic waste management. *SN Appl. Sci.* 1**,** 1402. 10.1007/s42452-019-1468-2.

Jehanno, C., Alty, J. W., Roosen, M., De Meester, S., Dove, A. P., Chen, E. Y. X., Leibfarth, F. A., Sardon, H., 2022. Critical advances and future opportunities in upcycling commodity polymers. *Nature.* 603**,** 803-814. 10.1038/s41586-021-04350-0.

Jensen, K., Østergaard, P. R., Wilting, R., Lassen, S. F., 2010. Identification and characterization of a bacterial glutamic peptidase. *BMC Biochemistry.* 11**,** 47. 10.1186/1471-2091-11-47.

Joo, S., Cho, I. J., Seo, H., Son, H. F., Sagong, H. Y., Shin, T. J., Choi, S. Y., Lee, S. Y., Kim, K. J., 2018. Structural insight into molecular mechanism of poly(ethylene terephthalate) degradation. *Nat Commun.* 9**,** 382. 10.1038/s41467-018-02881-1.

Jumper, J., Evans, R., Pritzel, A., Green, T., Figurnov, M., Ronneberger, O., Tunyasuvunakool, K., Bates, R., Žídek, A., Potapenko, A., Bridgland, A., Meyer, C., Kohl, S. A. A., Ballard, A. J., Cowie, A., Romera-Paredes, B., Nikolov, S., Jain, R., Adler, J., Back, T., Petersen, S., Reiman, D., Clancy, E., Zielinski, M., Steinegger, M., Pacholska, M., Berghammer, T., Bodenstein, S., Silver, D., Vinyals, O., Senior, A. W., Kavukcuoglu, K., Kohli, P., Hassabis, D., 2021. Highly accurate protein structure prediction with AlphaFold. *Nature*. 596**,** 583-589. 10.1038/s41586-021-03819-2.

Jung, H., Shin, G., Kwak, H., Hao, L. T., Jegal, J., Kim, H. J., Jeon, H., Park, J., Oh, D. X., 2023. Review of polymer technologies for improving the recycling and upcycling efficiency of plastic waste. *Chemosphere*. 320**,** 138089. 10.1016/j.chemosphere.2023.138089.

Jurado, A. R., Huang, C. S., Zhang, X., Zhou, Z. H., Tong, L., 2015. Structure and substrate selectivity of the 750-kDa α6β6 holoenzyme of geranyl-CoA carboxylase. *Nat. Commun*. 6**,** 8986. 10.1038/ncomms9986.

Kakudo, S., Negoro, S., Urabe, I., Okada, H., 1993. Nylon oligomer degradation gene, *nylC*, on plasmid pOAD2 from a *Flavobacterium* strain encodes endo-type 6-aminohexanoate oligomer hydrolase: purification and characterization of the *nylC* gene product. *Appl. Environ. Microbiol*. 59**,** 3978-80. 10.1128/aem.59.11.3978-3980.1993.

Kampers, L. F. C., Volkers, R. J. M., Martins Dos Santos, V. A. P., 2019. *Pseudomonas putida* KT2440 is HV1 certified, not GRAS. *Microb. Biotechnol*. 12**,** 845-848. 10.1111/1751-7915.13443.

Kenny, S. T., Runic, J. N., Kaminsky, W., Woods, T., Babu, R. P., O'Connor, K. E., 2012. Development of a bioprocess to convert PET derived terephthalic acid and biodiesel derived glycerol to medium chain length polyhydroxyalkanoate. *Appl. Microbiol. Biotechnol.* 95**,** 623-633. 10.1007/s00253-012-4058-4.

Kim, H. T., Kim, J. K., Cha, H. G., Kang, M. J., Lee, H. S., Khang, T. U., Yun, E. J., Lee, D.-H., Song, B. K., Park, S. J., Joo, J. C., Kim, K. H., 2019. Biological Valorization of Poly(ethylene terephthalate) Monomers for Upcycling Waste PET. *ACS Sus. Chem Eng.*. 7**,** 19396-19406. 10.1021/acssuschemeng.9b03908.

Kim, M. S., Chang, H., Zheng, L., Yan, Q., Pfleger, B. F., Klier, J., Nelson, K., Majumder, E. L. W., Huber, G. W., 2023. A Review of Biodegradable Plastics: Chemistry, Applications, Properties, and Future Research Needs. *Chemical Reviews*. 123**,** 9915-9939. 10.1021/acs.chemrev.2c00876.

Kinoshita, S., Kageyama, S., Iba, K., Yamada, Y., Okada, H., 1975. Utilization of a Cyclic Dimer and Linear Oligomers of ε-Aminocaproic Acid by *Achromobacter guttatus* KI 72. *Agri. Biol. Chem.*. 39**,** 1219-1223. 10.1271/bbb1961.39.1219.

Kinoshita, S., Negoro, S., Muramatsu, M., Bisaria, V. S., Sawada, S., Okada, H., 1977. 6-Aminohexanoic acid cyclic dimer hydrolase. A new cyclic amide hydrolase produced by *Achromobacter guttatus* KI74. *Eur J Biochem*. 80**,** 489-95. 10.1111/j.1432-1033.1977.tb11904.x.

Kinoshita, S., Terada, T., Taniguchi, T., Takene, Y., Masuda, S., Matsunaga, N., Okada, H., 1981. Purification and characterization of 6-aminohexanoic-acid-oligomer hydrolase of *Flavobacterium* sp. Ki72. *Eur J Biochem*. 116, 547-51. 10.1111/j.1432-1033.1981.tb05371.x.

Klement, T., Büchs, J., 2013. Itaconic acid – A biotechnological process in change. *Bioresour. Technol.* 135, 422-431. 10.1016/j.biortech.2012.11.141.

Kolganov, A. A., Sreenithya, A., Pidko, E. A., 2023. Homogeneous Catalysis in Plastic Waste Upcycling: A DFT Study on the Role of Imperfections in Polymer Chains. *ACS Catalysis*. 13310-13318. 10.1021/acscatal.3c03269.

Korman, S. H., Andresen, B. S., Zeharia, A., Gutman, A., Boneh, A., Pitt, J. J., 2005. 2-Ethylhydracrylic Aciduria in Short/Branched-Chain Acyl-CoA Dehydrogenase Deficiency: Application to Diagnosis and Implications for the R-Pathway of Isoleucine Oxidation. *Clin. Chem.* 51, 610-617. 10.1373/clinchem.2004.043265.

Kosior, E., Mitchell, J., 2020. Chapter 6 - Current industry position on plastic production and recycling. In: Letcher, T. M., (Ed.), Plastic Waste and Recycling. Academic Press, pp. 133-162.

Krieger, E., Vriend, G., 2014. YASARA View - molecular graphics for all devices - from smartphones to workstations. *Bioinformatics*. 30, 2981-2. 10.1093/bioinformatics/btu426.

Kronen, M., Sasikaran, J., Berg, I. A., 2015. Mesaconase Activity of Class I Fumarase Contributes to Mesaconate Utilization by *Burkholderia xenovorans*. *Appl. Environ. Microbiol.* 81, 5632-8. 10.1128/aem.00822-15.

Kurihara, S., Oda, S., Kato, K., Kim, H. G., Koyanagi, T., Kumagai, H., Suzuki, H., 2005. A novel putrescine utilization pathway involves gamma-glutamylated intermediates of *Escherichia coli* K-12. *J Biol Chem*. 280, 4602-8. 10.1074/jbc.M411114200.

Lambert, S., Wagner, M., 2016. Characterisation of nanoplastics during the degradation of polystyrene. *Chemosphere*. 145, 265-8. 10.1016/j.chemosphere.2015.11.078.

Larkin, M. A., Blackshields, G., Brown, N. P., Chenna, R., McGettigan, P. A., McWilliam, H., Valentin, F., Wallace, I. M., Wilm, A., Lopez, R., Thompson, J. D., Gibson, T. J., Higgins, D. G., 2007. Clustal W and Clustal X version 2.0. *Bioinformatics*. 23, 2947-2948. 10.1093/bioinformatics/btm404.

Lebreton, L., Slat, B., Ferrari, F., Sainte-Rose, B., Aitken, J., Marthouse, R., Hajbane, S., Cunsolo, S., Schwarz, A., Levivier, A., Noble, K., Debeljak, P., Maral, H., Schoeneich-Argent, R., Brambini, R., Reisser, J., 2018. Evidence that the Great Pacific Garbage Patch is rapidly accumulating plastic. *Sci. Reports*. 8, 4666. 10.1038/s41598-018-22939-w.

Lee, R. P., Keller, F., Meyer, B., 2017. A concept to support the transformation from a linear to circular carbon economy: net zero emissions, resource efficiency and conservation through a coupling of the energy, chemical and waste management sectors. *Clean Energy*. 1, 102-113. 10.1093/ce/zkx004.

Lee, S., Lee, Y. R., Kim, S. J., Lee, J.-S., Min, K., 2023. Recent advances and challenges in the biotechnological upcycling of plastic wastes for constructing a circular bioeconomy. *Chem. Eng. J.*. 454, 140470. 10.1016/j.cej.2022.140470.

Li, H., Aguirre-Villegas, H. A., Allen, R. D., Bai, X., Benson, C. H., Beckham, G. T., Bradshaw, S. L., Brown, J. L., Brown, R. C., Cecon, V. S., Curley, J. B., Curtzwiler, G. W., Dong, S., Gaddameedi, S., García, J. E., Hermans, I., Kim, M. S., Ma, J., Mark, L. O., Mavrikakis, M., Olafasakin, O. O., Osswald, T. A., Papanikolaou, K. G., Radhakrishnan, H., Sanchez Castillo, M. A., Sánchez-Rivera, K. L., Tumu, K. N., Van Lehn, R. C., Vorst, K. L., Wright, M. M., Wu, J., Zavala, V. M., Zhou, P., Huber, G. W., 2022. Expanding plastics recycling technologies: chemical aspects, technology status and challenges. *Green Chem*. 24, 8899-9002. 10.1039/D2GC02588D.

Li, W.-J., Narancic, T., Kenny, S. T., Niehoff, P.-J., O'Connor, K., Blank, L. M., Wierckx, N., 2020. Unraveling 1,4-Butanediol Metabolism in *Pseudomonas putida* KT2440. *Front. Microbiol.* 11. 10.3389/fmicb.2020.00382.

Li, W. J., Jayakody, L. N., Franden, M. A., Wehrmann, M., Daun, T., Hauer, B., Blank, L. M., Beckham, G. T., Klebensberger, J., Wierckx, N., 2019. Laboratory evolution reveals the metabolic and regulatory basis of ethylene glycol metabolism by *Pseudomonas putida* KT2440. *Environ. Microbiol.* 21, 3669-3682. 10.1111/1462-2920.14703.

Li, Z., Yang, J., Loh, X. J., 2016. Polyhydroxyalkanoates: opening doors for a sustainable future. *NPG Asia Materials*. 8, e265-e265. 10.1038/am.2016.48.

Lin, S.-Y., Hameed, A., Liu, Y.-C., Hsu, Y.-H., Lai, W.-A., Young, C.-C., 2013. *Pseudomonas formosensis* sp. nov., a gamma-proteobacteria isolated from food-waste compost in Taiwan. *IJSEM*. 63, 3168-3174. 10.1099/ijs.0.049452-0.

Little, A., Pellis, A., Comerford, J. W., Naranjo-Valles, E., Hafezi, N., Mascal, M., Farmer, T. J., 2020. Effects of Methyl Branching on the Properties and Performance of Furandioate-Adipate Copolyesters of Bio-Based Secondary Diols. *ACS Sus. Chem. Eng*. 8, 14471-14483. 10.1021/acssuschemeng.0c04513.

Liu, J., He, J., Xue, R., Xu, B., Qian, X., Xin, F., Blank, L. M., Zhou, J., Wei, R., Dong, W., Jiang, M., 2021a. Biodegradation and up-cycling of polyurethanes: Progress, challenges, and prospects. *Biotechnol. Adv*. 48, 107730. 10.1016/j.biotechadv.2021.107730.

Liu, P., Zhang, T., Zheng, Y., Li, Q., Su, T., Qi, Q., 2021b. Potential one-step strategy for PET degradation and PHB biosynthesis through co-cultivation of two engineered microorganisms. *Eng. Microbiol*. 1, 100003. 10.1016/j.engmic.2021.100003.

Liu, S., Narancic, T., Tham, J. L., O'Connor, K. E., 2023. β-oxidation-polyhydroxyalkanoates synthesis relationship in *Pseudomonas putida* KT2440 revisited. *Appl. Microbiol. Biotechnol*. 107, 1863-1874. 10.1007/s00253-023-12413-7.

Loeschcke, A., Thies, S., 2015. *Pseudomonas putida*-a versatile host for the production of natural products. *Appl. Microbiol. Biotechnol*. 99, 6197-214. 10.1007/s00253-015-6745-4.

Lohkamp, B., Bäuerle, B., Rieger, P.-G., Schneider, G., 2006. Three-dimensional Structure of Iminodisuccinate Epimerase Defines the Fold of the MmgE/PrpD Protein Family. *J. Mol. Biol.* 362, 555-566. 10.1016/j.jmb.2006.07.051.

López, J. A., Naranjo, J. M., Higuita, J. C., Cubitto, M. A., Cardona, C. A., Villar, M. A., 2012. Biosynthesis of PHB from a new isolated *Bacillus megaterium* strain: Outlook on future developments with endospore forming bacteria. *Biotechnol. Bioprocess Eng.*. 17, 250-258. 10.1007/s12257-011-0448-1.

Lu, C.-D., Itoh, Y., Nakada, Y., Jiang, Y., 2002. Functional Analysis and Regulation of the Divergent *spuABCDEFGH-spuI* Operons for Polyamine Uptake and Utilization in *Pseudomonas aeruginosa* PAO1. *J Bacteriol*. 184, 3765-3773. 10.1128/jb.184.14.3765-3773.2002.

Luengo, J. M., Olivera, E. R., 2020. Catabolism of biogenic amines in *Pseudomonas* species. *Environ Microbiol*. 22, 1174-1192. 10.1111/1462-2920.14912.

Lutz, S., 2010. Beyond directed evolution-semi-rational protein engineering and design. *Curr Opin Biotechnol*. 21, 734-43. 10.1016/j.copbio.2010.08.011.

Lynd, L. R., Beckham, G. T., Guss, A. M., Jayakody, L. N., Karp, E. M., Maranas, C., McCormick, R. L., Amador-Noguez, D., Bomble, Y. J., Davison, B. H., Foster, C., Himmel, M. E., Holwerda, E. K., Laser, M. S., Ng, C. Y., Olson, D. G., Román-Leshkov, Y., Trinh, C. T., Tuskan, G. A., Upadhayay, V., Vardon, D. R., Wang, L., Wyman, C. E., 2022. Toward low-cost biological and hybrid biological/catalytic conversion of cellulosic biomass to fuels. *Energy Environ Sci*. 15, 938-990. 10.1039/D1EE02540F.

Ma, Y., Yao, M., Li, B., Ding, M., He, B., Chen, S., Zhou, X., Yuan, Y., 2018. Enhanced Poly(ethylene terephthalate) Hydrolase Activity by Protein Engineering. *Engineering*. 4, 888-893. 10.1016/j.eng.2018.09.007.

Madeira, F., Pearce, M., Tivey, A. R. N., Basutkar, P., Lee, J., Edbali, O., Madhusoodanan, N., Kolesnikov, A., Lopez, R., 2022. Search and sequence analysis tools services from EMBL-EBI in 2022. *Nucleic acids research*. 50, W276-W279. 10.1093/nar/gkac240.

Madhuri Indurthi, S., Chou, H.-T., Lu, C.-D., 2016. Molecular characterization of *lysR-lysXE*, *gcdR-gcdHG* and *amaR-amaAB* operons for lysine export and catabolism: a comprehensive lysine catabolic network in *Pseudomonas aeruginosa* PAO1. *Microbiology*. 162, 876-888. 10.1099/mic.0.000277.

Magnin, A., Entzmann, L., Pollet, E., Avérous, L., 2021. Breakthrough in polyurethane bio-recycling: An efficient laccase-mediated system for the degradation of different types of polyurethanes. *Waste Manage*. 132, 23-30. 10.1016/j.wasman.2021.07.011.

Magnin, A., Pollet, E., Phalip, V., Avérous, L., 2020. Evaluation of biological degradation of polyurethanes. *Biotechnol. Adv.* 39, 107457.

Martin, W. R., Frigan, F., Bergman, E. H., 1961. Noninductive metabolism of itaconic acid by *Pseudomonas* and *Salmonella* species. *J. Bacteriol.* 82, 905-8. 10.1128/jb.82.6.905-908.1961.

Martínez-García, E., de Lorenzo, V., 2011. Engineering multiple genomic deletions in Gram-negative bacteria: analysis of the multi-resistant antibiotic profile of *Pseudomonas putida* KT2440. *Environ. Microbiol.* 13**,** 2702-16. 10.1111/j.1462-2920.2011.02538.x.

Massy, J., 2017. Thermoplastic and Thermosetting Polymers. In: Massy, J., (Ed.), A Little Book about BIG Chemistry: The Story of Man-Made Polymers. Springer International Publishing, Cham, pp. 19-26.

McGettrick, A. F., O'Neill, L. A. J., 2022. The itaconate family of immunomodulators grows. *Nat. Metab.* 4**,** 499-500. 10.1038/s42255-022-00578-w.

McGettrick, A. F., O'Neill, L. A. J., 2023. Two for the price of one: itaconate and its derivatives as an anti-infective and anti-inflammatory immunometabolite. *Curr. Opin. Immunol.* 80**,** 102268. 10.1016/j.coi.2022.102268.

Mezzina, M. P., Manoli, M. T., Prieto, M. A., Nikel, P. I., 2021. Engineering Native and Synthetic Pathways in *Pseudomonas putida* for the Production of Tailored Polyhydroxyalkanoates. *Biotechnol. J.* 16**,** 2000165. 10.1002/biot.202000165.

Michelucci, A., Cordes, T., Ghelfi, J., Pailot, A., Reiling, N., Goldmann, O., Binz, T., Wegner, A., Tallam, A., Rausell, A., Buttini, M., Linster, C. L., Medina, E., Balling, R., Hiller, K., 2013. Immune-responsive gene 1 protein links metabolism to immunity by catalyzing itaconic acid production. *Proc. Natl. Acad. Sci.* 110**,** 7820. 10.1073/pnas.1218599110.

Mileva, D., Tranchida, D., Gahleitner, M., 2018. Designing polymer crystallinity: An industrial perspective. *Polym Crystallization.* 1**,** e10009. 10.1002/pcr2.10009.

Mills, E. L., Ryan, D. G., Prag, H. A., Dikovskaya, D., Menon, D., Zaslona, Z., Jedrychowski, M. P., Costa, A. S. H., Higgins, M., Hams, E., Szpyt, J., Runtsch, M. C., King, M. S., McGouran, J. F., Fischer, R., Kessler, B. M., McGettrick, A. F., Hughes, M. M., Carroll, R. G., Booty, L. M., Knatko, E. V., Meakin, P. J., Ashford, M. L. J., Modis, L. K., Brunori, G., Sévin, D. C., Fallon, P. G., Caldwell, S. T., Kunji, E. R. S., Chouchani, E. T., Frezza, C., Dinkova-Kostova, A. T., Hartley, R. C., Murphy, M. P., O'Neill, L. A., 2018. Itaconate is an anti-inflammatory metabolite that activates Nrf2 via alkylation of KEAP1. *Nature.* 556**,** 113-117. 10.1038/nature25986.

Minor, A.-J., Goldhahn, R., Rihko-Struckmann, L., Sundmacher, K., 2023. Chemical Recycling Processes of Nylon 6 to Caprolactam: Review and Techno-Economic Assessment. *Chem. Eng. J.* 474**,** 145333. 10.1016/j.cej.2023.145333.

Mirdita, M., Schütze, K., Moriwaki, Y., Heo, L., Ovchinnikov, S., Steinegger, M., 2021. ColabFold - Making protein folding accessible to all. *bioRxiv.* 2021.08.15.456425. 10.1101/2021.08.15.456425

Molitor, R., Bollinger, A., Kubicki, S., Loeschcke, A., Jaeger, K.-E., Thies, S., 2020. Agar plate-based screening methods for the identification of polyester hydrolysis by *Pseudomonas* species. *Microb. Biotechnol.* 13**,** 274-284. 10.1111/1751-7915.13418.

Mückschel, B., Simon, O., Klebensberger, J., Graf, N., Rosche, B., Altenbuchner, J., Pfannstiel, J., Huber, A., Hauer, B., 2012. Ethylene Glycol Metabolism by *Pseudomonas putida. AEM*. 78, 8531-8539. doi:10.1128/AEM.02062-12.

Mueller, W. F., 1962. The Origins of the Basic Inventions Underlying Du Pont's Major Product and Process Innovations, 1920 to 1950. The Rate and Direction of Inventive Activity. Princeton University Press, Princeton, pp. 323-358.

Müller, R. J., Schrader, H. C. G., Profe, J., Dresler, K., Deckwer, W. D., 2005. Enzymatic Degradation of Poly(ethylene terephthalate): Rapid Hydrolyse using a Hydrolase from *T. fusca. Macromol. Rapid Commun*. 26, 1400-1405.

Nagai, K., Iida, K., Shimizu, K., Kinugasa, R., Izumi, M., Kato, D., Takeo, M., Mochiji, K., Negoro, S., 2014. Enzymatic hydrolysis of nylons: quantification of the reaction rate of nylon hydrolase for thin-layered nylons. *Appl. Microbiol. Biotechnol*. 98, 8751-61. 10.1007/s00253-014-5885-2.

Narancic, T., Salvador, M., Hughes, G. M., Beagan, N., Abdulmutalib, U., Kenny, S. T., Wu, H., Saccomanno, M., Um, J., O'Connor, K. E., Jiménez, J. I., 2021. Genome analysis of the metabolically versatile *Pseudomonas umsongensis* GO16: the genetic basis for PET monomer upcycling into polyhydroxyalkanoates. *Microb. Biotechnol*. 14, 2463-2480. 10.1111/1751-7915.13712.

National Archives and Records Administration, 1982. Federal Register: 47 Fed. Reg. 17033 (Apr. 21, 1982) Appendix E, page 17197. https://www.loc.gov/item/fr047077/ (accessed 31.01.2024).

Negoro, S., 2000. Biodegradation of nylon oligomers. *Appl, Microbiol. Biotechnol*. 54, 461-466. 10.1007/s002530000434.

Negoro, S., Kakudo, S., Urabe, I., Okada, H., 1992. A new nylon oligomer degradation gene (*nylC*) on plasmid pOAD2 from a *Flavobacterium* sp. *J Bacteriol*. 174, 7948-7953. 10.1128/jb.174.24.7948-7953.1992.

Negoro, S., Kato, D.-i., Ohki, T., Yasuhira, K., Kawashima, Y., Nagai, K., Takeo, M., Shibata, N., Kamiya, K., Shigeta, Y., 2021. Structural and functional characterization of nylon hydrolases. In: Weber, G., Bornscheuer, U. T., Wei, R., Eds.), Methods in Enzymology. vol. 648. Academic Press, pp. 357-389.

Negoro, S., Shibata, N., Kato, D. I., Tanaka, Y., Yasuhira, K., Nagai, K., Oshima, S., Furuno, Y., Yokoyama, R., Miyazaki, K., Takeo, M., Hengphasatporn, K., Shigeta, Y., Lee, Y. H., Higuchi, Y., 2023. X-ray crystallographic and mutational analysis of the NylC precursor: catalytic mechanism of autocleavage and substrate hydrolysis of nylon hydrolase. *FEBS Journal*. 290, 3400-3421. 10.1111/febs.16755.

Negoro, S., Shibata, N., Lee, Y.-H., Takehara, I., Kinugasa, R., Nagai, K., Tanaka, Y., Kato, D.-I., Takeo, M., Goto, Y., Higuchi, Y., 2018. Structural basis of the correct subunit assembly, aggregation, and intracellular degradation of nylon hydrolase. *Sci Rep*. 8, 9725-9725. 10.1038/s41598-018-27860-w.

Negoro, S., Shibata, N., Tanaka, Y., Yasuhira, K., Shibata, H., Hashimoto, H., Lee, Y. H., Oshima, S., Santa, R., Oshima, S., Mochiji, K., Goto, Y., Ikegami, T., Nagai, K., Kato, D., Takeo, M., Higuchi, Y., 2012. Three-dimensional structure of nylon hydrolase and mechanism of nylon-6 hydrolysis. *J Biol Chem.* 287**,** 5079-90. 10.1074/jbc.M111.321992.

Nelms, S. E., Barnett, J., Brownlow, A., Davison, N. J., Deaville, R., Galloway, T. S., Lindeque, P. K., Santillo, D., Godley, B. J., 2019. Microplastics in marine mammals stranded around the British coast: ubiquitous but transitory? *Sci Rep.* 9**,** 1075. 10.1038/s41598-018-37428-3.

Nelson, K. E., Weinel, C., Paulsen, I. T., Dodson, R. J., Hilbert, H., Martins dos Santos, V. A., Fouts, D. E., Gill, S. R., Pop, M., Holmes, M., Brinkac, L., Beanan, M., DeBoy, R. T., Daugherty, S., Kolonay, J., Madupu, R., Nelson, W., White, O., Peterson, J., Khouri, H., Hance, I., Chris Lee, P., Holtzapple, E., Scanlan, D., Tran, K., Moazzez, A., Utterback, T., Rizzo, M., Lee, K., Kosack, D., Moestl, D., Wedler, H., Lauber, J., Stjepandic, D., Hoheisel, J., Straetz, M., Heim, S., Kiewitz, C., Eisen, J. A., Timmis, K. N., Düsterhöft, A., Tümmler, B., Fraser, C. M., 2002. Complete genome sequence and comparative analysis of the metabolically versatile *Pseudomonas putida* KT2440. *Environ Microbiol.* 4**,** 799-808. 10.1046/j.1462-2920.2002.00366.x.

Nikel, P. I., de Lorenzo, V., 2018. *Pseudomonas putida* as a functional chassis for industrial biocatalysis: From native biochemistry to *trans*-metabolism. *Metab. Eng..* 50**,** 142-155. 10.1016/j.ymben.2018.05.005.

Nolasco-Soria, H., Moyano-López, F., Vega-Villasante, F., del Monte-Martínez, A., Espinosa-Chaurand, D., Gisbert, E., Nolasco-Alzaga, H. R., 2018. Lipase and Phospholipase Activity Methods for Marine Organisms. In: Sandoval, G., (Ed.), Lipases and Phospholipases: Methods and Protocols. Springer New York, New York, NY, pp. 139-167.

Notredame, C., Higgins, D. G., Heringa, J., 2000. T-Coffee: A novel method for fast and accurate multiple sequence alignment. *J Mol Biol.* 302**,** 205-17. 10.1006/jmbi.2000.4042.

Ochsner, U. A., Fiechter, A., Reiser, J., 1994. Isolation, characterization, and expression in Escherichia coli of the *Pseudomonas aeruginosa rhlAB* genes encoding a rhamnosyltransferase involved in rhamnolipid biosurfactant synthesis. *J. Biol. Chem.* 269**,** 19787-19795. 10.1016/S0021-9258(17)32089-6.

Ohi, M., Li, Y., Cheng, Y., Walz, T., 2004. Negative staining and image classification — powerful tools in modern electron microscopy. *Biol Proced. Online.* 6**,** 23-34. 10.1251/bpo70

Okabe, M., Lies, D., Kanamasa, S., Park, E. Y., 2009. Biotechnological production of itaconic acid and its biosynthesis in *Aspergillus terreus. Appl. Microbiol. Biotechnol.* 84**,** 597-606. 10.1007/s00253-009-2132-3.

Okada, H., Negoro, S., Kimura, H., Nakamura, S., 1983. Evolutionary adaptation of plasmid-encoded enzymes for degrading nylon oligomers. *Nature.* 306**,** 203-6. 10.1038/306203a0.

Okui, N., 1990. Relationships between melting temperature, maximum crystallization temperature and glass transition temperature. *Polymer*. 31**,** 92-94. 10.1016/0032-3861(90)90355-3.

Otto, M., Wynands, B., Lenzen, C., Filbig, M., Blank, L. M., Wierckx, N., 2019. Rational Engineering of Phenylalanine Accumulation in *Pseudomonas taiwanensis* to Enable High-Yield Production of Trans-Cinnamate. *Front Bioeng Biotechnol*. 7. 10.3389/fbioe.2019.00312.

Otzen, M., Palacio, C., Janssen, D. B., 2018. Characterization of the caprolactam degradation pathway in *Pseudomonas jessenii* using mass spectrometry-based proteomics. *Appl Microbiol Biotechnol*. 102**,** 6699-6711. 10.1007/s00253-018-9073-7.

Paci, M., La Mantia, F. P., 1999. Influence of small amounts of polyvinylchloride on the recycling of polyethyleneterephthalate. *Polym. Degrad. Stab*. 63**,** 11-14. 10.1016/S0141-3910(98)00053-6

Paczia, N., Nilgen, A., Lehmann, T., Gätgens, J., Wiechert, W., Noack, S., 2012. Extensive exometabolome analysis reveals extended overflow metabolism in various microorganisms. *Microb. Cell Factories*. 11**,** 122. 10.1186/1475-2859-11-122.

Pandit, A. V., Harrison, E., Mahadevan, R., 2021. Engineering *Escherichia coli* for the utilization of ethylene glycol. *Microb. Cell Factories*. 20**,** 22. 10.1186/s12934-021-01509-2.

Pardo, I., Jha, R. K., Bermel, R. E., Bratti, F., Gaddis, M., McIntyre, E., Michener, W., Neidle, E. L., Dale, T., Beckham, G. T., Johnson, C. W., 2020. Gene amplification, laboratory evolution, and biosensor screening reveal MucK as a terephthalic acid transporter in *Acinetobacter baylyi* ADP1. *Metab. Eng*. 62**,** 260-274. 10.1016/j.ymben.2020.09.009.

Parke, D., Garcia, M. A., Ornston, L. N., 2001. Cloning and Genetic Characterization of *dca* Genes Required for β-Oxidation of Straight-Chain Dicarboxylic Acids in *Acinetobacter* sp. Strain ADP1. *AEM*. 67**,** 4817-4827. 10.1128/AEM.67.10.4817-4827.2001

Partenheimer, W., 2003. Valuable oxygenates by aerobic oxidation of polymers using metal/bromide homogeneous catalysts. *Catal. Today*. 81**,** 117-135. 10.1016/S0920-5861(03)00124-X.

Patel, R. N., Nanduri, V., Brzozowski, D., McNamee, C., Banerjee, A., 2003. Enantioselective Enzymatic Cleavage of N-Benzyloxycarbonyl Groups. *Adv. Synth Catal.*. 345**,** 830-834. 10.1002/adsc.200303038.

Paysan-Lafosse, T., Blum, M., Chuguransky, S., Grego, T., Pinto, B. L., Salazar, Gustavo A., Bileschi, Maxwell L., Bork, P., Bridge, A., Colwell, L., Gough, J., Haft, Daniel H., Letunić, I., Marchler-Bauer, A., Mi, H., Natale, Darren A., Orengo, Christine A., Pandurangan, Arun P., Rivoire, C., Sigrist, C. J. A., Sillitoe, I., Thanki, N., Thomas, P. D., Tosatto, S. C. E., Wu, Cathy H., Bateman, A., 2022. InterPro in 2022. *Nucleic Acids Research*. 51**,** D418-D427. 10.1093/nar/gkac993.

Peix, A., Ramírez-Bahena, M. H., Velázquez, E., 2018. The current status on the taxonomy of *Pseudomonas* revisited: An update. *Infect Genet Evol*. 57, 106-116. 10.1016/j.meegid.2017.10.026.

Pettersen, E. F., Goddard, T. D., Huang, C. C., Couch, G. S., Greenblatt, D. M., Meng, E. C., Ferrin, T. E., 2004. UCSF Chimera—A visualization system for exploratory research and analysis. *J. Comput. Chem*. 25, 1605-1612. 10.1002/jcc.20084

Pettinari, M. J., Vázquez, G. J., Silberschmidt, D., Rehm, B., Steinbüchel, A., Méndez, B. S., 2001. Poly(3-Hydroxybutyrate) Synthesis Genes in *Azotobacter* sp. Strain FA8. *AEM*. 67, 5331-5334. 10.1128/AEM.67.11.5331-5334.2001.

Philip, S., Keshavarz, T., Roy, I., 2007. Polyhydroxyalkanoates: biodegradable polymers with a range of applications. *J. Chem. Technol. Biotechnol*. 82, 233-247. 10.1002/jctb.1667.

Pietroluongo, M., Padovano, E., Frache, A., Badini, C., 2020. Mechanical recycling of an end-of-life automotive composite component. *SM&T*. 23, e00143. 10.1016/j.susmat.2019.e00143.

PlasticsEurope, 2022. Plastics - the Facts 2022: An analysis of European plastics production, demand and waste data.

PlasticsEurope, 2023. Plastics - the fast Facts 2023.

Prieto, A., Escapa, I. F., Martínez, V., Dinjaski, N., Herencias, C., de la Peña, F., Tarazona, N., Revelles, O., 2016. A holistic view of polyhydroxyalkanoate metabolism in *Pseudomonas putida*. *Environ. Microbiol*. 18, 341-357. 10.1111/1462-2920.12760.

Puetz, H., Janknecht, C., Contreras, F., Vorobii, M., Kurkina, T., Schwaneberg, U., 2023. Validated High-Throughput Screening System for Directed Evolution of Nylon-Depolymerizing Enzymes. *ACS Sus. Chem. Eng.*. 11, 15513-15522. 10.1021/acssuschemeng.3c01575.

Puiggalí, J., 2021. Aliphatic polyamides (nylons): Interplay between hydrogen bonds and crystalline structures, polymorphic transitions and crystallization. *Polym. Crystallization*. 4, e10199. 10.1002/pcr2.10199.

Puiggené, Ò., Espinosa, M. J. C., Schlosser, D., Thies, S., Jehmlich, N., Kappelmeyer, U., Schreiber, S., Wibberg, D., Kalinowski, J., Harms, H., Heipieper, H. J., Eberlein, C., 2022. Extracellular degradation of a polyurethane oligomer involving outer membrane vesicles and further insights on the degradation of 2,4-diaminotoluene in *Pseudomonas capeferrum* TDA1. *Sci Rep*. 12, 2666. 10.1038/s41598-022-06558-0.

Quienne, B., Kasmi, N., Dieden, R., Caillol, S., Habibi, Y., 2020. Isocyanate-Free Fully Biobased Star Polyester-Urethanes: Synthesis and Thermal Properties. *Biomacromolecules*. 21, 1943-1951. 10.1021/acs.biomac.0c00156.

Reinecke, F., Steinbüchel, A., 2009. *Ralstonia eutropha* strain H16 as model organism for PHA metabolism and for biotechnological production of technically interesting biopolymers. *J Mol Microbiol Biotechnol*. 16, 91-108. 10.1159/000142897.

Riquelme, S. A., Liimatta, K., Wong Fok Lung, T., Fields, B., Ahn, D., Chen, D., Lozano, C., Sáenz, Y., Uhlemann, A.-C., Kahl, B. C., Britto, C. J., DiMango, E., Prince, A., 2020. *Pseudomonas aeruginosa* Utilizes Host-Derived Itaconate to Redirect Its Metabolism to Promote Biofilm Formation. *Cell Metab.* 31**,** 1091-1106.e6. 10.1016/j.cmet.2020.04.017.

Rocco, C. J., Wetterhorn, K. M., Garvey, G. S., Rayment, I., Escalante-Semerena, J. C., 2017. The PrpF protein of *Shewanella oneidensis* MR-1 catalyzes the isomerization of 2-methyl-*cis*-aconitate during the catabolism of propionate *via* the AcnD-dependent 2-methylcitric acid cycle. *PLoS One*. 12**,** e0188130-e0188130. 10.1371/journal.pone.0188130.

Rognstad, R., Katz, J., 1979. Effects of 2,4-dihydroxybutyrate on lipogenesis in rat hepatocytes. *J. Biol. Chem.* 254**,** 11969-11972. 10.1016/S0021-9258(19)86412-8.

Rowe, L., Howard, G. T., 2002. Growth of *Bacillus subtilis* on polyurethane and the purification and characterization of a polyurethanase-lipase enzyme. *Int. Biodeterior. Biodegradation*. 50**,** 33-40. 10.1016/S0964-8305(02)00047-1.

Rudra, B., Gupta, R. S., 2021. Phylogenomic and comparative genomic analyses of species of the family *Pseudomonadaceae*: Proposals for the genera *Halopseudomonas* gen. nov. and *Atopomonas* gen. nov., merger of the genus *Oblitimonas* with the genus *Thiopseudomonas*, and transfer of some misclassified species of the genus *Pseudomonas* into other genera. *Int. J. System. Evolut. Microbiol*. 71. 10.1099/ijsem.0.005011.

Russell, J. R., Huang, J., Anand, P., Kucera, K., Sandoval, A. G., Dantzler, K. W., Hickman, D., Jee, J., Kimovec, F. M., Koppstein, D., Marks, D. H., Mittermiller, P. A., Núñez, S. J., Santiago, M., Townes, M. A., Vishnevetsky, M., Williams, N. E., Vargas, M. P. N., Boulanger, L. A., Bascom-Slack, C., Strobel, S. A., 2011. Biodegradation of polyester polyurethane by endophytic fungi. *AEM*. 77**,** 6076-6084. 10.1128/AEM.00521-11.

Sadler, J. C., Wallace, S., 2021. Microbial synthesis of vanillin from waste poly(ethylene terephthalate). *Green Chem*. 23**,** 4665-4672. 10.1039/d1gc00931a.

Saha, B. C., 2017. Emerging biotechnologies for production of itaconic acid and its applications as a platform chemical. *J. Ind. Microbiol. Biotechnol.* 44**,** 303-315. 10.1007/s10295-016-1878-8.

Salvachúa, D., Rydzak, T., Auwae, R., De Capite, A., Black, B. A., Bouvier, J. T., Cleveland, N. S., Elmore, J. R., Furches, A., Huenemann, J. D., Katahira, R., Michener, W. E., Peterson, D. J., Rohrer, H., Vardon, D. R., Beckham, G. T., Guss, A. M., 2020. Metabolic engineering of *Pseudomonas putida* for increased polyhydroxyalkanoate production from lignin. *Microb. Biotechnol*. 13**,** 290-298. 10.1111/1751-7915.13481.

Salvador, M., Abdulmutalib, U., Gonzalez, J., Kim, J., Smith, A. A., Faulon, J.-L., Wei, R., Zimmermann, W., Jimenez, J. I., Microbial Genes for a Circular and Sustainable Bio-PET Economy. *Genes*, Vol. 10, 2019.

Sanluis-Verdes, A., Colomer-Vidal, P., Rodriguez-Ventura, F., Bello-Villarino, M., Spinola-Amilibia, M., Ruiz-Lopez, E., Illanes-Vicioso, R., Castroviejo, P., Aiese Cigliano, R., Montoya, M., Falabella, P., Pesquera, C., Gonzalez-Legarreta, L., Arias-Palomo, E., Solà, M., Torroba, T., Arias, C. F., Bertocchini, F., 2022. Wax worm saliva and the enzymes therein are the key to polyethylene degradation by *Galleria mellonella*. *Nat: Commun*. 13**,** 5568. 10.1038/s41467-022-33127-w.

Sasikaran, J., Ziemski, M., Zadora, P. K., Fleig, A., Berg, I. A., 2014. Bacterial itaconate degradation promotes pathogenicity. *Nat. Chem. Biol.* 10**,** 371-7. 10.1038/nchembio.1482.

Sayers, E. W., Bolton, E. E., Brister, J. R., Canese, K., Chan, J., Comeau, D. C., Connor, R., Funk, K., Kelly, C., Kim, S., Madej, T., Marchler-Bauer, A., Lanczycki, C., Lathrop, S., Lu, Z., Thibaud-Nissen, F., Murphy, T., Phan, L., Skripchenko, Y., Tse, T., Wang, J., Williams, R., Trawick, B. W., Pruitt, K. D., Sherry, S. T., 2022. Database resources of the national center for biotechnology information. *Nucleic Acids Res*. 50**,** D20-d26. 10.1093/nar/gkab1112.

Sayqal, A., Xu, Y., Trivedi, D. K., AlMasoud, N., Ellis, D. I., Rattray, N. J. W., Goodacre, R., 2016. Metabolomics Analysis Reveals the Participation of Efflux Pumps and Ornithine in the Response of *Pseudomonas putida* DOT-T1E Cells to Challenge with Propranolol. *PLoS One*. 11**,** e0156509. 10.1371/journal.pone.0156509.

Schimerlik, M. I., Cleland, W., 1977. Inhibition and alternate-substrate studies on the mechanism of malic enzyme. *Biochemistry*. 16**,** 565-570.

Schmidt, J., Wei, R., Oeser, T., Dedavid e Silva, L. A., Breite, D., Schulze, A., Zimmermann, W., 2017. Degradation of Polyester Polyurethane by Bacterial Polyester Hydrolases. *Polymers*. 9**,** 65.

Schmidt, M., Pearson, A. N., Incha, M. R., Thompson, M. G., Baidoo, E. E. K., Kakumanu, R., Mukhopadhyay, A., Shih, P. M., Deutschbauer, A. M., Blank, L. M., Keasling, J. D., 2022. Nitrogen Metabolism in *Pseudomonas putida*: Functional Analysis Using Random Barcode Transposon Sequencing. *Appl Environ Microbiol*. 88**,** e0243021. 10.1128/aem.02430-21.

Schöne, A.-C., Kratz, K., Schulz, B., Lendlein, A., 2016. Polymer architecture versus chemical structure as adjusting tools for the enzymatic degradation of oligo(ε-caprolactone) based films at the air-water interface. *Polym. Degrad. Stability*. 131**,** 114-121. 10.1016/j.polymdegradstab.2016.07.010.

Schwanemann, T., Otto, M., Wierckx, N., Wynands, B., 2020. *Pseudomonas* as Versatile Aromatics Cell Factory. *Biotechnol. J.* 15**,** 1900569. 10.1002/biot.201900569.

Schyns, Z. O. G., Shaver, M. P., 2021. Mechanical Recycling of Packaging Plastics: A Review. *Macromol. Rapid Commun*. 42**,** 2000415. 10.1002/marc.202000415.

Sheng, Y., Lam, S. S., Wu, Y., Ge, S., Wu, J., Cai, L., Huang, Z., Le, Q. V., Sonne, C., Xia, C., 2021. Enzymatic conversion of pretreated lignocellulosic biomass: A review on influence of structural changes of lignin. *Bioresour. Technol*. 324**,** 124631. 10.1016/j.biortech.2020.124631.

Silva-Rocha, R., Martínez-García, E., Calles, B., Chavarría, M., Arce-Rodríguez, A., de Las Heras, A., Páez-Espino, A. D., Durante-Rodríguez, G., Kim, J., Nikel, P. I., Platero, R., de Lorenzo, V., 2013. The Standard European Vector Architecture (SEVA): a coherent platform for the analysis and deployment of complex prokaryotic phenotypes. *Nucleic Acids Res*. 41**,** D666-75. 10.1093/nar/gks1119.

Singh, A., Rorrer, N. A., Nicholson, S. R., Erickson, E., DesVeaux, J. S., Avelino, A. F., Lamers, P., Bhatt, A., Zhang, Y., Avery, G., 2021. Techno-economic, life-cycle, and socioeconomic impact analysis of enzymatic recycling of poly (ethylene terephthalate). *Joule*. 5**,** 2479-2503.

Son, H. F., Cho, I. J., Joo, S., Seo, H., Sagong, H.-Y., Choi, S. Y., Lee, S. Y., Kim, K.-J., 2019. Rational Protein Engineering of Thermo-Stable PETase from *Ideonella sakaiensis* for Highly Efficient PET Degradation. *ACS Catal*. 9**,** 3519-3526. 10.1021/acscatal.9b00568.

Spínola-Amilibia, M., Illanes-Vicioso, R., Ruiz-López, E., Colomer-Vidal, P., Rodriguez-Ventura, F., Peces Pérez, R., Arias, C. F., Torroba, T., Solà, M., Arias-Palomo, E., Bertocchini, F., 2023. Plastic degradation by insect hexamerins: Near-atomic resolution structures of the polyethylene-degrading proteins from the wax worm saliva. *Sci. Adv*. 9**,** eadi6813. 10.1126/sciadv.adi6813.

Steiger, M. G., Wierckx, N., Blank, L. M., Mattanovich, D., Sauer, M., 2017. Itaconic Acid – An Emerging Building Block. *Ind. Biotechnol*., pp. 453-472.

Streit, W. R., Schmitz, R. A., 2004. Metagenomics – the key to the uncultured microbes. *Curr. Opin. Microbiol*. 7**,** 492-498. 10.1016/j.mib.2004.08.002.

Strelko, C. L., Lu, W., Dufort, F. J., Seyfried, T. N., Chiles, T. C., Rabinowitz, J. D., Roberts, M. F., 2011. Itaconic Acid Is a Mammalian Metabolite Induced during Macrophage Activation. *J. Am. Chem. Soc.* 133**,** 16386-16389. 10.1021/ja2070889.

Sulaiman, S., Yamato, S., Kanaya, E., Kim, J.-J., Koga, Y., Takano, K., Kanaya, S., 2012. Isolation of a Novel Cutinase Homolog with Polyethylene Terephthalate-Degrading Activity from Leaf-Branch Compost by Using a Metagenomic Approach. *AEM*. 78**,** 1556-1562. doi:10.1128/AEM.06725-11.

Sullivan, K. P., Werner, A. Z., Ramirez, K. J., Ellis, L. D., Bussard, J. R., Black, B. A., Brandner, D. G., Bratti, F., Buss, B. L., Dong, X., Haugen, S. J., Ingraham, M. A., Konev, M. O., Michener, W. E., Miscall, J., Pardo, I., Woodworth, S. P., Guss, A. M., Román-Leshkov, Y., Stahl, S. S., Beckham, G. T., 2022. Mixed plastics waste valorization through tandem chemical oxidation and biological funneling. *Science*. 378**,** 207-211. doi:10.1126/science.abo4626.

Sun, Z., Ramsay, J. A., Guay, M., Ramsay, B. A., 2007. Carbon-limited fed-batch production of medium-chain-length polyhydroxyalkanoates from nonanoic acid by *Pseudomonas putida* KT2440. *Appl. Microbiol. Biotechnol*. 74**,** 69-77. 10.1007/s00253-006-0655-4

Taboada, B., Estrada, K., Ciria, R., Merino, E., 2018. Operon-mapper: a web server for precise operon identification in bacterial and archaeal genomes. *Bioinformatics*. 34**,** 4118-4120. 10.1093/bioinformatics/bty496.

Takehara, I., Fujii, T., Tanimoto, Y., Kato, D.-I., Takeo, M., Negoro, S., 2018. Metabolic pathway of 6-aminohexanoate in the nylon oligomer-degrading bacterium *Arthrobacter* sp. KI72: identification of the enzymes responsible for the conversion of 6-aminohexanoate to adipate. *Appl. Microbiol. and Biotechnol.* 102**,** 801-814. 10.1007/s00253-017-8657-y.

Teufel, F., Almagro Armenteros, J. J., Johansen, A. R., Gíslason, M. H., Pihl, S. I., Tsirigos, K. D., Winther, O., Brunak, S., von Heijne, G., Nielsen, H., 2022. SignalP 6.0 predicts all five types of signal peptides using protein language models. *Nature Biotechnol.* 40**,** 1023-1025. 10.1038/s41587-021-01156-3.

Textile Exchange, Preferred Fiber and Materials Market Report. 2022.

Thiounn, T., Smith, R. C., 2020. Advances and approaches for chemical recycling of plastic waste. *J. Polym Sci.* 58**,** 1347-1364. 10.1002/pol.20190261.

Thompson, M. G., Costello, Z., Hummel, N. F. C., Cruz-Morales, P., Blake-Hedges, J. M., Krishna, R. N., Skyrud, W., Pearson, A. N., Incha, M. R., Shih, P. M., Garcia-Martin, H., Keasling, J. D., 2019a. Robust Characterization of Two Distinct Glutarate Sensing Transcription Factors of *Pseudomonas putida* L-Lysine Metabolism. *ACS Synth Biol.* 8**,** 2385-2396. 10.1021/acssynbio.9b00255.

Thompson, M. G., Valencia, L. E., Blake-Hedges, J. M., Cruz-Morales, P., Velasquez, A. E., Pearson, A. N., Sermeno, L. N., Sharpless, W. A., Benites, V. T., Chen, Y., Baidoo, E. E. K., Petzold, C. J., Deutschbauer, A. M., Keasling, J. D., 2019b. Omics-driven identification and elimination of valerolactam catabolism in *Pseudomonas putida* KT2440 for increased product titer. *Metab. Eng. Commun.* 9**,** e00098. 10.1016/j.mec.2019.e00098.

Thompson, R. C., Swan, S. H., Moore, C. J., vom Saal, F. S., 2009. Our plastic age. *Philos Trans R Soc Lond B Biol Sci.* 364**,** 1973-6. 10.1098/rstb.2009.0054.

Thomsen, T. B., Hunt, C. J., Meyer, A. S., 2022. Influence of substrate crystallinity and glass transition temperature on enzymatic degradation of polyethylene terephthalate (PET). *Nat. Biotechnol.* 69**,** 28-35. 10.1016/j.nbt.2022.02.006.

Tiso, T., Ihling, N., Kubicki, S., Biselli, A., Schonhoff, A., Bator, I., Thies, S., Karmainski, T., Kruth, S., Willenbrink, A.-L., Loeschcke, A., Zapp, P., Jupke, A., Jaeger, K.-E., Büchs, J., Blank, L. M., 2020. Integration of Genetic and Process Engineering for Optimized Rhamnolipid Production Using *Pseudomonas putida*. *Front. Bioeng. Biotechnol.* 8. 10.3389/fbioe.2020.00976.

Tiso, T., Narancic, T., Wei, R., Pollet, E., Beagan, N., Schröder, K., Honak, A., Jiang, M., Kenny, S. T., Wierckx, N., Perrin, R., Avérous, L., Zimmermann, W., O'Connor, K., Blank, L. M., 2021a. Towards bio-upcycling of polyethylene terephthalate. *Metab. Eng.* 66**,** 167-178. 10.1016/j.ymben.2021.03.011.

Tiso, T., Winter, B., Wei, R., Hee, J., de Witt, J., Wierckx, N., Quicker, P., Bornscheuer, U. T., Bardow, A., Nogales, J., Blank, L. M., 2021b. The metabolic potential of plastics as biotechnological carbon sources – Review and targets for the future. *Metab. Eng.* 10.1016/j.ymben.2021.12.006.

Tiso, T., Zauter, R., Tulke, H., Leuchtle, B., Li, W.-J., Behrens, B., Wittgens, A., Rosenau, F., Hayen, H., Blank, L. M., 2017. Designer rhamnolipids by reduction of congener diversity: production and characterization. *Microb. Cell Factories*. 16**,** 225. 10.1186/s12934-017-0838-y

Tokiwa, Y., Calabia, B. P., Ugwu, C. U., Aiba, S., 2009. Biodegradability of Plastics. *Int. J. Mol. Sci*. 10**,** 3722-3742.

Tournier, V., Duquesne, S., Guillamot, F., Cramail, H., Taton, D., Marty, A., André, I., 2023. Enzymes' Power for Plastics Degradation. *Chem. Rev*. 123**,** 5612-5701. 10.1021/acs.chemrev.2c00644

Tournier, V., Topham, C. M., Gilles, A., David, B., Folgoas, C., Moya-Leclair, E., Kamionka, E., Desrousseaux, M. L., Texier, H., Gavalda, S., Cot, M., Guémard, E., Dalibey, M., Nomme, J., Cioci, G., Barbe, S., Chateau, M., André, I., Duquesne, S., Marty, A., 2020. An engineered PET depolymerase to break down and recycle plastic bottles. *Nature*. 580**,** 216-219. 10.1038/s41586-020-2149-4.

Trifunović, D., Schuchmann, K., Müller, V., 2016. Ethylene Glycol Metabolism in the Acetogen *Acetobacterium woodii*. *J Bacteriol*. 198**,** 1058-1065. 10.1128/jb.00942-15.

Tsuji, H., Miyauchi, S., 2001. Poly(l-lactide): VI Effects of crystallinity on enzymatic hydrolysis of poly(l-lactide) without free amorphous region. *Polym. Degrad. Stab*. 71**,** 415-424. 10.1016/S0141-3910(00)00191-9.

Ueda, K., Hosoda, M., Matsuda, T., Tai, K., 1998. Synthesis of High Molecular Weight Nylon 6 by Anionic Polymerization of ε-Caprolactam. Formation of Cyclic Oligomers. *Polym. J*. 30**,** 186-191. 10.1295/polymj.30.186.

Uekert, T., DesVeaux, J. S., Singh, A., Nicholson, S. R., Lamers, P., Ghosh, T., McGeehan, J. E., Carpenter, A. C., Beckham, G. T., 2022. Life cycle assessment of enzymatic poly(ethylene terephthalate) recycling. *Green Chem*. 24**,** 6531-6543. 10.1039/D2GC02162E.

Utomo, R. N. C., Li, W.-J., Tiso, T., Eberlein, C., Doeker, M., Heipieper, H. J., Jupke, A., Wierckx, N., Blank, L. M., 2020. Defined Microbial Mixed Culture for Utilization of Polyurethane Monomers. *ACS Sus. Chem. Eng*. 8**,** 17466-17474. 10.1021/acssuschemeng.0c06019.

Üzüm, Ö. B., Karadağ, E., 2006. Synthetic polymeric absorbent for dye based on chemically crosslinked acrylamide/mesaconic acid hydrogels. *J. Appl. Polym. Sci*. 101**,** 405-413. 10.1002/app.22248.

Valentini, M., García-Mauriño, S. M., Pérez-Martínez, I., Santero, E., Canosa, I., Lapouge, K., 2014. Hierarchical management of carbon sources is regulated similarly by the CbrA/B systems in *Pseudomonas aeruginosa* and *Pseudomonas putida*. *Microbiol*. 160**,** 2243-2252. 10.1099/mic.0.078873-0.

Van Cauwenberghe, L., Janssen, C. R., 2014. Microplastics in bivalves cultured for human consumption. *Environ Pollut*. 193**,** 65-70. 10.1016/j.envpol.2014.06.010.

Vockley, J., Mohsen al, W. A., Binzak, B., Willard, J., Fauq, A., 2000. Mammalian branched-chain acyl-CoA dehydrogenases: molecular cloning and characterization of recombinant enzymes. *Meth. Enzymol.* 324**,** 241-58. 10.1016/s0076-6879(00)24236-5.

Voit, B. I., Lederer, A., 2009. Hyperbranched and Highly Branched Polymer Architectures—Synthetic Strategies and Major Characterization Aspects. *Chem. Rev.* 109**,** 5924-5973. 10.1021/cr900068q.

Volke, D. C., Calero, P., Nikel, P. I., 2020. *Pseudomonas putida. Trends in Microbiol.* 28**,** 512-513. 10.1016/j.tim.2020.02.015.

Volke, D. C., Martino, R. A., Kozaeva, E., Smania, A. M., Nikel, P. I., 2022. Modular (de)construction of complex bacterial phenotypes by CRISPR/nCas9-assisted, multiplex cytidine base-editing. *Nat. Commun.* 13**,** 3026. 10.1038/s41467-022-30780-z.

Wang, H.-h., Zhou, X.-r., Liu, Q., Chen, G.-Q., 2011. Biosynthesis of polyhydroxyalkanoate homopolymers by *Pseudomonas putida. Appl. Microbiol Biotechnol.* 89**,** 1497-1507. 10.1007/s00253-010-2964-x.

Wang, H., Ye, J.-W., Chen, X., Yuan, Y., Shi, J., Liu, X., Yang, F., Ma, Y., Chen, J., Wu, F., Lan, Y., Wu, Q., Tong, Y., Chen, G.-Q., 2023. Production of PHA copolymers consisting of 3-hydroxybutyrate and 3-hydroxyhexanoate (PHBHHx) by recombinant *Halomonas bluephagenesis. Chem. Eng. J.* 466**,** 143261. 10.1016/j.cej.2023.143261.

Wang, Q., Nomura, C. T., 2010. Monitoring differences in gene expression levels and polyhydroxyalkanoate (PHA) production in *Pseudomonas putida* KT2440 grown on different carbon sources. *J. Biosci. Bioeng.* 110**,** 653-659. 10.1016/j.jbiosc.2010.08.001.

Wang, W., Cai, B., Shao, Z., 2014. Oil degradation and biosurfactant production by the deep sea bacterium *Dietzia maris* As-13-3. *Front. Microbiol.* 5. 10.3389/fmicb.2014.00711.

Wang, Y. Z., Zhou, Y., Zylstra, G. J., 1995. Molecular analysis of isophthalate and terephthalate degradation by *Comamonas testosteroni* YZW-D. *Environ Health Perspect.* 103 Suppl 5**,** 9-12. 10.1289/ehp.95103s49.

Wehrmann, M., Billard, P., Martin-Meriadec, A., Zegeye, A., Klebensberger, J., 2017. Functional Role of Lanthanides in Enzymatic Activity and Transcriptional Regulation of Pyrroloquinoline Quinone-Dependent Alcohol Dehydrogenases in *Pseudomonas putida* KT2440. *mBio.* 8**,** e00570-17. 10.1128/mBio.00570-17.

Wei, R., Tiso, T., Bertling, J., O'Connor, K., Blank, L. M., Bornscheuer, U. T., 2020. Possibilities and limitations of biotechnological plastic degradation and recycling. *Nat. Catal.* 3**,** 867-871. 10.1038/s41929-020-00521-w.

Wei, R., Zimmermann, W., 2017. Microbial enzymes for the recycling of recalcitrant petroleum-based plastics: how far are we? *Microb. Biotechnol.* 10**,** 1308-1322. 10.1111/1751-7915.12710.

Weimer, A., Kohlstedt, M., Volke, D. C., Nikel, P. I., Wittmann, C., 2020. Industrial biotechnology of *Pseudomonas putida*: advances and prospects. *Appl. Microbiol. Biotechnol*. 104**,** 7745-7766. 10.1007/s00253-020-10811-9.

Weisburg, W. G., Barns, S. M., Pelletier, D. A., Lane, D. J., 1991. 16S ribosomal DNA amplification for phylogenetic study. *J. Bacteriol*. 173**,** 697-703. 10.1128/jb.173.2.697-703.1991.

Welle, F., 2011. Twenty years of PET bottle to bottle recycling—An overview. *Resour. Conserv. Recycl*. 55**,** 865-875. 10.1016/j.resconrec.2011.04.009.

Werner, A. Z., Clare, R., Mand, T. D., Pardo, I., Ramirez, K. J., Haugen, S. J., Bratti, F., Dexter, G. N., Elmore, J. R., Huenemann, J. D., Peabody, G. L., Johnson, C. W., Rorrer, N. A., Salvachúa, D., Guss, A. M., Beckham, G. T., 2021. Tandem chemical deconstruction and biological upcycling of poly(ethylene terephthalate) to β-ketoadipic acid by *Pseudomonas putida* KT2440. *Metab. Eng.* 67**,** 250-261. 10.1016/j.ymben.2021.07.005.

Whinfield, J. R., Dickson, J. T., Improvements Relating to the Manufacture of Highly Polymeric Substances. Vol. UK Patent 578,079; "Polymeric Linear Terephthalic Esters", U.S. Patent 2,465,319 Publication date: 22 March 1949; Filing date: 24 September 1945; Priority date: 29 July 1941, 1941.

Wierckx, N., Agrimi, G., Lübeck, P. S., Steiger, M. G., Mira, N. P., Punt, P. J., 2020. Metabolic specialization in itaconic acid production: a tale of two fungi. *Curr. Opin. Biotechnol.* 62**,** 153-159. 10.1016/j.copbio.2019.09.014.

Wierckx, N., J. P., Ballerstedt, H., de Bont Jan, A. M., Wery, J., 2005. Engineering of Solvent-Tolerant *Pseudomonas putida* S12 for Bioproduction of Phenol from Glucose. *Appl. Environ. Microbiol.* 71**,** 8221-8227. 10.1128/AEM.71.12.8221-8227.2005.

Wierckx, N., Prieto, M. A., Pomposiello, P., de Lorenzo, V., O'Connor, K., Blank, L. M., 2015. Plastic waste as a novel substrate for industrial biotechnology. *Microb. Biotechnol.* 8**,** 900-903.

Willis, R. B., Montgomery, M. E., Allen, P. R., 1996. Improved Method for Manual, Colorimetric Determination of Total Kjeldahl Nitrogen Using Salicylate. *J. Agric. Food Chem*. 44**,** 1804-1807. 10.1021/jf950522b.

Willke, T., Vorlop, K. D., 2001. Biotechnological production of itaconic acid. *Appl. Microbiol. Biotechnol.* 56**,** 289-95. 10.1007/s002530100685.

Winnacker, M., Rieger, B., 2016. Poly(ester amide)s: recent insights into synthesis, stability and biomedical applications. *Polym. Chemistry*. 7**,** 7039-7046. 10.1039/C6PY01783E

Winsor, G. L., Griffiths, E. J., Lo, R., Dhillon, B. K., Shay, J. A., Brinkman, F. S., 2016. Enhanced annotations and features for comparing thousands of *Pseudomonas* genomes in the *Pseudomonas* genome database. *Nucleic Acids Res*. 44**,** D646-53. 10.1093/nar/gkv1227.

Wirtz, L., Eder, M., Schipper, K., Rohrer, S., Jung, H., 2020. Transport and kinase activities of CbrA of *Pseudomonas putida* KT2440. *Sci. Reports*. 10**,** 5400. 10.1038/s41598-020-62337-9.

Wu, D., Li, Q., Shang, X., Liang, Y., Ding, X., Sun, H., Li, S., Wang, S., Chen, Y., Chen, J., 2021a. Commodity plastic burning as a source of inhaled toxic aerosols. *J. Hazard. Materials*. 416**,** 125820. 10.1016/j.jhazmat.2021.125820.

Wu, Y., Shetty, M., Zhang, K., Dauenhauer, P. J., 2021b. Sustainable Hybrid Route to Renewable Methacrylic Acid via Biomass-Derived Citramalate. *ACS Eng. Au.* 10.1021/acsengineeringau.1c00021.

Wynands, B., Lenzen, C., Otto, M., Koch, F., Blank, L. M., Wierckx, N., 2018. Metabolic engineering of *Pseudomonas taiwanensis* VLB120 with minimal genomic modifications for high-yield phenol production. *Metab. Eng.* 47**,** 121-133. 10.1016/j.ymben.2018.03.011.

Wynands, B., Otto, M., Runge, N., Preckel, S., Polen, T., Blank, L. M., Wierckx, N., 2019. Streamlined *Pseudomonas taiwanensis* VLB120 Chassis Strains with Improved Bioprocess Features. *ACS Synth. Biol.* 8**,** 2036-2050. 10.1021/acssynbio.9b00108.

Xie, T., Gao, C., Wang, C., Shen, S. e., Wu, Y., 2014. Application of Poly(butylenes 2-methylsuccinate) as Migration Resistant Plasticizer for Poly(vinyl chloride). *Poly. Plast. Technol. Eng.* 53**,** 465-471. 10.1080/03602559.2013.845207.

Xu, L., Liaqat, F., Sun, J., Khazi, M. I., Xie, R., Zhu, D., 2024. Advances in the vanillin synthesis and biotransformation: A review. *Renew. Sustain. Energy Reviev*. 189**,** 113905. 10.1016/j.rser.2023.113905.

Yadav, G., Singh, A., Dutta, A., Uekert, T., DesVeaux, J. S., Nicholson, S. R., Tan, E. C. D., Mukarakate, C., Schaidle, J. A., Wrasman, C. J., Carpenter, A. C., Baldwin, R. M., Román-Leshkov, Y., Beckham, G. T., 2023. Techno-economic analysis and life cycle assessment for catalytic fast pyrolysis of mixed plastic waste. *Energy & Environ. Sci*. 16**,** 3638-3653. 10.1039/D3EE00749A.

Yasbin, R. E., Wilson, G. A., Young, F. E., 1975. Transformation and transfection in lysogenic strains of *Bacillus subtilis*: evidence for selective induction of prophage in competent cells. *J Bacteriol*. 121**,** 296-304. 10.1128/jb.121.1.296-304.1975.

Yasuhira, K., Tanaka, Y., Shibata, H., Kawashima, Y., Ohara, A., Kato, D., Takeo, M., Negoro, S., 2007. 6-Aminohexanoate oligomer hydrolases from the alkalophilic bacteria *Agromyces* sp. strain KY5R and *Kocuria* sp. strain KY2. *AEM*. 73**,** 7099-102. 10.1128/aem.00777-07.

Ye, S., Xiang, X., Wang, S., Han, D., Xiao, M., Meng, Y., 2020. Nonisocyanate CO2-Based Poly(ester-co-urethane)s with Tunable Performances: A Potential Alternative to Improve the Biodegradability of PBAT. *ACS Sus. Chem. Eng.* 8**,** 1923-1932. 10.1021/acssuschemeng.9b06294.

Yoshida, S., Hiraga, K., Takehana, T., Taniguchi, I., Yamaji, H., Maeda, Y., Toyohara, K., Miyamoto, K., Kimura, Y., Oda, K., 2016. A bacterium that degrades and assimilates poly(ethylene terephthalate). *Science*. 351**,** 1196-1199. 10.1126/science.aad6359.

Zalasiewicz, J., Waters, C. N., Ivar do Sul, J. A., Corcoran, P. L., Barnosky, A. D., Cearreta, A., Edgeworth, M., Gałuszka, A., Jeandel, C., Leinfelder, R., McNeill, J. R., Steffen, W., Summerhayes, C., Wagreich, M., Williams, M., Wolfe, A. P., Yonan, Y., 2016. The geological cycle of plastics and their use as a stratigraphic indicator of the Anthropocene. *Anthropocene*. 13**,** 4-17. 10.1016/j.ancene.2016.01.002.

Zampolli, J., Mangiagalli, M., Vezzini, D., Lasagni, M., Ami, D., Natalello, A., Arrigoni, F., Bertini, L., Lotti, M., Di Gennaro, P., 2023. Oxidative degradation of polyethylene by two novel laccase-like multicopper oxidases from *Rhodococcus opacus* R7. *Environ. Technol. Innov.*. 32**,** 103273. 10.1016/j.eti.2023.103273.

Zhai, W., Jiang, J., Park, C. B., 2022. A review on physical foaming of thermoplastic and vulcanized elastomers. *Polym Rev*. 62**,** 95-141. 10.1080/15583724.2021.1897996.

Zhang, M., Gao, C., Guo, X., Guo, S., Kang, Z., Xiao, D., Yan, J., Tao, F., Zhang, W., Dong, W., Liu, P., Yang, C., Ma, C., Xu, P., 2018. Increased glutarate production by blocking the glutaryl-CoA dehydrogenation pathway and a catabolic pathway involving l-2-hydroxyglutarate. *Nat. Commun*. 9**,** 2114. 10.1038/s41467-018-04513-0.

Zhang, M., Kang, Z., Guo, X., Guo, S., Xiao, D., Liu, Y., Ma, C., Xu, P., Gao, C., 2019. Regulation of Glutarate Catabolism by GntR Family Regulator CsiR and LysR Family Regulator GcdR in *Pseudomonas putida* KT2440. *mBio*. 10**,** 10.1128/mbio.01570-19. 10.1128/mbio.01570-19.

Zhang, Y., Liu, H., Liu, Y., Huo, K., Wang, S., Liu, R., Yang, C., 2021. A promoter engineering-based strategy enhances polyhydroxyalkanoate production in *Pseudomonas putida* KT2440. *Int. J. Biolog. Macromol*. 191**,** 608-617. 10.1016/j.ijbiomac.2021.09.142.

Zhou, J., Chen, Y., Zhang, Y., Sun, S., Ullah, M. W., Xu, W., 2021. Biotransformation of nylon-6,6 hydrolysate to bacterial cellulose. *Green Chem*. 23**,** 7805-7815. 10.1039/D1GC02129J.

Zhu, B., Wang, D., Wei, N., 2022a. Enzyme discovery and engineering for sustainable plastic recycling. *Trends Biotechnol*. 40**,** 22-37. 10.1016/j.tibtech.2021.02.008.

Zhu, F., Liu, D., Chen, Z., 2022b. Recent advances in biological production of 1,3-propanediol: new routes and engineering strategies. *Green Chem.* 10.1039/D1GC04288B.

Zobel, S., Benedetti, I., Eisenbach, L., de Lorenzo, V., Wierckx, N., Blank, L. M., 2015. Tn7-based device for calibrated heterologous gene expression in *Pseudomonas putida*. *ACS Synth. Biol.* 4**,** 1341-1351.

Zuin, V. G., Kümmerer, K., 2022. Chemistry and materials science for a sustainable circular polymeric economy. *Nat. Rev. Materials*. 7**,** 76-78. 10.1038/s41578-022-00415-2.

5 Appendix

5.1 Supplementary data to Chapter 2.1:

Microbial upcycling of polyamides using engineered Pseudomonas putida.

de Witt, J.[1], Luthe, T.[1], Jensen, K.[2], Polen, T.[1], Wirtz, A.[1], Frunzke, J.,[1], Wynands, B.[1], and Wierckx, N.[1*] (2024).

[1] Institute of Bio- and Geosciences IBG-1: Biotechnology, Forschungszentrum Jülich, Jülich, Germany

[2] Novozymes A/S, Biologiens Vej 2, Kgs. Lyngby DK-2800, Denmark

[*] Corresponding author
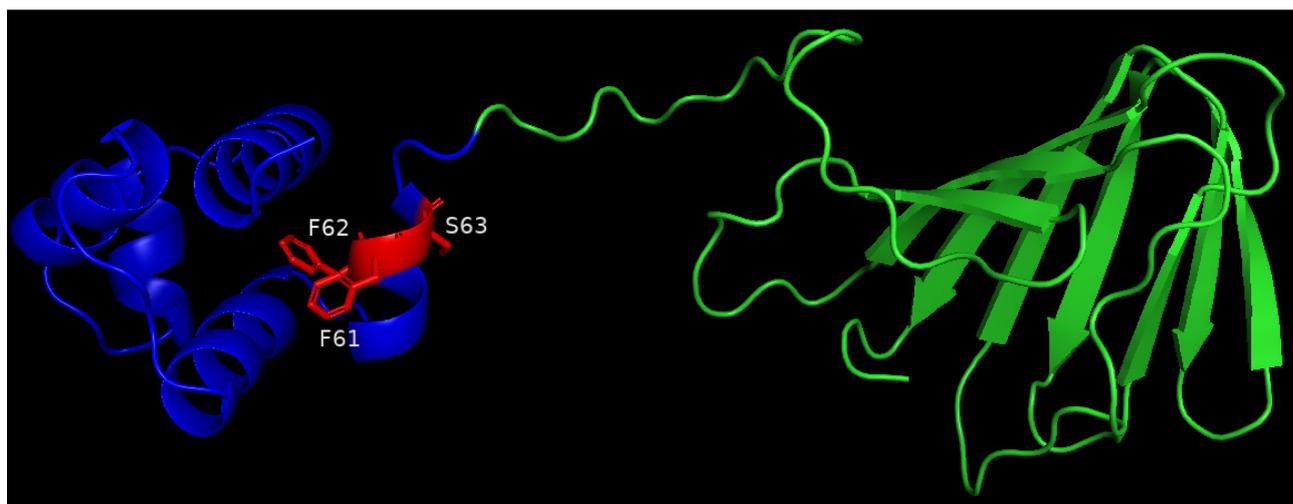
Figure S5.1-1. Predicted AlphaFold structure of the XRE family transcriptional regulator encoded by PP_2884. The DNA-binding domain is colored in blue and amino acids deleted in PP_2884$^{\Delta3}$ are labelled red and displayed as sticks (F61, F62, and S63).
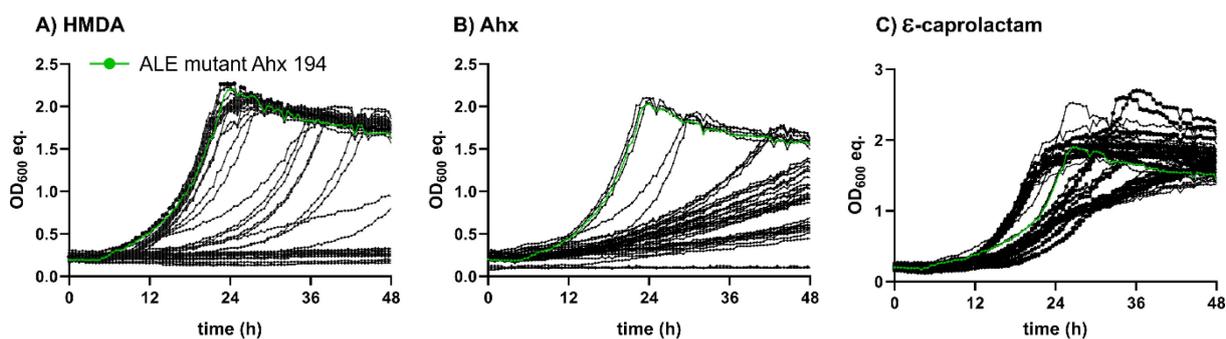
Figure S5.1-2. Screening of ALE mutants on C$_6$-PA monomers. Single clones were obtained from adaptive laboratory evolution of PP_2884$^{\Delta3}$ on Ahx and screened in MSM supplemented with 15 mM of the indicated substrate. ALE mutant Ahx-194 that was selected for whole-genome sequencing is highlighted in green.
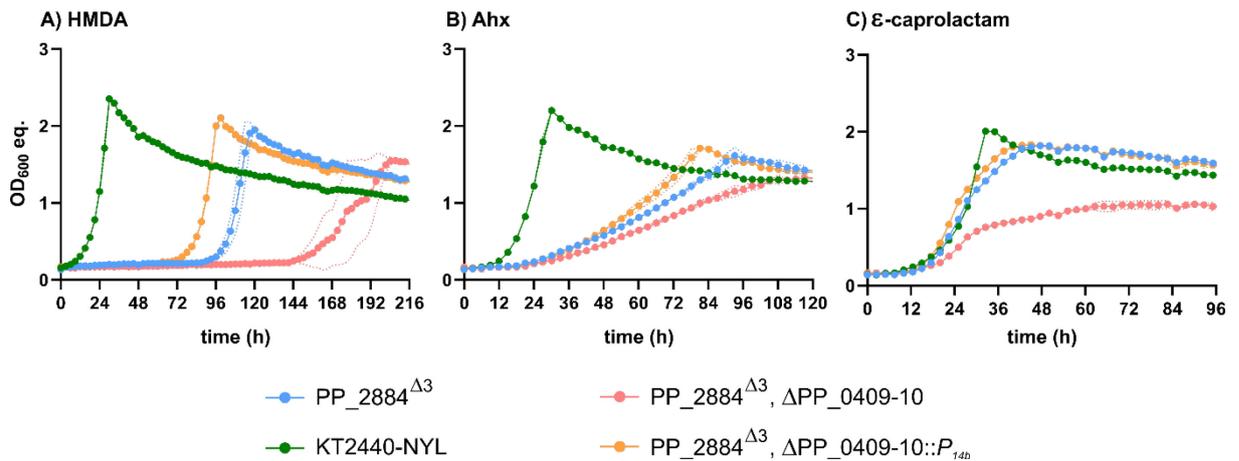
Figure S5.1-3. Effect of PP_0409-10 modifications in partly reverse engineered PP_2884$^{\Delta 3}$ strain. All strains were cultivated in MSM supplemented with 15 mM of the indicated carbon source. Deletion of PP_0409-10 (red) resulted in decreased growth with all C$_6$-PA monomers, whereas replacement by the constitutive promoter P_{14b} upstream of PP_0411-4 (ΔPP_0409-10::P_{14b}) (orange) increased growth. The mean values and standard deviations of three replicates are shown (n=3).
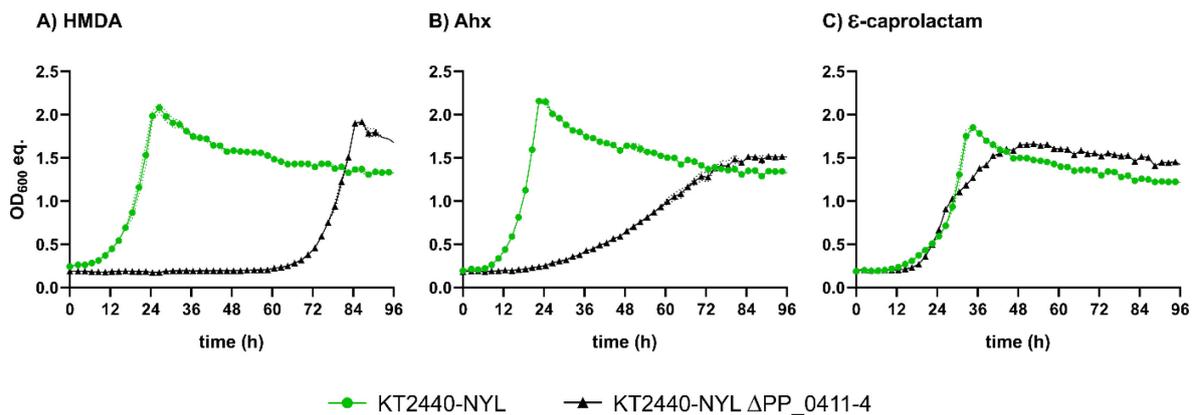
Figure S5.1-4. Effect of PP_0410-14 deletion on C$_6$-PA monomer metabolism. All strains were cultivated in MSM supplemented with 15 mM of the indicated carbon source. Deletion of PP_0410-4 resulted in decreased growth with all C$_6$-PA monomers. The mean values and standard deviations of three replicates are shown (n=3).
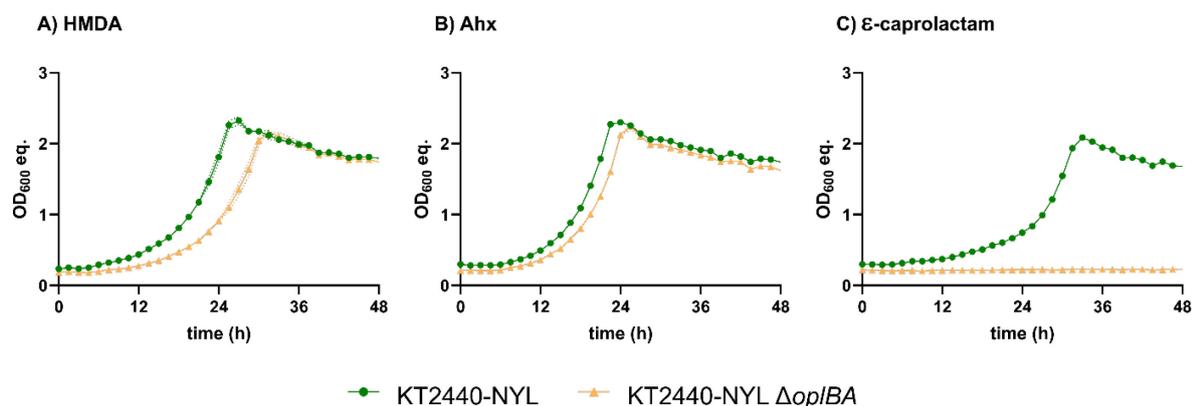
Figure S5.1-5. Effect of *oplBA* (PP_3514-5) deletion on growth with ε-caprolactam. Strains were cultivated in MSM supplemented with 15 mM of the indicated substrate. Deletion of *oplBA* (orange) abolished growth with ε-caprolactam while growth with HMDA and Ahx was not significantly altered. Hence, OplBA was revealed as ε-caprolactamase. The mean values and standard deviations of three replicates are shown (n=3).
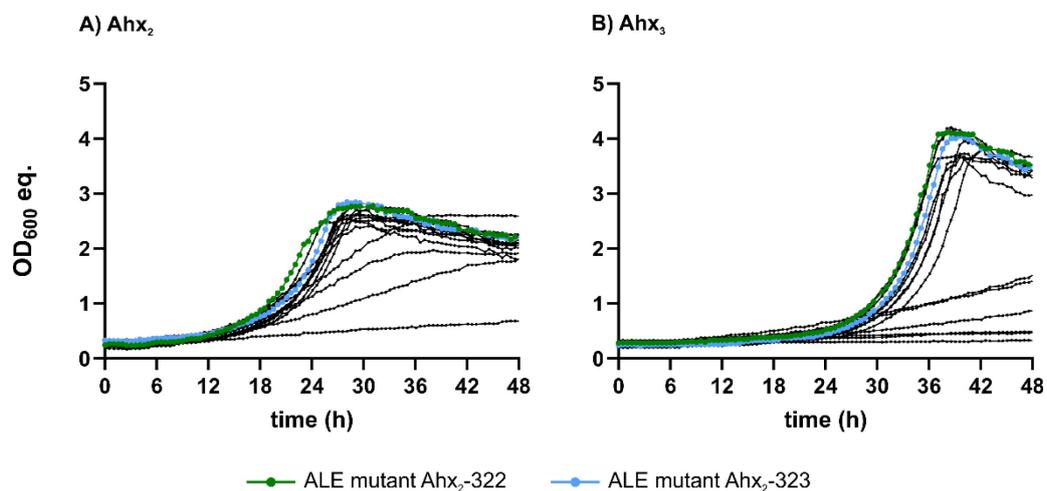
Figure S5.1-6. Screening of ALE mutants on Ahx-oligomers. Single clones were obtained from adaptive laboratory evolution of PP_2884$^{\Delta 3}$, PP_0409^{W676L}, P_{14f}-*nylB* on Ahx$_2$ and screened in MSM supplemented with 15 mM of the indicated oligomer. ALE mutant Ahx$_2$-322 (green) and ALE mutant Ahx$_2$-323 (blue) were selected for whole-genome sequencing.
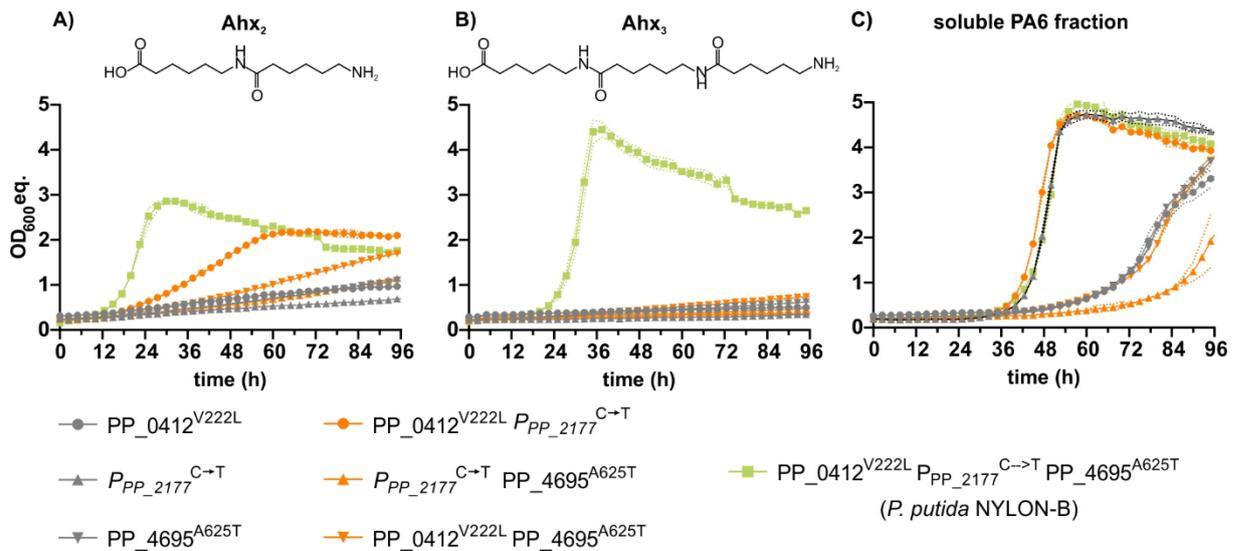
Figure S5.1-7. Reverse engineering of *P. putida* ALE-mutant Ahx₂-322. Combinations of the identified mutations were implemented in *P. putida* NYL P_{14f}–*nylB* and screened individually or in combination yielding the final reverse engineered strain *P. putida* NYLON-B. Strains were cultivated in MSM supplemented with 15 mM of the indicated oligomer or the PA6 soluble fraction. The mean values and standard deviations of three replicates are shown (n=3).
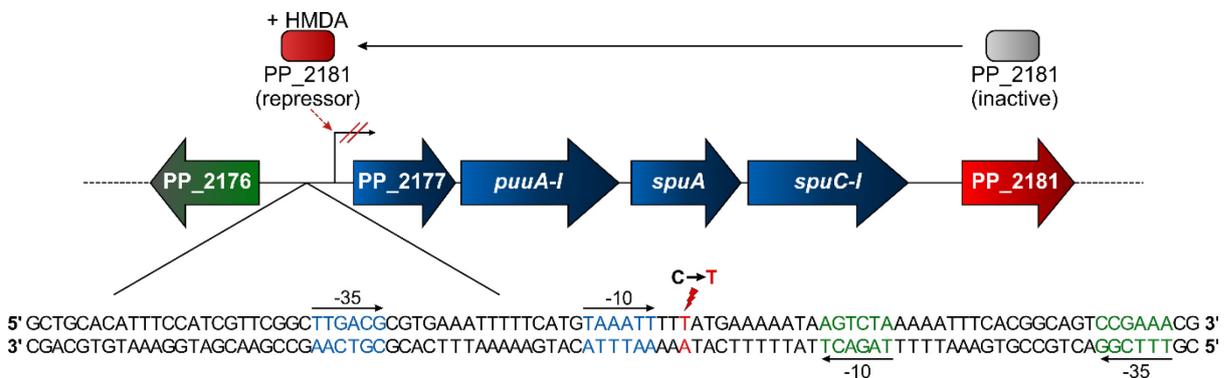
Figure S5.1-8. Genetic context of the identified mutation in ALE mutant Ahx₂-322. The mutation (C→T) (red flash) was located in close proximity to the predicted promoter regions of PP_2176 (green) and PP_2177-80 (blue). Downstream of PP_2177-80, its repressor PP_2181 is encoded that represses expression of the operon in the presence of HMDA and other amines (Schmidt et al., 2022). The mutation might enable constitutive expression of PP_2177-80 or prevent binding of PP_2181 thereby activating expression of PP_2177-80 in the absence of inducers. Promoter regions were predicted using SAPPHIRE (Coppens and Lavigne, 2020).

A) Linear Ahx$_{1-7}$
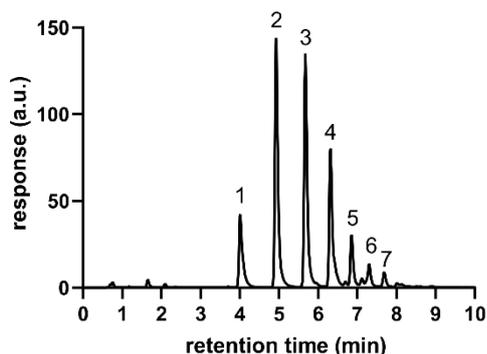
linear	concentration
Ahx$_1$	17.64 ± 1.96 µM
Ahx$_2$	95.03 ± 3.70 µM
Ahx$_3$	93.89 ± 3.36 µM
Ahx$_4$	56.67 ± 4.74 µM
Ahx$_5$	18.07 ± 1.88 µM
Ahx$_6$	10.96 ± 1.16 µM
Ahx$_7$	3.89 ± 0.48 µM

B) Cyclic Ahx$_{1-6}$
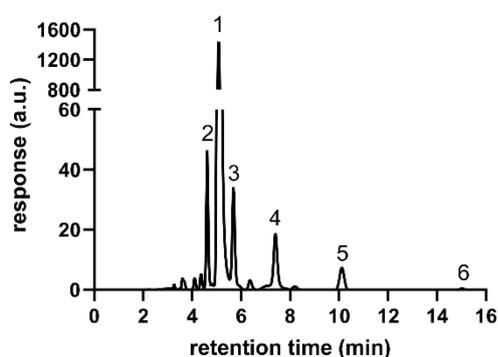
cyclic	concentration
Ahx$_1$	42.37 ± 0.41 mM
Ahx$_2$	unknown
Ahx$_3$	unknown
Ahx$_4$	unknown
Ahx$_5$	unknown
Ahx$_6$	unknown

Figure S5.1-9. Composition of the soluble PA6-fraction. HPLC chromatograms showing the separation of Ahx and linear Ahx$_{2-7}$ (A) or ε-caprolactam (cyclic Ahx$_1$) and cyclic Ahx$_{2-6}$ (B) that were detected using FLD and DAD, respectively. The concentration of the indicated compounds is shown. For cyclic Ahx$_{2-6}$, no standards were available preventing their quantification.

A) Acidic hydrolysis over time
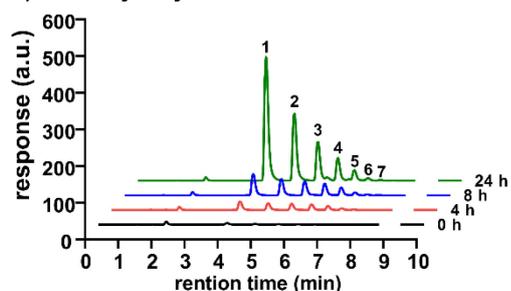
B) Composition in the PHB production medium

linear	concentration (mM)
Ahx$_1$	11.12 ± 0.41
Ahx$_2$	5.06 ± 0.11
Ahx$_3$	2.07 ± 0.01
Ahx$_4$	1.06 ± 0.03
Ahx$_5$	0.57 ± 0.03
Ahx$_6$	0.11 ± 0.01
Ahx$_7$	0.14 ± 0.00

Figure S5.1-10. Acidic hydrolysis of PA6. (A) HPLC chromatogram showing the release of soluble Ahx and Ahx$_{2-7}$ upon acidic hydrolysis after indicated hydrolysis time. Peak numbers correspond to the size (n) of Ahx$_n$. (B) Composition of the final MSM medium obtained from the PA6 hydrolysate that was used for the production of PHB.

Table S5.1-1. Up- and down-regulated genes in *P. putida P. putida* NYL compared to unevolved KT2440-AA under adipic acid-metabolizing conditions. Significant hits (FDR *p*-value < 0.01 and |log₂ fold change| > 1 are shown.

Name	Locus tag	Log₂ fold change	FDR p-value	Product
PP_0412	PP_0412	6.55354339	0	polyamine ABC transportersubstrate-binding protein
puuP	PP_1229	6.0237818	0	putrescine permease
PP_0414	PP_0414	5.75374521	0	polyamine ABC transporter permease
PP_0413	PP_0413	5.480252533	0	polyamine ABC transporter permease
PP_1228	PP_1228	4.754685153	0	methyl-accepting chemotaxis transducer
PP_2678	PP_2678	4.741244425	1.98848E-05	hydrolase
PP_2668	PP_2668	4.306936709	4.73141E-05	ABC transporter ATP-binding protein
PP_5538	PP_5538	4.286685901	0.001138722	ABC transporter substrate-binding protein
PP_2663	PP_2663	4.154316741	0.000813408	hypothetical protein
PP_2669	PP_2669	4.132807762	0.001038394	outer membrane protein
PP_2671	PP_2671	4.072046525	4.28975E-05	sensor histidine kinase
PedH	PP_2679	4.008935493	0.000793285	quinoprotein ethanol dehydrogenase
pqqD-II	PP_2681	3.988711887	0.004407143	coenzyme PQQ synthesis protein D
PP_2667	PP_2667	3.909554818	0.000422288	ABC transporter permease
PP_2677	PP_2677	3.872329565	0.000904126	hypothetical protein
PP_5279	PP_5279	3.757896509	0	hypothetical protein
exaE	PP_2672	3.68725639	0.000521384	transcriptional regulator ExaE
puuB	PP_2448	3.627270556	0	gamma-glutamylputrescine oxidase
PP_2676	PP_2676	3.586415556	0.009686807	substrate-binding protein
PP_2664	PP_2664	3.487122591	0.000254428	two-component system sensor histidine kinase/response regulator
PP_2666	PP_2666	3.412622208	0.005985024	hypothetical protein
spuC-II	PP_5182	3.19661723	0	polyamine:pyruvate transaminase
PP_3963	PP_3963	3.124548634	0	hypothetical protein
PP_5277	PP_5277	2.892572616	0	MFS transporter
spuB	PP_5183	2.847775771	0	glutamylpolyamine synthetase
PP_1227	PP_1227	2.803377699	0	membrane protein
kauB	PP_5278	2.688920996	0	4-guanidinobutyraldehyde dehydrogenase
PP_5393	PP_5393	2.492676072	0.003484579	metal-binding chaperone
PP_5398	PP_5398	2.490251377	0.008082868	transposase
spuH	PP_5177	2.421755271	0	spermidine/putrescine ABC transporter permease
PP_5729	PP_5729	2.400150429	0	hypothetical protein
pqqC	PP_0378	2.340271471	0.002776519	pyrroloquinoline-quinone synthase
PP_0375	PP_0375	2.322294231	0.000112931	prolyl oligopeptidase family protein
spuF	PP_5179	2.022531013	0	spermidine/putrescine ABC transporter ATP binding protein
PP_0875	PP_0875	2.014990825	7.10545E-06	hypothetical protein
PP_2134	PP_2134	1.989969966	0.000472841	transposase
PP_2257	PP_2257	1.961782675	1.54184E-08	aerotaxis receptor
spuE	PP_5180	1.829064364	2.60402E-14	spermidine/putrescine ABC transporter substrate-binding protein
pqqE	PP_0379	1.798713811	0.00404812	coenzyme PQQ synthesis protein E
pqqD-I	PP_0377	1.796915683	0.001439815	coenzyme PQQ synthesis protein D
PP_2737	PP_2737	1.779029147	0.000104737	short-chain dehydrogenase/reductase family oxidoreductase
spuG	PP_5178	1.739061297	9.03884E-14	spermidine/putrescine ABC transporter permease
PP_3875	PP_3875	1.706648365	3.61003E-05	hypothetical protein
PP_4443	PP_4443	1.671239702	2.00303E-07	transposase
PP_4605	PP_4605	1.562973163	1.2445E-11	AraC family transcriptional regulator
PP_2258	PP_2258	1.52553778	9.01892E-09	sensory box protein
lysA-I	PP_2077	1.521913938	0.00064205	diaminopimelate decarboxylase
PP_3877	PP_3877	1.456802022	0.000131043	hypothetical protein
PP_1935	PP_1935	1.434508933	8.42066E-05	Cro/CI family transcriptional regulator
PP_2532	PP_2532	1.432052545	4.80724E-07	hypothetical protein
PP_4604	PP_4604	1.413622585	3.06363E-07	DMT superfamily permease
PP_0874	PP_0874	1.407071699	1.47518E-05	hypothetical protein
PP_3871	PP_3871	1.401180421	0.00040189	hypothetical protein
PP_3883	PP_3883	1.37274629	0.001279833	holin
potF-I	PP_0873	1.34301109	8.30229E-05	putrescine-binding protein
PP_5176	PP_5176	1.339677267	0.000738421	hypothetical protein
PP_2736	PP_2736	1.326411393	0.001374222	hypothetical protein
PP_2861	PP_2861	1.321007679	0.003719498	methyl-accepting chemotaxis transducer
PP_3873	PP_3873	1.297755402	0.00169182	hypothetical protein
pcaY	PP_2643	1.293905122	7.5849E-06	aromatic acid chemoreceptor
PP_2511	PP_2511	1.288312628	0.00408432	hypothetical protein
PP_4589	PP_4589	1.28206728	8.39461E-05	D-isomer specific 2-hydroxyacid dehydrogenase family protein
cfa	PP_2734	1.257537877	0.000272856	cyclopropane-fatty-acyl-phospholipid synthase
PP_2729	PP_2729	1.256158464	0.009643762	hypothetical protein
PP_3863	PP_3863	1.224160001	0.006807305	tail protein
fliE	PP_4370	1.19320485	0.000957187	flagellar hook-basal body complex protein FliE
grx	PP_2958	1.186334339	0.000599448	glutaredoxin
PP_1487	PP_1487	1.186193818	0.007435816	hypothetical protein

PP_3864	PP_3864	1.159756795	0.001272126	FluMu DNA circulation protein
PP_1272	PP_1272	1.133846454	0.000272596	multidrug MFS transporter membrane fusion protein
PP_2730	PP_2730	1.121016297	0.008409583	lipoprotein
PP_2159	PP_2159	1.102773239	0.004632633	plastocyanin/azurin family copper-binding protein
PP_2884	PP_2884	1.101487096	0.000557674	XRE family transcriptional regulator
PP_3869	PP_3869	1.098436544	0.001077441	sheath protein
PP_4969	PP_4969	1.092796943	0.000655528	hypothetical protein
PP_2070	PP_2070	1.092601451	0.004658636	AraC family transcriptional regulator
PP_3598	PP_3598	1.092564579	0.001077441	peptidase C26
PP_2766	PP_2766	1.058570099	0.008412058	long-chain-fatty acid--CoA ligase-like protein
PP_3661	PP_3661	1.055702191	0.000962294	membrane protein
PP_2735	PP_2735	1.055034739	0.003824943	hypothetical protein
PP_3404	PP_3404	1.00696166	0.009643762	hypothetical protein
sodB	PP_0915	-1.004302367	0.008416083	superoxide dismutase
sahR	PP_4966	-1.005229609	0.009978945	methionine metabolism transcriptional regulator
PP_1846	PP_1846	-1.006492171	0.000598925	group II intron-encoding maturase
rpoA	PP_0479	-1.00685332	0.003613523	DNA-directed RNA polymerase subunit alpha
pvdY	PP_4245	-1.008389327	0.000266232	hydroxyproline acetylase
kgtP	PP_1400	-1.014612146	0.004066017	alpha-ketoglutarate permease
rplE	PP_0466	-1.015866692	0.000112453	50S ribosomal protein L5
PP_1508	PP_1508	-1.022112134	0.001281632	hypothetical protein
rnz	PP_4033	-1.022421123	0.009724391	ribonuclease Z
PP_1790	PP_1790	-1.024505433	0.004027313	acylneuraminate cytidylyltransferase
PP_5247	PP_5247	-1.024806435	0.005292642	hypothetical protein
PP_0870	PP_0870	-1.025095046	0.000958589	glycine betaine/carnitine/choline ABC transporter substrate-binding protein
rplS	PP_1465	-1.027521066	8.52797E-05	50S ribosomal protein L19
PP_5454	PP_5454	-1.03167671	0.000672661	membrane protein
PP_0103	PP_0103	-1.033110718	0.007717321	cytochrome c oxidase subunit 2
PP_4547	PP_4547	-1.035355365	0.00029706	glutamine synthetase
PP_5673	PP_5673	-1.035995186	0.007786679	D-alanine--D-alanine ligase
PP_1631	PP_1631	-1.040158748	0.000242966	hypothetical protein
PP_5467	PP_5467	-1.042089391	0.006523309	hypothetical protein
rpsK	PP_0477	-1.044377341	0.004091211	30S ribosomal protein S11
glpE	PP_3098	-1.049727437	0.00028722	thiosulfate sulfurtransferase GlpE
PP_5628	PP_5628	-1.056566356	0.000103451	hypothetical protein
PP_2126	PP_2126	-1.061771107	0.000473209	LuxR family transcriptional regulator
tsaA	PP_1084	-1.065241884	0.000227977	peroxiredoxin
PP_5667	PP_5667	-1.069049183	0.007409917	McbC family microcin B17-like processing protein
PP_5582	PP_5582	-1.069140706	0.006523309	hypothetical protein
pydB	PP_4036	-1.069887121	0.000933922	bifunctional D-hydantoinase/dihydropyrimidinase
arcC	PP_0999	-1.071511445	0.000167114	carbamate kinase
PP_3788	PP_3788	-1.073914446	0.002598121	non-ribosomal peptide synthetase
rplN	PP_0464	-1.074605757	0.000112453	50S ribosomal protein L14
PP_5575	PP_5575	-1.077941673	8.73227E-05	hypothetical protein
PP_1756	PP_1756	-1.079076575	0.003643645	hypothetical protein
PP_1245	PP_1245	-1.080503262	0.001844198	hypothetical protein
clsB	PP_3264	-1.080557995	0.000604709	cardiolipin synthase
PP_0333	PP_0333	-1.08125923	0.000306709	hypothetical protein
PP_1737	PP_1737	-1.085026171	0.000123736	hypothetical protein
PP_2189	PP_2189	-1.089245426	0.000476062	hypothetical protein
PP_2256	PP_2256	-1.090028278	6.11773E-05	Cro/CI family transcriptional regulator
rplP	PP_0461	-1.090101968	2.19899E-05	50S ribosomal protein L16
potF-II	PP_3147	-1.092707033	0.000332082	putrescine-binding protein
paaZ	PP_3270	-1.099304097	0.004377992	bifunctional oxepin-CoA hydrolase/3-oxo-5,6-dehydrosuberyl-CoA semialdehyde dehydrogenase
PP_2655	PP_2655	-1.099326074	0.00321272	hypothetical protein
PP_4273	PP_4273	-1.10156443	0.00337115	MerR family transcriptional regulator
PP_1746	PP_1746	-1.10309935	0.00070597	CsrA-like carbon storage regulator
rpmC	PP_0462	-1.109857684	0.000585062	50S ribosomal subunit protein L29
treSB	PP_4059	-1.110682305	0.002491713	bifunctional trehalose synthase B/maltokinase
PP_5427	PP_5427	-1.11121707	0.003450236	hypothetical protein
pgl	PP_1023	-1.113015344	0.002155703	6-phosphogluconolactonase
PP_5319	PP_5319	-1.119542539	0.000647554	hypothetical protein
PP_0195	PP_0195	-1.123846324	1.14044E-05	hypothetical protein
PP_3775	PP_3775	-1.123878618	0.001636617	sarcosine oxidase
PP_5329	PP_5329	-1.124005556	0.005563441	phosphate ABC transporter substrate-binding protein
PP_4986	PP_4986	-1.126840464	8.94836E-05	hemolysin III family channel protein
PP_3389	PP_3389	-1.13154905	4.95857E-05	membrane protein
PP_2573	PP_2573	-1.131766202	0.008421261	hypothetical protein
rpoE	PP_1427	-1.132159874	7.397E-05	RNA polymerase sigma E factor
PP_0352	PP_0352	-1.132229866	1.57288E-05	ECF family RNA polymerase sigma-70 factor
PP_5627	PP_5627	-1.132782859	0.004400868	hypothetical protein
yhjG	PP-4857	-1.133773686	0.002598121	protein YhjG
PP_0803	PP_0803	-1.138136028	0.000155317	protein secretion ABC transporter permease
ybhP-II	PP_4056	-1.141773873	0.000106523	phosphohydrolase
fba	PP_4960	-1.144817369	0.000121741	fructose-bisphosphate aldolase
msrQ	PP_4675	-1.153281427	0.000623186	methionine sulfoxide reductase heme-binding subunit

PP_0355	PP_0355	-1.162898841	0.00376196	two-component system response regulator
PP_0678	PP_0678	-1.163023857	0.000452481	hypothetical protein
PP_2121	PP_2121	-1.179728862	4.28975E-05	lipoprotein
PP_5661	PP_5661	-1.180327394	2.37824E-06	putative lipoprotein
metF	PP_4977	-1.180931332	0.000186854	5,10-methylenetetrahydrofolate reductase
PP_5474	PP_5474	-1.183887746	4.42387E-05	hypothetical protein
PP_2707	PP_2707	-1.184507164	0.004456822	exodeoxyribonuclease III
PP_3401	PP_3401	-1.187290479	0.003719498	hypothetical protein
PP_0683	PP_0683	-1.189874213	0.00064205	hypothetical protein
PP_0913	PP_0913	-1.189913521	3.61564E-06	hypothetical protein
tufB	PP_0452	-1.19228303	0.007940653	elongation factor Tu-B
PP_5589	PP_5589	-1.198104603	0.000744491	rhs repeat-associated core domain-containing protein
PP_2370	PP_2370	-1.199190456	0.000119112	hypothetical protein
PP_5290	PP_5290	-1.209282687	0.004698756	transposase
PP_0804	PP_0804	-1.216328976	5.68455E-06	protein secretion ABC transporter permease/ATP-binding protein
PP_2059	PP_2059	-1.218955596	3.15652E-05	hypothetical protein
PP_4074	PP_4074	-1.221206178	0.008416083	hypothetical protein
PP_1418	PP_1418	-1.221383713	0.007984309	tricarboxylate transport protein TctC
PP_5583	PP_5583	-1.224137744	3.69208E-06	hypothetical protein
sucB	PP_4188	-1.224706926	0.000944649	2-oxoglutarate dehydrogenase dihydrolipoyltranssuccinylase subunit
hyuC	PP_4034	-1.225110191	0.003560469	bifunctional N-carbamoyl-beta-alanine amidohydrolase/allantoine amidohydrolase
PP_5365	PP_5365	-1.22686672	8.86699E-05	fatty acid methyltransferase
PP_1417	PP_1417	-1.231282606	0.00321272	tricarboxylate transport protein TctB
PP_3779	PP_3779	-1.23202369	6.13659E-06	LysR family transcriptional regulator
PP_1538	PP_1538	-1.232973142	0.001889195	hypothetical protein
galU	PP_3821	-1.234599466	7.63689E-06	UTP-glucose-1-phosphate uridylyltransferase
PP_5565	PP_5565	-1.236331214	0.00321272	hypothetical protein
PP_5569	PP_5569	-1.236918481	0.009222252	hypothetical protein
ahcY	PP_4976	-1.246251306	9.03689E-07	adenosylhomocysteinase
treSA	PP_2918	-1.254362455	0.000806431	trehalose synthase A
PP_3323	PP_3323	-1.257667977	0.009901004	CobW/P47K family protein
pfpI	PP_2725	-1.263744473	0.001189018	protease PfpI
PP_1122	PP_1122	-1.264961657	0.000422288	OmpA family protein
PP_4423	PP_4423	-1.265637372	6.61968E-05	hypothetical protein
PP_3110	PP_3110	-1.26600586	0.000265085	hypothetical protein
hutF	PP_5036	-1.270401078	2.18769E-06	formiminoglutamate deiminase
nhaP	PP_4974	-1.27349159	0.000292967	NhaP-type Na+(K+)/H+ antiporter
PP_4218	PP_4218	-1.275341362	0.000506649	lipase/esterase family protein
PP_3109	PP_3109	-1.27755034	0.001438889	hypothetical protein
PP_0861	PP_0861	-1.279081029	0.000255121	outer membrane ferric siderophore receptor
gnuK	PP_3416	-1.27926808	1.82792E-05	D-gluconate kinase
PP_3145	PP_3145	-1.282506835	8.86699E-05	hypothetical protein
PP_3801	PP_3801	-1.283897613	3.05407E-06	cation ABC transporter substrate-binding protein
PP_3385	PP_3385	-1.288221903	6.92365E-05	hypothetical protein
fnrC	PP_3287	-1.292226262	1.90133E-05	Crp/Fnr family transcriptional regulator
PP_4464	PP_4464	-1.297491091	0.000791034	LysR family transcriptional regulator
PP_3784	PP_3784	-1.302566982	0.001220561	hypothetical protein
algC	PP_5288	-1.302737702	1.04022E-07	phosphomannomutase/phosphoglucomutase
PP_5726	PP_5726	-1.303274828	0.001428148	hypothetical protein
pntAA	PP_0156	-1.306098221	6.36922E-06	pyridine nucleotide transhydrogenase subunit alpha
PP_5693	PP_5693	-1.31107082	0.00132388	hypothetical protein
PP_1546	PP_1546	-1.316718902	0.006103223	hypothetical protein
pvdP	PP_4212	-1.322645874	1.53923E-06	pyoverdine biosynthesis-like protein
benB	PP_3162	-1.330503192	6.52443E-05	benzoate 1,2-dioxygenase subunit beta
pydX	PP_4037	-1.332870819	4.48568E-06	NADP-dependent dihydropyrimidine dehydrogenase subunit
mucA	PP_1428	-1.334567603	2.3269E-06	sigma factor AlgU negative regulator
dsbG	PP_4237	-1.33665131	0.00314946	protein disulfide isomerase
PP_1690	PP_1690	-1.337553807	8.40802E-05	hypothetical protein
PP_0754	PP_0754	-1.340807114	0.000422288	hypothetical protein
PP_2900	PP_2900	-1.341236186	5.0059E-07	hypothetical protein
folEB	PP_3324	-1.342072466	0.00408432	GTP cyclohydrolase I
ybhN	PP_3263	-1.343813798	0.000549166	phospholipid modification enzyme
paaB	PP_3277	-1.345185137	0.002742925	ring 1,2-phenylacetyl-CoA epoxidase regulatory subunit
PP_3107	PP_3107	-1.350664985	3.01873E-08	hypothetical protein
PP_2297	PP_2297	-1.35158664	0.006577435	integrase
PP_4254	PP_4254	-1.354786155	0.0005813	hypothetical protein
PP_2419	PP_2419	-1.356774987	9.99069E-06	membrane protein
PP_4032	PP_4032	-1.358672698	8.62713E-05	lipoprotein Blc
PP_4041	PP_4041	-1.3594447	0.004632633	glycoside hydrolase
PP_2292	PP_2292	-1.362967522	9.15627E-05	hypothetical protein
paoB	PP_3309	-1.364702312	0.000266232	aromatic aldehyde dehydrogenase FAD-binding subunit
PP_5488	PP_5488	-1.368417649	0.000314497	hypothetical protein
PP_1533	PP_1533	-1.370097862	0.009375481	excisionase
gtsB	PP_1016	-1.370658257	2.34985E-05	ABC transporter permease
paaD	PP_3275	-1.371133126	0.001921771	1,2-phenylacetyl-CoA epoxidase subunit D
PP_5252	PP_5252	-1.373287676	3.60983E-07	hypothetical protein
hupN	PP_0975	-1.378492759	5.1216E-06	DNA-binding protein HU

paaI	PP_3281	-1.381835581	0.002014606	hydroxyphenylacetyl-CoA thioesterase
PP_3797	PP_3797	-1.382810696	1.77814E-05	membrane protein
pvdQ	PP_2901	-1.389547803	2.72893E-08	acyl-homoserine lactone acylase PvdQ
PP_5580	PP_5580	-1.392673389	1.59782E-05	hypothetical protein
PP_3785	PP_3785	-1.395136098	9.15627E-05	hypothetical protein
pydA	PP_3796	-1.395471237	0.008409583	NADP-dependent dihydropyrimidine dehydrogenase subunit PreA
benC	PP_3163	-1.3999966	0.000422288	benzoate 1,2-dioxygenase electron transfer component
PP_3090	PP_3090	-1.401828986	6.11431E-08	OmpA domain-containing protein
PP_1102	PP_1102	-1.415846613	0.000363678	hypothetical protein
PP_3823	PP_3823	-1.418055642	1.86916E-06	cytochrome c-type protein
paaE	PP_3274	-1.419263088	0.005551091	ring 1,2-phenylacetyl-CoA epoxidase reductase subunit
kdgD	PP_3599	-1.429055853	5.41911E-07	5-dehydro-4-deoxyglucarate dehydratase
glpK	PP_1075	-1.436546298	0.001132108	glycerol kinase
PP_5503	PP_5503	-1.438508424	1.97596E-07	CheA signal transduction histidine kinase
PP_0655	PP_0655	-1.441153754	6.63645E-06	fimbrial-like protein
PP_1545	PP_1545	-1.441613647	7.26721E-05	hypothetical protein
PP_1729	PP_1729	-1.447599679	0.000314497	hypothetical protein
PP_3273	PP_3273	-1.450100749	6.68559E-06	hypothetical protein
PP_1193	PP_1193	-1.45105709	0.009648958	membrane protein
mucB	PP_1429	-1.451375948	6.68698E-09	sigma factor AlgU regulator MucB
PP_2570	PP_2570	-1.452030292	8.86699E-05	transposase
katG	PP_3668	-1.468480511	0.000506649	catalase-peroxidase
PP_5568	PP_5568	-1.474349217	8.69497E-09	membrane protein
PP_3016	PP_3016	-1.486886643	7.51638E-05	lipopolysaccharide core biosynthesis protein
PP_2377	PP_2377	-1.491483951	9.57271E-09	acyltransferase
PP_4070	PP_4070	-1.492406043	2.80609E-06	hypothetical protein
yehW	PP_0869	-1.496961201	7.66932E-12	osmoprotectant ABC transporter permease
PP_2251	PP_2251	-1.498271516	8.31694E-07	membrane protein
PP_5266	PP_5266	-1.509181661	1.64107E-06	acetyl-CoA hydrolase family protein
opdP	PP_0883	-1.510408326	8.69157E-09	glycine-glutamate dipeptide porin
PP_3782	PP_3782	-1.511712392	1.86291E-07	hypothetical protein
PP_2474	PP_2474	-1.516785213	1.47697E-09	glutathione S-transferase family protein
paaA	PP_3278	-1.532642272	0.000325482	ring 1,2-phenylacetyl-CoA epoxidase subunit alpha
PP_5362	PP_5362	-1.534528652	0.000155317	hypothetical protein
PP_0319	PP_0319	-1.536999594	2.56727E-10	hypothetical protein
PP_3765	PP_3765	-1.539454235	0.000112453	H-NS family protein MvaT
yeaG	PP_0397	-1.548679981	2.77631E-10	protein kinase
cpo	PP_4021	-1.555666433	6.52443E-05	non-heme chloroperoxidase
PP_1105	PP_1105	-1.557022132	1.59643E-05	ATP-dependent DNA ligase
PP_1660	PP_1660	-1.563755253	1.93552E-06	hypothetical protein
PP_5363	PP_5363	-1.563842859	7.38193E-05	hypothetical protein
PP_3824	PP_3824	-1.569953483	7.5849E-06	hypothetical protein
ybhP-I	PP_3265	-1.570371642	0.000158589	phosphohydrolase
algP	PP_0194	-1.577046565	6.1179E-07	transcriptional regulator AlgP
PP_1473	PP_1473	-1.579585454	0.000189998	hypothetical protein
aspC	PP_3786	-1.579966998	2.64415E-10	aminotransferase
PP_3798	PP_3798	-1.581395948	7.77363E-08	hypothetical protein
PP_0805	PP_0805	-1.59099919	4.26278E-10	outer membrane efflux protein
dppA-I	PP_0882	-1.592351852	5.53788E-05	dipeptide ABC transporter substrate-binding protein
yiaD	PP_0773	-1.594230822	0.000326811	OmpA/MotB domain-containing protein
pstS	PP_2656	-1.596945932	0.001267452	phosphate ABC transporter substrate-binding protein
PP_3774	PP_3774	-1.596967847	0.0001502	hypothetical protein
PP_5238	PP_5238	-1.598394352	1.45936E-06	hypothetical protein
PP_3799	PP_3799	-1.598958571	3.14356E-06	hypothetical protein
PP_3158	PP_3158	-1.601612382	8.98679E-08	hypothetical protein
PP_3113	PP_3113	-1.602969267	4.28975E-05	transposase
PP_3091	PP_3091	-1.607907237	5.71967E-06	membrane protein
ygaU	PP_0258	-1.610290686	3.01888E-07	murein cross-linking regulator
phaK	PP_3271	-1.61069161	0.002559974	phenylacetic acid-specific porin
PP_5472	PP_5472	-1.611157835	0.000778498	hypothetical protein
fpvA	PP_4217	-1.613250913	0.000441106	TonB-dependent outer membrane ferripyoverdine receptor FpvA
PP_5699	PP_5699	-1.618839064	0.000477819	iron uptake protein
paaC	PP_3276	-1.621817601	0.001094803	ring 1,2-phenylacetyl-CoA epoxidase subunit beta
pagL-I	PP_0737	-1.621857944	9.14269E-06	lipid A 3-O-deacylase
PP_5473	PP_5473	-1.625984614	0.000211552	LuxR family transcriptional regulator
PP_5700	PP_5700	-1.631079853	0.000963047	hypothetical protein
algR	PP_0185	-1.63307748	0.000476062	alginate biosynthesis regulatory protein
glgE	PP_4060	-1.63589528	0.001077441	alpha-1,4-glucan:maltose-1-phosphate maltosyltransferase
PP_5596	PP_5596	-1.636142494	8.52797E-05	hypothetical protein
PP_2291	PP_2291	-1.644154184	5.24183E-06	hypothetical protein
PP_3096	PP_3096	-1.648480796	1.26174E-10	hypothetical protein
PP_5037	PP_5037	-1.658250956	8.2643E-08	lipocalin family lipoprotein
htrG	PP_3631	-1.659022289	7.31226E-05	signal transduction protein
metK	PP_4967	-1.660432738	2.70466E-11	methionine adenosyltransferase
PP_1246	PP_1246	-1.66295319	3.62051E-10	hypothetical protein
gpD	PP_3065	-1.668572541	4.57941E-08	tail formation
PP_1478	PP_1478	-1.671183531	0.000102088	xenobiotic reductase

PP_4557	PP_4557	-1.67135864	0.006376778	hypothetical protein
proP	PP_2914	-1.672397306	2.76723E-06	osmosensory proline/betaine/H+ permease
PP_3094	PP_3094	-1.676964043	1.55475E-09	hypothetical protein
PP_4415	PP_4415	-1.679378653	1.57756E-07	hypothetical protein
PP_2347	PP_2347	-1.695601636	0.000119112	two-component system response regulator
syrB	PP_3783	-1.716430652	2.26039E-06	syringomycin biosynthesis protein 2
PP_3092	PP_3092	-1.728884137	7.52907E-10	hypothetical protein
PP_0235	PP_0235	-1.729551437	3.53095E-12	peroxidase
PP_1659	PP_1659	-1.736111462	1.32932E-09	hypothetical protein
PP_5432	PP_5432	-1.747084663	2.77631E-10	hypothetical protein
PP_4118	PP_4118	-1.759138272	3.06363E-07	membrane protein
PP_2857	PP_2857	-1.76349642	6.65831E-05	hypothetical protein
oprF	PP_2089	-1.766506388	5.86462E-09	porin F
PP_1006	PP_1006	-1.768119591	8.30464E-09	heme receptor
PP_0150	PP_0150	-1.774952334	4.44721E-11	hypothetical protein
PP_0886	PP_0886	-1.777965648	0.003778516	hypothetical protein
PP_1357	PP_1357	-1.778313462	2.00303E-06	hypothetical protein
pvdD	PP_4219	-1.783008387	3.47911E-06	non-ribosomal peptide synthetase
PP_0255	PP_0255	-1.790998138	0.000583512	hypothetical protein
PP_5567	PP_5567	-1.795128471	5.31108E-10	hypothetical protein
yqaE	PP_0373	-1.795727631	3.04782E-06	membrane protein
PP_4470	PP_4470	-1.79904662	1.60037E-11	Arc domain-containing transcriptional regulator
clpV	PP_3095	-1.800823836	8.69157E-09	protein ClpV1
PP_5725	PP_5725	-1.806143756	3.79499E-09	hypothetical protein
PP_4139	PP_4139	-1.813822626	3.21119E-07	hypothetical protein
PP_3800	PP_3800	-1.839656559	3.13819E-10	hypothetical protein
glpF	PP_1076	-1.845096142	0	aquaglyceroporin
PP_3639	PP_3639	-1.845942135	0.001982003	alkylhydroperoxidase AhpD domain-containing protein
PP_1121	PP_1121	-1.849214371	3.30525E-10	OmpA family protein
PP_4504	PP_4504	-1.852131886	5.00394E-05	hypothetical protein
PP_5562	PP_5562	-1.852786743	1.01247E-11	hypothetical protein
PP_3928	PP_3928	-1.863223189	0.000106905	hypothetical protein
PP_1106	PP_1106	-1.869386075	7.6773E-06	hypothetical protein
yegS	PP_2125	-1.873595095	7.80425E-08	lipid kinase
PP_0330	PP_0330	-1.876841463	4.90562E-09	hypothetical protein
pntAB	PP_5747	-1.889956688	3.91659E-08	pyridine nucleotide transhydrogenase subunit alpha
ycfJ	PP_0837	-1.901149717	0.000549166	flagella biosynthesis regulator
PP_5334	PP_5334	-1.901732044	1.98372E-08	membrane protein
PP_1829	PP_1829	-1.911219443	5.08435E-13	alpha/beta family hydrolase
PP_3269	PP_3269	-1.912029822	0.00217261	hypothetical protein
PP_4176	PP_4176	-1.918238087	1.43673E-07	5-oxo-L-prolinase
PP_4096	PP_4096	-1.924589001	2.27516E-10	hypothetical protein
PP_2290	PP_2290	-1.929221396	0.000462611	hypothetical protein
PP_5702	PP_5702	-1.957134475	1.28897E-06	hypothetical protein
PP_3321	PP_3321	-1.960260836	5.41911E-07	hypothetical protein
PP_2346	PP_2346	-1.988371075	4.02134E-05	hypothetical protein
PP_5360	PP_5360	-2.01245328	8.53374E-07	hypothetical protein
PP_1446	PP_1446	-2.017292519	5.92452E-08	TonB-dependent receptor
PP_3100	PP_3100	-2.01830604	1.76081E-14	hypothetical protein
PP_5561	PP_5561	-2.020449262	7.18095E-11	hypothetical protein
PP_1370	PP_1370	-2.035738121	3.4238E-14	group 1 family glycosyl transferase
arcB	PP_1000	-2.053563284	6.43276E-07	ornithine carbamoyltransferase
PP_3097	PP_3097	-2.070777636	0	hypothetical protein
PP_1537	PP_1537	-2.11197458	0.007786679	hypothetical protein
pvdI	PP_4221	-2.118331884	1.21953E-08	non-ribosomal peptide synthetase
fadE	PP_1893	-2.147295851	7.26423E-06	medium-long chain acyl-CoA dehydrogenase
PP_2856	PP_2856	-2.148049858	2.64106E-05	hypothetical protein
PP_3093	PP_3093	-2.151385007	0	hypothetical protein
opdH	PP_1419	-2.156053163	1.29329E-08	tricarboxylate-specific outer membrane porin
PP_5520	PP_5520	-2.165895757	1.07228E-05	hypothetical protein
PP_4222	PP_4222	-2.173861375	4.22113E-14	protein SyrP
PP_3098	PP_3098	-2.175055082	0.00011267	hypothetical protein
PP_4296	PP_4296	-2.178385271	0.006235956	hypothetical protein
PP_3612	PP_3612	-2.225644254	5.23125E-12	TonB-dependent receptor
PP_4851	PP_4851	-2.227553202	3.58849E-13	phosphate starvation-inducible protein PsiF
pvdH	PP_4223	-2.233842612	0	diaminobutyrate-2-oxoglutarate transaminase
osmC	PP_0089	-2.244215152	2.63668E-09	stress-induced peroxiredoxin
acnA-I	PP_2112	-2.262418057	3.81338E-08	aconitate hydratase
PP_4978	PP_4978	-2.276630401	2.24547E-09	hypothetical protein
PP_5560	PP_5560	-2.285092727	0.006756275	hypothetical protein
PP_5151	PP_5151	-2.292918271	1.48379E-09	hypothetical protein
PP_1691	PP_1691	-2.295629553	6.13482E-07	hypothetical protein
pvdR	PP_4209	-2.295769234	3.52163E-12	ABC transporter permease
PP_4856	PP_4856	-2.337448971	3.00241E-13	Dps family ferritin
PP_0679	PP_0679	-2.340705498	1.37456E-10	hypothetical protein
ycaC-I	PP_0711	-2.341024739	2.3926E-11	putative hydrolase
PP_5361	PP_5361	-2.387410235	1.8841E-07	protein P47K

PP_3930	PP_3930	-2.390672708	2.70274E-12	hypothetical protein
pvdN	PP_4214	-2.411594053	0	pyoverdine biosynthesis-like protein
speC	PP_0864	-2.435615768	2.03915E-08	ornithine decarboxylase
pvdL	PP_4243	-2.440742369	0	non-ribosomal peptide synthetase
glpD	PP_1073	-2.447267258	3.86989E-07	aerobic glycerol-3-phosphate dehydrogenase
pvdM	PP_4213	-2.453350044	0	dipeptidase
PP_3266	PP_3266	-2.461750084	7.66932E-12	hypothetical protein
PP_0092	PP_0092	-2.461863333	1.76081E-14	putative lipoprotein
puuD	PP_3099	-2.473637182	2.08629E-11	uricase/urate oxidase
PP_3614	PP_3614	-2.49617172	1.15285E-11	membrane protein
PP_3088	PP_3088	-2.497084611	0	hypothetical protein
PP_3089	PP_3089	-2.506118062	0	hypothetical protein
fumC-II	PP_1755	-2.510916227	7.1404E-12	class 2 fumarate hydratase
PP_2858	PP_2858	-2.541692668	2.27516E-10	hypothetical protein
PP_0216	PP_0216	-2.542103244	0	sensory box/GGDEF family protein
PP_0085	PP_0085	-2.616077839	5.82972E-14	hypothetical protein
PP_1504	PP_1504	-2.625551534	7.64753E-12	hypothetical protein
PP_3743	PP_3743	-2.63445036	9.33765E-15	hypothetical protein
PP_4441	PP_4441	-2.65490085	0.000255121	transposase
pvdJ	PP_4220	-2.665947497	0	non-ribosomal peptide synthetase
pvdO	PP_4215	-2.704056493	0	pyoverdine biosynthesis-like protein
pvdE	PP_4216	-2.709396596	0	pyoverdine ABC transporter ATP-binding protein/permease
PP_2172	PP_2172	-2.709511875	1.76081E-14	hypothetical protein
PP_1744	PP_1744	-2.710056633	0	hypothetical protein
PP_2662	PP_2662	-2.710530648	1.60355E-05	hypothetical protein
PP_1101	PP_1101	-2.711266383	0	hypothetical protein
pvdS	PP_4244	-2.711930655	1.76081E-14	alternative sigma factor
PP_4738	PP_4738	-2.715221615	6.77152E-13	hypothetical protein
PP_1276	PP_1276	-2.72706299	9.0672E-10	hypothetical protein
PP_3807	PP_3807	-2.784875911	0	thioesterase
PP_4615	PP_4615	-2.809010736	0	membrane protein
sodA	PP_0946	-2.823824885	0	superoxide dismutase
PP_3325	PP_3325	-2.850177229	0	ferric siderophore receptor
PP_3241	PP_3241	-2.889819294	0	hypothetical protein
PP_1839	PP_1839	-2.906442435	0	hypothetical protein
PP_3326	PP_3326	-2.910098459	3.36342E-10	hypothetical protein
PP_3504	PP_3504	-3.048893359	0	hypothetical protein
PP_1157	PP_1157	-3.087601313	1.43549E-12	acetolactate synthase
PP_5525	PP_5525	-3.116210335	2.87264E-11	hypothetical protein
PP_1503	PP_1503	-3.257390765	0	hypothetical protein
asnB	PP_1750	-3.369189785	0	asparagine synthetase
PP_2345	PP_2345	-3.37016511	0	hypothetical protein
PP_1749	PP_1749	-3.388142291	0	acetyltransferase
PP_1748	PP_1748	-3.416425765	0	hypothetical protein
PP_4855	PP_4855	-3.417341486	2.96137E-13	osmotically-inducible lipoprotein OsmE
PP_3808	PP_3808	-3.437639537	0	antibiotic synthesis protein MbtH
pvdA	PP_3796	-3.572107993	0	L-ornithine 5-monooxygenase
fumC-I	PP_0944	-3.580357677	0	class 2 fumarate hydratase
PP_5073	PP_5073	-3.624012478	0	hypothetical protein
PP_4614	PP_4614	-3.643253049	1.86507E-13	hypothetical protein
PP_1502	PP_1502	-3.656799001	9.33765E-15	OmpA family protein
PP_0945	PP_0945	-3.788120643	0	hypothetical protein
PP_3929	PP_3929	-3.869598174	0	hypothetical protein
cynT	PP_0100	-3.995667181	0	carbonic anhydrase
algL	PP_1281	-4.347244734	0	alginate lyase
algG	PP_1283	-4.534529227	0	poly(beta-D-mannuronate) C5 epimerase
PP_0943	PP_0943	-4.704372216	0	hypothetical protein
PP_0101	PP_0101	-4.866188951	0	sulfate transporter
algA	PP_1277	-5.129290024	0	mannose-6-phosphate isomerase/mannose-1-phosphate guanylyltransferase
algX	PP_1282	-5.397827064	0	alginate biosynthesis protein AlgX
alg8	PP_1287	-5.44884335	0	glycosyltransferase Alg8
algJ	PP_1279	-5.689627184	0	alginate O-acetylase AlgJ
algI	PP_1280	-5.728188049	0	alginate O-acetylase AlgI
algF	PP_1278	-6.097672855	0	alginate biosynthesis protein AlgF
algE	PP_1284	-6.25043168	0	alginate production protein AlgE
alg44	PP_1286	-6.285596202	0	alginate biosynthesis protein Alg44
algK	PP_1285	-6.37866192	0	alginate biosynthesis protein AlgK
algD	PP_1288	-7.772824306	0	GDP-mannose 6-dehydrogenase

Table S5.1-2. Up- and down-regulated genes in *P. putida* NYL under Ahx-metabolizing conditions compared to AA-metabolizing conditions. Significant hits (FDR p-value < 0.01 and |log2 fold change| > 1 are shown.

Name	Locus tag	Log$_2$ fold change	FDR p-value	Product
PP_4437	PP_4437	10.014243	0.0062926	transposase
dadA-II	PP_5270	6.04273245	0	D-amino acid:quinone oxidoreductase
dadX	PP_5269	5.79951151	0	alanine racemase
dadA-I	PP_4434	4.73879331	0	D-amino acid dehydrogenase small subunit
PP_4435	PP_4435	4.3738703	0	hypothetical protein
PP_5242	PP_5242	3.98743461	0	GAF domain-containing sensor histidine kinase
norM	PP_5262	3.28700639	0	multidrug resistance protein NorM
ytnA	PP_1059	3.22024709	0	amino acid permease YtnA
ybgL	PP_2920	3.09394591	0	nitrogen-containing compound degradation protein
PP_2511	PP_2511	3.09106599	0	hypothetical protein
PP_2737	PP_2737	3.07356654	0	short-chain dehydrogenase/reductase family oxidoreductase
PP_2738	PP_2738	3.00128797	0	putative Transcriptional regulator
cfa	PP_2734	2.87182462	0	cyclopropane-fatty-acyl-phospholipid synthase
PP_5343	PP_5343	2.84314623	0	putative Transcriptional regulator
PP_2729	PP_2729	2.76674118	0	hypothetical protein
PP_2733	PP_2733	2.67311827	0	membrane protein
folEA-II	PP_2512	2.67121617	0	GTP cyclohydrolase I
PP_0596	PP_0596	2.62882683	0	omega-amino acid--pyruvate aminotransferase
PP_5344	PP_5344	2.53622609	0	acetyltransferase
PP_3504	PP_3504	2.48995148	0	hypothetical protein
PP_2735	PP_2735	2.45821976	0	hypothetical protein
pqqB	PP_0379	2.40102788	0.00034093	coenzyme PQQ synthesis protein B
ycaC-II	PP_5243	2.38545252	0	putative hydrolase
PP_5241	PP_5241	2.35939691	0	LuxR family transcriptional regulator
PP_2736	PP_2736	2.29021961	0	hypothetical protein
PP_0874	PP_0874	2.2503197	0	hypothetical protein
mmsA-I	PP_0597	2.21951782	0	methylmalonate-semialdehyde dehydrogenase
potF-I	PP_0873	2.2108787	0	putrescine-binding protein
PP_5345	PP_5345	2.16387924	0	acetyltransferase
PP_5535	PP_5535	2.14111467	0	membrane protein
PP_5240	PP_5240	2.09396608	1.8622E-10	two-component system response regulator
PP_4488	PP_4488	2.09097956	0.00911996	hypothetical protein
PP_2730	PP_2730	2.06033611	3.2017E-11	lipoprotein
galD	PP_2513	2.00137345	0	4-oxalomesaconate tautomerase
gabT	PP_0214	1.97773269	0	5-aminovalerate aminotransferase DavT
fdhA	PP_0328	1.96964085	0	formaldehyde dehydrogenase
PP_0875	PP_0875	1.84999985	0	hypothetical protein
PP_2731	PP_2731	1.82166972	8.9101E-14	hypothetical protein
PP_2728	PP_2728	1.78234917	1.4485E-07	hypothetical protein
ribB	PP_0530	1.74365344	0	3,4-dihydroxy-2-butanone-4-phosphate synthase
PP_0544	PP_0544	1.7418056	0.0062926	ethanolamine transporter
PP_2732	PP_2732	1.68577459	0	hypothetical protein
dapA-II	PP_2639	1.67534268	0	4-hydroxy-tetrahydrodipicolinate synthase
PP_4547	PP_4547	1.67349526	0	glutamine synthetase
PP_5729	PP_5729	1.6148288	0	hypothetical protein
aceA	PP_4116	1.57459117	0.0004611	isocitrate lyase
glyA-I	PP_0322	1.57046425	0	serine hydroxymethyltransferase
soxB	PP_0323	1.55997657	4.4572E-09	sarcosine oxidase subunit beta
gabD-I	PP_0213	1.53814503	7.2428E-05	succinate-semialdehyde dehydrogenase
PP_0643	PP_0643	1.52994561	0.00803794	hypothetical protein
PP_5659	PP_5659	1.50070312	1.1039E-12	hypothetical protein
actP-I	PP_1743	1.48781425	0.00593401	acetate permease
PP_4665	PP_4665	1.46404113	2.5097E-09	hypothetical protein
aspA	PP_5338	1.44535534	0	aspartate ammonia-lyase
PP_0313	PP_0313	1.43918159	0.00048226	electron transfer flavoprotein subunit beta
bioF	PP_0363	1.42627211	0.00014442	8-amino-7-oxononanoate synthase
davB	PP_0383	1.36416828	2.8971E-11	lysine 2-monooxygenase
PP_5244	PP_5244	1.34523473	0.00015259	AraC family transcriptional regulator
catB	PP_3715	1.30247017	0	muconate cycloisomerase 1
PP_2922	PP_2922	1.29153134	6.1012E-11	urea amidolyase-like protein
PP_5279	PP_5279	1.28665795	0.0061008	hypothetical protein
PP_2446	PP_2446	1.2833956	0.00156909	hypothetical protein
PP_2875	PP_2875	1.27089459	8.1836E-06	hypothetical protein
PP_0275	PP_0275	1.26266719	0.00012215	hypothetical protein
bioC	PP_0365	1.23193864	0.00346877	malonyl-ACP O-methyltransferase
PP_5176	PP_5176	1.22698111	4.7122E-11	hypothetical protein
betX	PP_1741	1.2085547	8.0037E-15	choline/betaine/carnitine ABC transporter substrate-binding protein BetX
catC	PP_3714	1.20305616	0	muconolactone delta-isomerase
dgcA	PP_0310	1.18750745	0	dimethylglycine dehydrogenase subunit

PP_0153	PP_0153	1.18629386	2.9149E-10	hypothetical protein
PP_2177	PP_2177	1.14892065	6.2909E-06	transcriptional regulator
soxA	PP_0325	1.1420592	0	sarcosine oxidase subunit alpha
PP_2086	PP_2086	1.14102141	0	CrfX family protein
PP_0738	PP_0738	1.12958407	0	hypothetical protein
betA-I	PP_0056	1.12752979	0	choline dehydrogenase
PP_0308	PP_0308	1.12360835	9.5377E-14	dipeptidase
bioH	PP_0364	1.11345206	0.00751616	pimeloyl-ACP methyl ester esterase
dgcB	PP_0311	1.11237141	8.628E-13	dimethylglycine dehydrogenase subunit
PP_2921	PP_2921	1.09428062	4.272E-13	hypothetical protein
caiX	PP_0304	1.09008365	3.5108E-06	carnitine uptake ABC transporter substrate-binding protein
ykgJ	PP_0819	1.08519744	0.00023098	ferredoxin
aphA	PP_5340	1.07981468	8.0037E-15	acetylpolyamine aminohydrolase
ggt	PP_4659	1.07440508	0.00054156	gamma-glutamyltranspeptidase
potF-IV	PP_5341	1.07326074	2.2825E-14	putrescine-binding protein
tdcG-I	PP_0297	1.07218527	3.7221E-06	L-serine dehydratase
mexC	PP_2817	1.07152935	0.00095003	multidrug RND transporter membrane fusion protein MexC
bioB	PP_0362	1.07105273	0.0046725	biotin synthase
PP_2970	PP_2970	1.06761016	1.2959E-05	hypothetical protein
PP_1846	PP_1846	1.05479237	6.4792E-07	group II intron-encoding maturase
PP_2447	PP_2447	1.05103744	4.9899E-12	hypothetical protein
catA-I	PP_3713	1.0487579	1.5291E-11	catechol 1,2-dioxygenase
livG	PP_1138	1.0410672	9.1769E-07	ABC transporter ATP-binding protein
soxD	PP_0324	1.03598106	0.00048201	sarcosine oxidase subunit delta
bioD	PP_0366	1.02005947	4.6442E-05	dethiobiotin synthetase
pntAB	PP_5747	1.01744206	2.1265E-05	pyridine nucleotide transhydrogenase subunit alpha
bvgA	PP_1090	1.01507744	0.00137257	virulence factors transcription regulator BvgA
yciH	PP_0566	1.01091632	9.3306E-07	translation-related factor
livM	PP_1139	1.00649101	4.1107E-05	branched-chain amino acid ABC transporter permease
PP_0740	PP_0740	1.00488569	5.394E-05	MerR family transcriptional regulator
livH	PP_1140	1.00325478	7.8556E-06	branched-chain amino acid ABC transporter permease
PP_2192	PP_2192	-1.00757345	1.4569E-06	ECF family RNA polymerase sigma-70 factor/transmembrane sensor protein
yhiI	PP_5206	-1.0143159	4.1654E-05	translation-like protein
PP_3768	PP_3768	-1.0167556	1.7199E-13	shikimate 5-dehydrogenase
PP_5568	PP_5568	-1.02805193	1.8882E-08	membrane protein
PP_0685	PP_0685	-1.03319155	0.00156424	hypothetical protein
PP_3877	PP_3877	-1.04661347	6.9054E-05	hypothetical protein
oprG	PP_0504	-1.06841583	0.00101953	outer membrane protein OprG
PP_5238	PP_5238	-1.08402194	2.17E-10	hypothetical protein
hemN	PP_4264	-1.08511747	0	oxygen-independent coproporphyrinogen III dehydrogenase
PP_3368	PP_3368	-1.09728149	2.2825E-14	MFS transporter
PP_1152	PP_1152	-1.10871741	0	membrane fusion efflux protein
PP_3878	PP_3878	-1.11788359	2.4507E-06	minor capsid protein C
PP_5391	PP_5391	-1.13011222	1.8052E-09	hypothetical protein
benE-II	PP_3167	-1.13037778	1.5829E-07	benzoate transport protein
gltR-I	PP_0271	-1.13100855	8.3774E-09	two-component system response regulator
mqo-II	PP_1251	-1.13188428	2.4402E-06	malate:quinone oxidoreductase
PP_5405	PP_5405	-1.13836034	9.0721E-08	transposase
ssuE	PP_0236	-1.14147995	1.5602E-14	NAD(P)H-dependent FMN reductase subunit
PP_5392	PP_5392	-1.16389928	1.3625E-06	WD40/YVTN repeat-containing protein
catA-II	PP_3166	-1.17713459	7.9216E-08	catechol 1,2-dioxygenase
PP_4637	PP_4637	-1.20631784	4.704E-07	5-methyltetrahydropteroyltriglutamate- homocysteine S-methyltransferase family protein
PP_2874	PP_2874	-1.24546851	1.2326E-13	hypothetical protein
aspC	PP_3786	-1.25017269	5.2945E-05	aminotransferase
PP_3873	PP_3873	-1.27959118	4.4276E-06	hypothetical protein
PP_1272	PP_1272	-1.28143693	7.5824E-09	multidrug MFS transporter membrane fusion protein
PP_3365	PP_3365	-1.28880049	0	acetolactate synthase
benC	PP_3163	-1.29932433	1.0749E-06	benzoate 1,2-dioxygenase electron transfer component
PP_3790	PP_3790	-1.30910982	0	diaminopimelate epimerase
PP_1151	PP_1151	-1.31851522	8.2091E-06	hypothetical protein
PP_5561	PP_5561	-1.35376558	0	hypothetical protein
PP_3787	PP_3787	-1.36061627	0.0021343	hypothetical protein
PP_5430	PP_5430	-1.36291058	1.6616E-05	hypothetical protein
syrB	PP_3783	-1.38911072	0.00078527	syringomycin biosynthesis protein 2
PP_3090	PP_3090	-1.39353616	0.0003483	OmpA domain-containing protein
sahR	PP_4966	-1.39936412	0.00450842	methionine metabolism transcriptional regulator
benD	PP_3164	-1.39997029	2.1095E-09	1,6-dihydroxycyclohexa-2,4-diene-1-carboxylate dehydrogenase
PP_3789	PP_3789	-1.4019562	1.3902E-07	efflux transporter
benK	PP_3165	-1.41642952	4.4564E-09	benzoate MFS transporter
PP_5467	PP_5467	-1.42730862	0	hypothetical protein
PP_3782	PP_3782	-1.42791162	1.5602E-14	hypothetical protein
fdhD	PP_0257	-1.43501725	0.00727643	protein sulfur transferase
PP_3843	PP_3843	-1.43580594	5.6667E-05	hypothetical protein
benB	PP_3162	-1.45012961	4.704E-07	benzoate 1,2-dioxygenase subunit beta
PP_1249	PP_1249	-1.45593022	0.00021188	DUF4223 domain-containing protein
PP_3784	PP_3784	-1.46210267	2.258E-05	hypothetical protein

PP_3785	PP_3785	-1.46887363	0.00024122	hypothetical protein
PP_3088	PP_3088	-1.48185966	0	hypothetical protein
PP_3788	PP_3788	-1.48590525	0.00468407	non-ribosomal peptide synthetase
PP_3098	PP_3098	-1.50590513	0	hypothetical protein
PP_3097	PP_3097	-1.53048147	0	hypothetical protein
PP_5562	PP_5562	-1.53108616	0	hypothetical protein
PP_5628	PP_5628	-1.53958935	0	hypothetical protein
PP_1246	PP_1246	-1.54909599	0	hypothetical protein
PP_1245	PP_1245	-1.58428707	0	hypothetical protein
puuD	PP_3099	-1.63138909	6.1628E-13	uricase/urate oxidase
yfeH	PP_2877	-1.67259376	0	osmotic pressure-regulated transporter
PP_3091	PP_3091	-1.70814057	3.7362E-05	membrane protein
PP_3093	PP_3093	-1.73151091	0	hypothetical protein
PP_3880	PP_3880	-1.74435235	0.00400154	hypothetical protein
PP_3092	PP_3092	-1.74767914	0	hypothetical protein
yehX	PP_0868	-1.75243559	0	ABC transporter ATP-binding protein
clpV	PP_3095	-1.76310543	1.4059E-05	protein ClpV1
kgtP	PP_1400	-1.76553238	0	alpha-ketoglutarate permease
PP_3871	PP_3871	-1.7999749	6.7396E-10	hypothetical protein
PP_3096	PP_3096	-1.80263649	0	hypothetical protein
asnB	PP_1750	-1.82613988	0	asparagine synthetase
PP_3094	PP_3094	-1.87669938	0	hypothetical protein
benA	PP_3161	-1.90885751	0	benzoate 1,2-dioxygenase subunit alpha
PP_3089	PP_3089	-1.91633403	8.9101E-14	hypothetical protein
PP_3100	PP_3100	-1.95862507	0	hypothetical protein
PP_2134	PP_2134	-1.98757261	3.1168E-13	transposase
yehW	PP_0869	-1.99165295	0	osmoprotectant ABC transporter permease
PP_0870	PP_0870	-2.01580198	0	glycine betaine/carnitine/choline ABC transporter substrate-binding protein
PP_0871	PP_0871	-2.05962034	0	glycine betaine/carnitine/choline ABC transporter permease
PP_5393	PP_5393	-2.36310371	0.00308446	metal-binding chaperone
PP_0818	PP_0818	-2.39703978	0	hypothetical protein
PP_1149	PP_1149	-2.48560554	0.00101973	hypothetical protein
PP_2052	PP_2052	-2.50153991	1.8711E-06	bifunctional sugar-phosphatase/mannitol-1-phosphate 5-dehydrogenase
PP_5500	PP_5500	-2.50282636	0	hypothetical protein
alaC	PP_0817	-4.57355145	0	aminotransferase

Table S5.1-3. DNA sequences of codon-optimized nylonase-encoding genes for P. putida KT2440. The upstream region containing P_{14f} is colored in orange. Nylonase-encoding genes are colored in green.

Construct	Sequence 5'-3'
P_{14f} -*nylA*	ACAGTTTACGAACCGAACAGGCTTATGTCAAGACGTCTTAATTAAGCCCGTTGACATGACATGGTTTTGAGGGTATAATGTGG CGACCTAGGGCCCAAGTTCACTTAAAAAGGAGATCAACAATGAAAGCAATTTTCGTACTGAAACATCTTAATCATGCTAAGGA GGTTTTCTAATGTCCAAGGTTGATCTGTGGCAGGACGCGACCGCCCAGGCCGAGCTGGTGCGTAGTGGTGAAATCTCCCGTAC TGAGCTGCTGGAGGCGACCATCGCTCACGTGCAGGCCGTGAACCCGGAGATCAACGCCGTCATCATCCCACTGTTCGAAAAGG CTCGCCGCGAATCGGAACTGGCTTCGGGTCCGTTCGCCGGCGTTCCGTACCTGCTGAAAGACCTGACCGTGGTGTCCCAGGGC GACATCAACACCTCCAGCATTAAGGGCATGAAGGAGTCGGGTTACCGTGCTGACCACGACGCATACTTCGTTCAGCGTATGCG CGCAGCTGGTTTCGTTCTGCTGGGTAAGACCAACACCCCGGAAATGGGCAACCAGGTAACTACTGAACCGGAGGCCTGGGGTG CCACCCGCAACCCTTGGAACCTGGGTCGTAGCGTAGGTGGTTCGAGTGGTGGCAGCGGCGCGGCCGTGGCAGCCGCACTGAGT CCAGTTGCACATGGTAACGACGCAGCGGGCTCCGTGCGTATCCCTGCTAGTGTATGCGGCGTGGTCGGCCTGAAACCCACCCG TGGTCGTATCAGTCCTGGTCCGCTGGTGACCGACAGCGACAACGTCGCCGGCGCCGCACACGAAGGTTTGTTCGCACGCAGTG TACGTGACATCGCGGCGCTGCTGGACGTGGTTAGCGGCCACCGTCCTGGTGATACTTTCTGCGCCCCGACCGCGTCCCGTCCA TACGCTCAGGGTATCAGCGAAAATCCTGGCTCGCTGCGCGTCGGTGTGCTGACCCACAACCCGGTCGGCGACTTCGCATTGGA CCCTGAATGCGCAGCAGCCGCACGTGGTGCAGCCGCTGCATTGGCCCGCACTGGGCCATGATGTGAACGACGCCTACCCAGAAG CCCTGGGCGACCGTTCGTTCCTGAAGGATTATTCGACCATCTGCGACGTGGCAATCGCTCGTGAGATCGAACGCAACGGCGAA CTCATCGGCCGCCCGCTGACCGAGGATGACGTGGAATGGACTAGTTGGGAAATGGTTAAACGCGCTGACCAGGTGACCGGCCG TGCTTTCGCCGCTTGTGTTGATGAACTGCGTTACTATGCCGGTAAGGTCGAACGTTGGTGGGAAGCCGGCTGGGACCTGCTGA TCCTGCCGACCGTGACTCGTCAAACCCCGGAGATCGGCGAGCTGATGCTGGCTAAAGGCACCGACCTGGAAGGCCGTCAAAGC GCCTTCATCTCCGGTTCGTTGCAAATGCTGGCCTTCACTGTTCCATTCAACGTCTCGGGCCAGCCGGCCATCTCGCTGCCCAT CGGCATGTCCTCGGACGGTATGCCCATTGGTGTCCAGATCGTGGCCGCCTACGGCCGTGAGGACCTGCTGTTGCAAGTTGCCG CACAGCTGGAAGGTGCTTTGCCTTGGGTTGCTCGTCGTCCACAACTGCTGAATCCAAGTCGTAAGATCCCTGCTGCCTAA
P_{14f} -*nylB*	ACAGTTTACGAACCGAACAGGCTTATGTCAAGACGTCTTAATTAAGCCCGTTGACATGACATGGTTTTGAGGGTATAATGTGG CGACCTAGGGCCCAAGTTCACTTAAAAAGGAGATCAACAATGAAAGCAATTTTCGTACTGAAACATCTTAATCATGCTAAGGA GGTTTTCTAATGAACGCTCGCAGTACTGGTCAACATCCAGCTCGCTATCCAGGTGCTGCGGCCGGCGAACCAACTTTGGATTC GTGGCAGGAAGCTCCACACAACCGTTGGGCATTCGCCCGTCTGGGCGAACTGCTGCCGACTGCGGCGGTTAGTCGTCGGGATC CAGCTACCCCAGCTGAGCCTGTTGTTCGCTTGGATGCTCTGGCGACTCGTTTGCCAGATCTGGAACAACGTCTGGAAGAAACC TGTACTGATGCTTTCCTGGTATTGCGCGGCAGTGAGGTTCTCGCTGAGTACTATCGCGCTGGCTTCGCCCCAGATGATCGCCA TCTGCTGATGTCGGTCAGCAAGTCGCTGTGCGGCACTGTAGTGGGCGCCCTGATCGACGAGGGCGTATCGACCCGGCTCAGC CCGTAACTGAATACGTCCCGGAGTTGGCCGGCTCGGTGTATGACGGTCCGAGCGTGTTGCAAGTACTGGACATGCAGATCAGT ATCGACTACAACGAGGACTACGTTGACCCAGCGTCGGAGGTGCAAACCCACGACCGCTCGGCCGGCTGGCGTACTCGTCGTGA CGGTGACCCGGCCGATACCTACGAGTTCCTGACCACCCTGCGTGGTGACGGCGGTACTGGCGAGTTCCAGTACTGTTCGGCTA ACACCGACGTGTTGGCTTGGATCGTTGAGCGTGTTACCGGCCTGCGTTACGTCGAAGCCCTGAGCACCTACCTGTGGGCCAAG CTGGACGCCGACCGTGACGCCACCATTACCGTGGATCAGACCGGTTTCGGCTTCGCCAACGGTGGCGTAAGTTGCACTGCTCG TGACCTGGCTCGCGTTGGCCGTATGATGCTGGATGGCGGTGTCGCTCCAGGTGGTCGCGTGGTGAGCCAGGGCTGGGTTGAGT CCGTCCTCGCTGGCGGCTCGCGTGAAGCCATGACCGACGAAGGTTTCACGAGCGCCTTCCCAGAGGGTAGTTACACTCGCCAG TGGTGGTGCACCGGTAACGAACGCGGTAACGTTTCGGGCATCGGTATCCACGGTCAGAACCTCTGGCTGGACCCACGCACCGA CAGCGTGATCGTCAAGCTGTCGAGCTGGCCGGACCCAGATACTCGCCATTGGCACGGTTTGCAATCGGGCATCCTGCTGGATG TGTCCCGTGCGCTCGACGCTGTATAA
P_{14f} -*nylC*	ACAGTTTACGAACCGAACAGGCTTATGTCAAGACGTCTTAATTAAGCCCGTTGACATGACATGGTTTTGAGGGTATAATGTGG CGACCTAGGGCCCAAGTTCACTTAAAAAGGAGATCAACAATGAAAGCAATTTTCGTACTGAAACATCTTAATCATGCTAAGGA GGTTTTCTAATGAACACTACCCCAGTACATGCCTTGACCGATATCGATGGTGGCATCGCTGTTGATCCAGCCCCACGGTTGGC TGGTCCTCCAGTGTTCGGTGGCCCTGGTAACGATGCCTTCGACCTGGCCCCAGTACGCTCGACCGGCCGCGAAATGCTGCGCT TCGACTTCCCTGGTGTCTCCATCGGTGCCGCGCACTATGAAGAAGGTCCAACTGGTGCGACCGTGATCCACATCCCAGCCGGC GCCCGCACCGCTGTTGACGCTCGTGGCGGCGCTGTTGGTTTGTCGGGTGGCTACGACTTCAACCACGCTATTGCTTGGCCGG CGGTGCTGGTTACGGTCTGGAAGCTGGCGCTGGTGTCAGTGACGCCCTGCTGGAACGTCTGGAGCATCGCACCGGCTTCGCCG AGTTGCAACTGGTCTCGTCCGCAGTAATCTACGACTTCTCCGCTCGTAGTACTGCTGTTTACCCAGACAAGGCTCTGGGTCGT GCTGCCCTGGAGTTCGCAGTTCCTGGTGAGTTTCCTCAAGGCCGTGCTGGCGCGGGCATGAGTGCTAGTGCTGGCAAGGTAGA TTGGGATCGTACTGAAATCACGGGCCAAGGCGCGGCATTCCGTCGCTTGGGCGATGTCCGTATCCTGGCCGTTGTTGTGCCAA ACCCGGTTGGTGTAATCGTTGATCGCGCGGGCACGGTCGTTCGCGGTAATTACGATGCCCAGACCGGCGTGCGCCGCCACCCG GTTTTCGATTACCAGGAGGCCTTTGCCGAACAAGTGCCGCCGGTGACCGAGGCCGGCAACACCACCATCTCCGCAATCGTTAC CAACGTCCGTATGTCGCCGGTAGAACTGAACCAGTTCGCTAAGCAGGTACACTCGTCGATGCACCGTGGCATCCAGCCTTTTC ATACCGATATGGACGGTGACACTCTGTTCGCCGTTACCACCGACGAGATCGACCTGCCAACCACTCCTGGTTCGAGCCGCGGT CGTCTGTCCGTTAACGCCACCGCGCTGGGCGCTATCGCATCGGAAGTGATGTGGGACGCCGTCCTGGAGGCCTAA

5.2 Supplementary data to Chapter 2.2:

Increasing the diversity of nylonases for polyamide degradation.

de Witt, J.[1], Ostheller, M-E.[2], Jensen, K.[3], van Slagmaat C.A.M.R.[4], Polen, T.[1], Wynands, B.[1], and Wierckx, N.[1*] (2024).

[1] Institute of Bio- and Geosciences IBG-1: Biotechnology, Forschungszentrum Jülich, Jülich, Germany

[2] Aachen-Maastricht Institute for Biobased Materials (AMIBM), Maastricht University, Brightlands Chemelot Campus, Urmonderbaan 22, 6167 RD Geleen, The Netherlands

[3] Novozymes A/S, Biologiens Vej 2, Kgs. Lyngby DK-2800, Denmark

[4] B4Plastics BV, IQ-parklaan 2A, 3650, Dilsen-Stokkem, Belgium

[*] Corresponding author

Table S5.2-1. Amino acid sequences of NylC$_{1-6}$.

Protein ID	Donor organism	Sequence
NylC$_1$	*Leucobacter chromiiresistens* JG 31	MNPSSHEPHALAEIDSGAVIDPAPRLAGAPVF GGPGNGDFDLVPQRSDGRERLRFDFPGVRIGS AHYAEGPTGATVIHLPAGARTAVDARGGAV GLAGGYDFNHAICLAGGSVYGLEAGAGVSD ALLERFENRTGFADLQLVSSAIIYDFSARSTSV YPDRELGRAAFDFAVEGEFAQGRAGAGMSA SSGKVDWERTEITGQGAAFRQIGDVRILAVV VPNPVGVILDRAGRVVRGNYDAATGERRHP VFDYAEAFAEHRAAETQSGNTTISALITNVKM STVELNQFAKQVHSSMHRGIQPFHTDMDGDT LFAVTTDEIDLPISPGSSRGRLSVNATALGAIA SEVMWDALLEAAK
NylC$_2$	*Microbacterium oxydans*	MTDIHRLAPVLPAGPRRSNGDYALAPVHGTD RGQVEYDFPGVLLGTAEYAEGPTGATVMSIP AGARTFTDRRGGAVGASGLYGYNHAICLAG GSVYGLSAVAGVSEALFERAEHRSGFDQLQL VSGAIIYDYSVRENSVFPDTALGKAALQAAR QGVIEVGRVGGGASASSGKVDPARVEFTGQG AAFRQVGDVKVLVVTVLNPYGVIVDRAGRII RGNFDATTGERRHPALDYEEAIGESRLVESMS GNTTITAVITNVQLSDVELKQFGLQVHSSMHR GIQPFHTPLDGDTLFALTTDEVALPEDPGTSR GRLSLNSTAVATLAGETAWDAILCAAG
NylC$_3$	*Streptomyces* sp. 63005	MTVTDRAGTPARAIPAPSFGPARTNDDFELTP QPSPGQGTVEFDFPGVEVGTAEYAEGPTGTT VVHVPAGARMFIDERGGAIGLSYGDKQFAHA ICLSGGSLYGLGACAGVADELRSRVDNRVGW NDLKCVSGAIIYDFATRDNAVVPDAALGRAA LRTAEPGRFPVGRAGAGISASVGKIDWTRCEF SGQGAAFRQVGDVKILAATVVNAVGVVVDR DGTVVRGNHDPATGTRRLPHLDYEAAFAGD GPTTMQGNTTISVLVTNVRLDDRALEQFGRQ VHGSMNRGIQPFHTSLDGDTLFTLTTDEVDLP TTPSRIGAHALNAVGLGSIAAEVMWDAILSSA R
NylC$_4$	*Variovorax boronicumulans*	MKNDVKAKQDLVPRLWQGPSDGRALSFDFP QLKIGIAEYEEGPTGCTVLHVEGGADCEVDV RGGAPGLLGGYTRVDAISLAGGSLYGLEAAT GVTSRMLAERDGAVGWGKIALVSGAIIYDFG GRTNSIYPDKALGAAAYRSAQVGTFPLGARG AGRSAAVGKFAAYPDYEREAGGQGAAFAMV GGTRVFVATVVNALGVIVDRQGRVVRGLRH RRTGVRHHPREVLVPTASATVEAPVTPGNTV ATTENTTLTVLVTDQPMPPLFLRQLGRQVHSS MARAIQPFHTPHDGDILFALSTGTGTASVDPF VLAEAASDLAWDAVLQAVDF
NylC$_5$	*Gordonia* sp.	MTFLARAGNRITDVAGIAVGHHDRIDDEVVV ATGTEPGVGWATGTTVVTVDAGATSAVDVR GGGPGTRETDLLEPGNSVRGANAIVLTGGSA YGLSAADGVMRGLEARGIGLPMDEQGHVVPI VPAAVIFDLPVGEWARRPDEEFGALALDAAD

216

		ADFAVGSVGAGAGARAGALKGGVGTASITL ADGPARGLTVGALVVANPVGQVIDPATGLP WGGDDLAAYGLGAPAAGELTRLRELEAKGT VLNTTIGVVATDATLSVPSVRRLAMSGHDGL ARAVRPAHSPLDGDTLFAVATGRRTADPEAA VDIPPGMEPEIAVVAALAEASATVVQRAIVSA VVHATSVAGIPSYRDVVASAFGWDSP
NylC$_6$	*Rhodococcus* sp.	MIVPGPTDSLLDVAGLSVGHWQRLDPEVTVG TPEIPGTGAATGCTVVLADPSAVASVDVRGG GPGTRETDLLDPSHSVQRVDAVLLTGGSAYG LAAADGVMRYLEKNGKGIPMGAPGAVVPIVP GAVIFDLPVGQWSARPTADSGCTAAATACST HLERGSAGAGTGARAGALKGGIGSASVRITD GPAAGVTVAALMVANPVGSVFDPVTGLPWG VDAARAEELGLSSPSASDLAAARALGDKGTV LNTTIGVVATDAPLSKAACRRVAVTGHDGLG RAIRPAHSPLDGDTIFALSTGTADVTDALRDS PSIPAFAAELPILAAVCEAAAVVVERAIVDAIL SATSVADIPAYRDVLPSVFGR

Table S5.2-2. Composition of PEA in mol percent (mol %). Monomers are abbreviated as followed: Adipic acid (AA), sebacic acid (SA), 1,6-hexamethylenediamine (HMDA), 1,6-hexanediol (HDO), and 3-methylpentanediol (3-MPDO).

polymer	AA	SA	HMDA	HDO	3-MPDO
PEA1	50	0	37.5	12.5	0
PEA2	0	50	37.5	12.5	0
PEA3	25	25	37.5	12.5	0
PEA4	0	50	37.5	0	12.5

5.3 Supplementary data to Chapter 2.3:

Bio-upcycling of even and uneven medium-chain-length diols and dicarboxylates using engineered Pseudomonas putida.

Ackermann Y. S.[1†], **de Witt J.** [1†]**,** Mezzina M. P.[2], Schroth C[1]., Polen T[1]., Nickel, P. I.[2], Wynands B.[1], and Wierckx N.[1*] (2024). Bio-upcycling of even and uneven medium-chain-length diols and dicarboxylates using engineered *Pseudomonas putida*. *Microb. Cell Factories – in press*, doi:10.1186/s12934-024-02310-7

[1] Institute of Bio- and Geosciences IBG-1: Biotechnology, Forschungszentrum Jülich, Jülich, Germany

[2] The Novo Nordisk Foundation Center for Biosustainability, Technical University of Denmark, Kongens Lyngby, Denmark

[†] these authors contributed equally to this study.

[*] Corresponding author

A) KT2440

B) KT2440-AA

Figure S5.3-1. Adaptive laboratory evolution of *P. putida* KT2440 wild type (A) and KT2440-AA (B) on 1,6-hexanediol. ALE was performed by iterative inoculation after the stationary phase was reached. Since *P. putida* KT2440 did not grow with HDO as sole carbon source, 15 mM HDO and 15 mM BDO were used for the first two stages of ALE to enable growth. This concentration was shifted to 20 mM HDO and 10 mM BDO (stages 3-5), and to 30 mM HDO (stages 6-14). *P. putida* KT2440-AA could grow with 30 mM HDO.
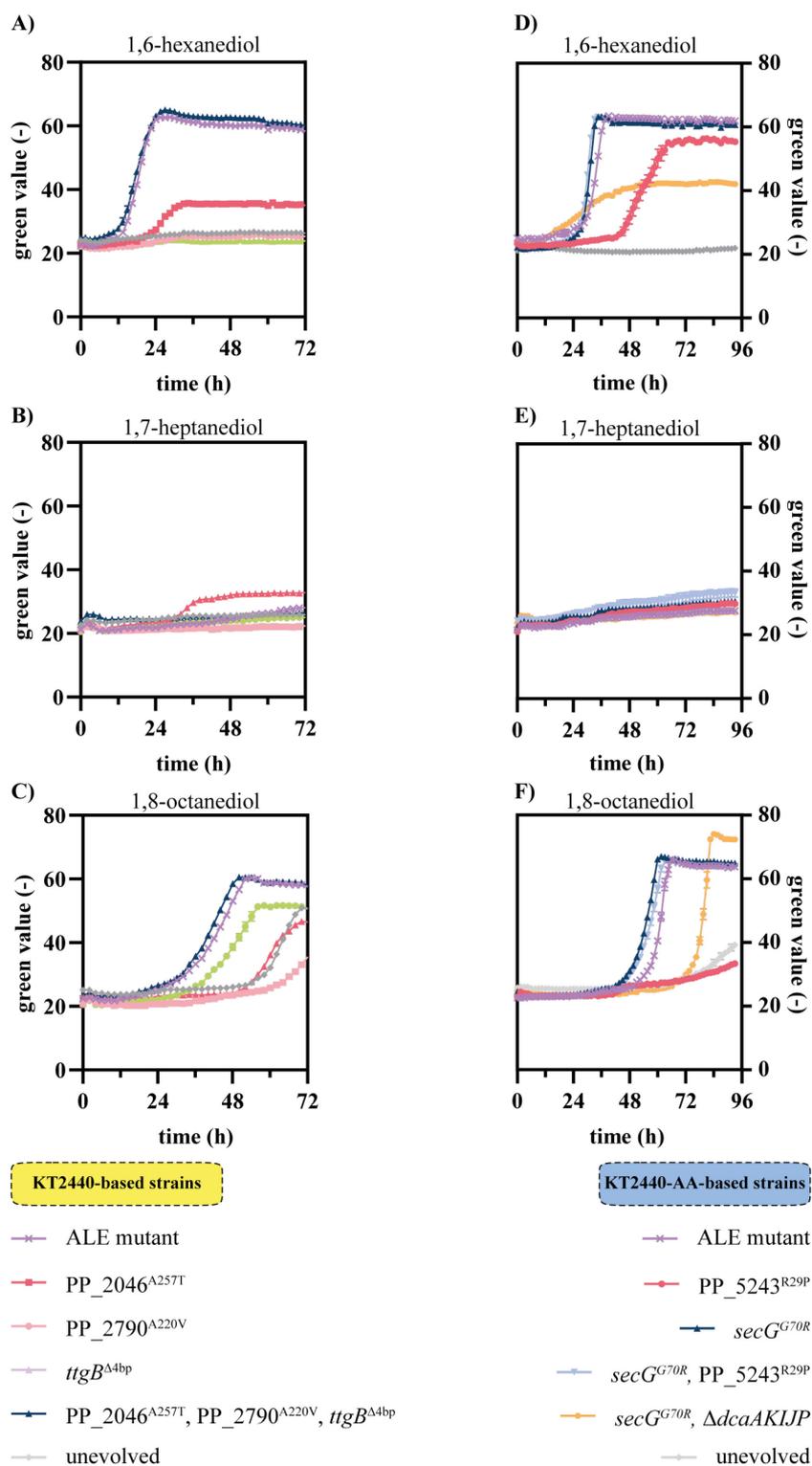
Figure S5.3-2. Metabolic pathways of aliphatic diols in engineered *P. putida* KT2440. Extension of Figure 1. *P. putida* KT2440 wild type-based strains (A-C) and *P. putida* KT2440-AA-based strains (D-F) were cultivated in mineral salts medium (MSM) supplemented with 1,6-hexanediol, 1,7-heptanediol, or 1,8-octanediol in concentrations that are C-mol equivalent to 30 mM 1,6-hexanediol. Growth was monitored using a Growth Profiler. Error bars indicate the standard error of the mean (n=3).
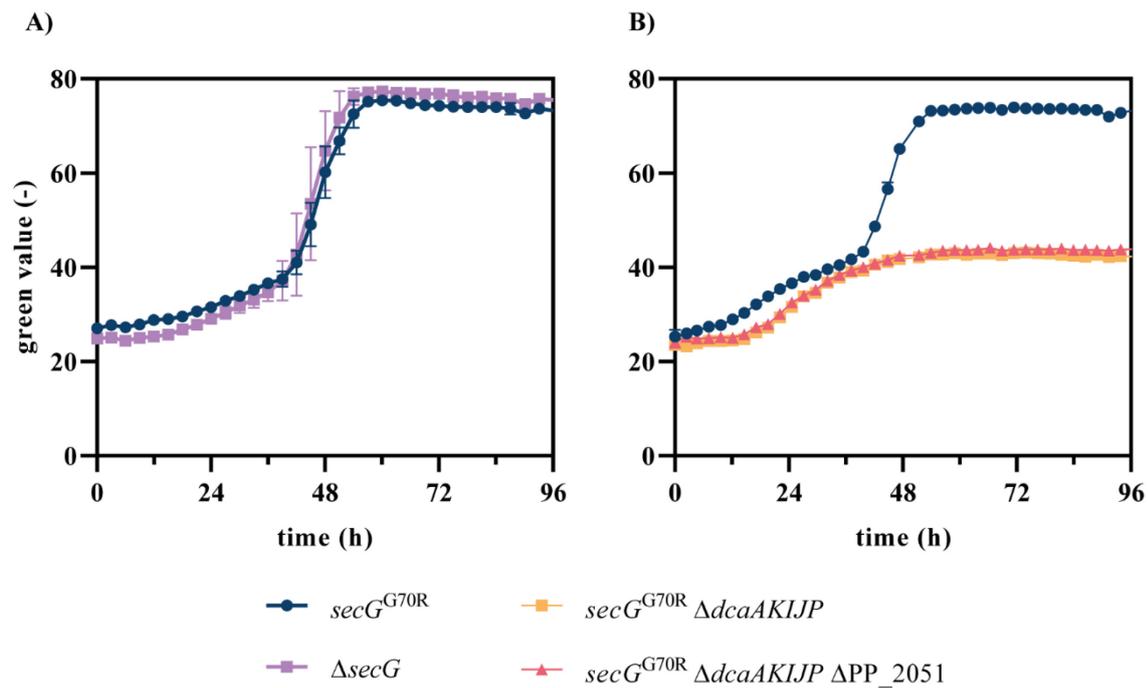
Figure S5.3-3. Growth of *P. putida* KT2440-AA mutants on HDO. Strains were cultivated in MSM supplemented with 15 mM of HDO as sole carbon source. (A) Effect of *secG*^{G70R} mutation on HDO metabolism. (B) Effect of Δ*dcaAKIJP* and ΔPP_2051.
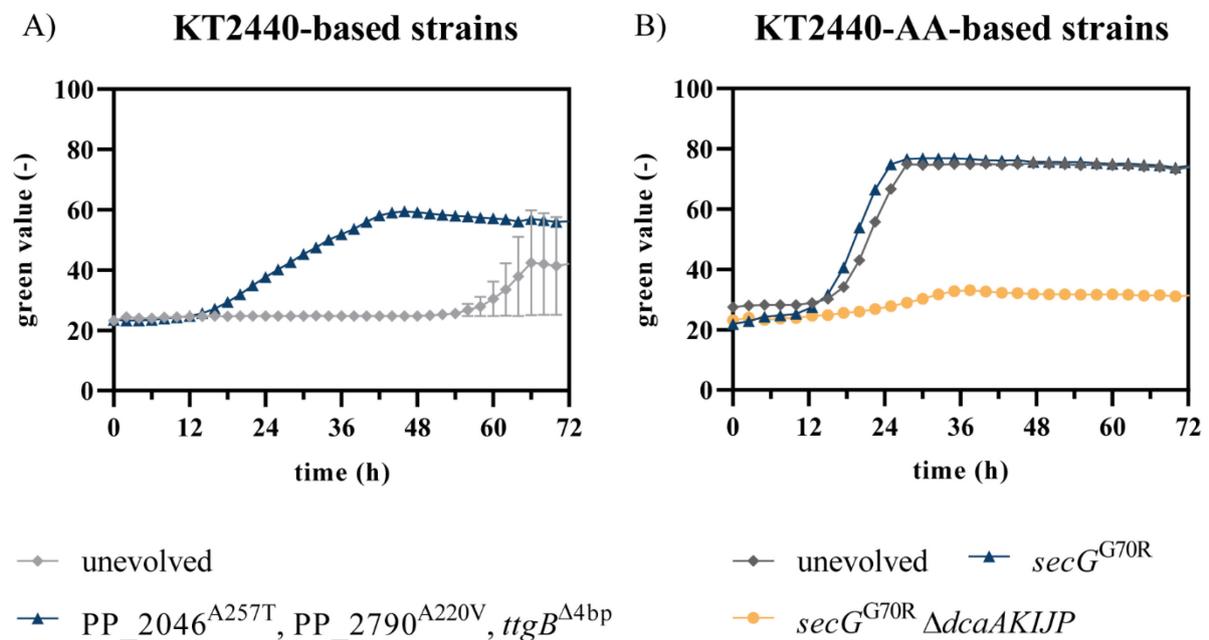
Figure S5.3-4. **Growth of *P. putida* KT2440-AA mutants on 6-hydroxyhexanoate.** Strains were cultivated in MSM supplemented with 15 mM of 6-hydroxyhexanoate as sole carbon source.
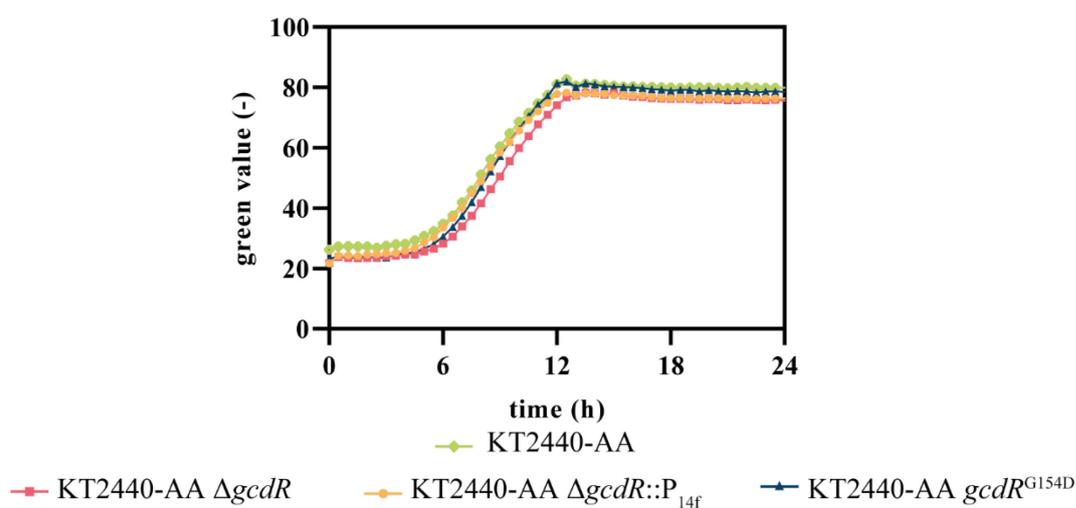
Figure S5.3-5. Growth of *P. putida* KT2440-AA mutants on glutarate. Strains were cultivated in MSM supplemented with 36 mM glutarate as sole carbon source.
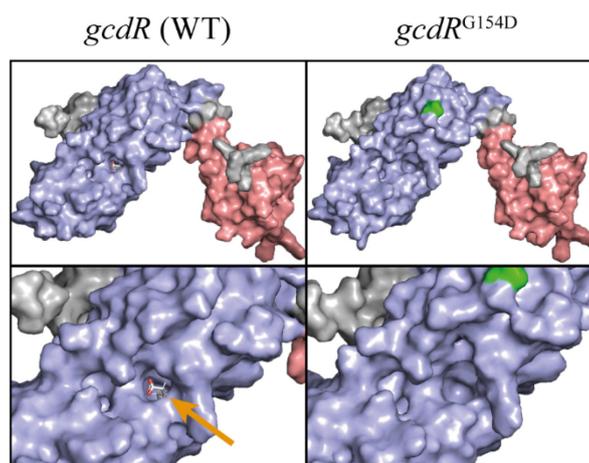
Figure S5.3-6. Three-dimensional structures of GcdR predicted with ColabFold and visualized with PyMOL. Docking of glutaric acid was calculated using YASARA (orange arrow). Mutated amino acid (D154) is marked in green. The blue surface color indicates the effector binding domain and the red surface color indicates the DNA binding domain.

A)

B)
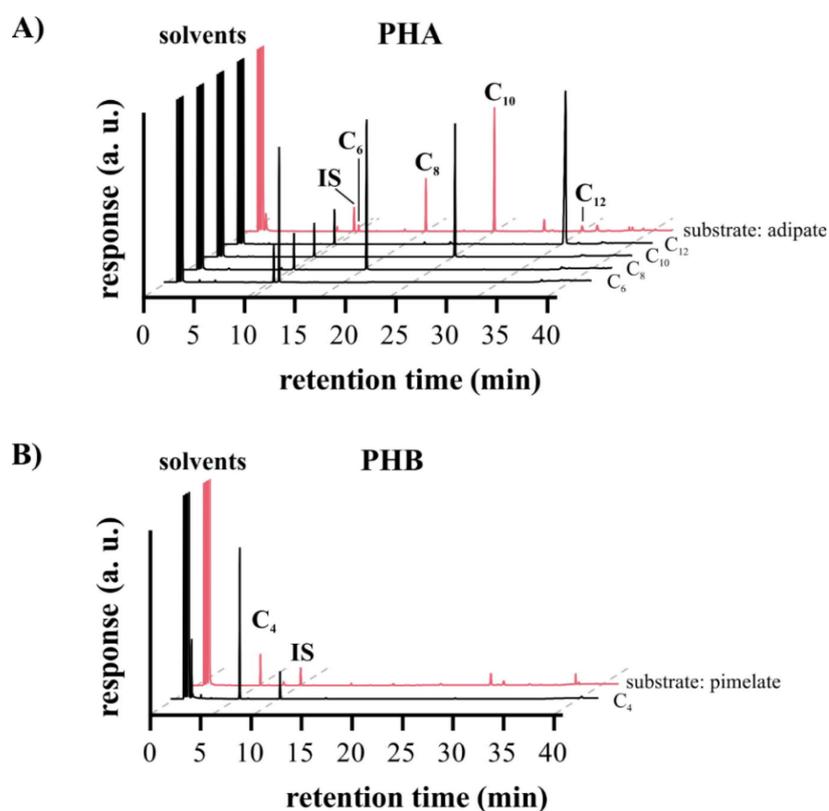
Figure S5.3-7. Exemplary gas chromatography chromatograms of polyhydroxyalkanoates (A) and polyhdroxybutyrate (B). Methyl esters of 3-hydroxyacids (C_4-C_{12}) were quantified using analytical standards (black lines). As internal standard (IS) methyl benzoate was used. PHA production from adipate (A) and PHB production from pimelate (B) are shown in red. For better visibility, the y-axis was capped due to high responses of chloroform and methanol.

5.4 Supplementary data to Chapter 2.4:

Characterization and engineering of branched short-chain dicarboxylate metabolism in Pseudomonas reveals resistance to fungal 2-hydroxyparaconate.

de Witt, J.[1], Ernst, P.[1], Gätgens, J.[1], Noack, S.[1], Hiller, D.[2], Wynands, B.[1], Wierckx, N.[1*], (2023). Characterization and engineering of the branched short-chain dicarboxylate metabolism of *Pseudomonas* reveals resistance to fungal 2-hydroxyparaconate. *Metabolic Engineering*, 75, 205-216. doi:10.1016/j.ymben.2022.12.008

[1] Institute of Bio- and Geosciences IBG-1: Biotechnology, Forschungszentrum Jülich, Jülich, Germany

[2] Institut für Mikrobiologie, Technische Universität Braunschweig, Germany

[*] Corresponding author
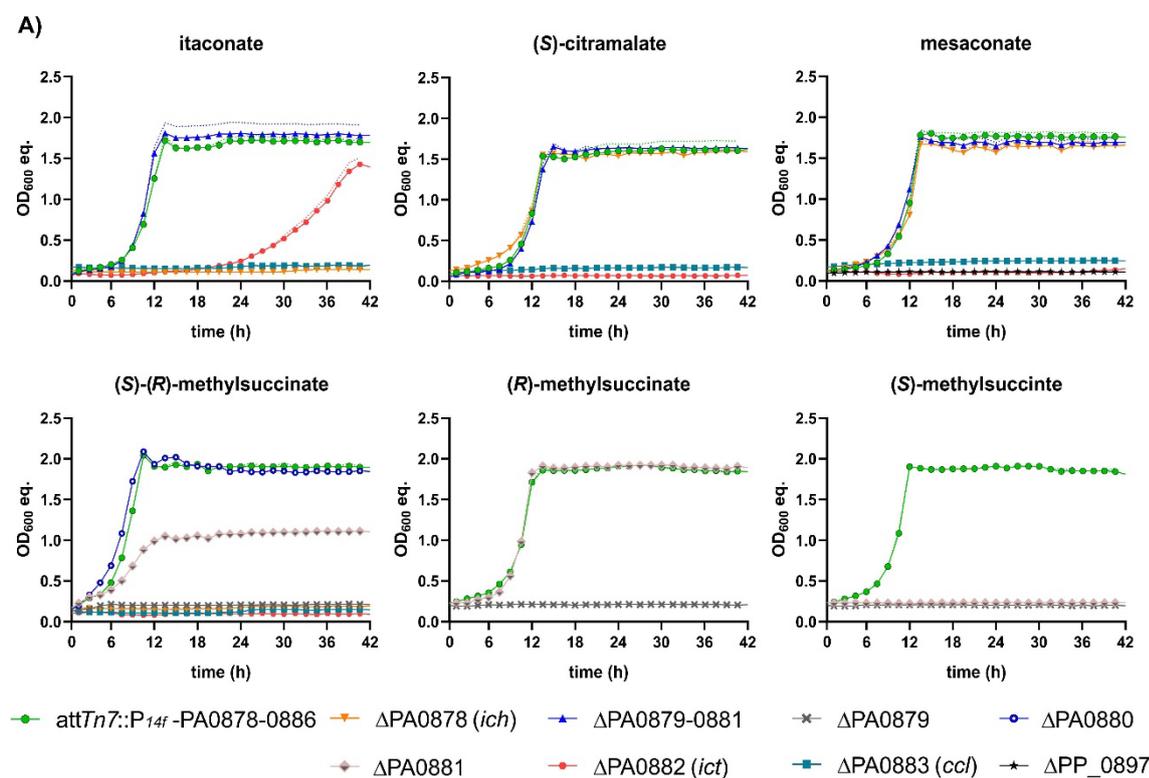
Figure S5.4-1. Growth of *P. putida* KT2440 strains on indicated BSCD. Strains were grown in a Growth Profiler in 96-well microtiter plates with MSM supplemented with 20 mM of the indicated substrate. OD_{600} equivalents (OD_{600} eq.) were derived from green-values obtained from the Growth Profiler using a calibration curve. The mean values with standard deviation (SD) of three replicates are shown.
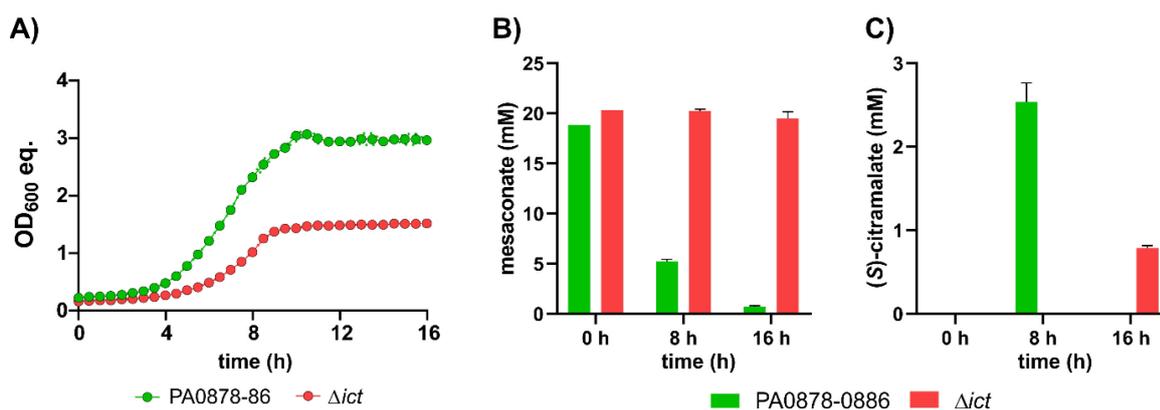
Figure S5.4-2. Growth of *P. putida* KT2440 *attTn7::P14f*-PA0878-86 and Δ*ict* mutant with mesaconate and glucose as mixed substrates. Strain were cultivated with 15 mM glucose and 20 mM mesaconate in a Growth Profiler in 96-well microtiter plates with MSM supplemented with 20 mM of the indicated substrate. **(A)** OD_{600} equivalents (OD_{600} eq.) were derived from green-values obtained from the Growth Profiler using a calibration curve. The mean values with standard deviation (SD) of three replicates are shown. The Δ*ict* mutant was not able to metabolize mesaconate (see Figure S1). HPLC analysis of culture supernatants for quantifying mesaconate **(B)** and (*S*)-citramalate **(C)** concentrations.
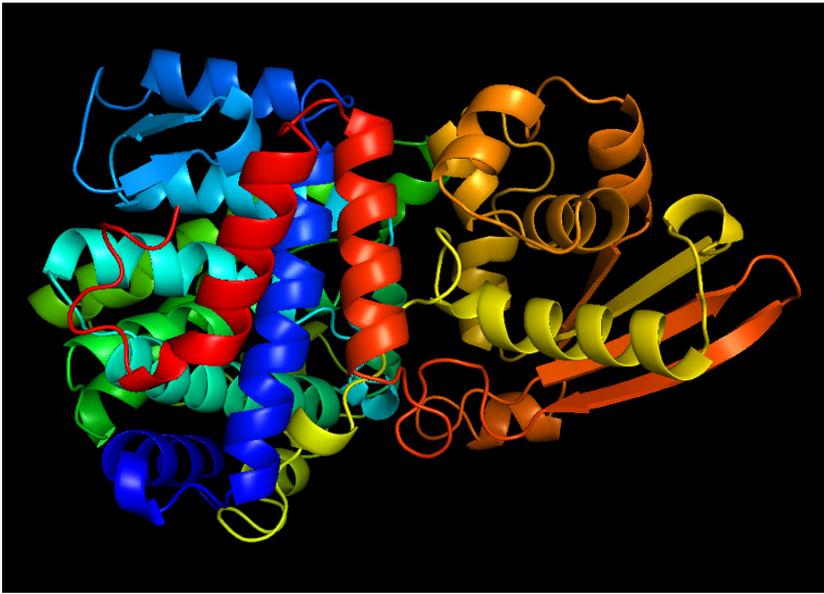
Figure S5.4-3. Predicted structure of PA0881. Structure was predicted using ColabFold (Mirdita et al., 2021) with N to C rainbow color code.

Figure S5.4-4. m/z-spectrum of 2-HP (A) and 2-HP* (B). Both compounds exhibit the same mass and similar MS-spectra. Hence, they might be (*S*)-(*R*)-isomers. Only one form was found to be cleaved by Rdo$_{PA}$.
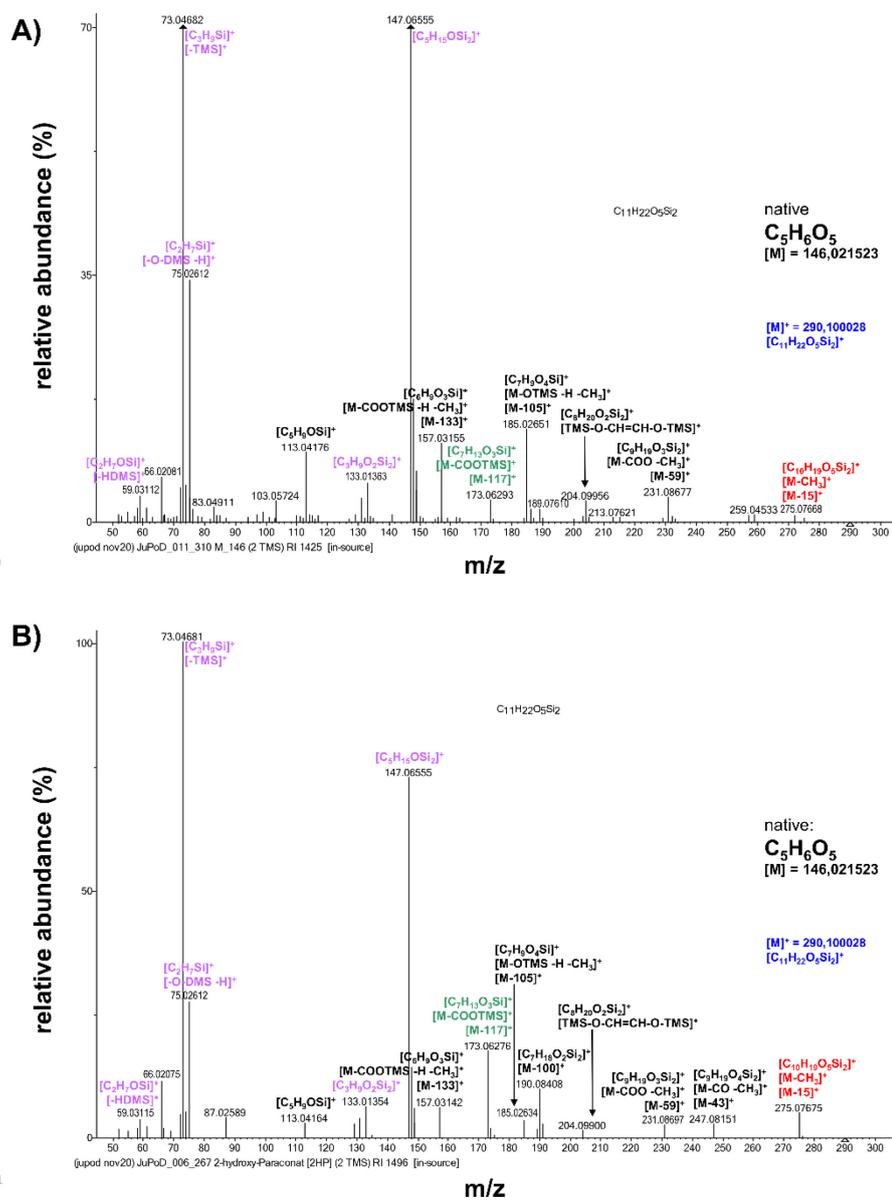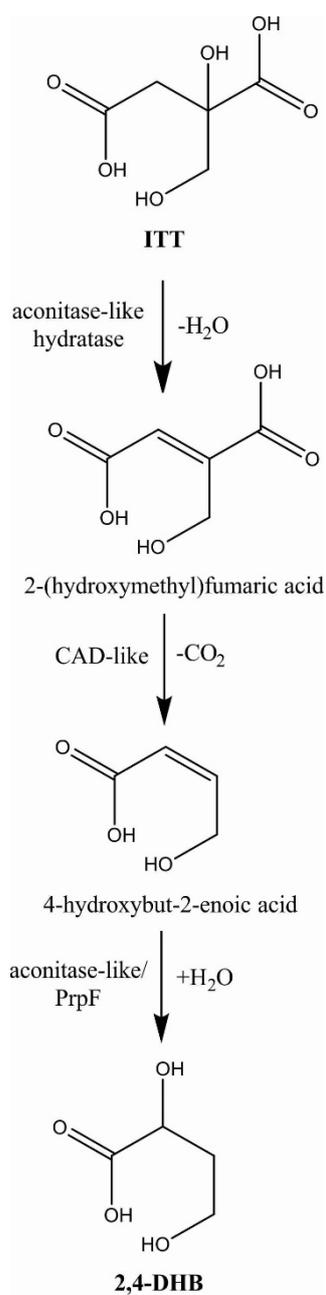
Figure S5.4-5. Proposed conversion of ITT to 2,4-DHB. Since activity of Ict towards ITT was indicated, this pathway might proceed *via* the CoA-activated forms starting with ITT-CoA.

Figure S5.4-6. m/z-spectrum of ITT (A) and probably methylated ITT (B).
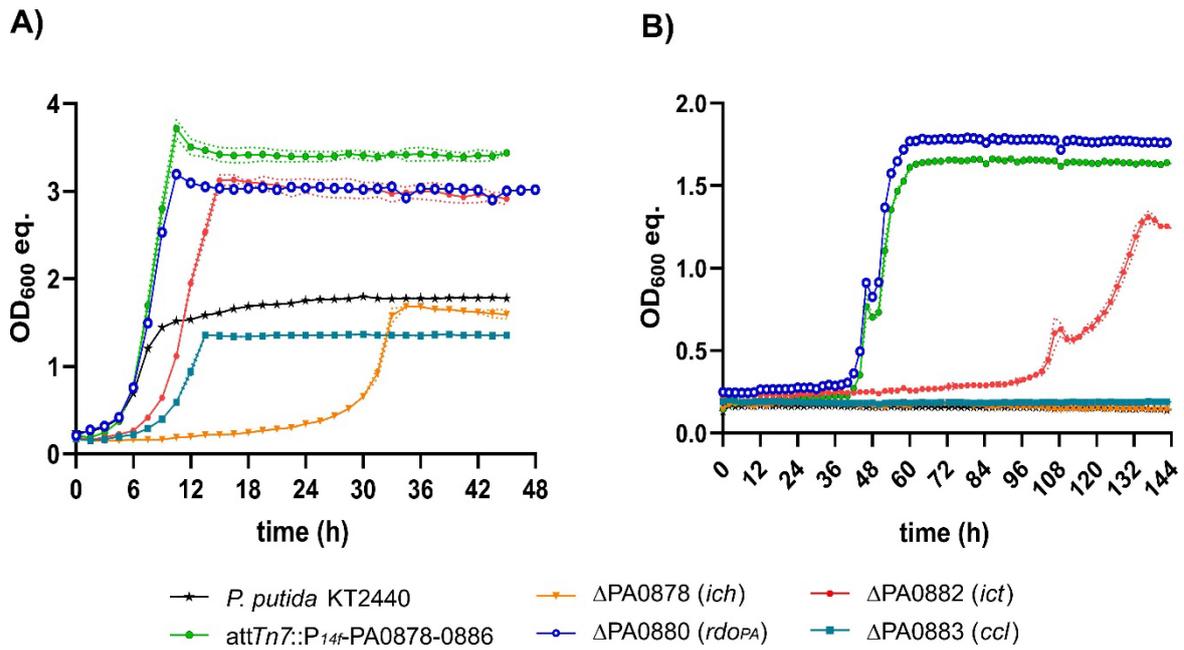
Figure S5.4-7. **Effect of CoA-intermediates originating from incomplete itaconate degradation on glucose and acetate metabolism.** Strains were grown in the presence of 20 mM itaconate and 15 mM glucose (A) or 60 mM acetate (B). The following accumulation products are expected for the tested mutants that impaired growth on the substrates: itaconyl-CoA (ΔIch), (*S*)-citramalyl-CoA (ΔCcl). Due to the putative side activity of the native SucCD on itaconate, the ΔIct mutant showed delayed growth but could metabolize itaconate. OD_{600} equivalents (OD_{600} eq.) were derived from green-values obtained from the Growth Profiler using a calibration curve. The mean values with standard deviation (SD) of three replicates are shown.
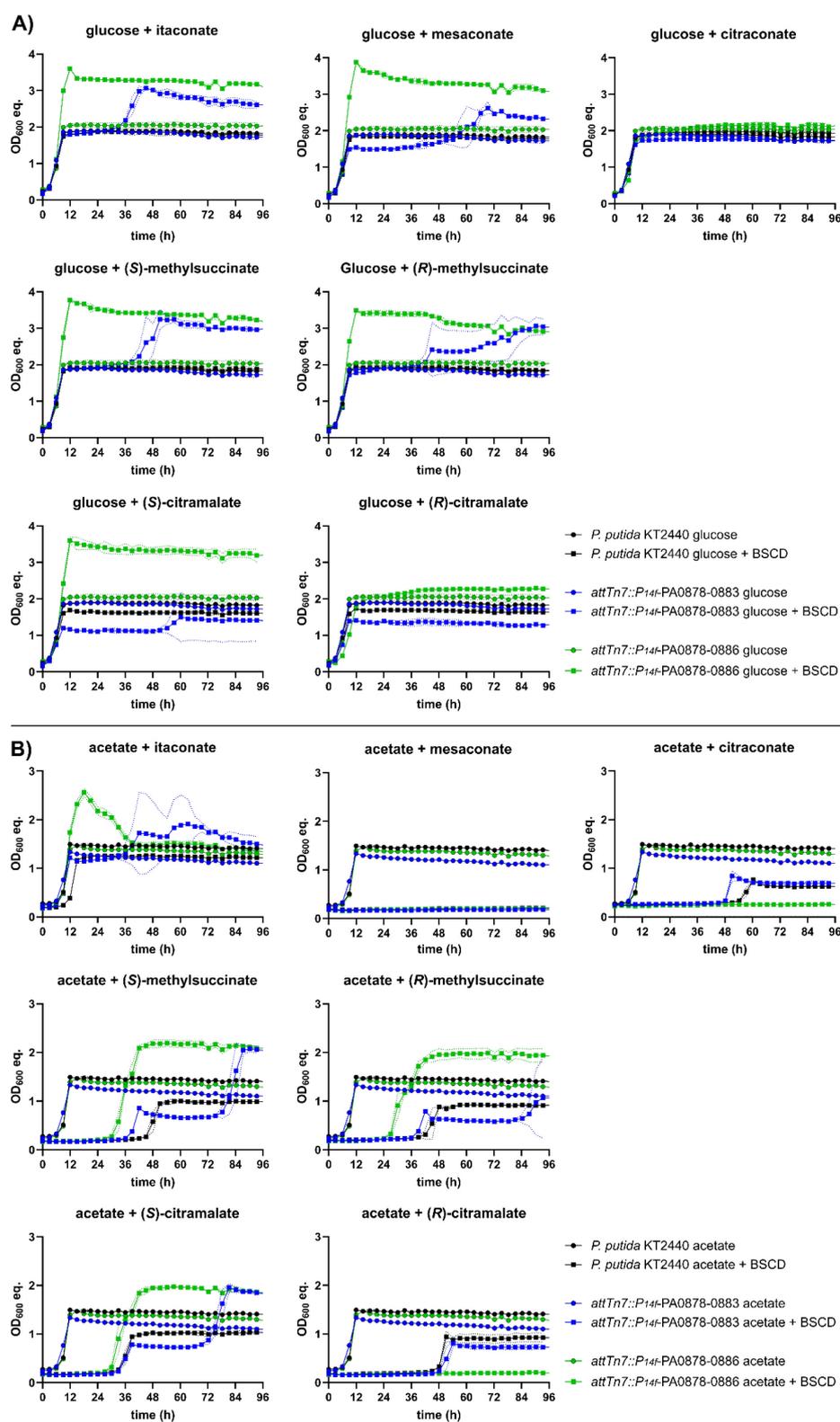
Figure S5.4-8. Toxicity of branched short-chain dicarboxylates for *P. putida* strains under glucose- and acetate-degrading conditions. Strains were cultivated in mineral salts medium with 15 mM glucose (A) or 60 mM acetate (B) supplemented with 20 mM of the indicated BSCD. OD_{600} equivalents (OD_{600} eq.) were derived from green-values obtained from the Growth Profiler using a calibration curve. The mean values with standard deviation (SD) of three replicates are shown.

Table S5.4-1. Growth rates of *P. putida* strains used in this study.

Figure 2.4-2			
Strain	**substrate**	**μ (h⁻¹)**	**SD**
P. putida KT2440 attTn7::P₁₄fPA0878-0883	itaconate	0.11	0.00
P. putida KT2440 attTn7::P₁₄fPA0878-0886	itaconate	0.39	0.02
P. putida KT2440 attTn7::P₁₄fPA0878-0883	mesaconate	0.04	0.00
P. putida KT2440 attTn7::P₁₄fPA0878-0886	mesaconate	0.42	0.02
P. putida KT2440 attTn7::P₁₄fPA0878-0883	(*S*)-citramalate	0.01	0.00
P. putida KT2440 attTn7::P₁₄fPA0878-0886	(*S*)-citramalate	0.40	0.01
P. putida KT2440 attTn7::P₁₄fPA0878-0883	(*R*)-citramalate	no growth	-
P. putida KT2440 attTn7::P₁₄fPA0878-0886	(*R*)-citramalate	no growth	-
P. putida KT2440 attTn7::P₁₄fPA0878-0883	citraconate	no growth	-
P. putida KT2440 attTn7::P₁₄fPA0878-0886	citraconate	no growth	-
P. putida KT2440 attTn7::P₁₄fPA0878-0883	(*S*)-(*R*)-methylsuccinate	0.02	0.00
P. putida KT2440 attTn7::P₁₄fPA0878-0886	(*S*)-(*R*)-methylsuccinate	0.40	0.02

| Figure 2.4-4			
Strain	**substrate**	**μ (h⁻¹)**	**SD**
P. putida KT2440	ITA, ITT, 2-HP	no growth	-
P. putida KT2440 attTn7::P₁₄fPA0878-0883	ITA, ITT, 2-HP	0.12	0.00
P. putida KT2440 attTn7::P₁₄fPA0878-0886	ITA, ITT, 2-HP	0.15	0.01
ΔPA0878 (*ich*)	ITA, ITT, 2-HP	no growth	-
ΔPA0879	ITA, ITT, 2-HP	0.13	0.01
ΔPA0880 (*rdoPA*)	ITA, ITT, 2-HP	no growth	-
ΔPA0881	ITA, ITT, 2-HP	0.14	0.00
ΔPA0882 (*ict*)	ITA, ITT, 2-HP	0.01	0.00
ΔPA0883 (*ccl*)	ITA, ITT, 2-HP	no growth	-

Figure 5			
Strain	**substrate**	**μ (h⁻¹)**	**SD**
P. putida KT2440	Glucose + ITT, 2-HP	0.32	0.00
P. putida KT2440 attTn7::P₁₄fPA0878-0883	Glucose + ITT, 2-HP	0.38	0.00
P. putida KT2440 attTn7::P₁₄fPA0878-0886	Glucose + ITT, 2-HP	0.23	0.00
ΔPA0878 (*ich*)	Glucose + ITT, 2-HP	0.31	0.00
ΔPA0879	Glucose + ITT, 2-HP	0.21	0.00
ΔPA0880 (*rdoPA*)	Glucose + ITT, 2-HP	0.20	0.01
ΔPA0881	Glucose + ITT, 2-HP	0.22	0.00
ΔPA0882 (*ict*)	Glucose + ITT, 2-HP	0.31	0.00
ΔPA0883 (*ccl*)	Glucose + ITT, 2-HP	0.20	0.00
P. putida KT2440	Acetate + ITT, 2-HP	0.22	0.01
P. putida KT2440 attTn7::P₁₄fPA0878-0883	Acetate + ITT, 2-HP	0.32	0.01
P. putida KT2440 attTn7::P₁₄fPA0878-0886	Acetate + ITT, 2-HP	0.25	0.00
ΔPA0878 (*ich*)	Acetate + ITT, 2-HP	0.22	0.02
ΔPA0879	Acetate + ITT, 2-HP	0.23	0.00
ΔPA0880 (*rdoPA*)	Acetate + ITT, 2-HP	no growth	-
ΔPA0881	Acetate + ITT, 2-HP	0.23	0.01
ΔPA0882 (*ict*)	Acetate + ITT, 2-HP	0.23	0.02
ΔPA0883 (*ccl*)	Acetate + ITT, 2-HP	0.23	0.01

Figure S1			
Strain	**substrate**	**μ (h⁻¹)**	**SD**
P. putida KT2440 attTn7::P₁₄fPA0878-0886	itaconate	0.36	0.01
ΔPA0878 (*ich*)	itaconate	no growth	-
ΔPA0879-81	itaconate	0.41	0.01
ΔPA0879	itaconate	0.38	0.02
ΔPA0880 (*rdoPA*)	itaconate	0.38	0.02
ΔPA0881	itaconate	0.37	0.01
ΔPA0882 (*ict*)	itaconate	0.11	0.00
ΔPA0883 (*ccl*)	itaconate	no growth	-
ΔPP_0897	itaconate	0.37	0.01

P. putida KT2440 attTn7::P14f*PA0878-0886*	(*S*)-citramalate	0.38	0.00
ΔPA0878 (*ich*)	(*S*)-citramalate	0.32	0.01
ΔPA0879-81	(*S*)-citramalate	0.40	0.01
ΔPA0879	(*S*)-citramalate	0.39	0.02
ΔPA0880 (*rdo*PA)	(*S*)-citramalate	0.37	0.02
ΔPA0881	(*S*)-citramalate	0.00	
ΔPA0882 (*ict*)	(*S*)-citramalate	no growth	-
ΔPA0883 (*ccl*)	(*S*)-citramalate	no growth	-
ΔPP_0897	(*S*)-citramalate	0.37	0.01
P. putida KT2440 attTn7::P14f*PA0878-0886*	mesaconate	0.36	0.00
ΔPA0878 (*ich*)	mesaconate	0.37	0.01
ΔPA0879-81	mesaconate	0.36	0.00
ΔPA0879	mesaconate	0.38	0.02
ΔPA0880 (*rdo*PA)	mesaconate	0.39	0.01
ΔPA0881	mesaconate	0.38	0.02
ΔPA0882 (*ict*)	mesaconate	no growth	-
ΔPA0883 (*ccl*)	mesaconate	no growth	-
ΔPP_0897	mesaconate	no growth	-
P. putida KT2440 attTn7::P14f*PA0878-0886*	(*S*)-(*R*)-methylsuccinate	0.36	0.00
ΔPA0878 (*ich*)	(*S*)-(*R*)-methylsuccinate	no growth	-
ΔPA0879-81	(*S*)-(*R*)-methylsuccinate	no growth	-
ΔPA0879	(*S*)-(*R*)-methylsuccinate	no growth	-
ΔPA0880 (*rdo*PA)	(*S*)-(*R*)-methylsuccinate	0.36	0.01
ΔPA0881	(*S*)-(*R*)-methylsuccinate	0.18	0.00
ΔPA0882 (*ict*)	(*S*)-(*R*)-methylsuccinate	no growth	-
ΔPA0883 (*ccl*)	(*S*)-(*R*)-methylsuccinate	no growth	-
ΔPP_0897	(*S*)-(*R*)-methylsuccinate	0.36	0.02
P. putida KT2440 attTn7::P14f*PA0878-0886*	(*R*)-methylsuccinate	0.36	0.00
ΔPA0878 (*ich*)	(*R*)-methylsuccinate	no growth	-
ΔPA0879-81	(*R*)-methylsuccinate	no growth	-
ΔPA0879	(*R*)-methylsuccinate	no growth	-
ΔPA0880 (*rdo*PA)	(*R*)-methylsuccinate	0.35	0.01
ΔPA0881	(*R*)-methylsuccinate	0.36	0.01
ΔPA0882 (*ict*)	(*R*)-methylsuccinate	no growth	-
ΔPA0883 (*ccl*)	(*R*)-methylsuccinate	no growth	-
ΔPP_0897	(*R*)-methylsuccinate	0.37	0.01
P. putida KT2440 attTn7::P14f*PA0878-0886*	(*S*)-methylsuccinate	0.36	0.00
ΔPA0878 (*ich*)	(*S*)-methylsuccinate	no growth	-
ΔPA0879-81	(*S*)-methylsuccinate	no growth	-
ΔPA0879	(*S*)-methylsuccinate	no growth	-
ΔPA0880 (*rdo*PA)	(*S*)-methylsuccinate	0.36	0.02
ΔPA0881	(*S*)-methylsuccinate	no growth	-
ΔPA0882 (*ict*)	(*S*)-methylsuccinate	no growth	-
ΔPA0883 (*ccl*)	(*S*)-methylsuccinate	no growth	-
ΔPP_0897	(*S*)-methylsuccinate	0.39	0.01

Figure S5.4-8			
Strain	**substrate**	**μ (h^{-1})**	**SD**
P. putida KT2440	glucose	0.38	0.01
P. putida KT2440 attTn7::P14f*PA0878-0883*	glucose	0.38	0.01
P. putida KT2440 attTn7::P14f*PA0878-0886*	glucose	0.37	0.01
P. putida KT2440	glucose + itaconate	0.41	0.00
P. putida KT2440 attTn7::P14f*PA0878-0883*	glucose + itaconate	0.40	0.02
P. putida KT2440 attTn7::P14f*PA0878-0886*	glucose + itaconate	0.42	0.01
P. putida KT2440	glucose + mesaconate	0.39	0.00
P. putida KT2440 attTn7::P14f*PA0878-0883*	glucose + mesaconate	0.39	0.01
P. putida KT2440 attTn7::P14f*PA0878-0886*	glucose + mesaconate	0.41	0.01

P. putida KT2440	glucose + (*S*)-citramalate	0.39	0.01
P. putida KT2440 attTn7::P$_{14f}$*PA0878-0883*	glucose + (*S*)-citramalate	0.40	0.00
P. putida KT2440 attTn7::P$_{14f}$*PA0878-0886*	glucose + (*S*)-citramalate	0.41	0.02
P. putida KT2440	glucose + (*R*)-citramalate	0.40	0.01
P. putida KT2440 attTn7::P$_{14f}$*PA0878-0883*	glucose + (*R*)-citramalate	0.39	0.00
P. putida KT2440 attTn7::P$_{14f}$*PA0878-0886*	glucose + (*R*)-citramalate	0.39	0.02
P. putida KT2440	glucose + (*S*)-methylsuccinate	0.40	0.01
P. putida KT2440 attTn7::P$_{14f}$*PA0878-0883*	glucose + (*S*)-methylsuccinate	0.39	0.01
P. putida KT2440 attTn7::P$_{14f}$*PA0878-0886*	glucose + (*S*)-methylsuccinate	0.43	0.02
P. putida KT2440	glucose + (*R*)-methylsuccinate	0.39	0.00
P. putida KT2440 attTn7::P$_{14f}$*PA0878-0883*	glucose + (*R*)-methylsuccinate	0.39	0.01
P. putida KT2440 attTn7::P$_{14f}$*PA0878-0886*	glucose + (*R*)-methylsuccinate	0.42	0.01
P. putida KT2440	glucose + citraconate	0.39	0.01
P. putida KT2440 attTn7::P$_{14f}$*PA0878-0883*	glucose + citraconate	0.39	0.01
P. putida KT2440 attTn7::P$_{14f}$*PA0878-0886*	glucose + citraconate	0.39	0.01
P. putida KT2440	acetate	0.41	0.00
P. putida KT2440 attTn7::P$_{14f}$*PA0878-0883*	acetate	0.39	0.01
P. putida KT2440 attTn7::P$_{14f}$*PA0878-0886*	acetate	0.40	0.01
P. putida KT2440	acetate + itaconate	0.37	0.00
P. putida KT2440 attTn7::P$_{14f}$*PA0878-0883*	acetate + itaconate	0.38	0.01
P. putida KT2440 attTn7::P$_{14f}$*PA0878-0886*	acetate + itaconate	0.40	0.01
P. putida KT2440	acetate + mesaconate	no growth	-
P. putida KT2440 attTn7::P$_{14f}$*PA0878-0883*	acetate + mesaconate	no growth	-
P. putida KT2440 attTn7::P$_{14f}$*PA0878-0886*	acetate + mesaconate	no growth	-
P. putida KT2440	acetate + (*S*)-citramalate	0.36	0.01
P. putida KT2440 attTn7::P$_{14f}$*PA0878-0883*	acetate + (*S*)-citramalate	0.36	0.01
P. putida KT2440 attTn7::P$_{14f}$*PA0878-0886*	acetate + (*S*)-citramalate	0.37	0.01
P. putida KT2440	acetate + (*R*)-citramalate	0.33	0.01
P. putida KT2440 attTn7::P$_{14f}$*PA0878-0883*	acetate + (*R*)-citramalate	0.32	0.02
P. putida KT2440 attTn7::P$_{14f}$*PA0878-0886*	acetate + (*R*)-citramalate	no growth	-
P. putida KT2440	acetate + (*S*)-methylsuccinate	0.33	0.02
P. putida KT2440 attTn7::P$_{14f}$*PA0878-0883*	acetate + (*S*)-methylsuccinate	0.31	0.01
P. putida KT2440 attTn7::P$_{14f}$*PA0878-0886*	acetate + (*S*)-methylsuccinate	0.35	0.01
P. putida KT2440	acetate + (*R*)-methylsuccinate	0.28	0.01
P. putida KT2440 attTn7::P$_{14f}$*PA0878-0883*	acetate + (*R*)-methylsuccinate	0.30	0.01
P. putida KT2440 attTn7::P$_{14f}$*PA0878-0886*	acetate + (*R*)-methylsuccinate	0.35	0.07
P. putida KT2440	acetate + citraconate	0.26	0.01
P. putida KT2440 attTn7::P$_{14f}$*PA0878-0883*	acetate + citraconate	0.30	0.06
P. putida KT2440 attTn7::P$_{14f}$*PA0878-0886*	acetate + citraconate	no growth	-

Table S5.4-2. Structure-based similarity search of PA0881 using Distance Matrix Alignment (DALI). Structures are labeled with their Protein Data Bank (PDB) identifier (ID). According to Holm, a Z-score greater than 20 indicates homology of two structures (Holm, 2020). The lower the root mean square deviation of aligned C_α atoms (rmsd) score is, the less the average deviation in distance of C_α atoms in the 3D superimposition. The number of aligned C_α atoms is indicated by lali. IDS = iminodisuccinate, CAD = *cis*-aconitate decarboxylase, PrpD = 2-methylcitrate dehydratase.

PDB ID	Z-score	rmsd	lali	description	origin	reference
2HP3	52.9	1.9	435	IDS epimerase	*Agrobacterium tumefaciens* BY6	Lohkamp et al. (2006)
7BR9	49.3	2.4	432	CAD	*Mus musculus*	Chun et al. (2020a)
6R6U	48.9	2.4	434	CAD	*Homo sapiens*	(Chen et al., 2019)
7BRA	46.1	2.7	429	CAD	*Bacillus subtilis*	Chun et al. (2020b)
6S62	41.8	2.6	432	PrpD	*Pseudomonas aeruginosa* PAO1	Unpublished, Protein Data Bank

Table S5.4-3. Compounds identified by GC-ToF-MS analysis. Retention time (R.T.) and corresponding retention index are displayed. Area percentage is shown for samples obtained from cultivation of indicated strains with the itaconate/2-HP/ITT mixture. Area percentage can be used to perform semi-quantitative analysis.

Compound	R.T. (min)	Retention index	Area % ΔPA0880	Area % $attTn7::P_{14f}-$ PA0878-0886
unknown	5.20	951.9	ND	0.2
1,-hexanol	5.56	982.8	0.4	0.3
N-morpholin	5.69	994.2	ND	0.1
pyruvate	6.94	1095.7	0.3	0.3
Carbonat-methoxyamin	7.41	1133.3	0.8	0.8
3-hydroxy-isovalerat	8.24	1201.1	ND	0.2
unknown	8.51	1224.0	1.7	1.6
phosphate	8.95	1261.9	62.5	64.0
unknown	9.19	1283.0	0.5	1.8
unknown	9.68	1325.5	ND	0.1
itaconate	9.81	1336.1	17.3	ND
unknown	10.27	1376.4	ND	0.2
2,4-dihydroxybutyrate (2,4-DHB)	10.52	1397.9	ND	6.4
2-hydroxyparaconate	10.92	1436.0	9.0	ND
tetradecamethyl-cyclo-Heptasiloxane	11.07	1450.5	1.8	1.8
citramalate	11.19	1462.1	0.3	ND
2-hydroxyparaconate*	11.55	1496.2	0.6	0.7
$C_6H_{10}O_6$ methylated ITT?	12.61	1598.1	ND	0.6
unknown	12.80	1618.3	0.7	ND
unknown	13.08	1648.7	ND	0.2
unknown	13.15	1656.6	ND	0.4
itatartarate	13.23	1664.6	3.5	20.0
unknown	16.81	2080.7	0.3	ND
unknown	17.98	2234.4	0.5	ND
unknown	19.64	2474.8	0.2	0.3

5.5 Supplementary data to Chapter 2.5:

Biodegradation of poly(ester-urethane) coatings by Halopseudomonas formosensis.

de Witt, J.[1]**,** Molitor, R.[2], Gätgens, J.[1], Ortmann de Percin Northumberland, C.[3], Kruse, L.[2], Polen, T.[1], Wynands, B.[1], van Goethem, K.[4], Thies, S.[2], Jaeger, K-E.[1,2], Wierckx, N.[1], (2023). Biodegradation of poly(ester-urethane) coatings by *Halopseudomonas formosensis*. *Microbial Biotechnology*, 17, e14362. doi:10.1111/1751-7915.1436

[1]Institute of Bio- and Geosciences IBG-1: Biotechnology, Forschungszentrum Jülich, Jülich, Germany

[2] Institute of Molecular Enzyme Technology, Heinrich-Heine-University Düsseldorf, Forschungszentrum Jülich, Jülich, Germany

[3] Ernst Ruska-Centre for Microscopy and Spectroscopy with Electrons: ER-C-3: Structural Biology, Forschungszentrum Jülich, Jülich, Germany

[4] I-COATS N.V. 2600 Antwerp, Belgium

[*] Corresponding author

Figure S5.5-1. Growth parameters of *H. formosensis* FZJ. Colony forming units (cfu) of *H. formosensis* FZJ were investigated in MSM supplemented with 1 % (v/v) Impranil DLN-SD as sole carbon source to confirm growth of the strain with the substrate (A). Consumption of NH_4^+ and OD_{600} was quantified over time in MSM supplemented with 22.5 mM suberic acid as sole carbon source (B) to reveal the correlation between both parameters (C). Hence, consumption of NH_4^+ was confirmed as suitable parameter for revealing growth of *H. formosensis* FZJ with Impranil DLN-SD as sole carbon source (Figure 2.5-1).
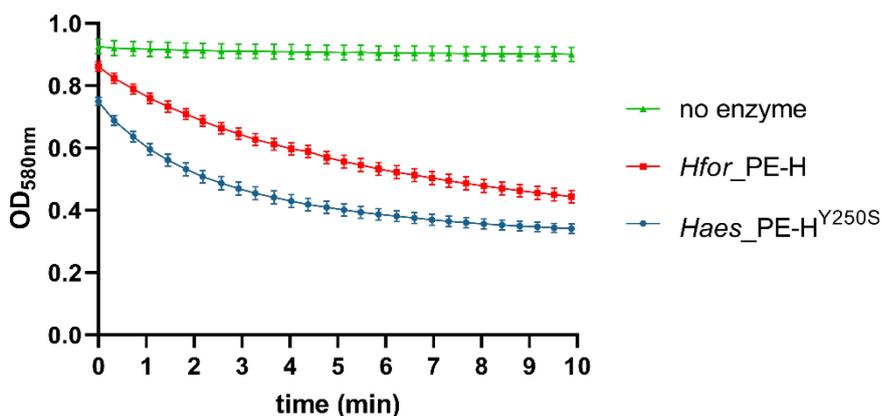
Figure S5.5-2. Decrease of turbidity by enzymatic depolymerization of Impranil DLN-SD over time. The loss of turbidity was measured by the decrease in OD_{580nm}. Reactions were performed in 100 mM potassium phosphate buffer with 100 mM NaCl (pH 7.2) and 1 % (v/v) Impranil DLN-SD. The final enzyme concentration used in the assays was 50 nM.
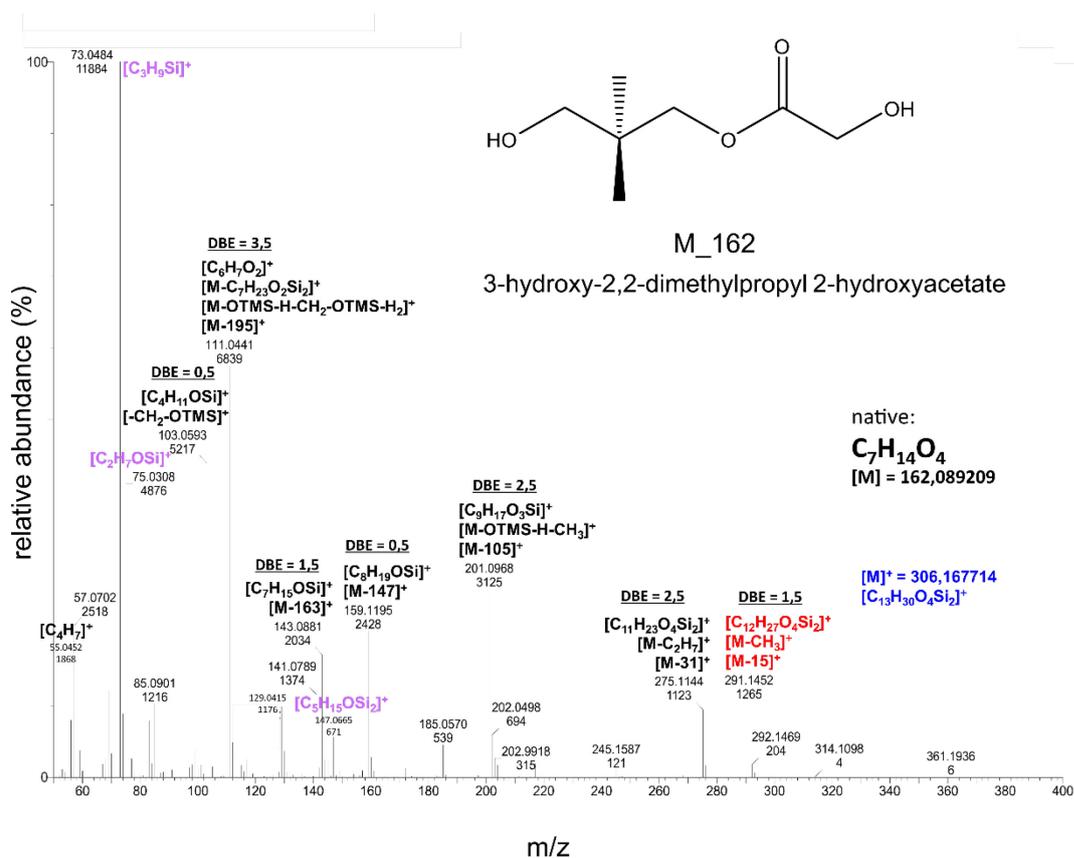
Figure 5.5-3. m/z Spectrum of M_162. Spectral analysis indicates that M_162 is 3-hydroxy-2,2-dimethylpropyl 2-hydroxyacetate that is a dimer of neopentyl glycol and glycolic acid.

Table S5.5-1. Predicted hydrolases encoded in the genome of *H. formosensis* FZJ. The genome was blasted against the TREMBL database and SignalP-6.0 was used to predict signal peptides and the translocation mechanism (Teufel et al., 2022). Sec/SPI: standard secretory signal peptides transported by the Sec translocon and cleaved by Signal Peptidase I (Lep). Sec/SPII: lipoprotein signal peptides transported by the Sec translocon and cleaved by Signal Peptidase II (Lsp). The sequence identity towards *Hfor*_PE-H from *H. formosensis* CC-CY503[T] is shown.

Enzyme	signal peptide	annotation	% identity CC-CY503[T] _PE-H
*Hfor*_PE-H	Sec/SPI	dienelactone hydrolase family protein	99.7
Hydrolase-1	Sec/SPI	arylesterase	<20
Hydrolase-2	Sec/SPII	carboxylesterase family protein	<20
Hydrolase-3	Sec/SPII	lipase secretion chaperone	<20
Hydrolase-4	Sec/SPI	lipase	<20
Hydrolase-5	Sec/SPII	alpha-beta hydrolase	<20
Hydrolase-6	Sec/SPI	serine hydrolase	<20
Hydrolase-7	no	alpha-beta hydrolase	<20

Hydrolase-8	Sec/SPII	SGNH/GDSL hydrolase family protein	<20
Hydrolase-9	no	carboxylesterase family protein	<20
Hydrolase-10	Sec/SPII	carboxylesterase family protein	<20
Hydrolase-11	Sec/SPI	alpha-beta hydrolase	27.2
Hydrolase-12	no	serine hydrolase	<20
Hydrolase-13	no	EstA family serine hydrolase	<20
Hydrolase-14	Sec/SPI	serine hydrolase	<20
Hydrolase-15	no	alpha-beta hydrolase	<20
Hydrolase-16	no	alpha-beta hydrolase	<20
Hydrolase-17	no	alpha-beta hydrolase	<20
Hydrolase-18	no	alpha-beta hydrolase	<20
Hydrolase-19	Sec/SPII	carboxylesterase family protein	<20
Hydrolase-20	Sec/SPI	dienelactone hydrolase family protein	29.2
Hydrolase-21	no	carbon-nitrogen hydrolase family protein	<20
Hydrolase-22	no	peptidase S8 and S53 subtilisin kexin sedolisin	<20
Hydrolase-23	Sec/SPI	phospholipase	<20

Table S5.5-2. Full GC-ToF-MS data.

Enzymatic degradation + Impranil DLN-SD (Figure 2.5-6 a)				
Compound	**Retention time (min)**	**Retention Index**	**Area TIC**	**Area %**
JuPoD_015_045 Methoxyamin [MeOX] (2 TMS) RI 956	5.24	956.4	3105873	0.0
JuPoD_003_113 1-Hexanol [C6ol] (TMS) RI 987	5.60	987.6	26304422	0.3
Peak 3	5.77	1002.3	1660821	0.0
Peak 4	6.05	1025.1	3931733	0.1
JuPoD_015_019 2-hydroxy-pyridin (TMS) RI 1037	6.21	1037.6	2648225	0.0
JuPoD_006_263 Lactat (2 TMS) RI 1055	6.39	1052.9	28271782	0.4
Peak 7	6.45	1057.1	9660357	0.1
Peak 8	6.51	1062.6	4163143	0.1
JuPoD_003_147 Neopentyl glycol [2,2-dimethyl-Propan-1,3-diol] (2 TMS) RI 1077	6.65	1074.1	5161727	0.1
JuPoD_011_362 M_75 (2 TMS) RI 1101	6.96	1098.8	26755404	0.3
JuPoD_005_198 n-Undecane [n-C11] (wo) RI 1100	6.99	1101.6	7956251	0.1
JuPoD_015_046 Hydroxylamin (3 TMS) RI 1114	7.11	1110.8	4593973	0.1
JuPoD_007_037 Carbonat-methoxyamin (2 TMS) RI 1139	7.41	1135.7	69923835	0.9
JuPoD_013_014 dodecamethyl-x-Pentasiloxane [xSi5] (wo) RI 1158	7.62	1152.5	11289119	0.1
JuPoD_005_161 n-Dodecane [n-C12] (wo) RI 1200	8.22	1201.2	4382761	0.1
JuPoD_011_290 unident_M_189 (xxx) RI 1226	8.49	1224.9	183070397	2.4
Peak 17	8.50	1225.4	185383422	2.4
Peak 18	8.91	1261.2	25357472	0.3
JuPoD_007_039 Phosphat (3 TMS) RI 1267	8.94	1263.6	2729724059	35.3
Peak 20	8.96	1265.3	799445745	10.4
Peak 21	8.97	1266.3	446600492	5.8

JuPoD_011_367 M_212 [unident_CnHm] (wo) RI 1277	9.09	1276.9	4632397	0.1
JuPoD_011_367 M_212 [unident_CnHm] (wo) RI 1277	9.19	1285.6	2053872	0.0
Peak 24	9.20	1286.6	2053872	0.0
JuPoD_006_378 3-hydroxy-Caproat [3-hydroxy-Hexanoat] (2 TMS) RI 1299	9.35	1299.1	102419060	1.3
JuPoD_011_363 M_198 [unident_CnHm] (wo) RI 1323	9.62	1323.1	9372030	0.1
JuPoD_011_357 unident_M_300 (xxx) RI 1333	9.71	1330.5	5580239	0.1
JuPoD_003_095 1,6-Hexan-diol (2 TMS) RI 1343	9.84	1341.4	106704702	1.4
JuPoD_010_080 Pelargonat [Nonanoat] (TMS) RI 1359	10.03	1358.1	8645965	0.1
Peak 30	11.08	1455.0	4450896	0.1
Peak 31	11.11	1457.1	4727600	0.1
JuPoD_010_082 3-hydroxy-Caprylat [3-hydroxy-Octanoat] (2 TMS) RI 1464	11.17	1463.8	60933891	0.8
JuPoD_006_379 Adipat (2 TMS) RI 1501	11.56	1500.9	512731177	6.6
JuPoD_005_202 n-Pentadecane [n-C15] (wo) RI 1500	11.58	1502.8	31470180	0.4
JuPoD_003_146 2,4-di-tertbutyl-Phenol (TMS) RI 1539	11.96	1539.2	2555082	0.0
JuPoD_005_203 n-Hexadecane [n-C16] (wo) RI 1600	12.59	1599.9	34652207	0.4
Peak 37	13.93	1744.2	13186032	0.2
Peak 38	14.06	1758.3	3511462	0.0
JuPoD_011_374 M_162 (2 TMS) RI 1902	15.30	1900.5	62366440	0.8
Peak 40	15.57	1932.0	2803183	0.0

Enzymatic degradation no Impranil DLN-SD (Figure 2.5-6 a)				
Compound	**Retention time (min)**	**Retention Index**	**Area TIC**	**Area %**
JuPoD_015_045 Methoxyamin [MeOX] (2 TMS) RI 956	5.25	957.2	3126014	0.0
JuPoD_016_016 Carbodiimid (2 TMS) RI 953	5.26	958.1	3126014	0.0
JuPoD_007_021 Borat (3 TMS) RI 973	5.44	974	14573577	0.1
JuPoD_003_113 1-Hexanol [C6ol] (TMS) RI 987	5.60	988.1	30941966	0.3
Peak 5	5.78	1003.2	1222521	0.0
Peak 6	6.06	1025.5	3748902	0.0
JuPoD_015_019 2-hydroxy-Pyridin (TMS) RI 1037	6.21	1038	3199180	0.0
JuPoD_006_263 Lactat (2 TMS) RI 1055	6.40	1053.3	11488166	0.1
Peak 9	6.45	1057.3	10738753	0.1
Peak 10	6.52	1062.9	5687671	0.1
JuPoD_011_362 M_75 (2 TMS) RI 1101	6.96	1099.3	27383921	0.3
JuPoD_005_198 n-Undecane [n-C11] (wo) RI 1100	7.00	1101.8	9383288	0.1
JuPoD_005_186 n-Undecane [n-C11] (wo) RI 1100	7.06	1107.4	2985218	0.0
JuPoD_015_046 Hydroxylamin (3 TMS) RI 1114	7.11	1111	4940395	0.0
JuPoD_007_037 Carbonat-methoxyamin (2 TMS) RI 1139	7.42	1136	71911826	0.7
JuPoD_013_014 dodecamethyl-x-Pentasiloxane [xSi5] (wo) RI 1158	7.62	1152.6	13115843	0.1
JuPoD_005_161 n-Dodecane [n-C12] (wo) RI 1200	8.22	1201.2	5082386	0.0
JuPoD_005_175 n-Dodecane [n-C12] (wo) RI 1200	8.36	1213.8	5561166	0.1
Peak 19	8.46	1222.2	1925280	0.0
JuPoD_011_276 unident_M_189 (xxx) RI 1226	8.49	1225	184894575	1.7
Peak 21	8.50	1225.5	192303016	1.8
Peak 22	8.91	1261.1	11432570	0.1
Peak 23	8.94	1263.6	2895071513	27.3
JuPoD_007_039 Phosphat (3 TMS) RI 1267	8.94	1263.8	2901936236	27.4
Peak 25	8.96	1265.1	1133420635	10.7

Peak 26	8.97	1266.4	545544755	5.1
Peak 27	8.98	1267.4	243415094	2.3
JuPoD_011_367 M_212 [unident_CnHm] (wo) RI 1277	9.09	1276.9	5348796	0.1
JuPoD_006_377 3-hydroxy-Caproat [3-hydroxy-Hexanoat] (2 TMS) RI 1299	9.35	1299.1	13946423	0.1
JuPoD_011_363 M_198 [unident_CnHm] (wo) RI 1323	9.63	1323.2	9772989	0.1
JuPoD_011_357 unident_M_300 (xxx) RI 1333	9.71	1330.6	8794637	0.1
JuPoD_010_072 Pelargonat [Nonanoat] (TMS) RI 1359	10.03	1358	4735544	0.0
Peak 33	10.79	1426.4	2386331	0.0
Peak 34	11.08	1455.1	21070627	0.2
JuPoD_010_082 3-hydroxy-Caprylat [3-hydroxy-Octanoat] (2 TMS) RI 1464	11.17	1463.8	37264643	0.4
JuPoD_005_201 n-Pentadecane [n-C15] (wo) RI 1500	11.58	1502.8	23982484	0.2
JuPoD_003_146 2,4-di-tertbutyl-Phenol (TMS) RI 1539	11.96	1539.2	3284150	0.0
JuPoD_005_177 n-Hexadecane [n-C16] (wo) RI 1600	12.59	1600	35307780	0.3
Peak 39	13.01	1645.6	22883188	0.2
JuPoD_005_199 n-Heptadecane [n-C17] (wo) RI 1700	13.54	1702.2	30463933	0.3
Peak 41	15.57	1932.2	3398829	0.0

Microbial degradation *H. formosensis* FZJ (Figure 2.5-6 b)				
Compound	**Retention time (min)**	**Retention Index**	**Area TIC**	**Area %**
JuPoD_015_045 Methoxyamin [MeOX] (2 TMS) RI 956	5.24	956.5	13378952	0.5
JuPoD_016_016 Carbodiimid (2 TMS) RI 953	5.25	957.7	1626381	0.1
JuPoD_003_113 1-Hexanol [C6ol] (TMS) RI 987	5.60	987.7	18368144	0.7
Peak 4	5.78	1002.9	1073601	0.0
JuPoD_015_019 2-hydroxy-Pyridin (TMS) RI 1037	6.21	1037.8	1283163	0.0
JuPoD_006_251 Lactat (2 TMS) RI 1055	6.39	1053.1	2514340	0.1
JuPoD_003_147 Neopentylglycol [2,2-dimethyl-Propan-1,3-diol] (2 TMS) RI 1077	6.65	1074.3	71277618	2.6
JuPoD_011_362 M_75 (2 TMS) RI 1101	6.96	1099.1	12898203	0.5
JuPoD_005_186 n-Undecane [n-C11] (wo) RI 1100	6.99	1101.7	2194956	0.1
JuPoD_013_014 dodecamethyl-x-Pentasiloxane [xSi5] (wo) RI 1158	7.62	1152.6	8975473	0.3
JuPoD_011_290 unident_M_189 (xxx) RI 1226	8.49	1224.9	62383557	2.3
JuPoD_006_067 4-hydroxy-Butyrat [GHB] (2 TMS) RI 1230	8.55	1230.0	22179229	0.8
JuPoD_007_039 Phosphat (3 TMS) RI 1267	8.94	1263.9	1953171598	71.6
Peak 14	8.96	1266.0	403538019	14.8
Peak 15	8.98	1267.3	135020003	5.0
JuPoD_003_094 1,6-Hexan-diol (2 TMS) RI 1343	9.83	1341.5	5112955	0.2
JuPoD_006_376 Adipat (2 TMS) RI 1501	11.57	1502.2	4910497	0.2
JuPoD_011_249 M_162 (2 TMS) RI 1902	15.31	1901.5	6152823	0.2

Microbial degradation abiotic control (Figure 2.5-6 b)				
Compound	**Retention time (min)**	**Retention Index**	**Area TIC**	**Area %**
JuPoD_015_045 Methoxyamin [MeOX] (2 TMS) RI 956	5.24	956.5	18272345	0.4
JuPoD_007_021 Borat (3 TMS) RI 973	5.43	973.5	8486759	0.2
JuPoD_003_113 1-Hexanol [C6ol] (TMS) RI 987	5.60	987.7	16716063	0.4

JuPoD_015_019 2-hydroxy-Pyridin (TMS) RI 1037	6.21	1037.8	1243795	0.0
JuPoD_011_362 M_75 (2 TMS) RI 1101	6.96	1098.9	13488524	0.3
JuPoD_007_035 Carbonat-methoxyamin (2 TMS) RI 1139	7.41	1135.5	4227397	0.1
JuPoD_013_014 dodecamethyl-x-Pentasiloxane [xSi5] (wo) RI 1158	7.62	1152.6	5908778	0.1
JuPoD_011_303 unident_M_189 (xxx) RI 1226	8.49	1224.9	60206996	1.4
JuPoD_007_039 Phosphat (3 TMS) RI 1267	8.94	1263.8	2019748849	47.8
Peak 10	8.95	1265.2	2039184788	48.3
Peak 11	9.22	1288.1	37202063	0.9

Table S1. Strains used in this thesis.

Strain	Description	Reference	Chapter
Escherichia coli			
HB101 pRK2013	*F⁻ mcrB mrr hsdS20(rB⁻ mB⁻) recA13 leuB6 ara-14 proA2 lacY1 galK2 xyl-5 mtl-1 rpsL20*(Smᴿ) *gln V44λ⁻*	Boyer and Roulland-Dussoix (1969)	2.1, 2.3, 2.4, 2.5
PIR2	F⁻ Δ*lac169 rpoS* (Am) *robA1 creC510 hsdR514 endA reacA1 uidA* (Δ*Mlui*)::*pir-116*	Life Technologies	2.1, 2.3, 2.4, 2.5
DH5α λpir	*endA1 hsdR17 glnV44 (= supE44) thi-1 recA1 gyrA96 relA1 Φ 80dlacΔ (lacZ)M15 Δ(lacZYA-argF)U169 zdg-232::Tn10 uidA::pir⁺*	de Lorenzo lab	2.3
DH5α λpir pTNS1	*endA1 hsdR17 glnV44* (= *supE44) thi-1 recA1 gyrA96 relA1* φ80*dlac*Δ(*lacZ)M15 Δ(lacZYA-argF)U169 zdg-232*::Tn10 *uidA*::*pir+*	de Lorenzo lab	2.4
EPI400 pQT8-*Pem7-sceI*	*F–mcrA Δ(mrr-hsdRMS-mcrBC) φ80dlacZ*Δ*M15 ΔlacX74 recA1 endA1 araD139 Δ(ara, leu)7697 galU galK λ–rpsL nupG tonA ΔpcnBdhf*	This study MiCat #700	2.5
EC100D pir-116 pEMG-TS1-TS2ΔPE-H	*F–mcrA Δ(mrr-hsdRMS-mcrBC) φ80dlacZ*Δ*M15 ΔlacX74 recA1 endA1 araD139 Δ(ara, leu)7697 galU galK λ–rpsL nupG pir-116(DHFR)*	This study MiCat #1080	2.5
Pseudomonas putida			
KT2440	Strain derived from *P. putida* mt-2 cured of the pWW0 plasmid.	Bagdasarian *et al.* (1981) MiCat #30	2.1, 2.3, 2.4
KT2440 PP_2884^Δ3, PP_0409^W676L	PP_2884^Δ3, PP_0409^W676L.	This work MiCat #1100	2.1
KT2440-AA	Metabolizes AA. Genomic integration of *att*Tn7::*P₁₄ₑ-dcaAKIJP* and removal of the resistance marker. Exchange of the natural promoter *P_paaF* for the synthetic *P₁₄g* promoter together with knockout of *paaYX*, knockout of *psrA*.	Ackermann *et al.* (2021) MiCat #618	2.1, 2.3
HMDA-1 mutant	Mutant of KT2440-AA isolated after prolonged incubation on HMDA.	This work MiCat #1282	2.1
KT2440-AA ΔPP_2884	Deletion of PP_2884.	This work MiCat #1083	2.1
KT2440-AA PP_2884^Δ3	Deletion of 9 bp in PP_2884 resulting in the loss of F61, F62, and F63 in the encoded regulator.	This work MiCat #1099	2.1
ALE mutant Ahx-194	ALE mutant of KT2440-AA PP_2884^Δ3 after ALE on Ahx.	This work MiCat #1553	2.1

P. putida NYL	KT2440-AA PP_2884$^{\Delta3}$, PP_0409^{W676L}. Final reverse engineered strain for growth on C$_6$-PA-monomers.	This work MiCat #1570	2.1
P. putida NYL ΔPP_0411-4	Deletion of PP_0411-4.	This work MiCat #1741	2.1
P. putida NYL Δ*oplBA*	Deletion of *oplBA* PP_3514-5.	This work MiCat #1974	2.1
KT2440-AA PP_2884$^{\Delta3}$, ΔPP_0409-10	Deletion of PP_0409-10.	This work MiCat #1504	2.1
KT2440-AA PP_2884$^{\Delta3}$, ΔPP_0409-10::$_{P14b}$	Deletion of PP_0409-10 and insertion of the constitutive P$_{14b}$ promoter upstream of PP_0411-4.	This work MiCat #1506	2.1
P. putida NYL-P_{14f}-*nylB*	Constitutive expression of codon-optimized *nylB* from *Paenarthrobacter ureafaciens* in landing pad PP_0340-1.	This work MiCat #1586	2.1
P. putida NYL-P_{14f}-*nylB* ALE mutant Ahx$_2$ -322	ALE mutant of *P. putida* NYL-P_{14f}-*nylB* isolated from ALE on Ahx$_2$.	This work MiCat #1688	2.1
P. putida NYL-P_{14f}-*nylB* ALE mutant Ahx$_2$ -323	ALE mutant of *P. putida* NYL-P_{14f}-*nylB* isolated from ALE on Ahx$_2$.	This work MiCat #1689	2.1
P. putida NYL-P_{14f}-*nylB* PP_0412^{V222L}	Partly reverse engineered. PP_0412^{V222L}.	This work MiCat #1784	2.1
P. putida NYL-P_{14f}-*nylB* CbrA^{A625T}	Partly reverse engineered. CbrA^{A625T} (PP_4695^{A625T}).	This work MiCat #1786	2.1
P. putida NYL-P_{14f}-*nylB*, $P_{PP_2177}$$^{C\rightarrow T}$	Partly reverse engineered. Introduced the SNV in the intergenic region of PP_2176 and PP_2177-80.	This work MiCat #1789	2.1
P. putida NYL-P_{14f}-*nylB* PP_0412^{V222L} CbrA^{A625T}	Partly reverse engineered. PP_0412^{V222L} CbrA^{A625T}	This work MiCat #2703	2.1
P. putida NYL-P_{14f}-*nylB* PP_0412^{V222L} $P_{PP\_2177}$$^{C\rightarrow T}$	Partly reverse engineered. PP_0412^{V222L} $P_{PP_2177}$$^{C\rightarrow T}$	This work MiCat #1818	2.1
P. putida NYL-P_{14f}-*nylB* CbrA^{A625T} $P_{PP\_2177}$$^{C\rightarrow T}$	Partly reverse engineered. CbrA^{A625T} $P_{PP_2177}$$^{C\rightarrow T}$	This work MiCat #2704	2.1
P. putida NYLON-B	*P. putida* NYL P_{14f}-*nylB*, PP_0412^{V222L}, CbrA^{A625T}, $P_{PP\_2177}$$^{C\rightarrow T}$. Final reverse engineered strain for C$_6$-PA monomer and linear Ahx-oligomer metabolism.	This work MiCat #1831	2.1
P. putida NYLON-B ΔPP_0411-4	Deletion of PP_0411-4	This work MiCat #1893	2.1
P. putida NYLON-A	*P. putida* NYLON-B, in which *nylB* was replaced by *nylA*	This work MiCat #2085	2.1

P. putida NYLON-C	*P. putida* NYLON-B, in which *nylB* was replaced by *nylC*	This work MiCat #2086	2.1
P. putida NYLON-ABC	*P. putida* NYLON-B, in which *nylB* was replaced by a synthetic operon of *nylABC*. Expression of all three nylonases.	This work MiCat #2087	2.1
P. putida NYLON-ABC ΔPP_5003-6	Deletion of PP_5003-6 PHA cluster of *P. putida* KT2440.	This work MiCat #2170	2.1
P. putida NYLON-PHB	*P. putida* NYLON-ABC ΔPP_5003-6 harboring pSEVA6311::*phaCAB* for inducible PHB production.	This work MiCat #2176	2.1
A12.1p	Evolved KT2440 strain bearing the evolved plasmid pBNT-*dcaAKIJJP*	Ackermann et al. (2021)	2.3
A12.1ge	A12.1 after genomic integration of *attTn7*::P_{14e}-*dcaAKIJP* and removal of the resistance marker	Ackermann et al. (2021)	2.3
PA1.1	Evolved A12.1ge strain for growth on pimelate with *gcdR*^{G154D}	This work MiCat #2230	2.3
PA1.2	Evolved A12.1ge strain for growth on pimelate with *gcdR*^{G148D}	This work MiCat #2231	2.3
KT2440-AA Δ*gcdR*	Knockout of *gcdR*	This work MiCat #1447	2.3
KT2440-AA Δ*gcdR*::P_{14f}	Exchange of the regulator gene *gcdR* for the synthetic P_{14f} promoter	This work MiCat #1446	2.3
KT2440-AA *gcdR*^{G154D}	*gcdR*^{G154D}	This work MiCat #1459	2.3
KT2440-AA *gcdR*^{G148D}	*gcdR*^{G148D}	This work MiCat #1454	2.3
KT2440 ALE HDO	Evolved KT2440 wild type on 1,6-hexanediol	This work MiCat #1560	2.3
KT2440 PP_2046^{A257T}	Partly reverse engineered, PP_2046^{A257T}	This study MiCat #1675	2.3
KT2440 PP_2790^{A220V}	Partly reverse engineered, PP_2790^{A220V}	This study MiCat #1712	2.3
KT2440 *ttgB*^{Δ4bp}	Partly reverse engineered, PP_1385^{Δ4bp}	This study MiCat #1713	2.3
KT2440 PP_2046^{A257T}, PP_2790^{A220V}, *ttgB*^{Δ4bp}	Fully reverse engineered strain	This study MiCat #1717	2.3
KT2400-AA ALE HDO	Evolved KT2440-AA on 1,6-hexanediol	This study MiCat #1558	2.3
KT2440-AA *secG*^{G70R}	Fully reverse engineered strain, *secG*^{G70R}	This work MiCat #1678	2.3

KT2440-AA PP_5423^{R29P}	Partly reverse engineered, PP_5423^{R29P}	This work MiCat #1677	2.3
KT2440-AA *secG*^{G70R} PP_5423^{R29P}	*secG*^{G70R}, PP_5423^{R29P} combined	This work MiCat #1718	2.3
KT2440-AA *secG*^{G70R} ΔP_{14e}-*dcaAKIJP*	Deletion of *dcaAKIJP* in KT2440-AA *secG*^{G70R}	This work MiCat #1758	2.3
KT2440-AA *secG*^{G70R} *gcdR*^{G154D}	Final strain for (u)mcl-DCA and -diol metabolism	This work MiCat #1834	2.3
KT2440-AA *secG*^{G70R} *gcdR*^{G154D} ΔPP_5003-6, pS6311·PHB	Strain for PHB production using pS6311·PHB, containing *phaCAB*, PHB biosynthesis pathway from *C. necator* H16	This work MiCat #2174	2.3
attTn7::P_{14f}-PA0878-0883	*P. putida* KT2440 with genomic integration of the PA0878-0883 cluster under control of the constitutive P_{14f}-promoter	This study MiCat #563	2.4
attTn7::P_{14f}-PA0878-0886	*P. putida* KT2440 with genomic integration of the PA0878-0886 cluster under control of the constitutive P_{14f}-promoter	This study MiCat #565	2.4
ΔPA0878	*P. putida* KT2440 *attTn7*::P_{14f}-PA0878-0886 with deletion of PA0878	This study MiCat #1072	2.4
ΔPA0879-0881	*P. putida* KT2440 *attTn7*::P_{14f}-PA0878-0886 with deletion of PA0879-0881	This study MiCat #566	2.4
ΔPA0879	*P. putida* KT2440 *attTn7*::P_{14f}-PA0878-0886 with deletion of PA0879	This study MiCat #1068	2.4
ΔPA0880	*P. putida* KT2440 *attTn7*::P_{14f}-PA0878-0886 with deletion of PA0880	This study MiCat #1069	2.4
ΔPA0881	*P. putida* KT2440 *attTn7*::P_{14f}-PA0878-0886 with deletion of PA0881	This study MiCat #1070	2.4
ΔPA0882	*P. putida* KT2440 *attTn7*::P_{14f}-PA0878-0886 with deletion of PA0882	This study MiCat #1071	2.4
ΔPA0883	*P. putida* KT2440 *attTn7*::P_{14f}-PA0878-0886 with deletion of PA0883	This study MiCat #1150	2.4
ΔPP_0897	*P. putida* KT2440 *attTn7*::P_{14f}-PA0878-0886 with deletion of PP_0897	This study MiCat #1074	2.4
P. putida KT2440 *attTn7*::P_{14f}-PA0878-0886 ΔPP_5003-6 Km^{R-}	*P. putida* KT2440 *attTn7*::P_{14f}-PA0878-0886 with deletion of ΔPP_5003-6, kanamycin-sensitive	This study MiCat #2527	2.4
P. putida KT2440 *attTn7*::P_{14f}-PA0878-0886 ΔPP_5003-6 pS6311·PHB	*P. putida* KT2440 *attTn7*::P_{14f}-PA0878-0886 ΔPP_5003-6 Km^{R-} harboring pS6311·PHB	This study MiCat #2534	2.4

Other microorganisms

Pseudomonas aeruginosa PAO1	Wild-type, originating from Dieter Haas laboratory (Lausanne, CH)	Holloway et al. (1979)	2.4

Ustilago cynodontis NRBC 9727 Δfuz^7	Δfuz^7	Hosseinpour Tehrani et al. (2019)	2.4
Ustilago cynodontis NBRC9727 Δfuz^7 $\Delta cyp3$ P$_{etef}$-mttA P$_{ria1}$ *ria1* P$_{etef}$-*cyp3*	Δfuz^7 $\Delta cyp3$ P$_{etef}$-*mttA* P$_{ria1}$ *ria1* P$_{etef}$-*cyp3*	Ernst *et al.*., Manuscript in preparation	2.4
Candida albicans SC5314	Wild type clinical isolate	Laboratory: Wilson RB, Davis D, Enloe BM, Mitchell AP	2.4
Halopseudomonas formosensis FZJ	Wild type isolate – Kompostanlage Würselen	This study MiCat #580	2.5
Halopseudomonas formosensis FZJ ΔPE-H	Deletion mutant lacking *Hfor*_PE-H	This study MiCat #2758	2.5
Bacillus sp.	Wild type isolate – Kompostanlage Würselen	This study MiCat #581	2.5

Table S2. Plasmids used in this thesis

Plasmid	Description	Reference	Chapter
pRK2013	Km^R, *oriV*(RK2/ColE1) -*mob*$^+$ *tra*$^+$	Figurski and Helinski (1979)	2.1, 2.3, 2.4
pSW-2	Gm^R, *oriV*(*RK2*), *xylS*, Pm I-SceI (transcriptional fusion of I-SceI to Pm)	Martínez-García and de Lorenzo (2011)	2.1, 2.3
pEMG	Km_R, *oriV*(R6K), *lacZ* α with two flanking I-SceI sites	Martínez-García and de Lorenzo (2011)	2.1, 2.3
pEMG ΔPP_2884	pEMG harboring flanking sequences for ΔPP_2884	This study Plasmid #359	2.1
pEMG PP_2884^{Δ3}	pEMG harboring flanking sequences for PP_2884^{Δ3}	This study Plasmid #361	2.1
pEMG PP_0409^{W676L}	pEMG harboring flanking sequences for PP_0409^{W676L}	This study Plasmid #498	2.1
pEMG ΔPP_0409	pEMG harboring flanking sequences for ΔPP_0409	This study Plasmid #452	2.1
pEMG ΔPP_0409::P_{14b}	pEMG harboring flanking sequences for ΔPP_0409::P_{14b}	This study Plasmid #453	2.1
pEMG ΔPP_0411-4	pEMG harboring flanking sequences for ΔPP_0411-4	This study Plasmid #550	2.1
pEMG Δ*oplBA*	pEMG harboring flanking sequences for Δ*oplBA*	This study Plasmid #603	2.1
pEMG P_{14f}-*nylA*	pEMG harboring P_{14f}-*nylA* for integration into landing pad PP_0340-1	This study Plasmid #350	2.1
pEMG P_{14f}-*nylB*	pEMG harboring P_{14f}-*nylB* for integration into landing pad PP_0340-1	This study Plasmid #351	2.1
pEMG P_{14f}-*nylC*	pEMG harboring P_{14f}-*nylC* for integration into landing pad PP_0340-1	This study Plasmid #352	2.1
pEMG P_{14f}-*nylABC*	pEMG harboring P_{14f}-*nylABC* for integration into landing pad PP_0340-1	This study Plasmid #353	2.1
pEMG PP_0412^{V222L}	pEMG harboring flanking sequences for PP_0412^{V222L}	This study Plasmid #558	2.1
pEMG CbrA^{A625T}	pEMG harboring flanking sequences for CbrA^{A625T}	This study Plasmid #560	2.1
pEMG $P_{PP\_2177}{}^{C\rightarrow T}$	pEMG harboring flanking sequences for $P_{PP\_2177}{}^{C\rightarrow T}$	This study Plasmid #563	2.1

pEMG ΔPP_5003-6	pEMG harboring flanking sequences for ΔPP_5003-6	This study Plasmid #624	2.1, 2.3, 2.4
pRK600	Cm^R, *oriV*(ColE1), *tra$^+$ mob$^+$* of RK2	Keen *et al.* (1988)	2.3
pBBFLP	Helper plasmid used for antibiotic markers excision in *P. putida* strains; *oriV*(pBBR1) *oriT*(RK2) *mob$^+$* λP$_R$::FLP λ(cI857) *sacB tet*, Tc^R	de las Heras *et al.* (2008)	2.3
pSNW2	pEMG with *msfGFP*,	Volke et al., (2020)	2.3
pEMG_PP_2051	pEMG harboring flanking sequences for ΔPP_2051	Li et al., (2020)	2.3
pEMG_*dcaAKIJP*	pEMG harboring flanking sequences for Δ*dcaAKIJP*	This study Plasmid #386	2.3
pEMG_*ttgB*^{Δ4bp}	pEMG harboring flanking sequences for *ttgB*^{Δ4bp}	This study Plasmid #533	2.3
pEMG_PP_2046^{A247T}	pEMG harboring flanking sequences for PP_2046^{A247T}	This study Plasmid #530	2.3
pEMG_PP_2790^{A222V}	pEMG harboring flanking sequences for PP_2790^{A222V}	This study Plasmid #531	2.3
pEMG_PP_5423^{R29P}	pEMG harboring flanking sequences for PP_5423^{R29P}	This study Plasmid #535	2.3
pEMG_*secG*^{G70R}	pEMG harboring flanking sequences for *secG*^{G70R}	This study Plasmid #534	2.3
pEMG_*secG*	pEMG harboring flanking sequences for Δ*secG*	This study Plasmid #633	2.3
pS648::(sRBS)*phaCAB*	introduce synthetic RBSs upstream PHB operon	This study	2.3
pS341·PHA	For amplification of *phaCAB*	Durante-Rodríguez et al., (2018)	2.3
pS6311·PHB	Derivative of pSEVA631 harboring a synthetic operon for inducible expression of the *phaCAB* genes from *C. necator*	This study Plasmid #630	2,1, 2.3, 2.4
pSNW2_*gcdR*	pSNW2 harboring flanking sequences for Δ*gcdR*	This study Plasmid #479	2.3
pSNW2_*gcdR*_P$_{14f}$	pSNW2 harboring flanking sequences for Δ*gcdR* and Integration of P$_{14f}$	This study Plasmid #478	2.3
pSNW2_*gcdR*^{G148D}	pSNW2 harboring flanking sequences for *gcdR*^{G148D}	This study Plasmid #481	2.3
pSNW2_*gcdR*^{G154D}	pSNW2 harboring flanking sequences for *gcdR*^{G154D}	This study Plasmid #481	2.3
pBG14f_FRT_Kan	Km^R flanked with FRT sites, *oriV*(R6K), pBG-derived, promoter 14f, *msfGFP*	Ackermann et al. (2021)	2.4

pBG14f_FRT_Kan PA0878-0883	*attTn7* integration of PA0878-0883	This study Plasmid #335	2.4
pBG14f_FRT_Kan PA0878-0886	*attTn7* integration of PA0878-0886	This study Plasmid #337	2.4
pBG14f_FRT_Kan PA0878-0886 ΔPA0878	*attTn7* integration of PA0878-0886 ΔPA0878	This study Plasmid #348	2.4
pBG14f_FRT_Kan PA0878-0886 ΔPA0879-0881	*attTn7* integration of PA0878-0886 ΔPA0879-0881	This study Plasmid #338	2.4
pBG14f_FRT_Kan PA0878-0886 ΔPA0879	*attTn7* integration of PA0878-0886 ΔPA0879	This study Plasmid #347	2.4
pBG14f_FRT_Kan PA0878-0886 ΔPA0880	*attTn7* integration of PA0878-0886 ΔPA0880	This study Plasmid #344	2.4
pBG14f_FRT_Kan PA0878-0886 ΔPA0881	*attTn7* integration of PA0878-0886 ΔPA0881	This study Plasmid #345	2.4
pBG14f_FRT_Kan PA0878-0886 ΔPA0882	*attTn7* integration of PA0878-0886 ΔPA0882	This study Plasmid #346	2.4
pBG14f_FRT_Kan PA0878-0886 ΔPA0883	*attTn7* integration of PA0878-0886 ΔPA0883	This study Plasmid #371	2.4
pSEVA512S	Tc^R, *oriV*(R6K), mob$^+$, *lacZα*-MCS flanked by two I-SceI sites	de Lorenzo lab	2.4
pSEVA512S PP_0897	pSEVA512S with flanking regions TS1 and TS2 for PP_0897 knockout	This study Plasmid #349	2.4
pQT8-*sce-I*	*sce-I* expression	This study Plasmid #232	2.5
pEMG-Δ*Hfor*_PE-H	flanking region for *Hfor*_PE-H deletion	This study Plasmid #358	2.5

Table S3. Oligonucleotides used in this thesis.

Oligonucleotide	Sequence 5'-3'	Description	Chapter
JDW075	GATCCTCTAGAGTCGACCTGCAG	pEMG Backbone_fw	2.1
JDW076	CCCGGGTACCGAGCTCGA	pEMG Backbone_rv	2.1
JDW077	ATTCGAGCTCGGTACCCGGGCGTGACCGTGTCACAGATC	TS1 ΔPP_2884_fw	2.1
JDW078	TGGGTCAAGAAGCCGCCTTGTAATCAGAG	TS1 ΔPP_2884_rv	2.1
JDW079	CAAGGCGGCTTCTTGACCCACAGACGTTC	TS2 ΔPP_2884_fw	2.1
JDW080	CAGGTCGACTCTAGAGGATCGATCGGTTCGAGGCATTG	TS2 ΔPP_2884_rv	2.1
JDW088	ATTCGAGCTCGGTACCCGGGCGCTGAAGATGATCCGGG	TS1 PP_2884$^{\Delta 3}$_fw	2.1
JDW120	CCTCACGCACCGGCTCGTCGAACTCCGCCAGGCTCATG	TS1 PP_2884$^{\Delta 3}$_rv	2.1
JDW091	CAGGTCGACTCTAGAGGATCGCGGGGTTGGTGCCATAG	TS2 PP_2884$^{\Delta 3}$_fw	2.1
JDW121	CGACGAGCCGGTGCGTGA	TS2 PP_2884$^{\Delta 3}$_rv	2.1
JDW194	ATTCGAGCTCGGTACCCGGGTCCCTATATCAGTGAGGGTAGC	TS1-TS2-PP_0409^{W676L}_fw	2.1
JDW195	CAGGTCGACTCTAGAGGATCGCTGGAGCATCGTGCAGC	TS1-TS2-PP_0409^{W676L}_rv	2.1
JDW239	ATTCGAGCTCGGTACCCGGGATCCGGCGTTGTTGTTGAC	TS1 ΔPP_0411-4_fw	2.1
JDW240	CAAGCCATCAGCCTGCACCTTCTTGTTG	TS1 ΔPP_0411-4_rv	2.1
JDW241	AGGTGCAGGCTGATGGCTTGCCTGTACCG	TS2 ΔPP_0411-4_fw	2.1
JDW242	CAGGTCGACTCTAGAGGATCGCTTGTCGAGGGTGCCGG	TS2 ΔPP_0411-4_rv	2.1
JDW291	ATTCGAGCTCGGTACCCGGGAATCGAGATGATCCAGCAG	TS1 Δ*oplBA*_fw	2.1
JDW292	GACCGCAAGAAGGTCACCAACGTTTGTTC	TS1 Δ*oplBA*_rv	2.1
JDW293	TTGGTGACCTTCTTGCGGTCGGCGCGCG	TS2 Δ*oplBA*_fw	2.1
JDW294	CAGGTCGACTCTAGAGGATCGCGTCGAAGCAATGCCGGGTATAG	TS2 Δ*oplBA*_rv	2.1
JDW177	ATTCGAGCTCGGTACCCGGGATCGGCTGCGGTGGCTTG	TS1 ΔPP_0409-10_fw	2.1
JDW186	TATGTCGCAACTATACGCTCGACTTGGCAAAGAC	TS1 ΔPP_0409-10_rv	2.1
JDW187	GAGCGTATAGTTGCGACATACGGGTGCC	TS2 ΔPP_0409-10_fw	2.1
JDW188	CAGGTCGACTCTAGAGGATCGCCAGGTTCTCGGCCACG	TS2 ΔPP_0409-10_rv	2.1
JDW178	CGTAAACTGTCTATACGCTCGACTTGGCAAAGAC	TS1 ΔPP_0409-10::*P₁₄ᵦ*_rv	2.1
JDW179	GAGCGTATAGACAGTTTACGAACCGAAC	*P₁₄ᵦ* ΔPP_0409-10::*P₁₄ᵦ*_fw	2.1
JDW180	CCTCGCTCATTAGAAAACCTCCTTAGCATG	*P₁₄ᵦ* ΔPP_0409-10::*P₁₄ᵦ*_rv	2.1
JDW181	AGGTTTTCTAATGAGCGAGGCGAAGTCG	TS2 ΔPP_0409-10::*P₁₄ᵦ*_fw	2.1
JDW182	CAGGTCGACTCTAGAGGATCGTCACGTACACCACGGTC	TS2 ΔPP_0409-10::*P₁₄ᵦ*_rv	2.1
JDW122	CACTGCTCAGGGCCTGTG	pEMG backbone_fw	2.1
JDW125	GAATTCGAGCTCGGTACCC	pEMG backbone_rv	2.1
JDW123	TGCACAGGCCCTGAGCAGTGACAGTTTACGAACCGAAC	*P₁₄f–nylonase*_fw	2.1
JDW124	CGGGTACCGAGCTCGAATTCTTAGGCAGCAGGGATCTTAC	*P₁₄f-nylA*_rv	2.1

JDW135	CGGGTACCGAGCTCGAATTCTTATACAGCGTCGAGCGC	P_{14f}-*nylB*_rv	2.1
JDW139	CGGGTACCGAGCTCGAATTCTTAGGCCTCCAGGACGGC	P_{14f}-*nylC*_rv	2.1
JDW252	ATTCGAGCTCGGTACCCGGGTTGGGGCTGTTCACCGCTG	TS1-TS2-PP_0412^{V222L}_fw	2.1
JDW253	CAGGTCGACTCTAGAGGATCGCAGGCCGCCGACCACTT	TS1-TS2-PP_0412^{V222L}_rv	2.1
JDW255	ATTCGAGCTCGGTACCCGGGTACTCTACTGGCCAACCGC	TS1-TS2-CbrA^{A625T}_fw	2.1
JDW256	CAGGTCGACTCTAGAGGATCGCTCCTCGCTGTTCTGGTG	TS1-TS2-CbrA^{A625T}_rv	2.1
JDW266	ATTCGAGCTCGGTACCCGGGACTGCGAGATTCACGCCG	TS1-TS2- $P_{PP_2177}$$^{C\rightarrow T}$_fw	2.1
JDW267	CAGGTCGACTCTAGAGGATCGCAGATCCGGAAAGATGACAC	TS1-TS2- $P_{PP\_2177}$$^{C\rightarrow T}$_rv	2.1
JDW303	CATTAGAAAACCTCCTTAGCATTTAGTTGCCGGCCTCGGTCACC	P_{14f}-*nylC$_\alpha$C$_\beta$*_fw	2.1
JDW304	TAAATGCTAAGGAGGTTTTCTAATGACCACCATCTCCGCAATCGTTAC	P_{14f}-*nylC$_\alpha$C$_\beta$*_rv	2.1
JDW297	ATTCGAGCTCGGTACCCGGGAAGCCTCCAAGACCCTCAG	TS1 ΔPP_5003-6_fw	2.1
JDW298	TCCAGCAGGCCTACGACGCTCCGTTGTC	TS1 ΔPP_5003-6_rv	2.1
JDW299	AGCGTCGTAGGCCTGCTGGAGATGTAGTG	TS2 ΔPP_5003-6_fw	2.1
JDW300	CAGGTCGACTCTAGAGGATCGCGAACTTGAAGAAGCCTTC	TS2 ΔPP_5003-6_rv	2.1
JDW363	GAGGACGAAATCCCCGGGTACCGAGCTC	pBAM1-backbone_fw	2.1
JDW364	TGTTCAACACTCCTCTAGAGTCGACCTGCAG	pBAM1-backbone_rv	2.1
JDW365	CTCTAGAGGAGTGTTGAACAACCAACGAAC	*oppABCDF-nylC$_{JW-1}$* pBAM-1_fw	2.1
JDW366	TACCCGGGGATTTCGTCCTCTCAGTCTG	*oppABCDF-nylC$_{JW-1}$* pBAM-1_rv	2.1
JDW267	CAGGTCGACTCTAGAGGATCGCAGATCCGGAAAGATGACAC	TS1-TS2- $P_{PP_2177}$$^{C\rightarrow T}$_rv	2.1
JDW303	CATTAGAAAACCTCCTTAGCATTTAGTTGCCGGCCTCGGTCACC	P_{14f}-*nylC$_\alpha$C$_\beta$*_fw	2.1
JDW304	TAAATGCTAAGGAGGTTTTCTAATGACCACCATCTCCGCAATCGTTAC	P_{14f}-*nylC$_\alpha$C$_\beta$*_rv	2.1
JDW297	ATTCGAGCTCGGTACCCGGGAAGCCTCCAAGACCCTCAG	TS1 ΔPP_5003-6_fw	2.1
JDW298	TCCAGCAGGCCTACGACGCTCCGTTGTC	TS1 ΔPP_5003-6_rv	2.1
JDW299	AGCGTCGTAGGCCTGCTGGAGATGTAGTG	TS2 ΔPP_5003-6_fw	2.1
JDW300	CAGGTCGACTCTAGAGGATCGCGAACTTGAAGAAGCCTTC	TS2 ΔPP_5003-6_rv	2.1
JDW363	GAGGACGAAATCCCCGGGTACCGAGCTC	pBAM1-backbone_fw	2.1
JDW364	TGTTCAACACTCCTCTAGAGTCGACCTGCAG	pBAM1-backbone_rv	2.1
JDW365	CTCTAGAGGAGTGTTGAACAACCAACGAAC	*oppABCDF-nylC$_{JW-1}$* pBAM-1_fw	2.1
JDW366	TACCCGGGGATTTCGTCCTCTCAGTCTG	*oppABCDF-nylC$_{JW-1}$* pBAM-1_rv	2.1
JDW169	ATTCGAGCTCGGTACCCGGGAATGGCTGCTCACAGAAC	TS1 Δ*dcaAKIJP*	2.3
JDW170	TTTTAGAGAATTAAAACTGTCGCTAGAGAATTAAAG		2.3
JDW171	ACAGTTTTAATTCTCTAAAACCAGTTGATCAACACC	TS2 Δ*dcaAKIJP*	2.3
JDW172	CAGGTCGACTCTAGAGGATCAAGCCGGTGTCGAAGCTG		2.3
JDW208	ATTCGAGCTCGGTACCCGGGACGCTGGGCCAGGGCGAA	TS1 *ttgB*$^{\Delta 4bp}$	2.3
JDW209	GCGCCCTGGTATCGCCCTGGTGCTCTCGG		2.3
JDW210	CCAGGGCGATACCAGGGCGCCCTGGATC	TS2 *ttgB*$^{\Delta 4bp}$	2.3
JDW211	CAGGTCGACTCTAGAGGATCGCCTGCAAACCGCCGAGC		2.3

JDW215	ATTCGAGCTCGGTACCCGGGATGGTCATGTTGGCCAGGTCCAG	TS1 - PP_2046^{A247T} - TS2	2.3
JDW216	CAGGTCGACTCTAGAGGATCCGCTGCTGGTCCGCGTGG		2.3
JDW218	ATTCGAGCTCGGTACCCGGGTGTGCTGCTTCGAACAGG	TS1 - PP_2790^{A222V} - TS2	2.3
JDW219	CAGGTCGACTCTAGAGGATCGCTGATCAGCCACTTGCAG		2.3
JDW223	ATTCGAGCTCGGTACCCGGGAGCTGTACTGTCACGTCAATATTC	TS1 - PP_5423^{R29P} - TS2	2.3
JDW224	CAGGTCGACTCTAGAGGATCGCGGTTTGGTGAGTTTTTC		2.3
JDW228	ATTCGAGCTCGGTACCCGGGAAGGCCTGCAACTGTTCTAGCTTGC	TS1 - *secG*^{G70R} - TS2	2.3
JDW229	CAGGTCGACTCTAGAGGATCGCGGCCCAGGCCAAAGGC		2.3
JDW297	ATTCGAGCTCGGTACCCGGGAAGCCTCCAAGACCCTCAG	TS1 ΔPP_5003-6	2.3
JDW298	TCCAGCAGGCCTACGACGCTCCGTTGTC		2.3
JDW299	AGCGTCGTAGGCCTGCTGGAGATGTAGTG	TS2 ΔPP_5003-6	2.3
JDW300	CAGGTCGACTCTAGAGGATCGCGAACTTGAAGAAGCCTTC		2.3
JDW305	ATTCGAGCTCGGTACCCGGGACATCGAGGATTGCGCTG	TS1 Δ*secG*	2.3
JDW306	AACTGAACAACGGGTTTCAAGTAGTAGTATTGC		2.3
JDW307	TTGAAACCCGTTGTTCAGTTTCCTGCGG	TS2 Δ*secG*	2.3
JDW308	CAGGTCGACTCTAGAGGATCATTGATGGCCTGGCAGGTAAAG		2.3
YA89	TAACAGGGTAATCTGAATTCGTCCAGGCTCTGCGCCCG	TS1 Δ*gcdR,* also used for SNV	2.3
YA90	GTTGACGTACCCCTGTAGTCAATTATTTTAAACACCTACAGATGTATG TATATGTCGC		2.3
YA91	GACTACAGGGGTACGTCAACCTCACTTGTAAG	TS2 Δ*gcdR,* also used for SNV	2.3
YA92	GCCTGCAGGTCGACTCTAGAGAACACATTGTCCATGAC		2.3
YA95	CCCTGTAGTCAATTATTTTAAACACCTACAGATGTATGTATATGTCGC	TS1 Δ*gcdR* and P_{14f} integration	2.3
YA96	TAAAATAATTGACTACAGGGTTAATTAAGCCCGTT GACATGACATGGTTTTGAGGGTATAATGTGGCGACC TAGGGTACGTCAACCTCACTTGTAAG	TS2 Δ*gcdR* and P_{14f} integration	2.3
YA145	GCAACCATCCCCGAGCAATACG	qPCR amplicon *gcdH*	2.3
YA146	ATCACCAGCGACGACTGCACAC		2.3
SEM_MM_99	AGGATCCUCTAGAGTCGACCTGCAGGC	pS648 amplification	2.3
SEM_MM_101	ATGTTTTUCCTCCTTCATGACTCCATTATTATTGTTTC	pS648 amplification	2.3
SEM_MM_97	AAAAACAUATGGCGACCGGCAAAGGC	sRBS + *phaC* amplification	2.3
YA91	GACTACAGGGGTACGTCAACCTCACTTGTAAG	TS2 Δ*gcdR,* also used for SNV	2.3
YA92	GCCTGCAGGTCGACTCTAGAGAACACATTGTCCATGAC		2.3
YA96	TAAAATAATTGACTACAGGGTTAATTAAGCCCGTTGACATGAC ATGGTTTTGAGGGTATAATGTGGCGACCTAGGGTACGTCAACCTC ACTTGTAAG	TS2 Δ*gcdR* and P_{14f} integration	2.3
YA145	GCAACCATCCCCGAGCAATACG	qPCR amplicon *gcdH*	2.3
YA146	ATCACCAGCGACGACTGCACAC		2.3
SEM_MM_99	AGGATCCUCTAGAGTCGACCTGCAGGC	pS648 amplification	2.3

SEM_MM_101	ATGTTTTUCCTCCTTCATGACTCCATTATTATTGTTTC	pS648 amplification	2.3
SEM_MM_97	AAAAACAUATGGCGACCGGCAAAGGC	sRBS + *phaC* amplification	2.3
SEM_MM_103	ATGTTTTTCCUCCTGAATTCTCATGCCTTGGCTTTGACGTATCGC	*phaC* amplification	2.3
SEM_MM_104	AGGAAAAACAUATGACTGACGTTGTCATCGTATC	sRBS + *phaA* amplification	2.3
SEM_MM_105	ATGTTTTCCTCCTGAATTCTTATTTGCGCTCGACTGCC	*phaA* amplification	2.3
SEM_MM_106	AAAAACAUATGACTCAGCGCATTGCGTAT	sRBS + *phaB* amplification	2.3
SEM_MM_98	AGGATCCUCAGCCCATATGCAGGCCG	*phaB* amplification	2.3
SEM_MM-121	ATTAAACGUTCAAAAAACAATAGAGGAGACTGAATTTTCAGACACG	ChnR/P*chnB* amplification	2.3
SEM_MM_79	ATCCCCGGGUACCGAGCTCGAATTCGCGCGGC	ChnR/P*chnB* amplification	2.3
SEM_MM_80	ACCCGGGGAUCCTAAGGAGGAAAAACATATGGCGACC	(sRBS)*phaCAB* amplification	2.3
SEM_MM_120	AGCTTGCAUTCAGCCCATATGCAGGCC	(sRBS)*phaCAB* amplification	2.3
JDW001	GAATTCGAGCTCGGTACC	pBG14f_FRT_Kan backbone	2.4
JDW002	TAGAAAACCTCCTTAGCATG	pBG14f_FRT_Kan backbone	2.4
JDW003	CATGCTAAGGAGGTTTTCTAATGAGTGAGTCCGCTTTCGCCC	PA0878 fw cluster	2.4
JDW004	CGGGTACCGAGCTCGAATTCTCAGCCACCCTCCCCGGC	PA0883 rv cluster	2.4
JDW005	GTTCGGTTGATCAGTCGAATTCCACGTC	PA0878 rv for ΔPA0879-0881	2.4
JDW006	ATTCGACTGATCAACCGAACCAGCCGCACC	PA0882 fw for ΔPA0879-0881	2.4
JDW007	TCAGCCACCCTCCCCGGC	PA0883 rv	2.4
JDW009	CGGGTACCGAGCTCGAATTCTCAGCTCATGCCCAGCAG	PA0886 rv cluster	2.4
JDW010	GGGTAGTCGGTATGCAAATG	Mapping *Tn7* insertion PP_5408 fw	2.4
JDW011	TAGACGATGTCGTGCTCTTC	Mapping *Tn7* insertion PA0878 rv	2.4
JDW037	GGCTCCCGCTTCAGTCGAATTCCACGTC	PA0878 rv for ΔPA0879	2.4
JDW038	ATTCGACTGAAGCGGGAGCCGCCCATGC	PA0880 fw for ΔPA0879	2.4
JDW039	GGCACGCGGCTCAGAACGAGCGCGGCAG	PA0879 rv for ΔPA0880	2.4
JDW040	CTCGTTCTGAGCCGCGTGCCTCGGGACA	PA0881 fw for ΔPA0880	2.4
JDW041	GTTCGGTTGACTACAGCGGGTTGCTCAG	PA0880 rv for ΔPA0881	2.4
JDW042	CCCGCTGTAGTCAACCGAACCAGCCGCA	PA0882 fw for ΔPA0881	2.4
JDW043	GTCCGCCTCCTCAGATCAGCGGCGCTAC	PA0881 rv for ΔPA0882	2.4
JDW044	GCTGATCTGAGGAGGCGGACATGAACCG	PA0883 fw for ΔPA0882	2.4
JDW047	TCGAACGCGTTCATACCGTTCCGGTCGC	PA0882 rv for ΔPA0883	2.4
JDW048	AACGGTATGAACGCGTTCGACAGACGCG	PA0884 fw for ΔPA0883	2.4
JDW050	GAGGATCCCCGGGTACCG	pSEVA512S backbone	2.4
JDW051	AGAGTCGACCTGCAGGC	pSEVA512S backbone	2.4
JDW052	ATGCCTGCAGGTCGACTCTAGCAACCGCAGGCGCAACA	PP_0897 TS1 fw	2.4
JDW053	TTACATCAGGGCAGCGCGCTCCTCTTAAAG	PP_0897 TS1 rv	2.4
JDW054	AGCGCGCTGCCCTGATGTAACTGCGGCGGC	PP_0897 TS2 fw	2.4
JDW055	CTCGGTACCCGGGGATCCTCGCAGGCCAGGGGCTGCAG	PP_0897 TS2 rv	2.4

JDW065	CCGGGGATCCTCTAGAGTCGGCTCAGTACGGCATCGGAG	TS1 *Hfor*_PE-H fw	2.5
JDW066	CCGGGGATCCTCTAGAGTCGGCTCAGTACGGCATCGGAG	TS1 *Hfor*_PE-H rv	2.5
JDW067	TGGAGTAACAGTCTGACAGCCGGCCCTTCG	TS2 *Hfor*_PE-H fw	2.5
JDW068	AAGCTTGCATGCCTGCAGGTCGCACCGGACGGCGCCAT	TS2 *Hfor*_PE-H rv	2.5
JDW069	AAGCCGTTGCGCGAGTTCAC	Mapping knock-out	2.5
JDW072	GCCATAGAGCATCCGATGAC	Mapping knock-out	2.5

Danksagung

An erster Stelle möchte ich meinem Doktorvater Prof. Dr. Nick Wierckx danken, der mir die Forschung an diesem hochspannenden Thema ermöglicht hat. Nick, ich danke dir für die fantastische Betreuung und Unterstützung sowie für die vielfältigen Diskussionen und Anregungen über den gesamten Zeitraum meiner Doktorarbeit. Die schönen und produktiven Dienstreisen für Glaukos sowie zur GRC in die USA mit dir werde ich immer gerne in Erinnerung behalten. Besonders dankbar bin ich dir für die organisatorische Unterstützung während meines Forschungsaufenthalts bei Novozymes. Vielen Dank für die unvergesslichen Jahre in deiner Arbeitsgruppe am Forschungszentrum, die ich sehr geschätzt habe!

Des Weiteren möchte ich mich bei Prof. Dr. Karl-Erich Jaeger bedanken, der mich während des gesamten Zeitraums als Mentor begleitet hat und sich als Zweitgutachter meiner Doktorarbeit zur Verfügung gestellt hat.

Next, I would like to give a special thanks to Kenneth Jensen for giving me the opportunity to perform an amazing 3-month research stay at Novozymes in Copenhagen during my PhD. Kenneth, many thanks for being a great supervisor, both scientifically and personally, and thanks for 'delegating' all the cool science. Also many thanks to the entire Glaukos consortium for sharing a wonderful time and productive project meetings.

Natürlich danke ich auch dir Benedikt - dem einzig wahren Postdoc (oder auch **the** Postdoc). Deinen ständigen Support und deine gute Laune schätze ich sehr und es war mir eine Ehre, dein „Quatschkopp" zu sein („52531 … bei Aachen!").

Ein riesen Dankeschön geht auch an alle (ehemaligen) Mitglieder der MiCat Gruppe für das stets fantastische Arbeitsklima und die super Zusammenarbeit. Besonders hervorheben möchte ich die Fußballrunde bestehend aus Philipp „Schmepsi" Ernst, Thorsten „Totti" Lechtenberg, Thomas „Figo" Konjetzko, Felix „Herbie" Herrmann (immerhin 1 Spiel), und natürlich meinen Lieblingsbürokollegen und IT-Experten Yannic „Aggi" Ackermann. Besten Dank euch für die „ehrliche Arbeit"! Danke auch an dich Christoph Schroth, dass ich deine Masterarbeit betreuen durfte und wir so tolle Ergebnisse erzielen konnten.

Zum Abschluss danke ich natürlich meiner Familie, nämlich Beate, Uwe, und Stefan, für die ständige Unterstützung meiner gesamten bisherigen Laufbahn. Ohne euch hätte ich es nicht bis hierhin geschafft! Zu guter Letzt danke ich meiner Verlobten Victoria Pieper - bald de Witt ;) - für den stetigen Support und ich freue mich riesig auf unser nächstes Kapitel in Hamburg.

Eidesstattliche Erklärung

Ich versichere an Eides Statt, dass die Dissertation von mir selbständig und ohne unzulässige fremde Hilfe unter Beachtung der „Grundsätze zur Sicherung guter wissenschaftlicher Praxis an der Heinrich-Heine-Universität Düsseldorf" erstellt worden ist. Die Dissertation wurde in der vorgelegten oder in ähnlicher Form noch bei keiner anderen Institution eingereicht. Ich habe bisher keine erfolglosen Promotionsversuche unternommen.

_____
Jan Alexander de Witt